

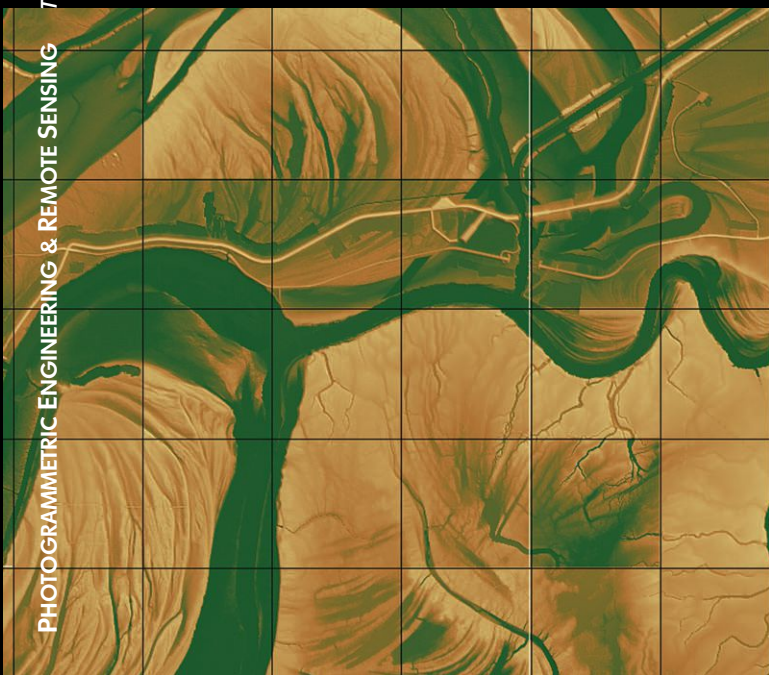
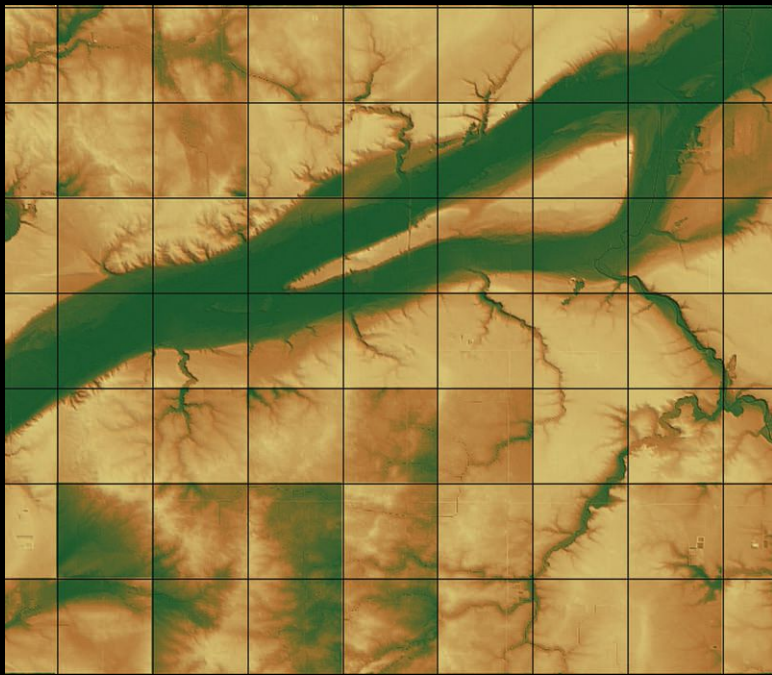
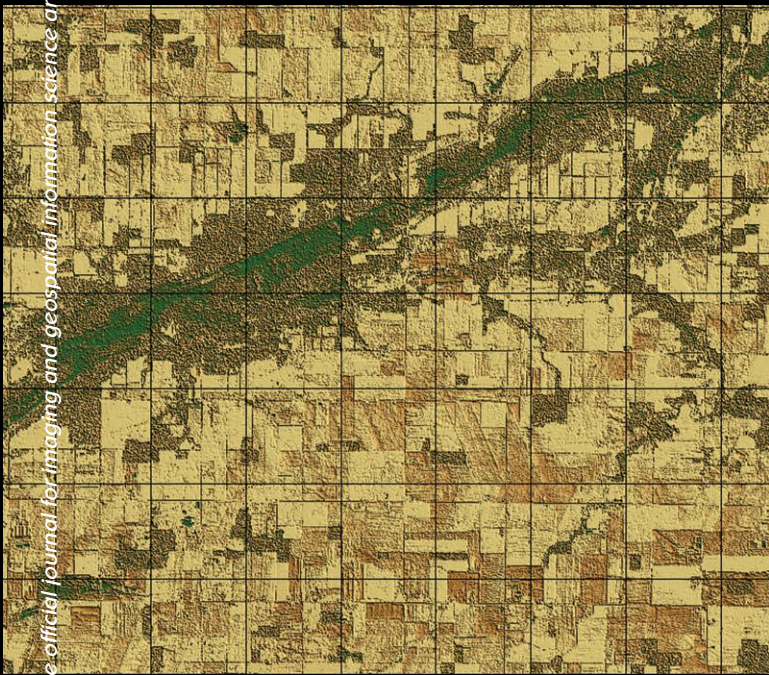
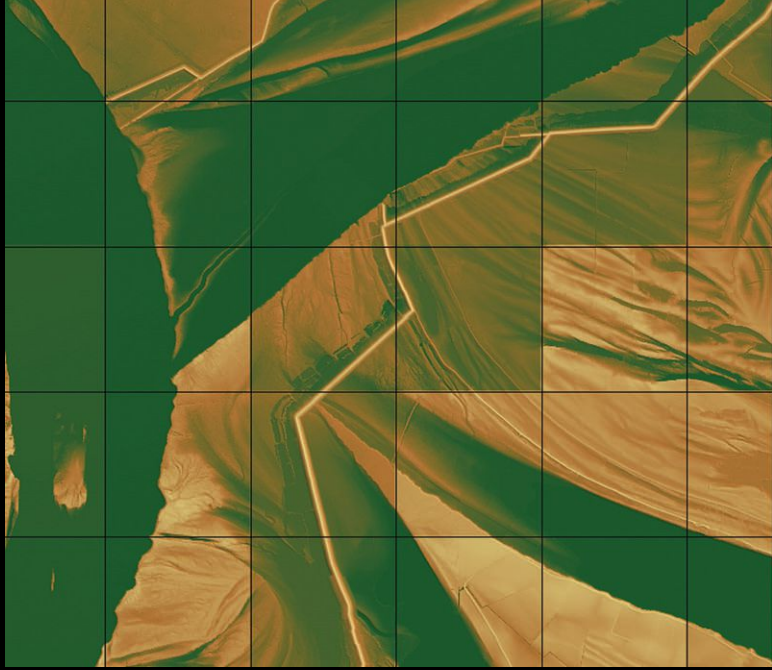
PE&RS

November 2011

Volume 77, Number 11

The official journal for imaging and geospatial information science and technology

PHOTOGRAMMETRIC ENGINEERING & REMOTE SENSING



We Get the Point



Together with Leica Geosystems, we offer the complete LiDAR workflow from capturing to delivering. Learn more about point clouds in ERDAS IMAGINE®, LPS, ERDAS APOLLO and Intergraph's GeoMedia® at www.erdas.com/lidar.



PECORA18

18th William T. Pecora Memorial Remote Sensing Symposium

www.asprs.org/Pecora18

November 14–17, 2011

Hilton Washington Dulles Hotel
Herndon, Virginia



ASPRS Conferences from Coast to Coast

IMAGING AND GEOSPATIAL TECHNOLOGIES – INTO THE FUTURE

ASPRS ANNUAL CONFERENCE

March 19–23, 2012

**Sacramento Convention Center
Sacramento, California**

www.asprs.org/Annual-Conferences/Sacramento-2012



The world around us is not flat. You often need a solution that allows you to get information from more than just two dimensional imagery and data. Introducing E3De™, an interactive geospatial software environment that allows you to extract important situational awareness from three dimensional data – providing you with more information about an area of interest than ever before. E3De has advanced tools to utilize raw LiDAR point cloud data and create photorealistic 3D visualizations, extract 3D features from a scene, or produce 3D products and layers. Derived results can be included in your GIS, fused with 2D data for further analysis, and more. When you analyze the world in all three dimensions, you discover the full potential of your data and can make better, more informed decisions. Learn more at www.ittvis.com/E3De.

E3De. Discover the Next Dimension of Your Data.



- ▶ **See how to extract 3D features from LiDAR data with E3De.**
Booth 205 at the 2011 ASPRS Pecora Symposium in Herndon, Virginia.

EXELIS

Visual Information Solutions

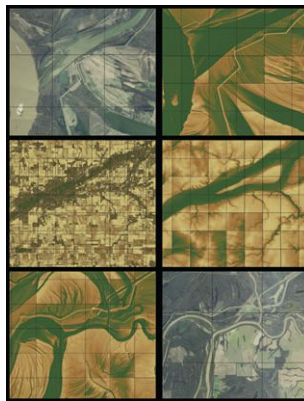


This month's cover shows elevation data from large-area lidar data

collections as well as derived information products and orthophotos.

Three pairs of images show lidar elevation data with orthophotos (top and bottom pairs) or with a lidar intensity image (middle pair) for the same area. The upper pair (collected by Photo Science for the Vicksburg District U.S. Army Corps of Engineers) shows orthophotos and elevation data for a segment of the Mississippi River along "The Delta" emphasizing the mainline levee system that provides flood protection for areas along the Mississippi River. The middle images (collected in Michigan by Woolpert for USGS) show lidar intensity and elevation data depicting the complex data returns in flood plains and riparian zones and the refined elevation data products. The lower pair shows elevation data and orthophotos for the lower part of "The Delta" where levees and flood control structures protect the Yazoo Basin from backwater flooding that occurs when the Mississippi River is at high stages. These views of lidar and derived data products were generated in Topo Analyst, a new product from Spatial Information Solutions (SIS) of Starkville, MS, a spin out from Mississippi State University.

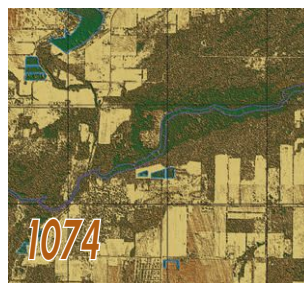
For additional information, contact Spatial Information Solutions (cgothara@spatialis.com) or visit <http://www.spatialis.com/>.



Highlight Article

1074 Cross-Walking "Lidar Guidelines and Base Specification" to Data Lifecycle Verification Approaches

Charles O'Hara



Feature Article

1081 ASPRS Ten-Year Remote Sensing Industry Forecast: Phase VI

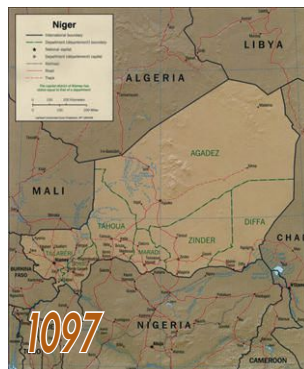
Charles Mondello, George Hepner, and Stephanie Boerman

Columns & Updates

1097 Grids and Datums – Republic of Niger

1099 Book Review – *Land Administration for Sustainable Development*

1106 Industry News



Announcements

1096 In Memoriam – Maurice Otto Nyquist

1101 Geoleague Challenge

1105 January 2013 Special Issue Call for Papers – *The Future of National-Scale Three-Dimensional Landscape Mapping*

Departments

1098 Certification List

1098 Region of the Month

1100 Member Champions

1103 New Members

1104 Calendar

1108 Who's Who in ASPRS

1109 Sustaining Members

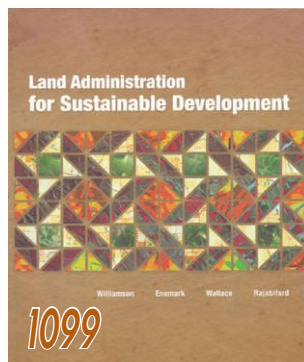
1111 Instructions for Authors

1132 Forthcoming Articles

1144 Advertiser Index

1144 Professional Directory

1180 Membership Application



PE&RS

November 2011 Volume 77, Number 11

PHOTOGRAMMETRIC ENGINEERING & REMOTE SENSING
The official journal for imaging and geospatial information science and technology

JOURNAL STAFF

Publisher

James R. Plasker
jplasker@asprs.org

Editor

Russell G. Congalton
russ.congalton@unh.edu

Executive Editor

Kimberly A. Tilley
kimt@asprs.org

Technical Editor

Michael S. Renslow
renslow76@comcast.net

Assistant Editor

Jie Shan
jshan@ecn.purdue.edu

Assistant Director – Publications

Rae Kelley
rkelley@asprs.org

Publications Production Assistant

Matthew Austin
maustin@asprs.org

Manuscript Coordinator

Jeanie Congalton
jcongalton@asprs.org

Circulation Manager

Sokhan Hing
sokhanh@asprs.org

Advertising Sales Representative

The Townsend Group, Inc.
asprs@townsend-group.com

CONTRIBUTING EDITORS

Grids & Datums Column

Clifford J. Mugnier
cjmce@lsu.edu

Book Reviews

John Iames
liames.john@epamail.epa.gov

Mapping Matters Column

Qassim Abdullah
Mapping_Matters@asprs.org

Website

webmaster@asprs.org



Immediate electronic access to all peer-reviewed articles in this issue is available to ASPRS members at www.asprs.org. Just log in to the ASPRS web site with your membership ID and password and download the articles you need.

Peer-Reviewed Articles

1113 Quantifying Urban Landscape Water Conservation Potential Using High Resolution Remote Sensing and GIS

Fayek A. Farag, Roger K. Kjelgren, and Joanna Endter-Wada

Urban landscaped areas in two suburbs of Salt Lake City, Utah were quantified through remote sensing and subsequent geographic information systems analysis that integrated localized reference evapotranspiration and municipal property and water billing data to determine amounts of urban landscape irrigation water that potentially could be conserved.

1123 Estimating Aboveground Carbon of Moso Bamboo Forests Using the k Nearest Neighbors Technique and Satellite Imagery

Guomo Zhou, Xiaojun Xu, Huaqiang Du, Hongli Ge, Yongjun Shi, and Yufeng Zhou

The k Nearest Neighbors technique with the new SCID metric was used to estimate aboveground carbon of Moso bamboo forests.

1133 Daily MODIS Data Trends of Hurricane-induced Forest Impact and Early Recovery

Elijah Ramsey III, Joseph Spruce, Amina Rangoonwala, Yukihiko Suzuoki, James Smoot, Jerry Gasser, and Terri Bannister

MODIS and 25 m optical and radar satellite data integrated for tracking daily wetland forest trends

1145 A Volumetric Approach to Population Estimation Using Lidar Remote Sensing

Zhenyu Lu, Jungho Im, and Lindi Quackenbush

The applicability of lidar data for population estimation at the census block level using various modeling techniques based on the volume of the residential buildings that were delineated using a modified building detection algorithm.

1157 Automatic Georeferencing of Aerial Images Using Stereo High-Resolution Satellite Images

Jaehong Oh, Charles K. Toth, and Dorota A. Grejner-Brzezinska

A new method for automated aerial image georeferencing based on image-to-image matching, using stereo high-resolution satellite images as reference data.

1169 Detection of Swimming Pools by Geographic Object-based Image Analysis to Support West Nile Virus Control Efforts

Minho Kim, James B. Holt, Rebecca J. Eisen, Kerry Padgett, William K. Reisen, and Janet B. Croft

Automatic detection of swimming pools was conducted using geographic object-based image analysis with very high spatial resolution satellite imagery, i.e., GeoEye-1, to aid in West Nile Virus control efforts.

PHOTOGRAMMETRIC ENGINEERING & REMOTE SENSING is the official journal of the American Society for Photogrammetry and Remote Sensing. It is devoted to the exchange of ideas and information about the applications of photogrammetry, remote sensing, and geographic information systems.

The technical activities of the Society are conducted through the following Technical Divisions: Geographic Information Systems, Photogrammetric Applications, Primary Data Acquisition, Professional Practice, and Remote Sensing Applications. Additional information on the functioning of the Technical Divisions and the Society can be found in the Yearbook issue of *PE&RS*.

Correspondence relating to all business and editorial matters pertaining to this and other Society publications should be directed to the American Society for Photogrammetry and Remote Sensing, 5410 Grosvenor Lane, Suite 210, Bethesda, Maryland 20814-2144, including inquiries, memberships, subscriptions, changes in address, manuscripts for publication, advertising, back issues, and publications. The telephone number of the Society Headquarters is 301-493-0290; the fax number is 301-493-0208; email address is asprs@asprs.org.

PE&RS. *PE&RS* (ISSN0099-1112) is published monthly by the American Society for Photogrammetry and Remote Sensing, 5410 Grosvenor Lane, Suite 210, Bethesda, Maryland 20814-2144. Periodicals postage paid at Bethesda, Maryland and at additional mailing offices.

SUBSCRIPTION. Effective January 1, 2011, the Subscription Rate for non-members per calendar year (companies, libraries) is \$410 (USA); \$426 for **Canada Airmail** (includes **5% for Canada's Goods and Service Tax** (GST#135123065)); \$420 for all other foreign.

POSTMASTER. Send address changes to *PE&RS*, ASPRS Headquarters, 5410 Grosvenor Lane, Suite 210, Bethesda, Maryland 20814-2144. CDN CPM #(40020812)

MEMBERSHIP. Membership is open to any person actively engaged in the practice of photogrammetry, photointerpretation, remote sensing and geographic information systems; or who by means of education or profession is interested in the application or development of these arts and sciences. Membership is for one year, with renewal based on the anniversary date of the month joined. Membership Dues include a 12-month subscription to *PE&RS* valued at \$68. Subscription is part of membership benefits and cannot be deducted from annual dues. Annual dues for Regular members (Active Member) is \$135; for Student members it is \$45; for Associate Members it is \$90 (see description on application in the back of this Journal). An additional postage surcharge is applied to all International memberships: Add \$40 for **Canada Airmail**, and 5% for **Canada's Goods and Service Tax (GST #135123065)**; all other foreign add \$60.00.

COPYRIGHT 2011. Copyright by the American Society for Photogrammetry and Remote Sensing. Reproduction of this issue or any part thereof (except short quotations for use in preparing technical and scientific papers) may be made only after obtaining the specific approval of the Managing Editor. The Society is not responsible for any statements made or opinions expressed in technical papers, advertisements, or other portions of this publication. Printed in the United States of America.

PERMISSION TO PHOTOCOPY. The appearance of the code at the bottom of the first page of an article in this journal indicates the copyright owner's consent that copies of the article may be made for personal or internal use or for the personal or internal use of specific clients. This consent is given on the condition, however, that the copier pay the stated per copy fee of \$3.00 through the Copyright Clearance Center, Inc., 222 Rosewood Drive, Danvers, Massachusetts 01923, for copying beyond that permitted by Sections 107 or 108 of the U.S. Copyright Law. This consent does not extend to other kinds of copying, such as copying for general distribution, for advertising or promotional purposes, for creating new collective works, or for resale.

Is your contact information current?

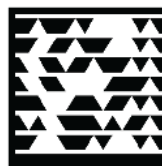
Contact us at members@asprs.org

or log on to <http://www.asprs.org/Member-Area/>
to update your information.

We value your membership.



Xiang Yu,
Peace Map Co., Ltd.



Visit **iFlyUltraCam.com**
to see the PMC video.
Or scan tag and watch on
your mobile phone.

Download the free tag reader app at <http://gettag.mobi>.

“Reliability, efficiency, and exceptional picture quality. That’s why I fly UltraCam.”



ULTRACAM
EAGLE

With plans to establish a high-resolution aerial image library of China and customers across 30 different government departments, Peace Map Co., Ltd. (PMC) needs a quality digital photogrammetric system to effectively serve their large market. That’s why PMC chooses Microsoft UltraCam for their digital-image acquisition.

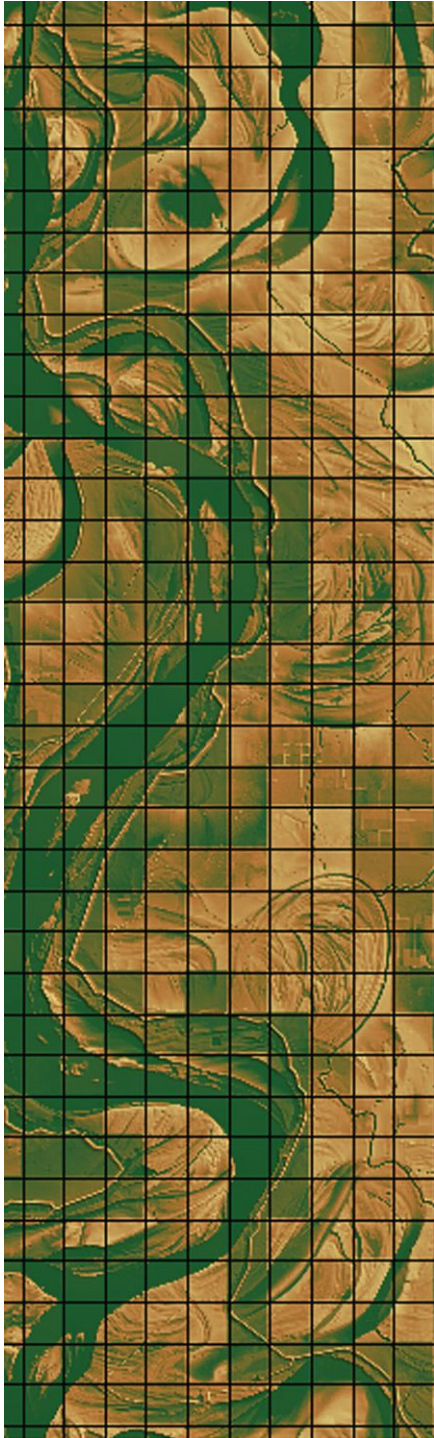
Mr. Xiang knows that the cost to fly missions is his greatest operational expense. Thanks to the large image footprint and stable performance of the UltraCam, he has seen a significant increase in efficiency compared to other digital aerial cameras. The continual innovation of the UltraCam helps PMC deliver breathtaking images to customers, reduce costs, and plan for steady growth into the future.

The UltraCam Eagle is the latest technological advance, featuring an ultra-large image footprint and revolutionary enhancements for high-quality imagery at unprecedented efficiencies. For details, visit www.UltraCamEagle.com.

Microsoft

Cross-Walking “Lidar Guidelines and Base Specification” to Data Lifecycle Verification Approaches

by Charles O'Hara



Evolution in Aerial Lidar Data Accuracy Verification and Review

Rapid advances in aerial lidar technologies, growth in useful applications of the data from lidar acquisition projects, and increasing demand for improved elevation data and derived information products combine to drive the need for consistent and unified specifications as well as efficient, cost effective, and standardized lidar data accuracy and verification methods which are aligned with those specifications. According to version 13 of the U.S. Geological Survey National Geospatial Program “Lidar Guidelines and Base Specification”¹

“The U.S. Geological Survey National Geospatial Program (NGP) has cooperated in the collection of numerous lidar datasets across the nation for a wide array of applications. These collections have used a variety of specifications and required a diverse set of products, resulting in many incompatible datasets and making cross-project analysis extremely difficult. The need for a single base specification, defining minimum collection parameters and a consistent set of deliverables, is apparent.

Beginning in late 2009, an increase in the rate of lidar data collection due to American Reinvestment and Recovery Act (ARRA) funding for The National Map makes it imperative that a single data specification be implemented to ensure consistency and improve data utility. Although the development of this specification was prompted by the ARRA stimulus funding, the specification is intended to remain durable beyond ARRA funded NGP projects.”

Lidar acquisition projects are evolving to include partnering of federal, state, county, and local participants. Partnering at multiple levels (federal, state, and local) on projects enables leveraging of funding resources while also requiring adjustments in the project acquisition data requirements and specification so that products deliver maximum benefits to the customers and the public and meet the combined requirements of the project partners. Differing participation can have significant impacts on the project specifications and requirements for their testing and verification. Major federal agencies such as the U.S. Geological Survey (USGS), the Federal Emergency Management Agency (FEMA), the U.S. Army Corps of Engineers (USACE), and the National Oceanic and Atmospheric Administration (NOAA) are providing leadership in developing specifications for lidar projects that are becoming increasingly a part of project requirements and specifications.

Vendor partnering for complex or large projects is also becoming commonplace. Projects that combine data from aerial rotary and fixed wing acquisitions of lidar and orthophotography, as well as terrestrial and mobile lidar, are delivering products that fuse data to include the best aspects of each sensor system involved. Such projects (Figure 1) will become more common as high resolution multi-scale, multi-source data are more effectively integrated with mapping and engineering software solutions. As the data become more complex, gathered from multiple sources, and collected to suit multi-scale applications, the methods for verifying the data must evolve to provide “best-practice” solutions that may be implemented across data sets, regardless of vendor specific systems or data types.

1. USGS, 2010. “U.S. Geological Survey National Geospatial Program: Lidar Guidelines and Base Specification,” version 13 ([http://lidar.cr.usgs.gov/USGS-NGP Lidar Guidelines and Base Specification, v13 ILMF.pdf](http://lidar.cr.usgs.gov/USGS-NGP%20Lidar%20Guidelines%20and%20Base%20Specification,%20v13%20ILMF.pdf)).

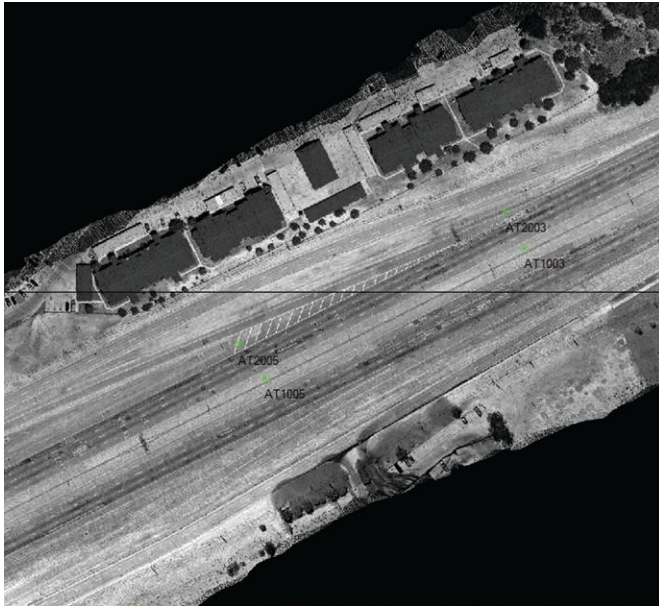


Figure 1. Surveyed checkpoint locations shown on intensity image derived from helicopter-based lidar acquired by Tuck Mapping as part of a multi-source lidar demonstration project conducted for the Texas Department of Transportation. (Data provided and used with the permission of Tuck Mapping)

Across the mapping industry, data vendors have made enormous investments in aircraft, lidar instruments, inertial measurement units and GPS navigation systems, as well as project planning and data production processing capabilities. Accompanying these investments in tangible assets, data producers have made further investments in both their production processes and personnel to develop and adhere to highly technical workflows, data processing, and internal quality control and assurance for delivering data products which will be acceptable to their customers. Despite the emergence of increasingly thorough guidelines and specifications for data and derived products, as well as vendors' production criteria, there exists a lack of commonly accepted best practices and standardized methods for verifying compliance to specifications.

Lidar – The Project Lifecycle Disconnect

A fundamental disconnect exists between lidar project data production and product delivery approaches, which inhibits the development of best practices that may be implemented across the project data production lifecycle. Lidar data and derived products are typically delivered at the end of the project; review, verification, and acceptance by customers typically await the delivery of final products. End-of-project delivery and verification approaches do not provide vendors with incentives for verifying, documenting, or delivering incremental products. At the same time, wide variation in the current "state-of-the-practice" for end-of-project delivery and verification highlights the fact that there are no mutually agreed-upon best practices or commodity software tools for verifying and accepting final products let alone practices and tools which could be accepted as sufficient, best practices for authoritatively testing incremental products against specifications and requirements.

New guidelines and specifications include unprecedented attention to the accuracy, quality, correctness, compliance, and completeness of lidar point cloud data which include flightline swath data, tiled data products, and final classified tiled LAS data. The new specifications for lidar data and derived information products require testing of various data products developed during phases of the data project. As part

of deliverable products verification, these tests are performed after-the-fact. Unless there are specific interim deliverables defined as project milestones, there are no mechanisms for engaging the producer and customer in "real time" verification of incremental products as data flow through the project. These emerging guidelines imply that lidar data must be tested and verified at key project phases by vendors to ensure that data meet eventual delivery guidelines and specifications. Specifications present a framework for verifying products developed across the lidar project lifecycle process or face the prospect that downstream products will ultimately fail due to flaws that were not addressed in earlier acquisition, calibration, and processing phases.

This article suggests that there is a pressing need for an effective cross-walking that maps lidar data and derived information product guidelines and specifications to project data lifecycle phases. As an initial step in that direction, this article proposes a simple cross-walking that identifies key phases of a typical lidar project life cycle and corresponding verification steps that may be conducted as gateways for assuring that products will meet specifications. Additionally, a collection of recent lidar projects is highlighted in summary with a brief description of the projects, technical challenges, and aspects of accuracy or quality characteristics. Some key tests and methods are presented that offer potential to be considered as part of a collection of industry best practices for key phases of lidar data verification.

Cross-Walking Specifications to Lidar Data Project Lifecycle Phases

Verifying lidar products as an industry standard practice currently emphasizes testing finished end products. This approach can lack rigor if testing focuses only on final delivered products which include uncertainties more ideally addressed in earlier phases of the data product's lifecycle. An approach to lidar data verification is presented which cross-walks guidelines and specifications to key phases of a typical lidar project. Four basic phases are proposed for a lidar project in which testing and verification tasks are suggested as starting points to address "gateway" questions that may be answered prior to subsequent tasks in the lidar data project lifecycle.

Phase 1 – Flight Planning, Operations, and Lidar Data Acquisition

Gateway Question: Are flight operations complete; have data been collected fully covering the project area without voids within flightlines, gaps between flightline data swaths, and at the pulse spacing and density specified?

Preliminary planning and data acquisition produce data which are converted to LAS files. The following tasks are presented as a possible subset for which best practice methods may be developed and addressed during this phase to comply with guidelines and specifications:

- **Collection Area:** Determine whether the data sets from initial flightlines completely and adequately cover the defined project area as well as any designated buffer area.
- **Overlap:** Generate swath boundary file polygons. Intersect adjacent boundary files and quantify percentage of swath width in the overlap to determine whether adjacent flightline swath data sufficiently overlap (Figure 2).
- **Spacing and Density:** Quantify point cloud spacing and density and determine if data are spaced at sufficient density to meet project requirements (Figure 2).
- **Gaps and Voids:** Identify gaps in data, voids that must be filled, or areas where additional flightlines are required. Employ vector boundaries containing holes as well as pulse

continued on page 1076

count rasters to quantify the spatially varying distribution of pulses.

- **LAS Compliance:** Test LAS files for size, multiple returns, scan angle, intensity, compliance to standard, contents, and for completeness of required information for header, variable length records, and data values.

Benefits: Completing these tasks in a timely and efficient manner is vital so that lidar equipment may be effectively used and so that any gaps, voids, or areas missed in initial flightlines may be acquired in conditions as similar as possible to those present during initial collections.

Phase 2 – Flightline Swath Data Calibration and Early Processing

Gateway Question: Are acquired data calibrated for instrument and systematic errors and have flightline swath LAS residual errors been minimized such that relative error within and between flightlines meets accuracy requirements?

Lidar flightline data has been acquired, converted to LAS format, and calibrated to remove system errors and systematic bias between flightlines. Relative accuracy of data must be tested by systematically investigating LAS elevations in the areas of overlap between adjacent flightlines. According to the USGS version 13 specification, “Accuracy for the lidar point cloud data is to be reported independently from accuracies of derivative products. Point cloud data accuracy is to be tested against a TIN constructed from bare earth lidar points.”¹ Therefore, verification of relative in-swath and between-swath accuracy should comprise the following tasks:

- **Bare Earth:** Preliminary classification of flightline swath data (or temporarily tiled in a reversible manner to enable compute effective preliminary classification) for bare earth lidar pulse returns.
- **Between Swath Relative Accuracy:** Quantify areas of overlap between adjacent swaths, segment overlap into desired sub-units, and identify common points per subunit for extracting Z-values from TINs constructed from bare earth returns in the immediate vicinity of the points (Figure 3).
- **Within Swath Relative Accuracy:** Identify areas within swath of single (first and only) returns and uniform surface characteristics for quantifying relative accuracy within that swath.

Relative accuracy testing is conducted using raster and vector methods, but methods must emphasize using point cloud data, bare earth classed points, and Z-values extracted from TINs. The use of boundaries, overlap extraction, using point cloud data and TINs to extract set Z-values from each swath corresponding to a common location is superior to raster-to-raster comparisons which compute Z-difference. These Z-difference rasters compute a difference surface from two preliminary surface models that are of limited confidence. Lacking an agreed upon best practice in this area, the use of the Z-difference surface for estimating RMSE Z between the two adjacent swaths is currently an accepted aspect of the “state-of-the-practice”. This practice may remain a “supplemental” relative accuracy test, but should be replaced by fully automated vector methods that might be similar to the overlap, segmentation, and centroid generation approach shown in Figure 3.

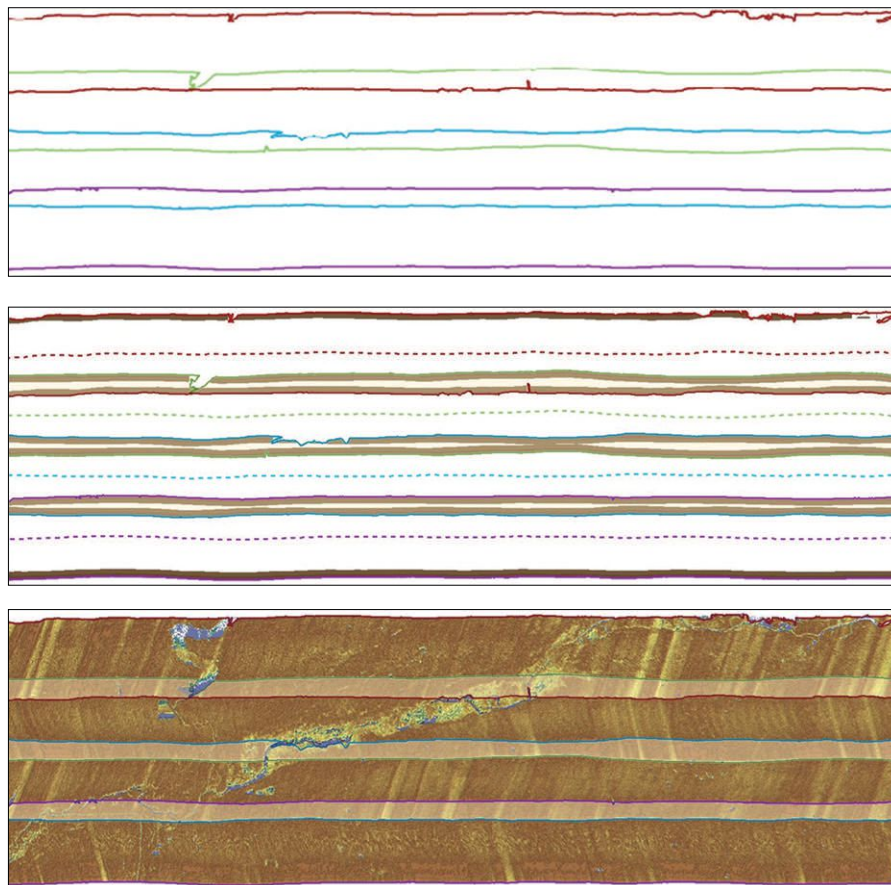


Figure 2. Boundary polygons created from lidar swaths (strips) shown in upper image quantify completeness of coverage, intersected overlap areas shown in the middle image with estimated centerline and outer 10% of the flightline swath shown for quantifying adequate overlap, and pulse count raster shown in the lower image created from first returns shows pulse distribution and voids or gaps in data.

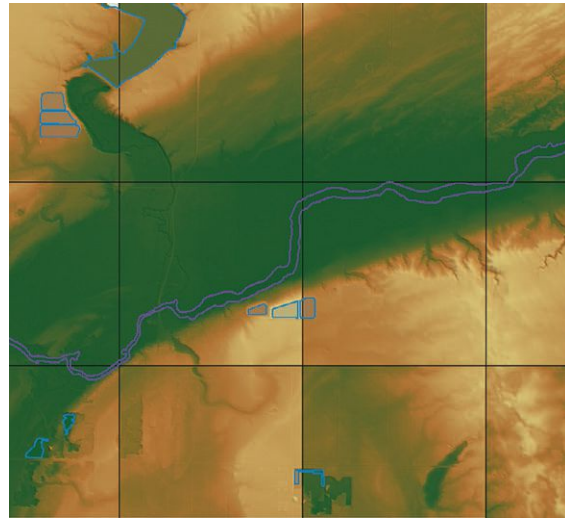
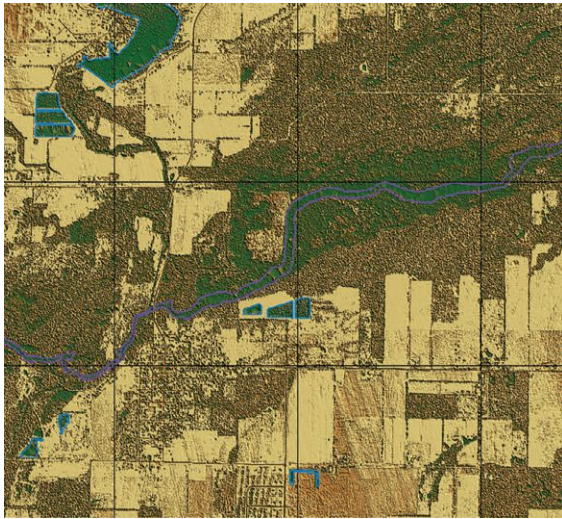


Figure 5. Breaklines for streams and waterbodies overlying intensity data on the left and hydro-flattened DEM data on the right. Note the TIN artifacts and data irregularities in the left-side image for areas within the breaklines and the smooth surface within the same areas in the right-side image. These forms of tests may be a typical part of the advanced visual checks performed on final data sets.

continued from page 1077

- Products, Documents, Reports, and Metadata:** There is a complex set of deliverable components in a lidar data project. Checksheets and methods are needed to compile a complete list of deliverable products and to verify them against requirements and specifications. Best practice methods are needed that might include a project data directory structure for data and derived information products, as well as a possible project documents, reports, and metadata repository to assure proper organization and delivery of final products.

Benefits: Standardizing the organization and delivery of components of project products will help assure consistent products that may be effectively tested against guidelines and specifications. Implementing streamlined capabilities that enable real-time testing of incremental products during the lidar project life cycle will ensure that post production tests of end products will meet product specifications and requirements and will help improve the accuracy and quality of lidar data and derived information products.

Focus Projects

Spatial Information Solutions (SIS) has compiled a collection of recently acquired sample lidar data sets from federal agencies as well as industry lidar data producers. In some cases, data were provided along with surveyed checkpoints which were used in the SIS software product, Topo Analyst, to verify accuracy and perform other quantitative and qualitative checks on the data sets. A brief description of the data sets, a view of the data and fundamental accuracy characteristics follow for a set of highlighted focus projects.

Channel Islands, California (USGS)

The USGS funded a lidar collection for the Channel Islands off the coast of California. The project presented challenges in terms of difficulty of access, lack of ability to establish ground survey base stations, and the rugged terrain and steep cliffs on the sides of the islands. These factors combined to add difficulties to aspects of data acquisition and processing. The lidar data were collected by helicopter and survey checkpoint locations were accessed by helicopter. As shown in figure 6, the fundamental vertical accuracy on this project was determined to be 5.8 cm.

Multi-County Project, Michigan (USGS)

A USGS-funded acquisition project collected lidar data for multiple counties in Michigan (Figure 7). This data collection illustrates what is becoming more of the norm for lidar acquisition projects in which data are collected for multiple counties and deliverables conform to specifications of the USGS and FEMA for elevation updates, map data enhancements, and flood plain mapping updates. Lidar was collected by a fixed-wing aerial platform. Data management and organization of data and derived products becomes more of a challenge with large projects, in this case comprising over 2,500 tiles of classified LAS data, DEM data, and other derived data products. Accuracy of the lidar point cloud data was determined to be .284 US Survey Feet (8.66 cm) at the 95% confidence level (FVA) and for the DEM to be .342 US Survey Feet (10.42 cm) at the 95% confidence level (FVA).

Texas DOT Demonstration Project (Industry Collaboration)

In a project aimed at highway transportation data acquisition for design and other applications, high-accuracy helicopter and terrestrial mobile lidar datasets were acquired for a segment of I-30 in Texas. Data were acquired to improve understanding of water accumulation of the interstate segment studied. Tuck Mapping flew helicopter lidar and other project partners collected terrestrial mobile lidar datasets. The lidar collected by Tuck Mapping (Figure 8) was found to have an RMSE Z of 0.039 US Survey Feet (1.19 cm) and a FVA 95% confidence level accuracy of 0.076 US Survey Feet (2.32 cm).

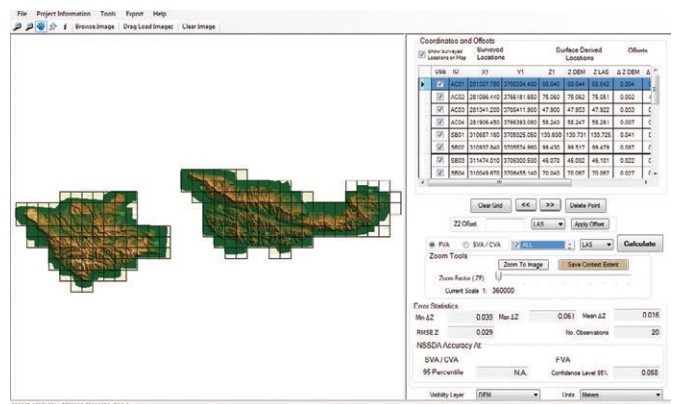


Figure 6. View of Channel Islands elevation data and absolute accuracy verification testing of LAS data by Fundamental Vertical Accuracy for quantifying accuracy to the 95 percent confidence level.

Mississippi River Alluvial Floodplain, Mississippi – The Delta (USACE)

The U.S. Army Corps of Engineers has been leading the way in developing lidar data for areas of need for flood protection, levee management, and flood control structures, as well as coastal areas within their jurisdiction. The Corps also leads the way in developing lidar technologies for advanced data acquisition. The Vicksburg District Corps acquired lidar data and updated ortho photos for the area commonly called “The Delta”. This area is the Mississippi River Alluvial Floodplain in the state of Mississippi and is an area of both historical and recent severe flooding. The area covers many counties in Mississippi and the lidar dataset required over 11,000 tiles (at 5000 × 5000 feet per tile) to cover the project area. The broad geographic extent of the Delta (Figure 9), the mostly flat-lying terrain, and the complex nature of the stream networks, waterbodies, oxbow lakes, levees, and flood control structures created challenges in data collection and processing. Projects such as this lidar project for “The Delta” will provide data and derived products of unprecedented accuracy and quality that will strengthen capabilities to plan infrastructure and to help protect our nation’s resources and population from the potentially disastrous impacts of flooding and other natural disasters.

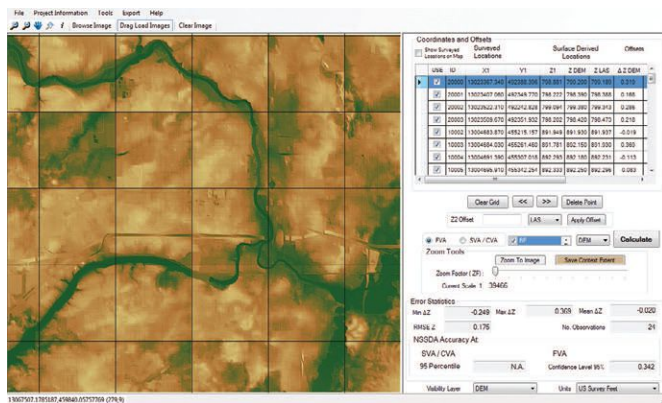


Figure 7. View of Michigan project elevation data and absolute accuracy verification testing of LAS as well as DEM data by Fundamental Vertical Accuracy for quantifying accuracy to the 95 percent confidence level.

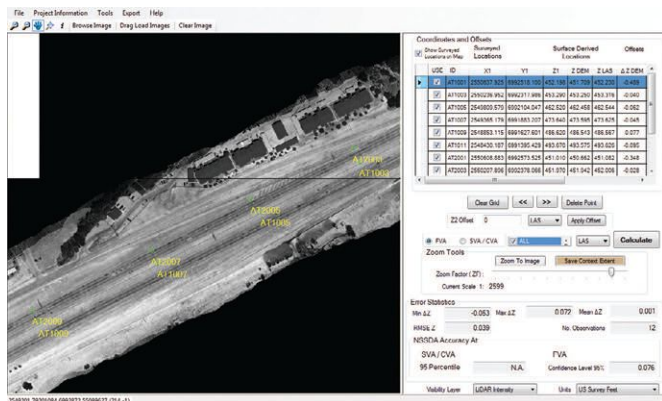


Figure 8. View of Tuck Mapping DOT demonstration project elevation data and absolute accuracy verification testing of LAS data by Fundamental Vertical Accuracy for quantifying accuracy to the 95 percent confidence level.

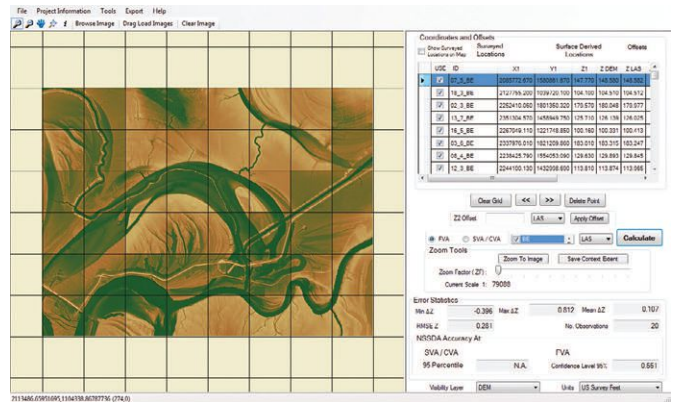


Figure 9. View of elevation data and absolute accuracy verification testing of LAS data by Fundamental Vertical Accuracy for quantifying accuracy to the 95 percent confidence level.

Conclusions

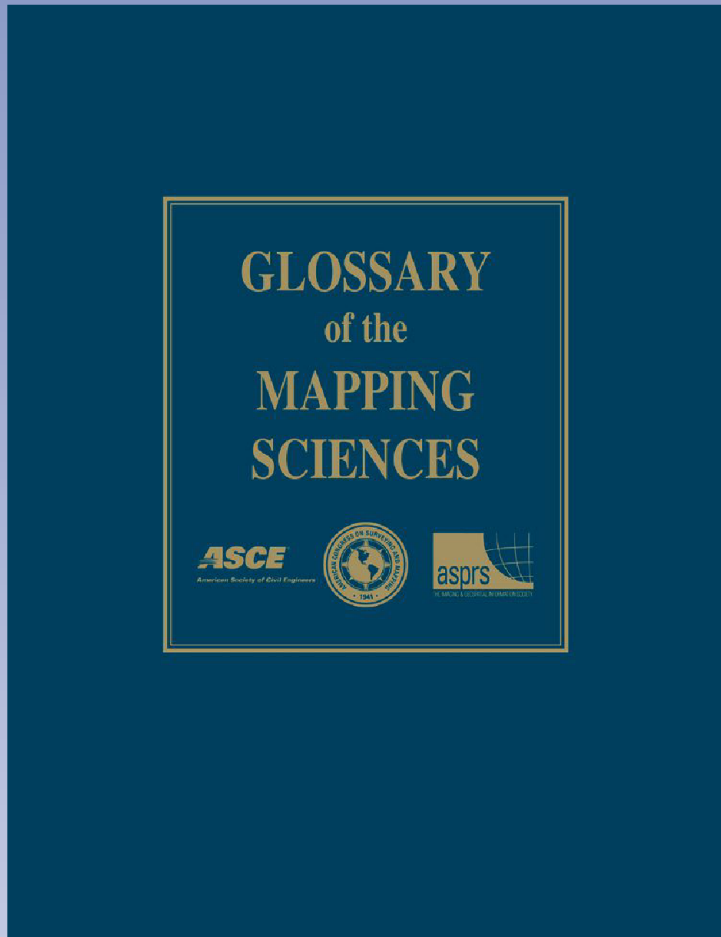
New lidar guidelines and specifications imply that incremental products must be verified to ensure the accuracy, quality, compliance, and completeness of final products. The implication of incremental product verification makes apparent the need for a set of best practices, not just for verifying final products, but for verifying products developed across the lidar project life cycle. Incremental product verification and best practices introduce an opportunity to transform industry practices for delivery and acceptance of products. Key to the transformation of industry practices would be the definition of specific interim deliverables defined as project milestones as well as best practices and mechanisms for engaging the producer and customer in “real time” verification of incremental products as data flow through the project.

Acceptance of incremental products opens the door to partial payment of project fees for partial completion of project deliverables. This transformation would improve project and product visibility and management capabilities for customers while improving data producers’ capabilities to improve cash flow during lengthy and cost-intensive lidar projects at the expense of verifying and delivering incremental products. The sum of these factors should have the cumulative effects of improving projects and products, providing a consistent set of best practices, and advancing industry and mapping community practices; ultimately leading to improvement in lidar data and derived mapping product quality, accuracy, and cost-benefits.

Author

Charles O'Hara, *Spatial Information Solution, Inc.*
Spatial Information Solution, Inc. (SIS) was formed as a spin-out from Mississippi State University with a focus on the commercialization of software technologies for map data accuracy and quality verification. Accuracy Analyst and Topo Analyst are an automated QA software solution for orthophoto verification and a software solution for automated accuracy verification and quality assurance of elevation data respectively.
coghara@spatialis.com
<http://www.spatialis.com/>

ASPRS, ACSM & ASCE present
Glossary of the Mapping Sciences



Everything you need to know about the mapping science from A to Z. The Glossary contains more than **11,000 definitions** that encompass every aspect of the mapping sciences. Definitions are included in the areas of **Photogrammetry, Remote Sensing, Cartography, Mapping, Land Surveying, Construction Surveying, Engineering Surveying, Geodesy, Hydrography, LIS/ GIS/LIM, Surveying Law, and Metrology.**



Member price: \$35
Non-member price: \$50
Student Member Price: \$25

Co-published by ASPRS, ACSM
and ASCE, 1994
Paperback, 576 pages
ISBN: 1-57083-011-8
Stock #5021

ORDER ONLINE NOW AT

<http://asprs.org/Publications-Other/Bookstore.html>

ASPRS TEN-YEAR REMOTE SENSING INDUSTRY FORECAST Phase VI

Mr. Charles Mondello, Chair ASPRS Ten-Year Remote Sensing Industry Forecast, *Pictometry International*

Dr. George Hepner, Co-Chair ASPRS Ten-Year Remote Sensing Industry Forecast, *University of Utah*

Ms. Stephanie Boerman, Team Member ASPRS Ten-Year Remote Sensing Industry Forecast, *Pictometry International*

<http://www.asprs.org/Forecast>

Executive Summary

The ASPRS Ten-Year Remote Sensing Industry Forecast began in 1999 with the goal of providing the remote sensing-based geospatial industry with an iterative, phased snapshot of key qualitative and quantitative metrics over time. The primary intent of Phase VI of the Forecast is to provide additional information about the industry in response to questions elicited by the results of the first five phases. In particular, Phase VI extended its inquiries into the areas of workforce issues, technology trends, information needs by users, and trends in U.S. leadership in the geospatial industry. Phase VI of the ASPRS Ten-Year Remote Sensing Industry Forecast developed a two prong approach to information gathering on the current issues of the industry. This approach consists of a Gross Revenue Survey (GRS) of private sector firms and an internet survey of individual members. This report summarizes the results and conclusions of these two separate, but complimentary data collection components. The Executive Summary of this report will address both the GRS and the internet survey results and conclusions. The specific methodology and results

of each of the information components will be described in detail in later sections.

The GRS component is a confidential, direct survey of industry private sector firms, including the Sustaining Members of ASPRS. This survey of revenues and business practices was done to complement a similar survey done in earlier phases of the Forecast to provide a financial snapshot of the industry. The GRS was sent to specific high level executives during April–May, 2011. Fifteen percent of those firms contacted, completed the survey in this period. Reported gross revenues of the respondent firms ranged from \$0.5M to over \$300M; total firm employee levels ranged from less than 10 to nearly 500. Given the general distribution of the responses, it is believed they represent a reasonable source of private sector information.

The internet survey of individual ASPRS members was launched between September, 2010 and November, 2010 to the approximately 6,000 members of ASPRS, which has nearly equal representation from the government, private sector and aca-

demia. Members were sent reminder email requests to complete the survey three times throughout this period. Approximately 450 ASPRS members responded to the internet survey, about seven percent (7%) of the target population. Based on self-identified job titles and salary ranges, most of the respondents to the Phase VI survey are in mid-level and upper management positions in all employment sectors.

Because of the limited nature of these surveys, the results cannot be used to definitively predict future trends, but rather to provide information and insights that can be used by industry, academia, and government in hiring, education and training, and policy making.

Industry Size and Growth

Total 2010 gross revenues for the remote sensing related portion of the geospatial industry are estimated at \$7.039 Billion (Figure 1). This estimate is made using actual revenues reported during the Gross Revenue Survey of Phase VI. A comparison of the Phase VI data with projections de-

continued on page 1082

veloped during Phases I–III of the Forecast (2001–2002) highlight a strong consistency in the rates of projected growth when comparing those from the 2001–2002 period with the 2010–2011 period. While the years 2011–2022 are projected using only the predicted growth levels provided by industry respondents in the most recent survey, the high level of consistency between the original projections and the latest data gives a high degree of confidence in the projections for the future. History would indicate the latest projections for the period 2011–2012 may actually be conservative.

Workforce Issues and Implications

Findings in Phase VI related to educational and workforce issues indicate that the industry has ample room for workers to enhance their employability by improving their geospatial educational level, especially with GIS applications that incorporate remote sensing. The GRS private firm respondents indicated that 34% anticipated they would have problems hiring qualified workers in the U.S. Sixty-six percent did not anticipate problems finding qualified employees. The internet survey results indicate that the educational community is not providing graduates with sufficient training in several skills, including geospatial applications tools, Lidar, photogrammetry, and verbal and writing skills. Spatial database understanding, Geodetic Science and Computer Programming were cited as important areas for future employees. The lack of sufficient verbal and written communication skills is a chronic problem faced by other industries as well, and corresponds with indications of a broad failing throughout all levels of the U.S. educational community.

The results suggest that U.S. academic institutions are attracting a large number of very qualified students from across the globe. In most cases, the students that can qualify to study in the U.S. are among the best students from a nation. This influx of foreign talent fosters improved graduate research in the U.S. system, and for those students who remain in the U.S. after graduation, an influx of talent into the geospatial industry.

An implication of these trends involves the basic research foundation of the geospatial industry. In an industry so linked to scientific and technological research and innovation, basic research is crucial to the future of the industry. Due to the nature of the geospatial industry in the U.S. (see Phase III–IV reports), a limited amount of basic geospatial research

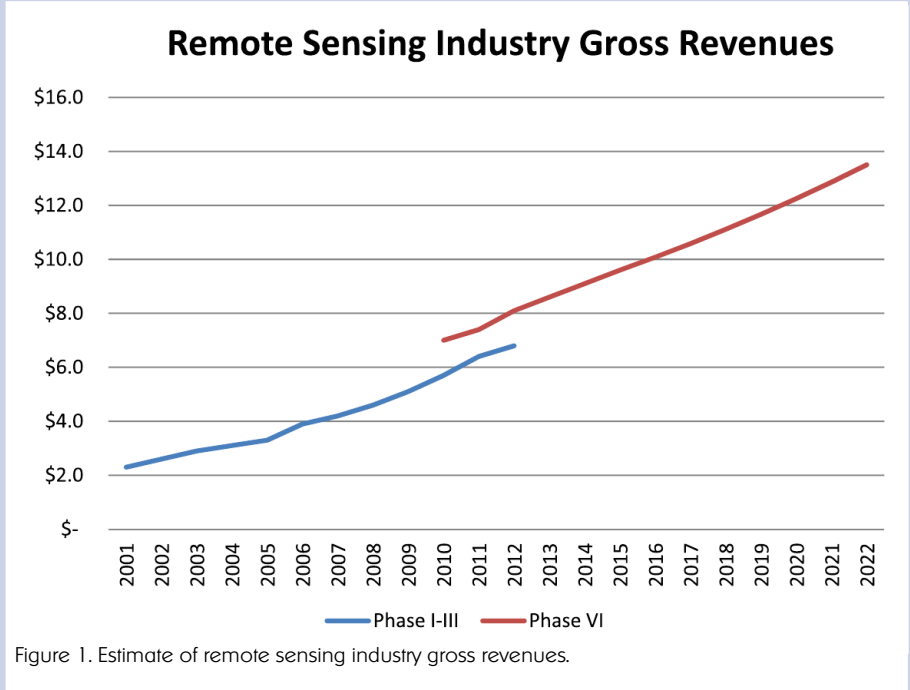


Figure 1. Estimate of remote sensing industry gross revenues.

is done in the government (especially the civilian area) and private sectors. The university academic sector is the primary basis of research and the source of researchers for the U.S. Thus, the longer term trend of increasing foreign-born graduate students will affect the foundation of geospatial research in the U.S. in ways that may conflict with immigration, national security and educational policies. This will affect the long term innovation and competitiveness of the industry in an increasingly international marketplace.

The hiring of employees who could obtain security clearances is a significant, but not critical issue. Most respondents reported limited problems in hiring employees who could be cleared.

Industry retention of trained employees is a major problem. Phase’s I–III found that many firms and agencies had a relatively high turnover of newer employees (less than five years). Responses to the Phase IV survey indicated that lack of advancement and adequate compensation are the two primary reasons for job dissatisfaction. Phase VI echoes the previous results regarding retention of employees. In the growing, competitive fields of high technology requiring skilled, educated employees, the remote sensing industry may not be providing sufficient compensation and advancement opportunities compared to other high technology opportunities to retain the needed workforce.

Further, with the exception of a few large Fortune 500 firms, the generally smaller size of geospatial firms compared to other high

technology fields may limit opportunities for advancement and the highest compensation. These results may also reflect the competition for trained civilian geospatial and remote sensing employees by the non-civilian contractor firms in the military and security arenas, which are not well sampled in Phases IV and VI.

International Issues

The issue of outsourcing of resources, primarily labor, for geospatial projects is a large economic and policy issue. Phase VI asked respondents to indicate whether more geospatial work is being performed or procured outside of the U.S. than 10 years ago. Respondents were asked to address two issues: 1) U.S.-based projects using foreign labor or 2) U.S. firms and agencies expanding into international markets. Definitely, respondents felt that more outsourcing of resources, including labor for U.S. projects was taking place. Many respondents to the internet survey indicated that the international market for U.S. firms was expanding as well. These results were bolstered by the GRS where the percent of business activities that are undertaken by U.S.-based organizations in non-U.S. or foreign areas was reported to be approximately 7.5% during 2010 and is projected to increase slightly to approximately 10% by 2020.

When governmental contracts are let, a mix of products and services may be requested in the request for proposal. These standardized product deliverables can be provided using international lower cost

labor. This process may cause further U.S. commercial provider consolidation, as well as, a U.S. skills shortfall.

Most of the respondents rated the U.S. as being equivalent to other nations in the majority of scientific/technology areas. A large number of respondents indicate that the U.S. is leading in key areas of Applications GIS Tools, Remote Sensing Tools, Hyperspectral, Consumer Mapping and Software as a Service, Lidar, Aerial and Satellite Data Capture, and Web Programming. They indicated that the U.S. was behind in Mathematics and Multi-lingual Skills.

The current skills advantage in the U.S. is a benefit to the U.S. domestic industry. Software development and consumer mapping may see future growth in offshore migration. This skills advantage, as yet, is not a large industry driver. Lidar technologies are a larger driver versus Hyperspectral, however offshore Lidar data processing is on the rise. Hyperspectral, which has shown promise in past Forecasts and fostered skills development in academia, has yet to have a large impact on our industry.

There has been a large change in the industry with the addition of consumer mapping and its associated technologies. The federal government is slow in its ability to release new “for the nation” programs. This fact, convolved with reductions in federal revenue base, is clearly affecting technology spending. This slowing of spending will directly affect the drive in new technology development.

Federal Government Policy

Governmental policy was not a primary focus of the Phase VI survey, but respondents have a generally favorable view of the role of government in the geospatial industry. Results indicate a change in the perception of government policy as being beneficial or neutral versus previous results indicating a more negative impact of government on the industry.

Government spending, while likely to decline in the future, is targeting basic programs driving sharing and leveraging data and processes. This is to some degree being supplanted by commercial firms using alternative methods of financial monetization. A future area of study should review the impacts of this change.

The ASPRS Forecast was initiated in 1999–

Purposes of the ASPRS Ten-Year Remote Sensing Industry Forecast 2000–2011

2000 to provide comprehensive data about the remote sensing geospatial industry, and reliable, unbiased assessments of the industry’s future. The remote sensing industry is viewed as those commercial firms, not-for-profit organizations, governmental agencies and academic institutions involved in the capture, production, distribution, and application of remotely sensed geospatial data and information. In recent years the complexion of the industry has changed from the remote sensing industry to a more integrated image-based geospatial industry (Figure 2). New advancements facilitate the application of remote sensing and geospatial science to many previously unrealized disciplines, from the sciences to a myriad of applications.

Phase VI of the ASPRS Ten-Year Remote Sensing Industry Forecast of the remote sensing and geospatial industry seeks to extend the results of the first five phases¹ and determine trends noted in the first phases. The Phase VI survey was extended explicitly to address questions of future workforce need and preparation, issues of employability of new entrants to the workforce and trends in the U.S. role in the geospatial science and technology community. Given the limited

nature of the survey, the results cannot be used to make explicit predictions, but do provide important information and indicate trends of interest.

In particular, ASPRS carried out the Phase VI survey in order to obtain current information and future expectations from a representative sample of the U.S. community regarding;

- “Use” of and “needs” for specific requirements in geospatial information
- Workforce hiring needs and requirements
- Role of U.S. in S&T trends
- The role of government policy in the geospatial industry
- Gross Revenue Trends in the geospatial remote sensing industry

These objectives formed the basis of a questionnaire that extended information gained from similar topics and questions in Phase I-V and questions designed to elicit new information. The initial portion of this report is description of the survey process and interpretation of the study sample. After this overview of results in selected areas, the responses for private and educational sector respondents are separated and discussed.

continued on page 1084

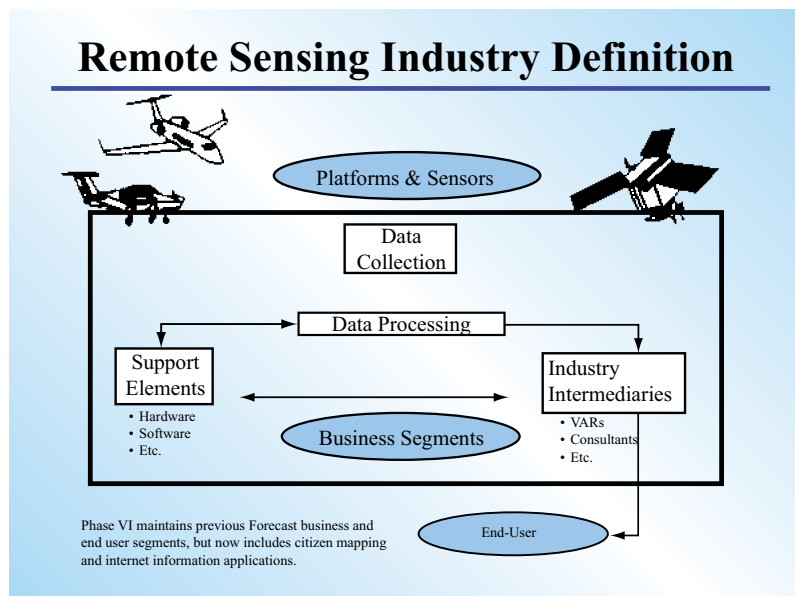


Figure 2. Business Segments and New Market Entrants for Phase VI.

1. Charles Mondello, George Hepner, and Ray A. Williamson, 2004. 10-Year industry forecast: phases I-III — Study documentation, *Photogrammetric Engineering and Remote Sensing*, 70(1):7–58.

Charles Mondello, George Hepner, and Ray A. Williamson, 2006. Ten year forecast of the U.S. remote sensing industry phase IV, *Photogrammetric Engineering and Remote Sensing*, 72(9):985–1000.

Charles Mondello, George Hepner, and Richard Medina, 2008. ASPRS Ten-year remote sensing industry forecast phase V, *Photogrammetric Engineering and Remote Sensing*, 74(11):1297–1306.

Two Components of Phase VI of the Forecast

The basis for Phase VI results and interpretations are an internet survey to individual members and a confidential, direct Gross Revenue Survey (GRS) of private sector, image-based geospatial firms. This approach is deemed the best to gather information and trends on issues across all employment sectors, as well as get a more detailed view of private sector activities.

Internet Survey of Individual Members

The internet-based survey was developed with input from the Phase VI sponsors, the U.S. Geological Survey (USGS) and the U.S. National Geospatial Intelligence Agency (NGA) in the summer, 2010. The survey was pretested on respondents from the three primary employment sectors in August, 2010. The survey was released in September, 2010 and closed to participation in November, 2010.

The internet survey was administered to the membership of ASPRS; approximately 6000 individuals, 86% of whom list the U.S.A as primary residence. Forty percent of the ASPRS members are employed in private sector, 20% Academic, 20% Government (all levels) and 20% list as other.

The membership of ASPRS represents the spectrum of geospatial information disciplines and interest areas with 31% being in the GIS technical division, 34% in the Remote Sensing division, 26% in Photogrammetry and 9% of the membership being in the Primary Data Acquisition and Professional Practice Divisions

The number of respondents to the internet survey varied depending on the individual question, but 420–450 complete and usable responses were obtained for most of the questions in the survey. Members were notified by email three times throughout this period with a request to complete the on-line survey. This response number amounts to slightly over 7% of the target population.

Gross Revenue Survey

The Gross Revenue Survey was a direct electronic and postal survey of the private sector firms only. The population of firms contacted to complete the survey was developed from the ASPRS Sustaining Members list supplemented by firms engaged in citizen-based commercial geospatial activities. Also, large technology and information firms participating in the geospatial arena were sent surveys.

In what discipline is your degree/certificate? Check all that apply.

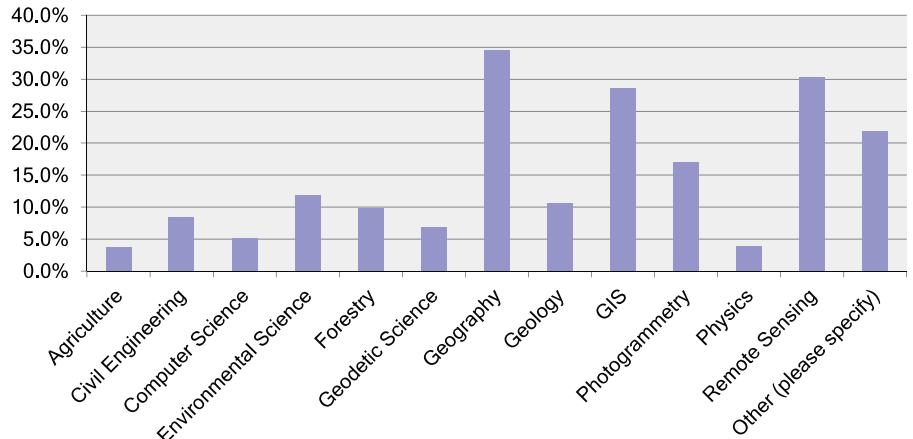


Figure 3. Educational degree areas of respondents

Each survey was posted and sent electronically to a specific high level management person in the firm. This person was contacted directly by email and phone as follow-up to help insure completion of the survey with the best information possible. The survey was conducted on behalf of ASPRS by the University of Utah Center for Public Policy and Administration (CPPA). Each firm was contacted by mail, telephone and through email in April-May, 2011. Recognizing the highly sensitive nature of the information being collected, all survey forms were returned to CPPA. CPPA removed all identifying information from the survey forms, which were provided to the Forecast Team for analysis.

Limitations on Interpretation

This report summarizes responses to the internet and confidential direct gross revenue survey. The report presents general trends occurring in the industry, not specific statistical information with confidence sufficient for prediction. Generally, the sample size for the internet survey has approximately a (±) 4.8 confidence interval at 95% confidence level. The sufficiency of the sample size issue is confounded by the inability to control properly for assumptions of sampling theory (random, unbiased samples) that would allow rigorous statistical procedures. The internet delivery of the survey does not allow rigorous sampling protocols as it depended on voluntary response from the respondent population. The GRS was targeted to the selected firms in the private sector with a 15% response rate. Both of these survey instruments primarily represent the trends and views of respondents from the civilian sector of the geospatial-remote sensing industry. Interpretations should be viewed with the survey limitations in mind. Although there was no means to randomize sampling within

the three employment sector stratifications, the results provide a useful stratification according to government, private and academic sectors.

Phase VI Internet Survey Results

The profile of the respondents to the Phase VI internet survey aligned with the ASPRS survey and the larger geospatial community in several ways. The respondent's primary employment sectors (Question 36) are 39% for the commercial-private sector; 28% for government at all levels; 30% in academic institutions, with 1-2% in both community college education and non-profit NGOs. This provides a representative basis for the analysis, approximately equaling the sector diversity of the ASPRS study population. More importantly, the results of the survey also represent the three primary employment sectors of the greater remote sensing community.

Approximately 34% of respondents have listed geography as one of their primary disciplines. This was followed by 30% in remote sensing, 28% in GIS and 23% "other", which includes numerous other disciplines from atmospheric science to urban planning (Figure 3). This result is consistent with the results in previous phases of the Forecast, where comprehensive academic programs in remote sensing and geospatial information are centered in geography departments, but employees in government and private sector achieve degrees in numerous other disciplines, as well.

Thirty-eight percent have master's degrees, 27% have a Ph.D., and 20% of the respondents have undergraduate degrees with approximately 10% having certificates, technical or two year college credentials.

Question 4 (Figure 4) asked respondents in

which sector of the industry do they primarily work. Most work in General Mapping (24%), with approximately 16% working in the National Security/Defense, Environmental and Civilian Government. Seventeen percent listed "other" as their primary sector.

As Figure 5 (Question 35) indicates, the majority of respondents have salaries greater than \$50,000 per year with 27% in the \$50,000-75,000 range, 35% in the \$75,000-\$150,000 range and 6% over \$150,000. Most of the respondents, 70% of the 440 who responded to Question 5, have eight years or more experience in the geospatial industry, with 36% having 20 or more years of experience. These values indicate the respondents are in the mid-level and upper management positions in the various employment sectors, which should be the group most informed and able to provide survey responses.

Workforce Issues: Need, Level of Education and Specializations

This section of the survey attempts to determine the level of demand for geospatial workers and the nature of the preparation necessary to fill future workforce demand. Question 49 asked whether their organization plans to replace employees in the next five years. Forty-five percent of the respondents indicate that their organization would be hiring in this time period. Twenty-five percent indicated no replacement hiring and 30% did not know.

The majority of the respondents (52%) indicate that the undergraduate degree is the preferred level of education for their workforce (Q 9 N=310). The master's degree was the second most preferred level of education at 21%. Technical training and certificates were listed as the preferred level by 12% and 6% of the respondents, respectively. Interestingly, only 2% of the respondents indicated that a Ph.D. is the preferred level of education. This certainly indicates support for higher education in geospatial workforce development, but not at the Ph.D. level. This may be an indicator of research funds slowing in a stagnant economy. Further study of this situation, together with a possible association with reduced research funding, is warranted.

Question 10 asked the respondents to rank the four most critical knowledge and skills needed by future employees. Figure 6 shows the response count of those areas listed as the four most critical. Applications GIS had the highest response count with

continued on page 1086

In which of the following Sectors and Sub-Sectors do you PRIMARILY work? (select one)

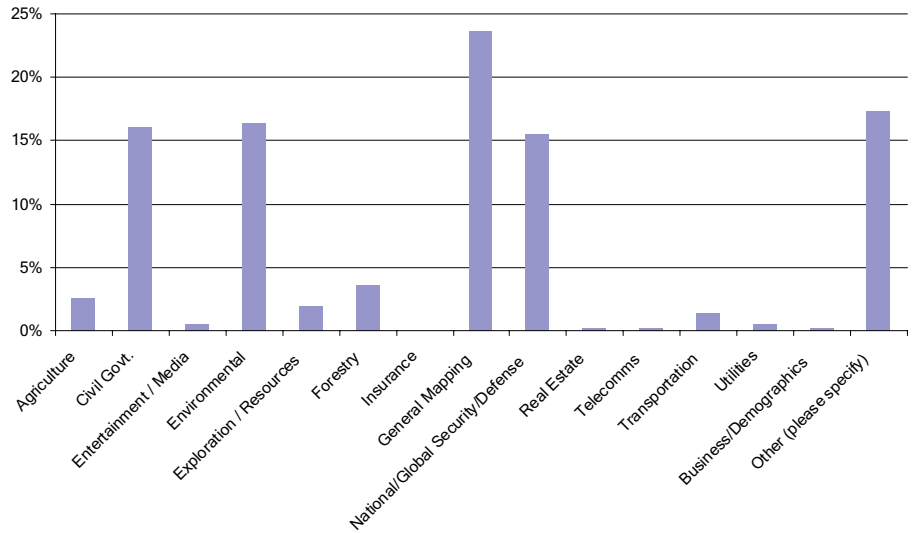


Figure 4. Primary sectors of respondent employment

What Is Your Annual Base Salary?

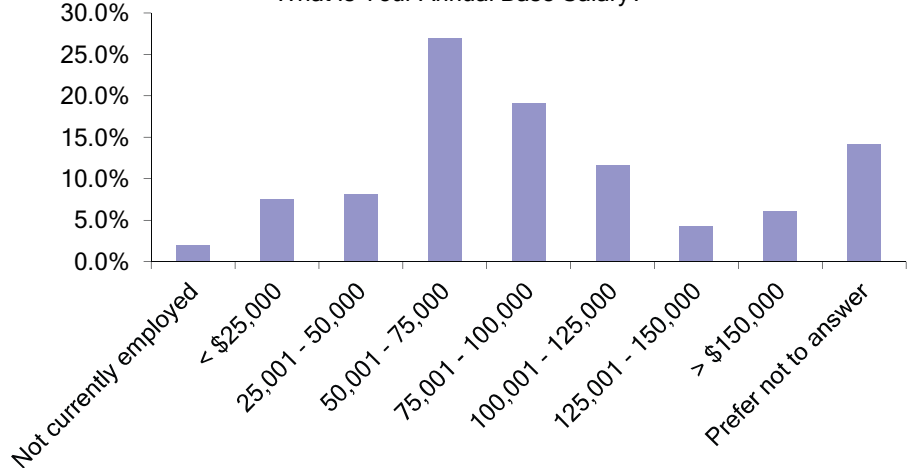


Figure 5. Base Salary for Respondents

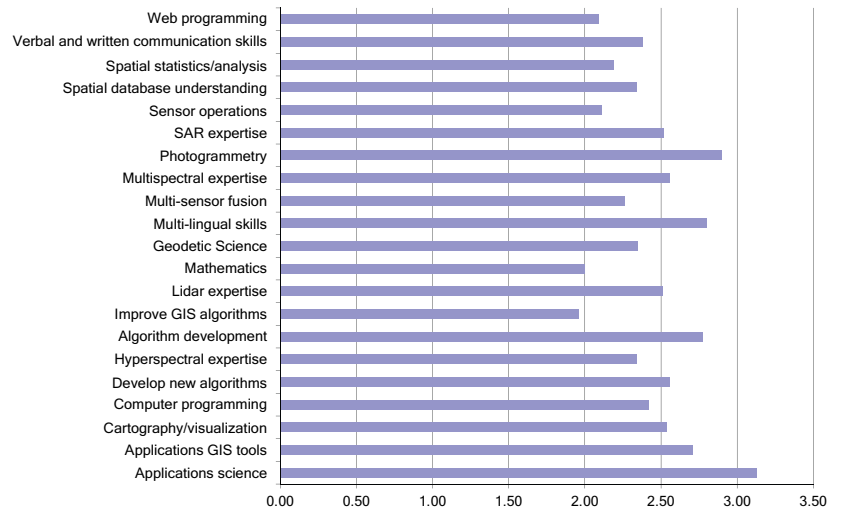


Figure 6. Most critical knowledge/skills needed by future employees

143 respondents listing it as one of the top four critical skills. Lidar, Photogrammetry and Communications Skills were ranked as the next three most critical.

In a related query to Question 10, Question 14 asked which areas of expertise were most difficult to recruit employees for over the last two years. The same four as in Question 10 were highest along with Spatial Database Understanding, Geodetic Science and Computer Programming.

Figure 7 shows that GIS, Lidar, Photogrammetry, Spatial Databases and Communications Skills are the areas that employers are finding most difficulty in recruiting employees. The Lidar, GIS and Spatial Databases are not too surprising given the great increase in civilian applications in recent years. Photogrammetry and Communication Skills are not a focus of our current educational preparation for students in geospatial areas.

Question 16 asked a similar type of question as a means of confirming future areas of knowledge between the responses to the two questions. Here the education segment can readily project its graduating class skills versus those needed by industry in the very near future. This match is critical to insure the domestic market doesn't experience a shortfall in skills.

The responses to Question 16 shown in Figure 8, when viewed with the responses to Question 10, reinforce the position that required skillsets will not change dramatically in the future. The primary areas are Remote Sensing Applications, GIS tools, Lidar, and Multispectral listed by greater than 40% of the respondents. Very closely behind, greater than 30% cited these areas as research /educational foci: Cartography Visualization, Multi-sensor Fusion, Photogrammetry, Spatial Database Understanding and Spatial Statistical Analysis. The single greatest difference in the response foci between Questions 10 and 16 was the cited need for Verbal and Written Communication skills. This highlights this need, but it was not reinforced in Question 16 responses due to the phrasing of Question 16.

The results provide knowledge of where the respondents believe the future lies for the industry. The important questions are whether the industry is developing the infrastructure to support these directions and whether the educational system is developing a workforce capable in these areas. It is critical for institutions of higher education to deliver work ready employees to the government and private sector.

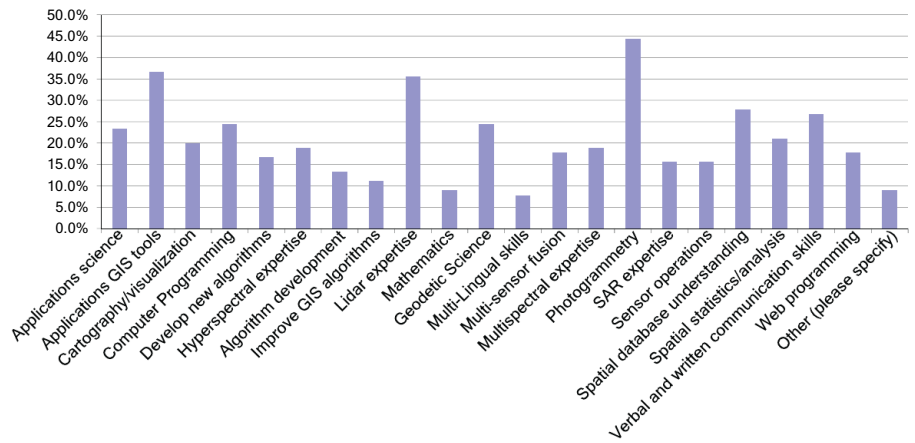


Figure 7. Area(s) of expertise for which employers experienced increased difficulty recruiting qualified applicants in the past two years.

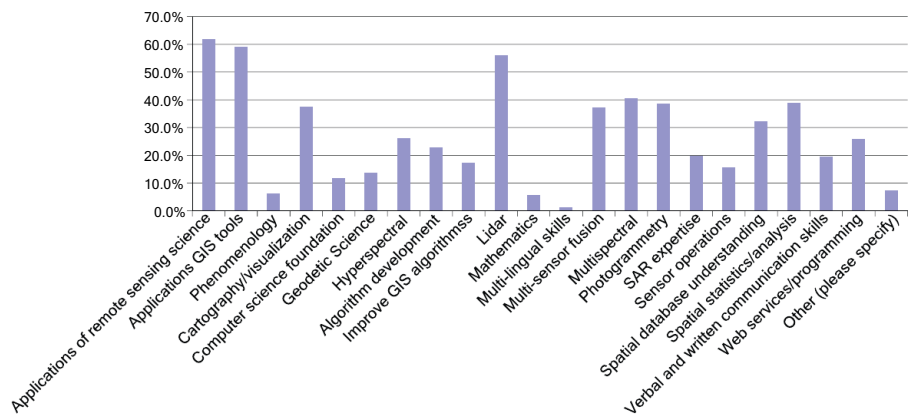


Figure 8. The technical focus areas of the respondents organization's educational and/or research programs in the remote sensing/geospatial areas for the next five years.

Security Clearances

The increased demand for employees who can be granted some form of a security clearance is a looming issue for most employers in the U.S. In Question 11, respondents were asked if their employer or contractors require governmental security clearances. With 297 responses, 54% indicated that clearances were needed and 40% responded that none were needed. On Question 12, 53% indicated that their employer or contractors do not have difficulty in recruiting individuals who can meet security clearance requirements (N=158). While the number of respondents is less, this result seems to counter the often heard perception from multiple government agencies and sponsors of the Forecast that employers cannot recruit sufficient numbers of employees who can meet clearance requirements, namely U.S. citizens with history and lifestyle matching the minimums needed for successful background testing. Twenty-two percent indicated that their employers did have problems. The primary reasons cited for

the difficulties are that the demand for skilled individuals who can qualify for clearances is so high, with several citing the need to pay new employees while the governmental clearance process is completed. Please recall that 39% of the respondents work in the private sector and 28% in government, with 16% in the Defense/National Security sector. Often a specific contract is required for contractors to begin the clearance process; if there are fewer of these the pool will continue to dwindle. The slowing in this sector may have a longer term effect on contractors and government entities abilities to hire cleared workers.

Workforce Retention Issues

Previous phases of the Forecast indicated that often professional/technical staff in agencies and firms leave the geospatial field within 5 years after initial employment. Phase VI asked for possible reasons for workforce departures. Question 15 asked, in an open ended format, for the three primary reasons why professional and technical staff leave

the geospatial field. Analysis of these 253 responses used a keyword search of the primary reported reasons for staff departures. The most often cited primary reason for departure (75) was related to compensation. The next most cited primary reason related to lack of career advancement opportunities (56). These responses are likely those of individuals who themselves have changed positions or those of management and coworkers familiar with staff who have changed.

Related comments were that compensation in other areas for employees with similar skills was higher than current job, lack of rewarding work and lack of job security. Phase VI results confirm the results of past surveys.

Technical Focus Areas

In the technologies associated with remote sensing and geospatial content, a limited number stand out as areas of focus (Figure 9). The Applications of Remote Sensing and GIS are seen as the most critical area of attention in the next five years. The goal of “solutions” carries the industry’s core technologies to new users. By developing end solutions in the integrated geospatial applications, customer solutions are provided with the integration of technologies and disparate geospatial datasets.

The second area standing out in technical interest is Lidar. With the number of systems now in operation and the drive toward end solutions Lidar provides many of the needed components for the final client solution set. These Lidar sets include not only cost effective elevation data, but new data, such as 3D, intensity data and phase content.

It is interesting to note that in previous Forecast Phases Hyperspectral and SAR were of higher technical weighting than in the Forecast Phase VI. Later sections in this document discussing data “used” versus “needed” quality; however, still show unmet content demand in these areas.

Most Important Geospatial Layers in Use

As Figure 10 indicates, Orthophoto, Elevation data, and Base Maps are the three primary data sets currently in use. These datasets provide the foundation of georeferencing, elevation and landscape features most needed for the majority of projects. As more attention is placed on end solutions, the importance of other layers should rise as content for new forms of decision support may be needed. These layers may play larger

What are the technical focus areas for your organization's educational and/or research programs in the remote sensing/geospatial areas for the next five years?
Please indicate all that apply.

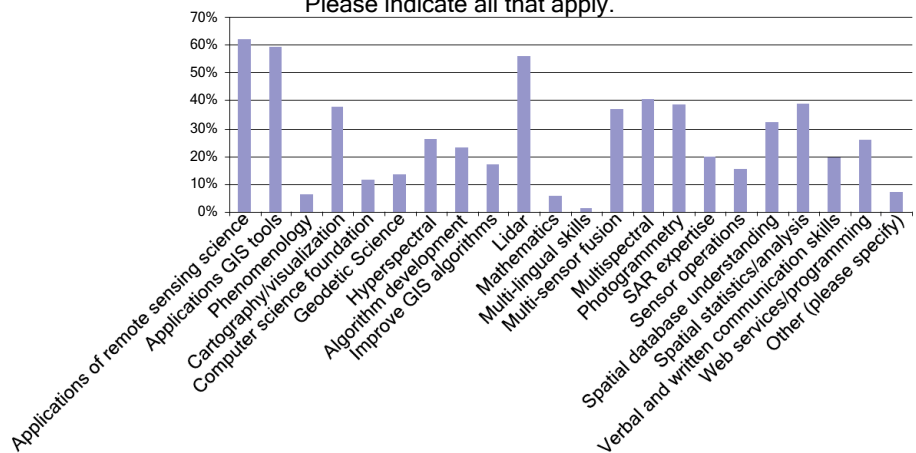


Figure 9. Technical focus areas for organization's education and research.

Which of the following are the three MOST important geospatial data layers that you currently use?

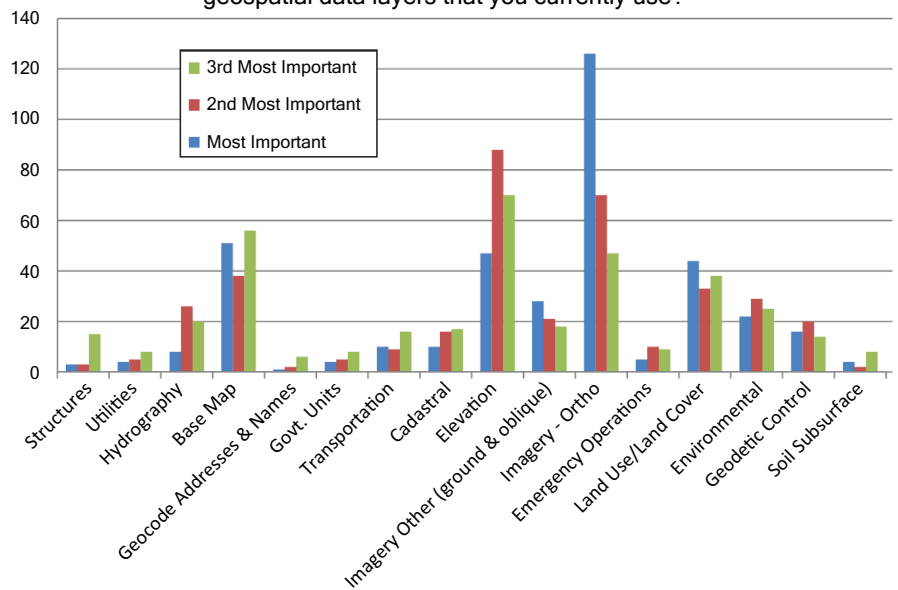


Figure 10. Three most important geospatial layers used.

roles, as unique solution sets will require additional dissimilar data from other sources.

Typical Remote Sensing Requirements

The importance of data characteristics reveals several interesting points (Figure 11). Spatial Resolution and Geolocation Accuracy are the two key metrics in Phase VI, and historically in past ASPRS Ten-Year Remote Sensing Industry Forecasts. However, the attention on Geolocation Accuracy would have led more to believe in a higher relative prioritization of the independent elevation layer. This answer shows that elevation as a component to the geolocation of an image data set is of far greater importance than as a separate layer. Elevation data is critical in positioning of an

image; however, the respondents to this survey did not consider the display of independent layers, such as contours, as critical as others to their general needs. For future studies a more detailed set of questions around Lidar data integration should be considered.

Additionally, since September 11, 2001 data currency has been a characteristic of importance in the past Forecast results. It appears now that either some of the need has been fulfilled or it has subsided in criticality.

Background on Data Characteristics: Data Used Today versus Data Needed in the Future

Figures 11–14 show responses on the relative importance of spatial resolution, geolocal, and elevation accuracy, image/

continued on page 1088

sensor types, primary and secondary data sets. The questions had two categories that the respondent could select from, “data used today”, and “data needed in the future”. The legend in each figure depicts the statistics between the two categories, and in example their respective cross category for image types: sensor technology , spatial resolution:GSD, or age of data: time, etcetera. These figures show the future need of each topic along with what is currently used today. Below, Figure 12 sensor type used today versus the future, is an example of how the use versus need series of questions are worded and formatted.

Data Characteristics: Spatial Resolution

The question on spatial resolution “needed” versus the data “used” reflects the continued demand for high-resolution data domestically (Figure 10). A greater separation exists between “used” versus “needed” in Phase VI compared to past phases.

The overall trends in the remaining spatial resolution data are similar to past studies. Phase V, while being international in scope, shows similar trends in resolution issues to Phase VI. Digital aerial sensors, as well as continued operation of high-resolution satellite systems, are meeting the domestic demand for better than half-meter resolution (Figure 13). A proliferation of new camera vendors has evolved developing low cost high resolution data capture in medium format sensors. These devices are now becoming certified by mapping agencies to validate systems attributes. By doing so, more vendors may enter the mapping market providing new capacity at lower cost. An overall trend versus past surveys shows that as digital imaging sensors continue to evolve, demand for better resolution follows.

Data Characteristics: Geospatial & Vertical Accuracy

As with past industry surveys the best quality geospatial locational accuracy data as an end deliverable is in high demand (Figure 14). The respondents indicate that a greater separation exists in Phase VI at the highest quality levels compared to past studies. This separation likely matches the demand at higher imaging spatial resolution. Technologies fulfilling this demand are growing with automated aero-triangulation, Lidar, and direct georegistration. Each of these technologies drives improvement in data overall. Most imaging

For your typical remote sensing requirements, please rank the following characteristics, from most important (1) to the least important (4).

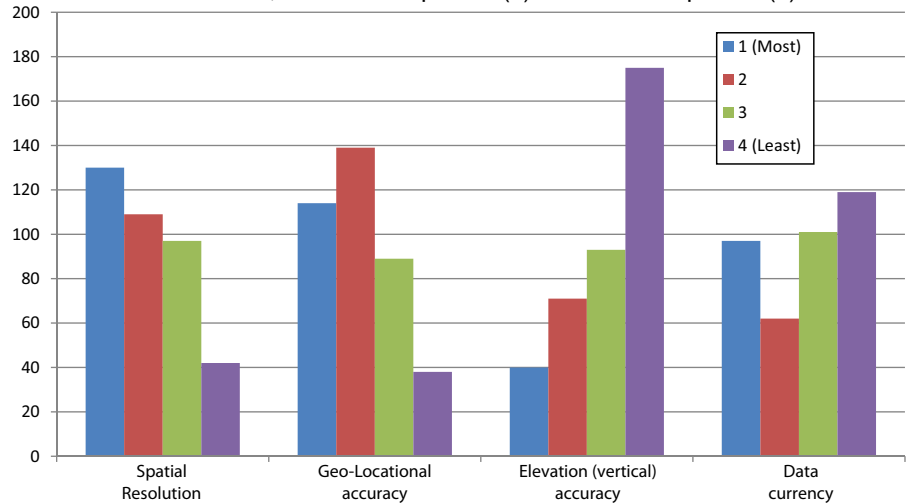


Figure 11. Most and least important remote sensing characteristics.

What image/sensor types do you currently WORK WITH today? What image types do you NEED most to do your job? (Could be the same - check all that apply)

Answer Options	Data Used Today	Data Needed in the Future	Response Count
Digitally captured B/W or Panchromatic	190	140	200
Digitally captured Color	263	211	282
Digitally captured IR	207	190	236
Pan Film analog captured	68	29	71
Color Film analog captured	96	37	96
Color IR Film analog captured	65	26	69
Lidar	220	243	292
SAR/IFSAR/INSAR	101	139	161
Multispectral	225	209	261
Hyperspectral	94	193	211
	answered question	371	371
	skipped question	79	79

Figure 12. Current use versus future need sample question.

What levels of Spatial Resolution do you currently WORK WITH today? What levels of Spatial Resolution do you NEED most to do your job? (Could be the same - check all that apply)

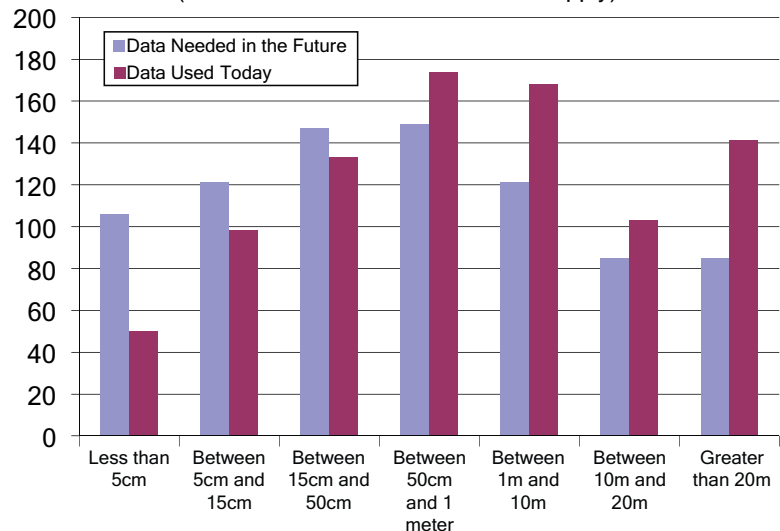


Figure 13. Spatial resolution use versus need

What levels of geo-locational accuracy do you currently WORK WITH today? What levels of geo-locational (horizontal) accuracy do you NEED most to do your job? (Could be the same - check all that apply)

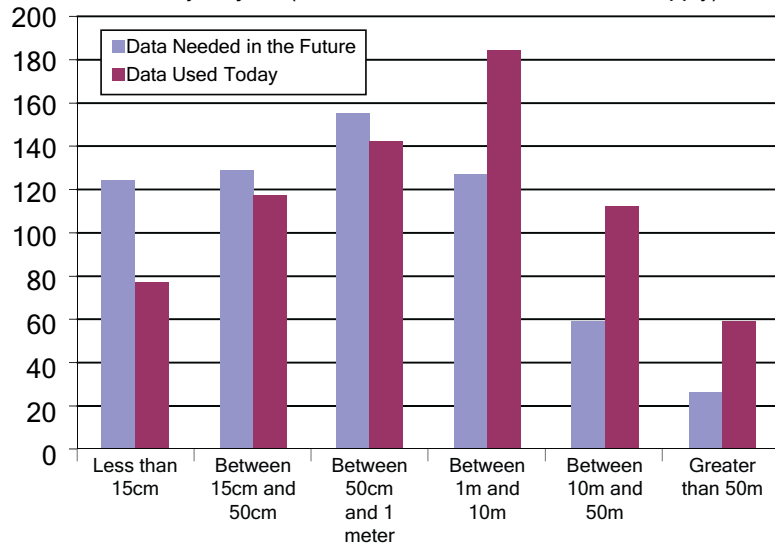


Figure 14. Geo-locational accuracy use versus need.

What levels of elevation (vertical) accuracy do you currently WORK WITH today? What levels of elevation (vertical) accuracy do you NEED most to do your job? (Could be the same - check all that apply)

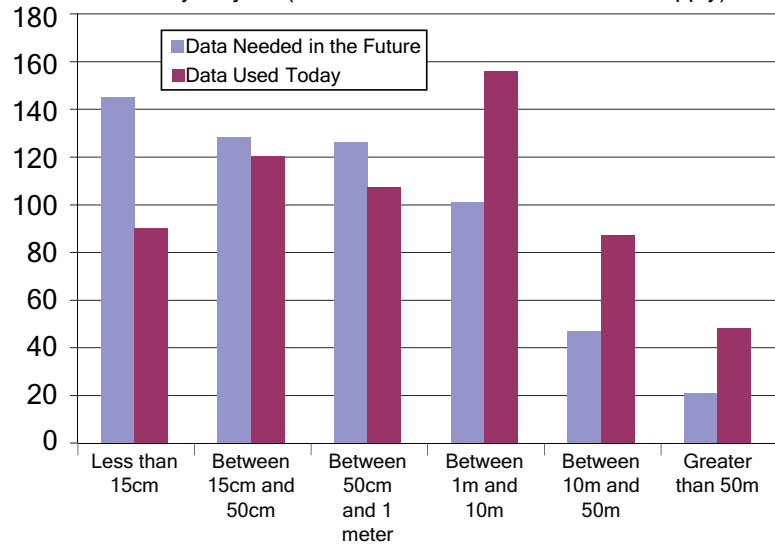


Figure 15. Elevation accuracy use versus need.

sensors with superior resolution and dynamic range require timely and current positional data to complete their data geo-registration process. Ground sample distances (GSD) of 4" and better are becoming more common. This offers users the ability to focus on smaller and smaller targets, each requiring better positional data for production. This is apparently continuing to drive this circular spiral between enhanced components and the increased demand for quality.

Vertical accuracy source data drives overall quality in many imaging systems that are classified as DEM-limited in performance

(Figure 15). The greatest error source in pixel placement for these systems is that associated with the source elevation data. Phase VI of the Forecast shows that technology has closed the previous gap in elevation data supply versus demand at the 15–50 cm level. The best levels of performance still show unmet demand, the overall match in “used” versus “needed” indicates a greater shortfall than in previous studies. The adoption of automated elevation extraction and Lidar still shows strong potential.

The industry continues its utilization of technologies comparable to those of previ-

ous ASPRS surveys. Film based image acquisition, which has shown a steady decline since the inception of the Forecast, appears to have leveled (Figure 16). Phase VI confirms this in comparison with the current U.S. versus International comparison involving Phase V. Phase VI responses continues to track with that of film versus digital transition in consumer and professional imaging markets. Phase VI reaffirms the excess capacity of digital imaging sensors versus industry need first seen in Phase IV, here we note the trend continues in “need” lower than “use”. While not a study, question reviewers familiar with the sales of data in the profession may note that imaging contract pricing has dropped in conjunction with vendor consolidation, from the author’s perspective, this drop in prices is a further indication of possible overcapacity. Hyperspectral, IFSAR, and Lidar appear to still outpace industry demand. Of these, Hyperspectral has the largest difference of future need compared to current use.

Data Characteristics: Currency

While resolution, accuracy and sensor type define the technologies employed, currency defines a critical component of the service aspect of the geospatial industry. The demand for “current” data is slightly increased over past studies (Figure 17). The only other change noted is at “under one year old” historically “used” exceeded “needed”, now parity exists. This appears to be addressed through commercial vendors who now have multiple online data access portals with optimal price points for new versus archival data.

Historically as data ages to greater than one year, its overall demand significantly decreases for many applications. This is an interesting area for future focus as the increasing amount of data hosted online increases the opportunity for change detection. As this capability becomes automated, it will further drive demand for historical content. This is already occurring in consumer online mapping sites where historic content is being merged with current collection data.

Data Characteristics: Air versus Space

The International Phase V study found that the ratio of aerial versus satellite data used varied on a regional basis; the pattern showed satellite data is utilized more in the developing regions of the world. Aerial and satellite data perform unique tasks in mapping, visualization, detailed target assessment, remote area

continued on page 1090

access, and multi-spectral content evaluation. Phase VI results indicate noteworthy changes in the 2010–2011 timeframe.

Since the survey began a series of data conclusions can be drawn:

- High-resolution satellites have proven themselves as commercially viable now in multiple generations of systems
- Consolidation has occurred both in air- and space-based data vendors
- The proportional use of satellite data has stabilized
- Respondents could chose more than one source for data capture

Figure 18 shows the relative weighting of aerial imagery having a slight edge in usage. Clearly, ground based data capture is growing. While not specified in the responses, it is presumed these are position orientation-based mobile systems versus stationary close range photogrammetric devices. This presumption is based on an increase in the number of industry announcements in product development and service requests in mobile mapping; while not specifically asked in this study, it is an area for future study.

Governmental Policy on Geospatial Industry

When asked whether various levels of government affect and impact the geospatial industry, the majority of respondents indicated that the federal government has the most effect. It is a positive one on the industry (Figure 19). Again, with the largest response group being from the private sector, the indication that government has a positive impact is an interesting result. Only a handful of years have passed since survey respondents considered government regulations burdensome. This turn in opinion is a good indicator that the federal government has responded to concerns in the profession and the industry.

International Linkages in the Geospatial Market

The issue of outsourcing of resources, primarily labor, for geospatial projects is an economic and policy issue. Our survey asked respondents to indicate whether more geospatial work is being performed or procured outside of the U.S. than 10 years ago. This question has three interpretations, 1) U.S.-based projects using foreign labor, 2) U.S. firms and agencies expanding into international markets, or 3) it could mean that more geospatial work is being done by other

What image/sensor types do you currently WORK WITH today?
What image types do you NEED most to do your job?
(Could be the same - check all that apply)

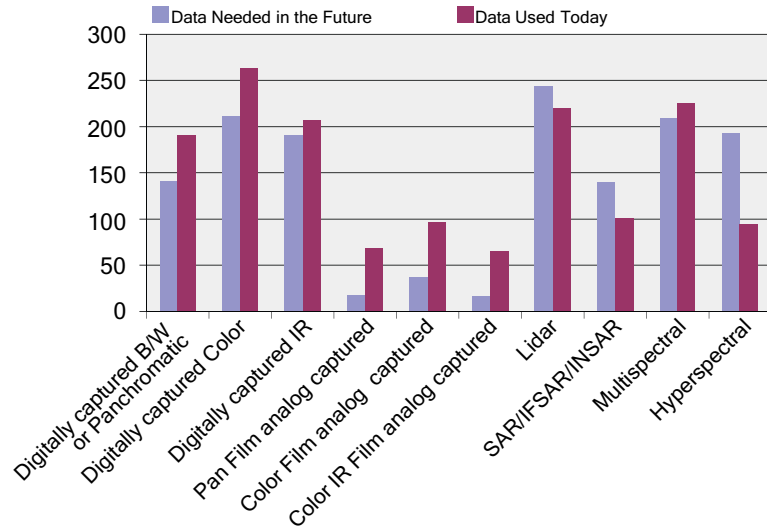


Figure 16. Image sensor types use versus need

How current are the PRIMARY data sets that you WORK WITH?
How current do you NEED your data to be?

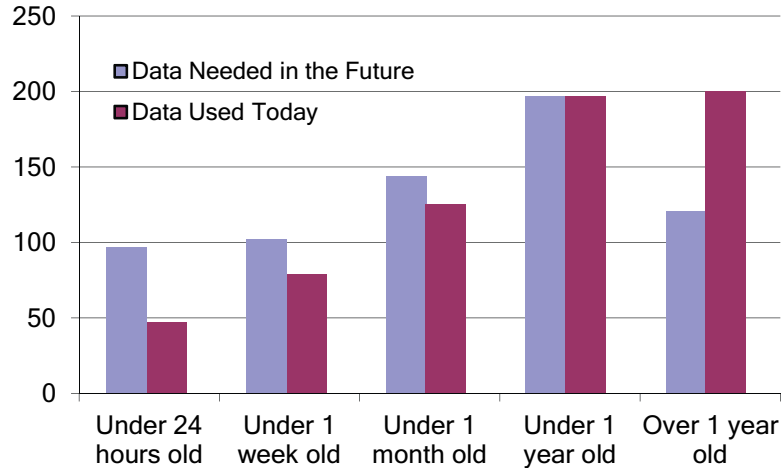


Figure 17. Primary data currency use versus need.

What portion of your remote sensing data/information is collected by aerial platforms versus space-based collection?

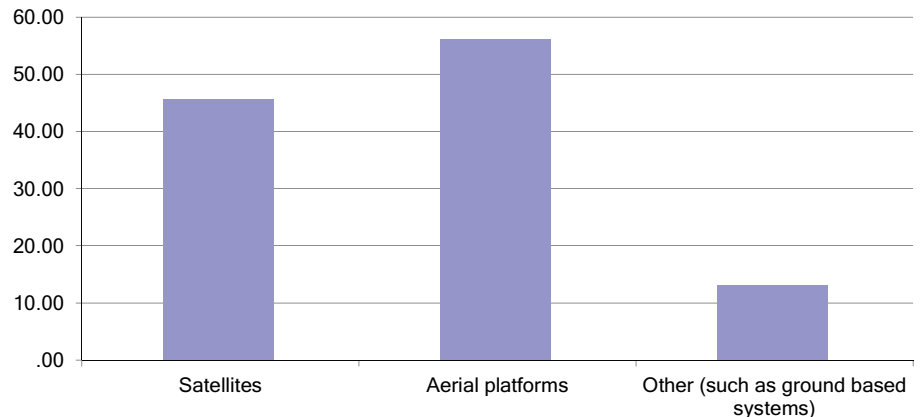


Figure 18. Relative weighting air, space and other data/information

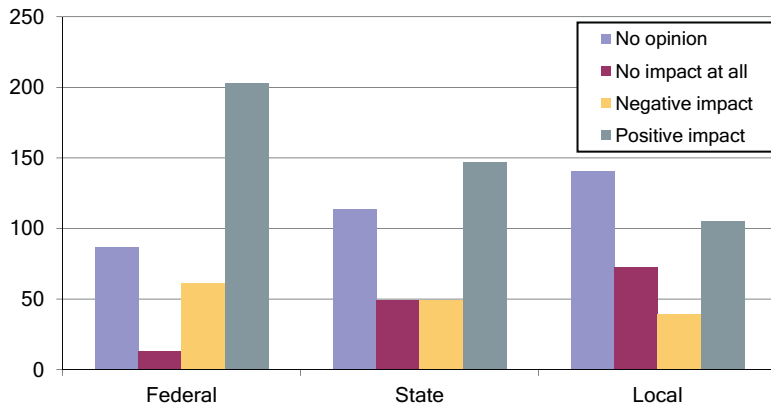


Figure 19. Do government policies affect the U.S. geospatial industry?

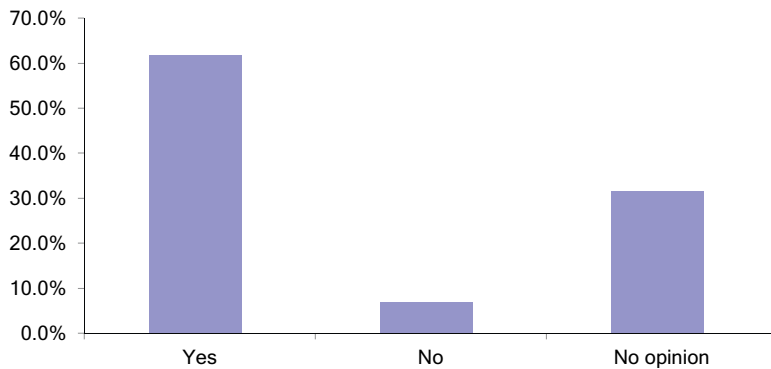


Figure 20. Do you find geospatial work being performed or procured more frequently outside of the U.S. now than 10 years ago?

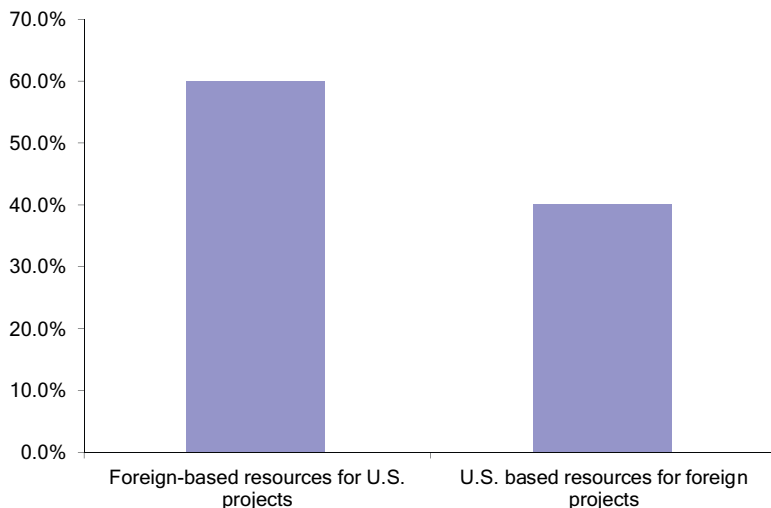


Figure 21. Respondents were asked to specify the relationship of the foreign linkages

nations for their own purposes. Assuming these interpretations, the clear outcome is that international relationships are an increasing part of the geospatial marketplace (Figure 20).

Among the respondents to the specific source and direction of resources for either U.S. or foreign projects, 60% indicated that foreign resources were being sourced to perform projects in the U.S. (Figure 21). As

an indication of the inverse trend, 40% of the respondents indicated that foreign projects were using U.S.-based resources. The assumption is that the respondents are referring to their firm's or agency's project work. When only the private sector respondents (N=83) are separated from the sample, over 71% of the respondents indicated that foreign based resources were being used in U.S. projects.

Leadership of the U.S. in the Geospatial Industry

The U.S. has been the world leader in the development of science and technology for aerial and satellite remote sensing and geographic information systems. The survey asked whether the U.S. is leading, equivalent or behind other nations' capabilities in several key geospatial arenas (Figure 19).

Most of the respondents rated the U.S. as being equivalent to other nations in the majority of areas (Figure 22). A large number of respondents indicate that the U.S. is leading in key areas of Applications GIS Tools, Remote Sensing Tools, Hyperspectral, Consumer Mapping and Software as a Service, Lidar, Aerial and Satellite Data Capture, and Web Programming. They indicated that the U.S. was behind in Mathematics and Multi-lingual Skills. The implication is that the U.S. firms and agencies will not have the workforce educated in mathematics to foster the advancement of geospatial science in the future, and the U.S. lacks language abilities to advance the industry to take advantage of foreign science advancements and foreign markets.

Academic/Educational Workforce Concerns

This section describes the sample stratified to be only those respondents in the academic/educational sector. The total number who identified themselves as academic in Question 36 is 105. Approximately 35 of these respondents were students and 70 were professors, research staff and academic managers.

Question 42 asked the approximate percentage of foreign students in various geospatial programs (Figure 23). The academic respondents indicated that 29% of their master's and Ph.D. students are foreign, 9% of their undergraduates are foreign and 12% of their certificate program students are foreign. Given the relatively small number of geospatial academic programs across the U.S., this sample, most of which were from different institutions, indicates that approximately 40% of students in these undergraduate and graduate programs are foreign.

Figure 24 indicates that the estimate from the academic respondents is that the number of foreign students in their programs is increasing. With the relaxation of some of the restrictions on foreign student visa allocation enforced after the 9/11 attacks, this estimate corresponds to the increased number of foreign students studying in the U.S. (Open Doors 2009, published by the Institute

continued on page 1092

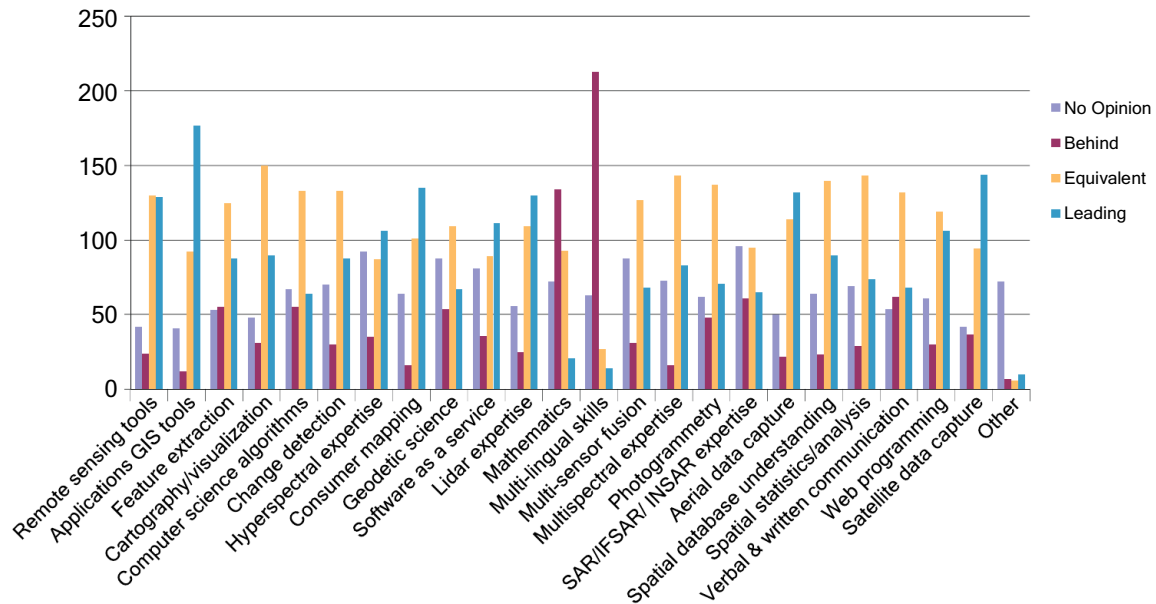


Figure 22. Rate each of the following areas in terms of whether the U.S. is leading, equivalent or behind other nations' capabilities.

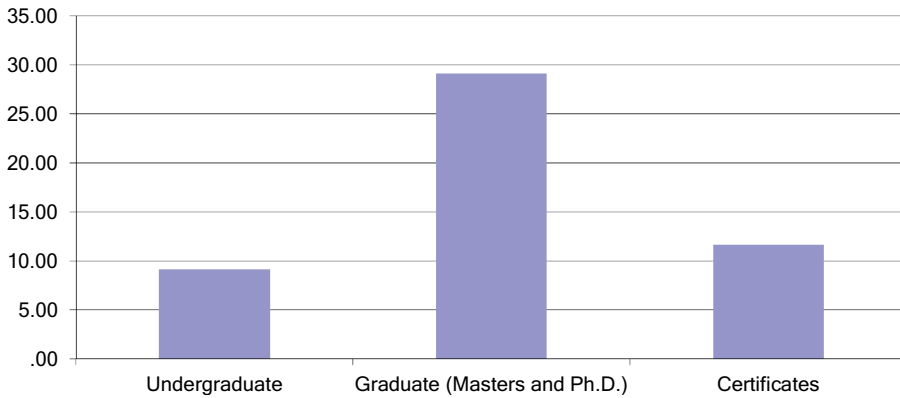


Figure 23. Estimate of the percentage of foreign students in your academic geospatial programs.

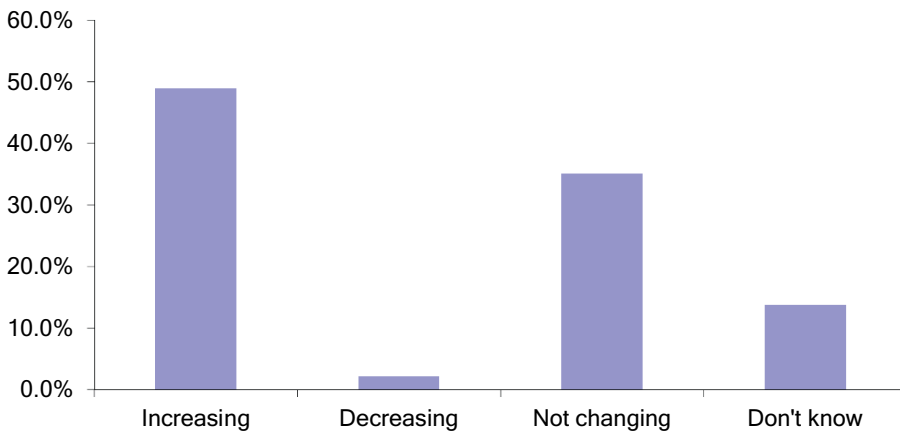


Figure 24. Estimate of the trend of foreign student enrollment in your academic geospatial programs

continued from page 1091

of International Education (IIE) with funding from the U.S. Department of State's Bureau of Educational and Cultural Affairs).

Question 43 asks academic respondents to estimate whether their foreign graduates will remain in the U.S. to work after graduation. Figure 25 shows the collective estimate

is that over 50% of the students will remain in the U.S.

The results from Questions 41–43, suggest that U.S. academic institutions are attracting a large number of very qualified students from across the globe. In most cases, the students that can qualify to study in the U.S.

are among the best students from a nation. This influx of foreign talent fosters improved graduate research in the U.S. system, and for those students who remain in the U.S. after graduation, an influx of talent into the geospatial industry.

A less apparent insight into the fact that such a relatively high percentage of graduate students are foreign is that other nations have a much more robust undergraduate system in geospatial related fields, such as geography, geodetic science and computer technology. Thus, there are many foreign students applying for U.S. graduate programs who are more qualified and prepared for graduate geospatial education than U.S. undergraduates.

A second insight is that many of the best U.S. students graduate with a BS degree in a geospatial area and can easily find a job in government or a private firm. The U.S. undergraduates can receive security clearances more easily and at less expense. Correspondingly, employment rules for foreign students (on student visas) do not allow them to work in the U.S. on student visas, so often they continue on for advanced graduate degrees. Thus, many master's and Ph.D. programs graduate a high percentage of foreign students.

An implication of these trends involves the basic research foundation of the geospatial industry. In an industry so linked to scientific and technological research and innovation, basic research is crucial to the future of the industry. Due to the nature of the geospatial industry in the U.S. (see Phase III–IV reports), limited basic geospatial research is done in the government

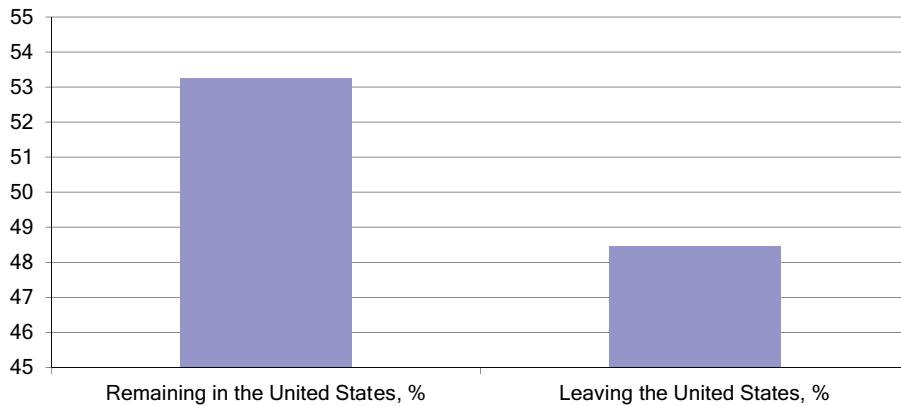


Figure 25. Estimate the percentage of foreign students likely to remain in the U.S. for employment after graduation

Remote Sensing Industry Gross Revenues

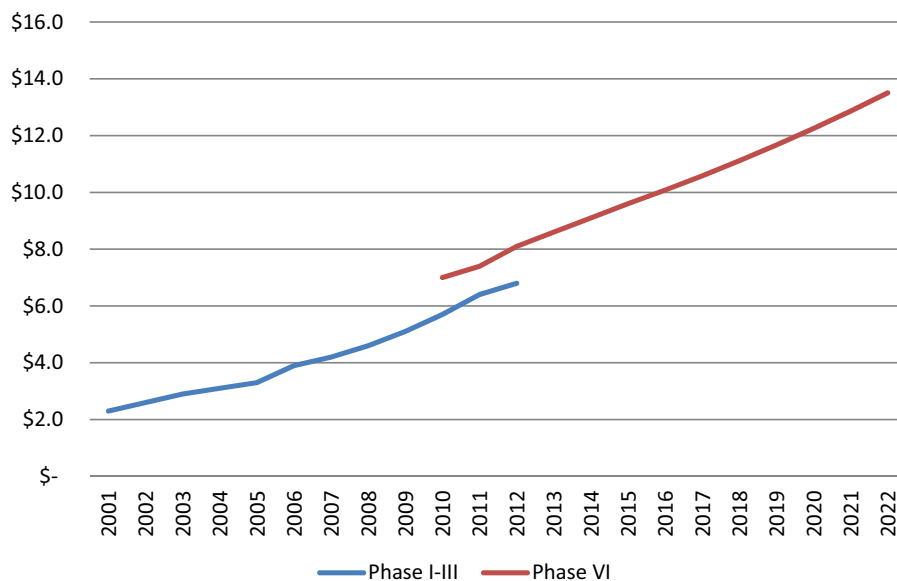


Figure 26. Estimate of remote sensing industry gross revenues from GRS.

(especially the civilian area) and private sector, compared to the university academic sector. Thus, the longer term trend of increasing foreign graduate students and graduates will affect the foundation of geospatial research in the U.S. in ways that may conflict with immigration, national security and educational policies. This will affect the long term innovation and competitiveness of the industry in an increasingly international marketplace.

Results of the 2010–2011 Gross Revenue Survey

The 2010-2011 Gross Revenue Survey (GRS) was administered to 248 firms comprising all segments of the remote sensing community (image-based geospatial activities). This survey was targeted to traditional image-based geospatial firms and to the newer firms performing exploitation of imagery for citizen-based applications.

The survey was conducted on behalf of ASPRS by the University of Utah Center for Public Policy and Administration (CPPA). Each firm was contacted by mail, telephone and through email in April-May, 2011. Recognizing the highly sensitive nature of the information being collected, all survey forms were returned to CPPA. CPPA removed all identifying information from the survey forms, which were provided to the Forecast Team for analysis.

Responses were received from approximately 15% of the firms surveyed. Reported gross revenues ranged from \$0.5 million to over \$300 million; total employee levels ranged from less than 10 to nearly 500. Given the general distribution of the responses, it is believed they represent a reasonable source from which to draw the following conclusions [Note--each of the summaries below is keyed to the question being asked on the survey form]:

Questions two and three of the GRS requested revenue estimates from the respondents. These estimates from the sample were used to estimate an industry total. Total 2010 gross revenues for the remote sensing industry are estimated at \$7.039 billion using actual revenues reported during the most recent survey (Figure 26). Figure 26 and Figure 1 are identical. A comparison of the most recent data with projections developed during Phases I-III of the Forecast (2001-2002) highlight several interesting points. There is strong consistency in the rates of projected growth when comparing those from the 2001-2002 period with the most recent (Phase VI-2011) projections -- the lines are nearly parallel. Considering that the years 2003 – 2012 were only projections in the initial Forecast Phases, and that years 2010 and 2011 were nearly at the extreme of the original projection, there is a high degree of correlation at the nexus of the two lines. Projected 2010 revenues (blue line) and the most recently enumerated 2010 revenues (red line) are within approximately 15% of each other, indicating the original projections were accurate. While the years 2011-2022 are projected using only the predicted growth levels provided by industry respondents in the most recent survey, the high level of consistency between the original projections and the latest data gives a high degree of confidence in the out years. History would indicate that the latest projections for the period 2011-2012 may actually be conservative.

Total employment in the remote sensing industry surveyed (Question 4) is estimated to be over 20,000 with an estimated average salary and benefits based on the revenue reports of just over \$120,000. However, these figures represent all employees associated with the business units reporting gross revenues, and should not be interpreted as including only remote sensing scientists. A good reference point for comparison is not available, as similar information was not collected in the earlier phases. However, both the total number of employees and the average salary and benefits appear to be higher than expected.

The breakout of market segments as reported in the Phases I-III surveys was approximately 66% aerial and 33% satellite. At the time, the commercial satellite market was in its infancy, and there were limited numbers of firms responding with satellite revenues. By comparison, the Phase VI survey (Q 5 and 6) indicates a significant growth in both overall revenues, as well as in the proportion of revenues attributable to the satellite market

continued on page 1094

segment. In addition, the “other” category is now becoming more significant, possibly given the recent inclusion of mobile mapping and other ground and airborne geospatial image-based services in the industry.

For 2010, the estimated market segment breakout is as follows:

Aerial	40%	\$2.8B
Satellite	48%	\$3.4B
Other	12%	\$0.9B

While it is possible to use the above breakout to project revenues by market segment for the period 2011-2022, given the recent trends and the significant changes in the industry such projections would not appear to be prudent at this time.

Question seven requested that the respondents estimate the percentage of activities conducted outside of the U.S. The percent of remote sensing business activities being conducted offshore are reported/projected as follows:

2010	2.29%	\$160M
2011	2.83%	\$210M
2015	3.66%	\$352M
2020	4.35%	\$534M

While these numbers appear to be relatively low, they represent a significant and apparently growing phenomenon. They represent between 1200 and 4000 U.S. jobs being outsourced on an annual basis. These results are consistent with the internet survey portion of Phase VI analysis of private firms that led to the conclusions that outsourcing of U.S.-based projects was increasing significantly.

The percent of business activities that are undertaken by U.S.-based organizations in non-U.S. or foreign areas (Q8) was reported to be approximately 7.5% during 2010 and is projected to increase slightly to approximately 10% by 2020, (Figure 27) as follows:

2010	7.5%	\$529M
2011	8.0%	\$588M
2015	8.7%	\$836M
2020	10.0%	\$1,226M

The issue of the impact of new entrants from the broader IT business and from WWW oriented, citizen based applications is impor-

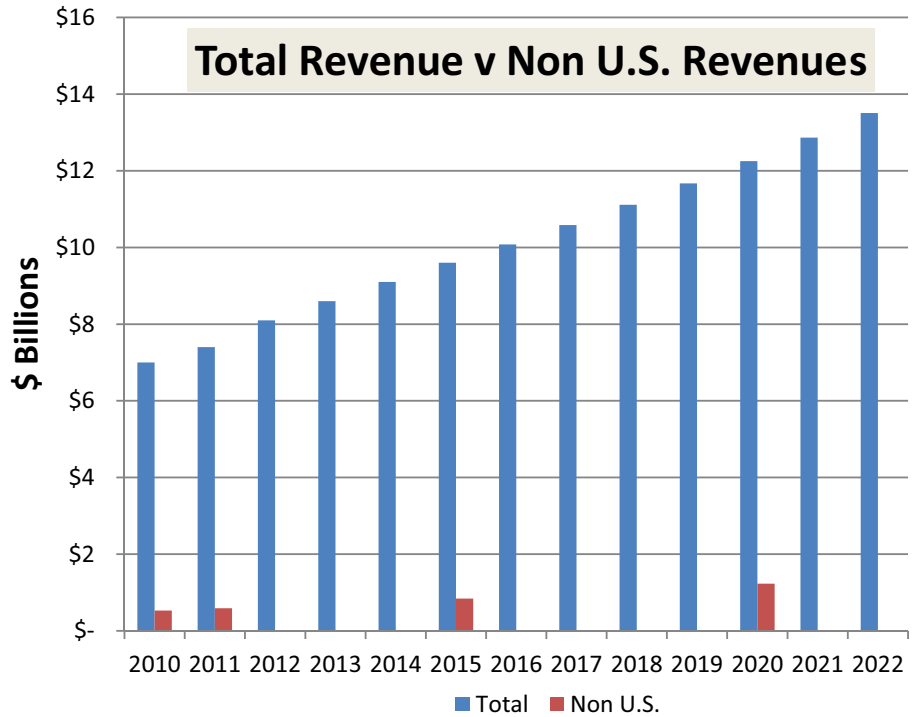


Figure 27. Total revenue versus non U.S. revenues.

tant to the future of the geospatial industry. When asked what strategies firms are developing to address changes in the market place caused by entry of firms such as Google, and the development of citizen imagery use and mapping in the remote sensing/geospatial market (Q9), responses were distributed among the following options:

- 34% Does not affect future activities
- 40% Partnership/joint activities with new entrants to market
- 26% Consolidation with other existing firms to compete
- 0% Other

Thus, 66% of the respondent firms are adapting to the changing competition and market opportunities to take advantage of the new citizen-based market. Also, they are acting to develop plans to accommodate their lines of business given the entry into the geospatial marketplace of large, diverse firms, such as Google and Microsoft.

Question 10 of the GRS asked the respondent whether his/her firm anticipates problems hiring qualified workers in the U.S. Thirty-four percent of the respondents stated Yes and 66% did not anticipate problems finding qualified employees. The respondents were asked to elaborate on strategies and/or suggestions for meeting future demand of qualified employees. Individual comments were aggregated into the following categories:

- Increasing use of H1 Visas
- Salary expectations are too high as projects are being contracted for less money
- Continued development and support for academic geospatial programs
- Train them ourselves
- Partnering within the profession and relying on U.S.-based contract labor
- Employment of staff with strong geospatial skills, but extensive in-house training and hiring foreign nationals is needed
- Internships starting early. Firm-based training. Generous education reimbursement.

Question 11. Summary categories, of text responses to the question: “What three specific science/business areas do you see the greatest shortcomings in U.S. geospatial capabilities in the next 10 years?”

Business

- Reduced funding to conduct environmental GIS projects
- Costs associated with keeping technology current
- Data becoming a commodity
- Too much Government regulation
- Potential lack of Federal funding
- Foreign competition – U.S. tax dollars going overseas
- Increase in the use of offshore labor
- Coastal zone mapping
- Commercial observation data

Technical

- Application development
- Geospatial modeling
- Current base maps
- Geospatial management
- Software to support
- Photogrammetric technicians
- Software specialists
- Labor costs
- Staffing adequately
- Project managers with expertise

In the Business-focused category of responses, the evident concerns are sufficient funding and pressures that affect pricing of geospatial products and services. This is noted in comments focusing on many areas of product and service monetization related items.

The Technical concerns are related to workforce issues of adequate education and training in specific specialties and applications. Also, the need for management level expertise for project administration.

The final question of the GRS was an open ended question regarding the industry's future growth areas (Question 12). The question was, "What major growth areas do you anticipate for our community, and how well do you believe we are prepared to meet these emerging needs?" The responses are summarized into Business and Technical categories.

Business

- Vertical market expertise in commercial and government sectors
- Vertical markets will grow with government policy cooperation
- Geospatial products entering new market segments

Technical

- Sensor processing
- Mobile mapping
- Rapid Response
- Open source

- Better than 3" GSD
- 3D
- QA/QC services
- Lidar will be well positioned

The converse to Question 11 focuses here on industry growth opportunities. The Business-oriented responses focus on both vertical penetration of the existing market and broadening the scope of geospatial usage across markets and into new markets.

The remaining open responses are aggregated under a Technology heading. These technical growth areas seem to focus on getting more out of existing sensor technologies, rather than new cutting edge sensors or platforms. This aligns well to the Business responses, both of which seem to indicate recognition of the new reality with lessening governmental spending and new markets in citizen geospatial usage.

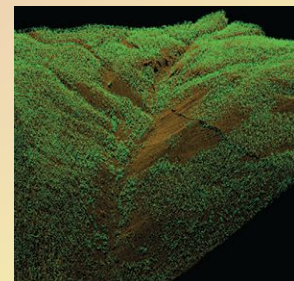
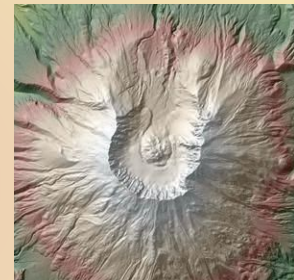
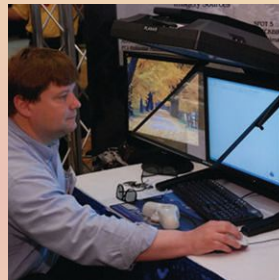
ASPRS Certification Program

ASPRS certification is official recognition by one's colleagues and peers that an individual has demonstrated professional integrity and competence in his or her field.

Apply for certification as a

- Photogrammetrist
- Mapping Scientist – Remote Sensing
- Mapping Scientist – GIS/LIS
- Photogrammetric Technologist
- GIS/LIS Technologist
- Remote Sensing Technologist

asprs.org/Certification-Program/



In Memoriam

Maurice Otto Nyquist

1944–2011

Maurice Otto (Maury) Nyquist, 67, ASPRS President (1994–1995), died September 20, 2011, in Lakewood, Colorado, and a private service for his family was held in Colorado.

Born May 30, 1944, in Fairmont, Minnesota to Carl Arther and Wilda Nyquist, he earned a bachelor of science in biology from Hamline University in 1966, a master of arts in biology from Mankato State University in 1968 and a PhD in zoology from Washington State University in 1973.



In 1974, after working for a year as an assistant professor of zoology at Washington State, Nyquist joined the National Park Service in Lakewood, Colorado and served as a manager from 1979–1993. He worked for the National Biological Service in Denver as a manager and scientist from 1993–1996. Then, he worked for the U.S. Geological Survey (USGS) Biological Resources Division from 1996 until he retired in 2004.

Nyquist earned a national and international reputation as a scientist and environmentalist. He was Faculty Affiliate of the College of Natural Resources at Colorado State University in Fort Collins (2001–2004); he was a member of many academic, government and private industry peer review committees; and, he contributed scientific articles to many professional journals.

Very active in the Federal Geographic Data Committee, Nyquist served as agency representative. He was chairman of its biological data working group and a member of its standards working group and coordination group. He also was director of production for the interactive computer exhibit on remote sensing at the Denver Museum of Natural History.

He received numerous awards for his government service, including a manager's award from the National Park Service in Lakewood in 1981 and a performance commendation award in 1988. He also was presented with an excellence of service team award from the U.S. Department of the Interior in 1999, and was named a NRA research grantee in 1972.

Nyquist was a leader in a number of professional organizations. He was named a Fellow of the American Society for Photogrammetry and Remote Sensing (ASPRS) in 1997. He served as the ASPRS Assistant Director and then Director of the Remote Sensing Applications Division from 1987–1991. In 1992 he was elected as the ASPRS National Vice President where he went up through the chairs to eventually serve as National President in 1994. Nyquist also served on the ASPRS National Board of Directors and the Executive Committee from 1988–1990.

In addition, he was a member of The Wildlife Society as well as the American Congress on Surveying and Mapping's Joint Satellite Mapping and Remote Sensing Committee. He was active in the GRASS Users Group, serving on its steering committee from 1986–2004 and as its treasurer from 1987–2004. Nyquist was a leader for the ELAS Users Group as its chairman from 1986–1987 and its co-chairman from 1985–1986. He was also a member of the national research society, Sigma Xi.

Nyquist lived by a personal philosophy that he adopted from Aldo Leopold's *A Sand County Almanac*: "We need to view the land as a community to which we belong, instead of a commodity for individual gain."

He is survived by his mother; his wife Mary Magee, whom he married in 1977; four children—Gretchen Salisbury (Shaun), Beth Nyquist, Krista Mullin (Bob) and Kyle Olson (Kim); and two grandchildren—Evan Mullin and Emerson Olson.

Donations in Nyquist's memory may be made to Trout Unlimited, 1300 North 17th Street, Suite 500, Arlington, VA 22209-3801, or your favorite charity.

"I had gotten an email from Maury on August 25, which was very upbeat, and then another on August 30 saying he wasn't good. I'm really sorry to see him go. I really enjoyed working with him, both in and outside of ASPRS. We'll really miss him."

Cliff Greve, ASPRS Past President

"Maury was a great member of ASPRS. I remember him reaching out and involving me in a number of ASPRS activities early in my career. He was always encouraging and upbeat with a great sense of humor. He is one of my many heroes in ASPRS and I will miss him."

Russell Congalton, ASPRS Past President

"When Maury was president of ASPRS, I did not know him very well, and, of course, I was in awe of him, as I still am. That year at the Alaska surveying conference, there was a break, and he turned to me and said, 'There is a great store of native art here, do you want to go look at it?' So we did, and I got to know him a little. I was just amazed that such a leader in our field could be so kind to such a flunky as me. He was a prince."

Kass Green, ASPRS Past President

"Before his diagnosis, Marilyn and I, together with Tom and Amy Budge, had several occasions to renew our ASPRS camaraderie with Maury. After his devastating diagnosis, we often asked ourselves how he was faring; and now are saddened by his passing. His last communiqué was very well stated and, to us, up-beat against the inevitable. He was a good-hearted and wonderful friend whom we shall sorely miss. We extend our best wishes to his family, and are thankful to have been able to know and work with him."

Stan Morain, ASPRS Past President

"Maury was a good friend with a warm smile and a big heart. He was a proud father, and a man who enjoyed his fishing, his beer and his pipe. He was involved in many remote sensing projects throughout his career and contributed significantly to the profession, and especially to ASPRS. He will be greatly missed."

Roger Hoffer, ASPRS Past President

"Maury left his mark on ASPRS and he will be missed by all."

Roger Crystal, ASPRS Past President

Grids & Datums

REPUBLIC OF NIGER

by Clifford J. Mugnier, C.P., C.M.S.

“Considerable evidence indicates that about 600,000 years ago, humans inhabited what has since become the desolate Sahara of northern Niger. Long before the arrival of French influence and control in the area, Niger was an important economic crossroads and the empires of Songhai, Mali, Gao, Kanem, and Bornu, as well as a number of Hausa states claimed control over portions of the area. During recent centuries, the nomadic Tuareg formed large confederations, pushed southward, and siding with various Hausa states, clashed with the Fulani Empire of Sokoto, which had gained control of much of the Hausa territory in the late 18th century. In the 19th century, contact with the West began when the first European explorers – notably Mungo Park (British) and Heinrich Barth (German) – explored the area searching for the mouth of the Niger River. Although French efforts at pacification began before 1900, dissident ethnic groups, especially the desert Tuareg, were not subdued until 1922, when Niger became a French colony” (*Niger – Country Studies, U.S. Dept. of State, 2011*).

“Before the Sahara started swallowing Niger around 2500 BC, it supported verdant grasslands, abundant wildlife and populations thriving on hunting and herding. Long after the desert pushed those populations south, Niger became a fixture on the trans-Saharan trade route. Between the 10th and 18th centuries, West African empires, such as the Kanem-Borno, Mali and Songhai flourished here, trafficking gold, salt, and slaves. The French strolled in late in the 1800s, meeting stronger-than-expected resistance. Decidedly un-amused, they dispatched the punitive Voulet-Chanoine expedition, destroying much of southern Niger in 1898–99. Although Tuareg revolts continued, culminating in Agadez’s siege in 1916–17; the French had control.

French rule wasn’t kind. They cultivated traditional chiefs’ power, whose abuses were encouraged as a means of control, and the enforced shift from subsistence farming to high-density cash crops compounded the Sahara’s ongoing migration. In 1958 France offered its West African colonies self-government in a French union or immediate independence. Countless votes conveniently disappeared, enabling France to claim that Niger wished to remain within its sphere of influence. Maintaining close French ties, Niger’s first president, Hamani Diori, ran a repressive one-party state. After surviving several coups, he was overthrown by Lieutenant Colonel Seyni Kountché after food stocks were discovered in ministerial homes during the Sahel drought of 1968–74. Kountché established a military ruling council. Kountché hit the jackpot in 1968 when uranium was discovered near Arlit. Mining incomes soon ballooned, leading to ambitious projects, including the ‘uranium highway’ to Agadez and Arlit. By the 1990s, Nigerians were aware of political changes sweeping West Africa and mass demonstrations erupted, eventually forcing the government into multiparty elections in 1993. However, a military junta overthrew the elected president, Mahamane Ousmane, in 1996. In 1999, during

widespread strikes and economic stagnation, president Mainassara (1996 coup leader) was assassinated and democracy re-established. Peaceful elections in 1999 and 2004 witnessed victory for Mamadou Tandja” (*Niger – Lonely Planet, 2011*).

Bordered by Algeria (956 km) (*PE&RS, October 2001*), Benin (266 km) (*PE&RS, July 2003*), Burkina Faso (628 km) (*PE&RS, January 2005*), Chad (1,175 km), Libya (354 km) (*PE&RS, June 2006*), Mali (821 km) (*PE&RS, October 2010*), and Nigeria (1,497 km) (*PE&RS, February 2009*); Niger has predominately desert plains and sand dunes, flat to rolling plains in the south and hills in the north. The lowest point is the Niger River (200 m), and the highest point is Idoùkâl-n-Taghès (2,022 m).

“Burkina Faso and Mali have jointly submitted a boundary dispute to the International Court of Justice (ICJ) for binding adjudication. The two states had signed an agreement to send their dispute to the ICJ on 24 February 2009 (entering into force on 20 November 2009) but the application was filed into the Court’s Registry on 20 July 2010. Burkina Faso and Niger have asked the ICJ to determine the course of their boundary between two identified endpoints, the survey pillar at Tong Tong (14° 25′ 04″ N, 00° 12′ 47″ E) in the north to the Boutou curve in the south (12° 36′ 18″ N, 01° 52′ 07″ E). This constitutes the vast majority of the central section of their boundary and the two parties made clear that the northern and southern extremities of the boundary (from Tong Tong to the tripoint with Mali, and Boutou to the tripoint with Benin) have already been demarcated by a Joint Technical Commission” (*International Boundaries Research Unit, Durham Univ., 22 July 2010*).

During WWII, the Niger Zone was established as a “British Grid” where: the Latitude of Origin (ϕ_0) = 13° N, Central Meridian (λ_0) = 0° (Equator), Scale Factor at Origin (m_0) = 0.99932, False Easting = 1,800 km, False Northing = 500 Km. The limits of the Grid were: North, 16° N.; East, 1° 30′ East; South: 10° N; and West, 14° West. The ellipsoid of reference was the Clarke 1880; the datum: ersatz (*Lambert Conical Orthomorphic Projection Tables, Niger Zone, RESTRICTED, Office of the Chief of Engineers, Washington, D.C., 1943*). (Later declassified – Ed.)

In December of 1945, the Institut Géographique National (IGN), issued SGC 1312 in which *I.A.E.F.* and *I.A.O.F.* (French East and West Africa) would employ a series of Gauss-Krüger Belts that included Niger. By 20 September 1950, that was rescinded in favor of the UTM Grid proposed by the U.S. Army Map Service.

The Chad-Niger Boundary is 1,175 km in length. In the south the Nigeria tripoint is situated in Lake Chad at about 13° 42′ 53″ N, 13° 38′ 20″ E, and in the north the Libya tripoint is situated northwest of the Tibesti at 23° N and 15° E. Northward the boundary traverses Lake Chad, crosses typical sandy and gravelly surfaces, and continues through a region of rocky ridges and steep-sided hills. There are

continued on page 1098

no known pillars demarcating the boundary (*Chad-Niger Boundary, International Boundary Study No. 73 – August 1, 1966, Bureau of Intelligence and Research, Department of State, USA*).

The Niger-Nigeria Boundary is 1,497 km in length. From the tri-point with Dahomey on the median line of the Niger River, it extends northward and then eastward to the Republic of Chad tripoint at 13° 42' 29" N, and approximately 13° 38' E. In the extreme eastern sector, the boundary follows the thalweg of the eastward flowing Komadugu Yobe for more than 272 km and then continues for about 25.6 km in Lake Chad to the Chad tripoint. The boundary is demarcated by pillars and the Komadugu Yobe (*Niger-Nigeria Boundary, International Boundary Study No. 93 – December 15, 1969, Bureau of Intelligence and Research, Department of State, USA*).

Located in the Sahara, the Algeria-Niger boundary is about 956 km in length. Northeastward from the tripoint with Mali, it consists of three straight-line sectors of 174.4 km, 227.2, and 548.8 km, respectively. The boundary is un-demarcated and traverses sparsely populated areas (*Algeria-Niger Boundary, International Boundary Study No. 99 – May 1, 1970, Bureau of Intelligence and Research, Department of State, USA*).

The Mali-Niger boundary extends for approximately 816 km between the Upper Volta and Algeria tripoints. The line is not demarcated by pillars. Although it follows several valleys, more than two-thirds of the boundary consists of straight-line segments (*Mali-Niger Boundary, International Boundary Study No. 150 – January 13, 1975, Bureau of Intelligence and Research, Department of State, USA*).

The only datum known for Niger has its origin at Point 58 east of the town of Dosso and near the border with Nigeria where: $\Phi_0 = 12^\circ 52' 44.045''$ N, $\Lambda_0 = 3^\circ 58' 37.040''$ E of Greenwich. Thanks to John W. Hager, "Azimuth is $97^\circ 30' 04.237''$ to C. F. L. 1 from north. Elevation = 266.71. Astro observed by IGN in 1968. This was used as a temporary datum pending the adjustment of the 12th Parallel to Adindan. It was for the section of the 12th Parallel in Niger and Upper Volta. Reference is *Final Report of the 12th Parallel Survey in the Republic of Niger*." Surveyed in 1969 by the French IGN, the ellipsoid of reference is the Clarke 1880 where: $a = 6,378,249.145$ m., $f/f_c = 293.465$. This was used as the basis for computation of the 12th Parallel traverse conducted 1966–70 from Senegal to Chad and connecting to the Adindan triangulation in Sudan. Remarkably, references to this datum origin point appear to have interchanged the values for Latitude and Longitude, incorrectly placing the point somewhere in Cameroon! According to TR 8350.2, the datum shift **from** Point 58 Datum **to** WGS84 Datum is: $\Delta X = -106$ m ± 25 m, $\Delta Y = -129$ m ± 25 m, and $\Delta Z = +169$ m ± 25 m, and is based on two points collocated in 1991.



The contents of this column reflect the views of the author, who is responsible for the facts and accuracy of the data presented herein. The contents do not necessarily reflect the official views or policies of the American Society for Photogrammetry and Remote Sensing and/or the Louisiana State University Center for Geoinformatics (C⁴G).

Stand out from the rest – earn ASPRS Certification

ASPRS congratulates these recently Certified and Re-certified individuals:

Certified Mapping Scientist Remote Sensing

Michael Tuffly, Certification #RS196,
effective 9/24/2011, expires 9/24/2016

Re-Certified Mapping Scientist GIS/LIS

Thomas R. Jordan, Certification #R184GS,
effective 9/6/2011, expires 9/6/2016

Certified Photogrammetric Technologists

Derege W. Kobre, Certification # 1505PT,
effective 9/24/2011, expires 9/24/2014

Joshua Quint, Certification # 1504PT,
effective 9/24/2011, expires 9/24/2014

Provisional Certified Photogrammetrist

Young-Jin Lee, Certification #1506P,
effective 9/24/2011, expires 9/24/2021

For more information on ASPRS Certification, visit
<http://www.asprs.org/membership/certification/>



Thank you to all the ASPRS regions that participated in the Region of the Month contest. and the Winner for the Month of SEPTEMBER is...

NORTHERN CALIFORNIA REGION

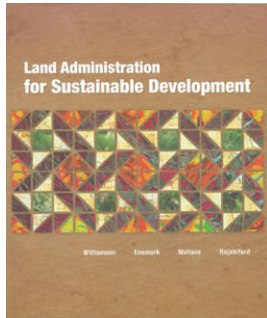
The Northern California Region sponsored 11 new members during the month of August.

In recognition of their commitment to the Society, they receive the following:

- A certificate from ASPRS acknowledging their work in membership recruitment.
- ASPRS Buck\$ vouchers valued at \$50 to be used toward merchandise in the ASPRS Bookstore.
- This special recognition in this issue of *PE&RS* of their designation as "Region of the Month," a true display of their commitment to the Society.

Northern California Region This is an ongoing regional recruitment campaign. We hope other regions will be listed here in future months.

Book Review



Land Administration for Sustainable Development

Ian Williamson, Stig Enemark, Jude Wallace and Abbas Rajabifard

ESRI Press Academic, Redlands California, 2010, 487 pp.

ISBN 978-1-58948-041-4

Paperback. \$49.95

Reviewed by John Stillwell, Professor, School of Geography, University of Leeds, Leeds, UK

The authors have created a very impressive volume focussing on the explanation of concepts and principles that underpin the role of land administration within the paradigm of land management. This volume also presents a review of the tools and mechanisms for dealing with processes leading to the achievement of sustainable land development. The aim of demonstrating the way in which infrastructures have been developed to administer the relationship between people and land so as to implement management strategies and land policies, has been realized, with examples from across the full spectrum of developed and developing countries. It is this global perspective that is one of the strengths of this book, but there are other key features too that indicate its excellence, not the least of which is the experience that its authors are able to contribute; all are professionals in fields such as land surveying, chartered engineering or land policy law, as well as holding academic posts in universities in either Australia or Denmark.

There are many excellent attributes about this book, but I choose to mention only three particular dimensions given the limited space for this review. First, the authors tackle a subject of immense importance which has responded to dramatic changes over time. Land administration is a subject which has evolved out of the attempts to define the relationship between people and land through land registration. The authors highlight the key role of the cadastre throughout while repeatedly acknowledging the functions or processes of land tenure, land value, land use and land development which collectively define the field.

Secondly, the book is very well organised and logical in its layout. It is organized into five main parts subdividing a collection of fourteen chapters. Part 1 (Introducing Land Management) is an introductory section comprised of two chapters, the first of which explains the universal land management paradigm and the four core administration functions. Within this chapter the authors explain that there are common processes and practices occurring in all countries while introducing the concept of the land administration “toolbox” that usefully sets out a set of ten principles that practitioners can use to help develop and manage assets and resources to secure sustainable development. The second chapter provides a chronological account of the evolution of land administrative systems from the early forms of surveying adopted by the ancient Egyptians through periods when cadastres were used as tools for taxation, land marketing and planning to the contemporary view of the multipurpose cadastre.

Part 2 (A New Theory) is comprised of three chapters that can be considered as theoretical contributions, although Chapter 3 (The

Discipline of Land Management) also takes a historical perspective in charting the evolution of land policy towards sustainability at the international level and the requirement for land administration systems (LAS) to embrace the need to manage rights, restrictions and responsibilities as well as rights in property-based commodities. Chapter 4 (Land Administration Processes) addresses the core processes of land administration and presents examples of tenure processes in particular, while Chapter 5 (Modern Land Administration Theory) explains the modern theory of land administration and how the core processes interact to create efficient land markets and effective land management. Here again the focus is on the national cadastre and how the data it contains (parcels, properties, buildings, roads) are an important part of the spatial data infrastructure (SDI) upon which a whole range of governance services rely for enhanced decision making. It is a touch disappointing that more detail is not provided on the relationship (integration) between the digital cadastral information and other digital information held in the GIS.

Part 3 (Building Modern Systems) is comprised of five chapters that purport to cover all the dimensions of building a modern LAS. Chapters 6 through 9 respectively cover the management of different types of land markets, the role of planning and regulation in controlling land use, the concept of the marine cadastre (i.e. marine administration), and the integration of the spatial data infrastructure with new technologies. Each chapter delivers valuable information, however it would have been useful to have read something in the land use management chapter (Chapter 7) on how the developments in modern LAS interface with the large body of work on land use simulation and the types of land use models developed by Dick Klosterman (What if?) or Keith Clarke (SLEUTH). Similarly, in Chapter 9 on SDIs and technology, it is surprising to find nothing about the European Unions’ ongoing preoccupation with interoperability as reflected in the INSPIRE initiative to create a regional SDI. INSPIRE sets out a framework and timetable that obliges public sector organizations to publish key spatial data sets in ways that support the discovery of the data and provide access to these resources via product-neutral visualization and downloading services. The final chapter in Part 3 reports on the Worldwide Cadastral Template Project, a global comparative analysis of cultural and technical descriptions of national cadastral systems, demonstrating the extent of the diversity of systems used by countries at different stages of development.

Chapters 11–14 constitute Parts 4 and 5 of the book and are primarily dedicated to implementation strategies, beginning with a chapter

continued on page 1100

on capacity-building and institutional development. The recognition that capacity-building is required at societal and organizational levels as well as at the individual level is critical. There is little doubt that huge technical skills shortages exist in many countries of the world. However, more importance might have been paid to the issue of ownership and accountability. In developing a system called "LANDADMIN" for the Lands Commission Secretariat (LCS) in Accra, Ghana, one of the most important considerations for successful system implementation was the involvement of the users (LCS staff) in the design and development process (Karikari et al., 2003); more generally, the need for greater user participation or collaboration is one of the lessons learned from the implementation of many planning support systems across a range of contexts (Geertman and Stillwell, 2009). The following chapter (Chapter 12: The Land Administration Toolbox) is considered by the authors to be the central chapter of the book because it describes the various "tools of the trade", using the analogy of the "toolbox". In this case the tools refer to a wide range of measures and methods categorized as "general", "professional" and "emerging". This extensive chapter, though not providing comprehensive coverage, is crucial in outlining the methodology that allows tools to be selected and applied that are context specific. Thereafter, Chapter 13 is dedicated to project management and evaluation in relation to land administration projects (LAPs) and explanation of "The Project Cycle", the World Bank model of how to undertake a large-scale project which is sustainable. The book ends with a short chapter in Part 5 that highlights the main issues and considers the challenges and opportunities that lie ahead.

The third and final thing that I like about this book is its standard of presentation. It is very readable. The color photographs and images enhance the text. There is a useful list of abbreviations at the beginning and an even more useful glossary of terms at the end. In summary, the authors are to be congratulated for bringing so many issues and ideas together into a document that is both fascinating yet authoritative; it deserves to be used by widely by scholars and practitioners alike.

References

Geertman, S. and Stillwell, J. (eds.), 2009. *Planning Support Systems Best Practice and New Methods*. Springer, Dordrecht.
 Karikari, I., Stillwell, J. and Carver, S., 2003. *Adoption of Geographic Information Systems in Accra lands Commission Secretariat, Our Common Estate*, RICS Foundation, London

ASPRS VICE PRESIDENTIAL CANDIDATES FOR 2012

This is a notice regarding the Official Nomination for the office of ASPRS Vice President for 2012, and the requirements for nomination by petition. The ASPRS Nominating Committee is pleased to announce its candidates for the office of ASPRS Vice President, to take office in March 2012.

Chris Aldridge

Continental Mapping Consultants
 Portland, Oregon

Dr. A. Stewart Walker

BAE Systems
 San Diego, California

Additional nominees for Vice President from the Private Sector should be submitted to the ASPRS Executive Director, 5410 Grosvenor Lane, Suite 210, Bethesda, MD 20814, no later than 14 weeks prior to the 2012 ASPRS Annual Conference. These nominations must be made by a nominating letter signed by not less than 250 voting members of ASPRS and must contain a biographical sketch of the nominee.

Deadline for nominations by petition: December 14, 2011.

ASPRS Nominating Committee:

- Carolyn Merry, Chair
- Brad Doorn
- Kass Green
- Marguerite Madden
- Kari Craun

BE AN ASPRS MEMBER CHAMPION

ASPRS is recruiting new members and YOU benefit from each new member YOU champion. Not only can you contribute to the growth of ASPRS, but you can earn discounts on dues and merchandise in the ASPRS Store.

**Member Champions by Region from
 January 1, 2011 – September 30, 2011**

Central New York
 Lindi J. Quackenbush, CMS
 William M. Stiteler, CMS

Columbia River
 Steven P. Lennartz
 James E. Meacham, CMS
 Brian Miyake

Eastern Great Lakes
 Jim Peters, CP

Florida
 Bon A. Dewitt
 Brian G. Ormiston
 Xiaojun Yang

Mid-South
 Thomas R. Jordan, CP

New England
 Daniel L. Civco
 Russell G. Congalton

Northern California
 Maggi Kelly
 Nathan P. Jennings

Potomac
 Karen L. Schuckman, CP
 Barry Haack

Puget Sound
 Eunju Kwak

Rocky Mountain
 Michaela Buenemann
 Roger H. Hanson, CP
 Mark Stanton

Saint Louis
 Rex G. Cammack
 Ming-Chih Hung

Western Great Lakes
 Mary E. Balogh
 Douglas H. Fuller, CP

**Member Champions
 By number of new
 members recruited**

**Recruited from 1 to 4 new
 members**

- Mary E. Balogh
- Rex G. Cammack
- Daniel L. Civco
- Russell G. Congalton
- Bon A. Dewitt
- Nathan P. Jennings
- Thomas R. Jordan, CP
- Barry Haack
- Roger H. Hanson, CP
- Maggi Kelly
- Eunju Kwak
- James E. Meacham, CMS
- Brian Miyake
- Brian G. Ormiston
- Jim Peters, CP
- Lindi J. Quackenbush, CMS
- Karen L. Schuckman
- Mark Stanton
- William M. Stiteler, CMS
- Xiaojun Yang

**Recruited 5 and more new
 members**

- Michaela Buenemann (5)
- Douglas H. Fuller, CP (5)
- Ming-Chih Hung (6)
- Steven P. Lennartz (23)

REMEMBER! To receive credit for a new member, the CHAMPION'S name and ASPRS membership number must be included on the new member's application.

CONTACT INFORMATION

For Membership materials, contact us at:
 301-493-0290, ext. 109/104 or email: members@asprs.org.
 Individuals who want to join ASPRS may sign up on-line at
<http://www.asprs.org/Join-Now/>.

RECRUIT

- **1 new member, earn a 10% DISCOUNT off your ASPRS DUES and \$5 in ASPRS BUCK\$.**
- **5 new members, earn a 50% DISCOUNT off your ASPRS DUES and \$25 in ASPRS BUCK\$.**
- **10 or more new members in a calendar year and receive the Ford Bartlett Award, one year of complimentary membership, and \$50 in ASPRS BUCK\$.**

All newly recruited members count toward the Region's tally for the Region of the Month Award given by ASPRS.

Those eligible to be invited to join ASPRS under the Member Champion Program are:

- Students and/or professionals who have never been ASPRS members.
- Former ASPRS members are eligible for reinstatement if their membership has lapsed for at least three years

ASPRS BUCK\$ VOUCHERS are worth \$5 each toward the purchase of publications or merchandise available through the ASPRS web site, catalog or at ASPRS conferences.

2nd Annual ASPRS GeoLeague Challenge to be presented at the ASPRS 2012 Annual Conference in Sacramento, California, March 19-23, 2012

Registration ends November 30th, 2011

For complete rules and information, visit <http://asprsignature.blogspot.com/>

Introduction: The 2011 ASPRS Annual Conference in Milwaukee, Wisconsin was the culmination of the first ever GeoLeague Challenge, where five different teams of students competed for the glory of being named the ASPRS GeoLeague Champions! The student teams were made up of both undergraduate and graduate students, each with one faculty mentor. The teams were charged with finding a suitable location in New Hampshire for a 90 MW capacity wind farm while minimizing the cost of the project and addressing the impacts that the wind farm may have on the chosen location. The teams presented their solutions in three different mediums: a paper, a poster, and a video. Each of these submissions were evaluated by our guest judges to determine the winner.

The participating teams in this year's competition were from Mississippi State University, University of Connecticut, University of Florida, University of Nebraska, and University of South Carolina. They each submitted unique and innovative solutions, but in the end, the team from the University of South Carolina took second place, and the University of Florida captured first place with its consistently strong performance. As the winning team, the University of Florida's student chapter received \$250, and the students who participated received books that were graciously donated by ESRI, one year complimentary membership in ASPRS, and their paper submission highlighted in the July issue of *Photogrammetric Engineering & Remote Sensing*.

Now it's your turn to enter the 2012 GeoLeague Challenge and compete for fame and prizes.

Premise: Coastal environments are renowned for their dynamics and vulnerability to both natural hazards of both extreme (hurricanes and nor'easters) and chronic nature (shoreline erosion and sea-level rise.) The rapid development of our coast witnessed by remote sensing of land use/land cover change (LULCC) is juxtaposed to these opposing forces of development and coastal processes, with wetland ecosystems often being squeezed between the two. Coastal resource management agencies struggle to acquire and maintain up-to-date geospatial information for dynamic features, particularly coastal land use/land cover, shorelines, and wetlands. No single remote sensing system (platform, sensor, and image processing approach) can meet the demand. Professionals trained broadly in available data and their integration and spatial analysis are poised to meet these needs, which in the future will become ever higher need as the inexorable process of sea-level rise and periodic coastal storms continue.

The Challenge: To apply remote sensing and GIS to solve vexing problems currently facing Federal, State, and non-profit natural resource managers who need timely information in order to develop policy and monitor the fate of our vital shore and coastal wetlands. Specifically, you are tasked to recommend a "remote sensing remedy," including sensors and spatial analytical techniques (in a cost- and time-efficient manner) to create coastal wetland inventories that can be efficiently updated at least every 5–10 years.

Stipulations for this challenge include:

- The thematic accuracy of the product should approach 90% overall
- Users and producers accuracy meeting National Map Accuracy Standards, using a minimum mapping unit of approximately 1 ha
- The ideal approach would also include regional demonstrations:
 - Target mapping of specific invasive species as an additional thematic class, e.g., *Phragmites australis*, ("common reed") an extensive, exotic species that is spectrally and ecologically similar to other intertidal marshes (e.g., *Spartina* spp.)
 - For a West Coast context, *Spartina* is typically invasive and would be a target of high interest.
 - The wetland maps and invasive species should be updated coast-wide every 5–10 years.

How to Participate: Form a group of at least 5 ASPRS Student Members (undergraduate and/or graduate students) and a faculty advisor in your region. If you have trouble meeting this requirement, please feel free to contact us. You may also enlist the help of ASPRS members in your surrounding communities; however, the students must do all of the work; non-students can only provide guidance!

To be eligible to win, please fill out a registration form, located on the ASPRS Student Blog (asprsignature.blogspot.com) and the ASPRS Student Advisory Council (SAC) Facebook page, and return it to the SAC Deputy Chair (abenjamin1@ufl.edu) prior to November 30, 2011.

How to Present Your Solutions: Your solutions will be presented in a session at the 2012 ASPRS Annual Conference in Sacramento, California. At least one representative from each team will be required to attend the conference to present the project. You will be required to present 3 things at the conference:

- 1) A poster that can be hung during the poster session (maximum size: 36 in tall by 48 in wide) that gives an overview of your solution and the process by which you created your solution.
- 2) A short 5 minute PowerPoint presentation to be made during the GeoLeague Challenge Session
- 3) A scientific paper (following the guidelines presented by Photogrammetric Engineering & Remote Sensing (PE&RS) for Highlight Articles online at <http://www.asprs.org/PE-RS-Submissions-Policy-and-Guidelines/PE-RS-Instructions-for-Authors-of-Highlight-Articles.html> describing in detail your solution to this years' challenge, including background on the project, your methods, graphic illustrations, and the results pertaining to your solution.

All materials must be submitted by February 27th, 2012.

How to Submit Your Solutions: Your PowerPoint presentation and paper should be uploaded to the ASPRS ftp site no later than 8:00pm EST on Monday, February 27, 2012.

FTP Site: <ftp://birdseye.asprs.org>

Login: ASPRS/FTP_USER (all caps)

Password: ASPRSgeneral

Please place your materials in the GeoLeague folder with the name of your team in the heading (ex. `teamname_paper.doc`, `teamname_presentation.ppt`).

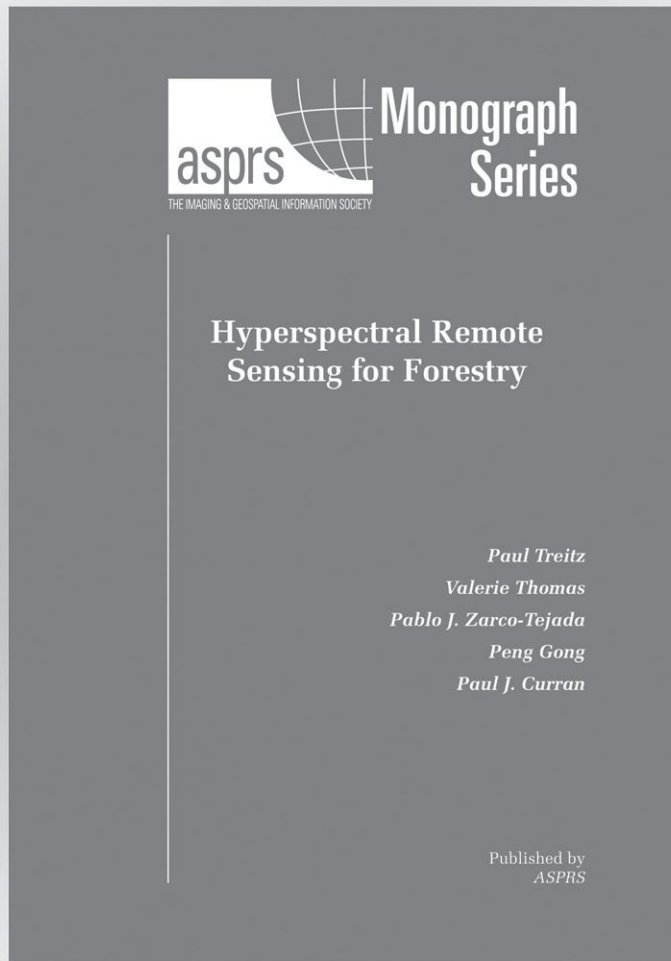
You should bring your poster along with you and set it up at the start of the conference.

Contact: Please contact the ASPRS SAC Deputy Chair with any questions you may have!

Adam Benjamin
ASPRS Student Advisory Council Deputy Chair
abenjamin1@ufl.edu

NOW AVAILABLE FROM ASPRS

Hyperspectral Remote Sensing for Forestry



Hyperspectral Remote Sensing for Forestry provides a clear and concise description of the role of hyperspectral remote sensing for the extraction of biophysical / biochemical information about forests. This monograph covers the fundamental principles related to the importance of high spectral resolution data for the identification of spectral features related to plant biochemistry and physiology. Various methods of hyperspectral data analysis are discussed, with specific attention given to spectral indices, spectral mixture analysis and canopy reflectance modeling. A number of case studies are presented that cover applications related to: (i) forest classification based on species biochemical composition; (ii) forest canopy structural analysis; (iii) spectral unmixing; and (iv) fusion of hyperspectral and lidar data for species mapping. This volume will be of significant interest to the remote sensing scientist and practitioner as well as senior undergraduate and graduate students interested in hyperspectral remote sensing for vegetation analyses.

107+ pp. Softcover. 2010
ISBN 1-57083-093-2
Stock # 4584
List Price: \$26
ASPRS Members: \$21

ORDER ONLINE AT

<http://asprs.org/Publications-Other/Bookstore.html>



ASPRS MEMBERSHIP

Your path to success in the geospatial community

ASPRS would like to welcome the following new members!

At Large

Hussein Elhadi
Andre' Jalobeanu
Mohannad Al-Durgham*
Abdulla Al-Rawabdeh*

Central NY

Robinson Dugan*
Aaron McVay*
Zhen Zhen*

Central US

Dawn Farver*

Columbia River

Kendal McDonald
Jersey Krueger*

Eastern Great Lakes

Stanley Chandra Budhram, CP
Daniel Ngoroi
Qiusheng Wu*
Kirk Zmijewski*

Florida

Richard Pryce

Intermountain

Joan Biediger*

Mid-South

Jason Combs
H. Alexis Londo
Emily Fraser*
Laura Gast*
Joshua Johnson*
Sachidananda Mishra*
Armando Morales*
Cara Valinoti*

North Atlantic

Fenton Wright
Matthew Fagan*

Northern California

Steve Weaver
Adrian Aguirre*
Jim Alford*
Mark Barry*
Chris Erickson*
Rob Jones*
Robert Mulford*
Carlos Quispe*
Theresa Stinchfield*
Andrew Tapley

Tiffany Tatum*

New England

Maria Diuk-Wasser
Xiaowen Song*
Shumei Zhou*

Potomac

Kathryn Clifton
James Huffines
Ramon Leonel Perez David

Andrea Pomrenke
Rodrigo Costas*
Michael DeMarr*
Virginia Gorsevski*
Gina Rumbolo*
Heather Williams*
Bum-Chong Yoo*

Puget Sound

Chao Han

Rocky Mountain

Mark Bowersox
David Brostuen, CMS
Courtney Hurst
Robert Jones

Jamie Fuller*

Lisa Lone Fight*

Saint Louis

Douglas Evans
Jeremy Holm*
Brandon Marini*

Southwest US

Aaryn Olsson, Ph.D.
Steve Shelton, CP
Michael Alonzo*
Christopher Galletti*
Catherine Hall*
Jeff Kling*
Allan Yiulun Ng
Kellie Uyeda*
Robert Walker*

Western Great Lakes

Elizabeth Banda*
Naime Celik*
Daryn Hardwick*
Hilary Morgan*
Eray Sevgen*

*indicates student member

For more information on ASPRS membership, visit <http://www.asprs.org/Join-Now/>

DAT/EM Systems International



Introducing AIRFIELD3D™

Obstruction identification tool for U.S. FAA 18B-compliant airfield projects

Features:

- Digitize directly into the FAA-supplied 18B compliant templates for ESRI® ArcGIS®.
- Integrate flawlessly with ArcGIS geodatabases, shapefiles, and tables.
- Automatically construct Airport Airspace Survey Surfaces for Vertically Guided (VG) and Non-Vertically Guided (NVG) surfaces from runway centerline and airport elevation.
- Automatically apply multiple 18B-required field values at once.



8240 Sandlewood Place, Suite 101 • Anchorage, Alaska 99507 USA • +907.522.3681 • www.datem.com

Calendar

OCTOBER 2011

5-7, **PIA11 - Photogrammetric Image Analysis, ISPRS working groups I/2, III/1, III/4 and III/5**, Munich, Germany. For more information, visit www.pia11.tum.de.

❖ 7, **Columbia River & Puget Sound Regions 15th Annual Joint Technical Exchange**, Vancouver Water Resource Education Center, Vancouver, Washington. For more information, email cr.asprs@gmail.com or jeff@glickman.com.

9-12, **Archean to Anthropocene – The Past is the Key to the Future**, *The Geological Society of America*, Denver, Colorado. For more information, visit <http://www.geosociety.org/meetings/2011/>

16-19, **LIDAR Applications for Assessing Forest Ecosystems, SilviLaser 2011 Conference**, *University of Tasmania, Hobart, Australia*. For more information, visit www.silvilaser2011.com

20-21, **Advances In RS And GIS Applications In Forest Fire Management: From Local To Global Assessment**, *8th International Workshop of the EARSeL Special Interest Group (SIG) on Forest Fires*, Stresa, Italy. For more information, visit <http://forest.jrc.ec.europa.eu/earsel>

NOVEMBER 2011

14-17, **ASPRS 2011 Fall Pecora Conference**, *ASPRS*, Herndon, Virginia. For more information, visit www.asprs.org.

14-18, **Regional Geographic Conference (UGI 2011)**, Santiago, Chile. For more information, visit <http://www.ugi2011.cl/>.

21-25, **Surveying and Spatial Sciences Conference 2011 – Innovation In Action – Working Smarter**, Wellington, New Zealand. For more information, visit www.sssc2011.org/

29-30, **European Lidar Mapping Forum (ELMF)**, Salzburg, Austria. For more information, visit <http://www.lidarmap.org/ELMF/>.

DECEMBER 2011

5-9, **AGU Fall Meeting 2011**, *American Geophysical Union*, San Francisco, California. For more information, visit <http://www.agu.org/meetings/>.

JANUARY 2012

23-25, **International Lidar Mapping Forum (ILMF)**, Denver, Colorado. For more information, visit <http://www.lidarmap.org/ILMF.aspx>.

FEBRUARY 2012

8-10, **EuroCOW 2012 – The Calibration and Orientation Workshop**, Castelldefels (Barcelona), Spain. For more information, visit www.ideg.es.

MARCH 2012

❖ 13-24, **GIS in Action**, Portland, Oregon. For more information, visit http://www.orurisa.org/GIS_In_Action

19-23, **ASPRS 2012 Annual Conference**, *ASPRS*, Sacramento, California. For more information, visit <http://www.asprs.org>.

APRIL 2012

23-27, **SPIE Defense, Security, and Sensing 2012**, *SPIE*, Baltimore, Maryland. For more information, visit http://spie.org/defense-security.xml?WT.mc_id=RCal-DSSW.

MAY 2012

❖ 14-17, **Global Geospatial Conference 2012**, Québec City, Canada. For more information, visit <http://www.gsdi.org/gsdiconf/gsdi13/>

AUGUST 2012

25-September 1, **The XXII Congress of the International Society of Photogrammetry & Remote Sensing, ISPRS**, Melbourne, Australia. Deadline for abstracts: October 24, 2011. For more information, visit <http://www.isprs2012.org>

SEPTEMBER 2012

3-7, **9th International Symposium on Tropospheric Profiling**, L'Aquila, Ital. For more information, visit <http://cetemps.aquila.infnet.it/istp>.

OCTOBER 2012

29-November 1, **ASPRS/MAPPS 2012 Fall Conference**, *ASPRS*, Tampa, Florida. For more information, visit www.asprs.org.

MARCH 2013

24-28, **ASPRS 2013 Annual Conference**, *ASPRS*, Baltimore, Maryland. For more information, visit www.asprs.org.

❖ = indicates a new listing

ASPRS CONFERENCE INFORMATION

• Abstract deadlines • Hotel information • Secure on-line registration

www.asprs.org

Photogrammetric Engineering & Remote Sensing (PE&RS)

January 2013 Special Issue Call for Papers

“The Future of National-Scale Three-Dimensional Landscape Mapping”

Guest Editors:

Jason Stoker, USGS

Gregory Snyder, USGS

Larry Sugarbaker, USGS

A National three-dimensional (3-D) landscape mapping program is being considered by the Federal government to provide seamless, National-scale landscape 3-D data for mapping, monitoring, and other operational and/or science uses. The ultimate vision is a program that collects, preserves, and makes publicly available 3-D landscape data acquired by various lidar instruments and other technologies to help address pressing issues, such as climate change to resource management and flood risk mitigation. To help inform program planning, the USGS is leading a National Enhanced Elevation Assessment under the auspices of the National Digital Elevation Program (NDEP), and in concert with many other stakeholders. The Assessment is using an inclusive approach, which incorporates public and private input to document business requirements supported by elevation data and the associated benefits. The Assessment will help discover economies of scale, potential multiple data uses, and universal business requirements that may be met through a more comprehensive national approach for improving elevation data in the United States and its territories, including coastlines.

This special issue will broadly highlight the importance of 3-D data and attempt to address potential issues inherent in applying 3-D at the National scale, were these data to be available. It will highlight 3-D applications for mapping and monitoring including but not limited to the following topics:

- 3-D data collection and information creation- from the plot to global levels
- Costs and benefits of a National 3-D monitoring program
- 3-D data needs and applications with National implications
- Advanced information technology developments for 3-D data
- Standards and specifications needed for nationally-consistent 3-D data
- Methodologies of quality assurance and quality control of 3-D data
- New applications facilitated by the availability of 3-D data

While all submitted papers do not need to be National in scope, the results and conclusions must demonstrate the importance, utility and/or application to the National scale. The special issue will follow a two-step review process. Interested authors should prepare a detailed abstract of two pages (about 800 words). The abstract should include the contact information of the authors, outline the scope of the work and its relevance to National 3-D information, describe the key principles and procedures of the methods, report the main results, and summarize the findings. The submitted abstracts will be reviewed by the guest editors. Authors of the selected abstracts will be invited to submit full manuscripts for peer review based on PE&RS policy. All manuscripts are to follow the PE&RS Instructions for Authors that are published in each issue of the Journal and are available on the ASPRS website (<http://www.asprs.org/pers/Submissions>). Final accepted papers will be collected in the special issue.

IMPORTANT DATES

Submission of Abstracts (~800 words; 2 pages):

January, 1, 2012

Notification of Abstract Acceptance:

February 1, 2012:

Manuscripts Due:

March 1, 2012

Guest Editor Notify Author of Decision:

June, 1, 2012

Final Papers Due:

July 1, 2012

Special issue:

January, 2013

Please submit your abstracts by email directly to:

Jason Stoker

Physical Scientist

USGS Earth Resources Observation and Science (EROS)

Mundt Federal Building

47914 252nd St.

Sioux Falls, SD 57198

jstoker@usgs.gov

605-594-2579

Industry News

Business

LizardTech® has reached an agreement with Esri CIS in Russia to become an authorized reseller for its GeoExpress®, Express Server® and LiDAR Compressor™ geospatial imaging products. Esri CIS, headquartered in Moscow, Russia, will sell LizardTech's software products to companies and organizations in the nine countries of the Commonwealth of Independent States (CIS), including Russia, Kazakhstan and Belarus. LizardTech's line of geospatial software products includes GeoExpress, which enables geospatial professionals to compress and manipulate satellite and aerial imagery, Express Server for high-performance delivery and publication and LiDAR Compressor, which turns giant point cloud datasets into efficient MrSID® files. For information, visit www.lizardtech.com.

Woolpert announced it was recently selected by Des Moines Water Works (DMWW) in Iowa for a five-year, \$2.5 million contract to develop an asset management system for the water utility company. Woolpert will assist DMWW to establish best management practices, implement the Infor™ Enterprise Asset Management (EAM) system, and integrate the EAM with key business support systems. Implementation of this system will help reengineer and transform DMWW's business processes and information systems to increase efficiencies for its staff and customers. Woolpert's multi-phased approach will include planning, data conversion, system configuration, testing, application development, systems integration and training. For information, visit www.woolpert.com.

Contracts

AeroMetric has completed 36 miles of High Accuracy Mapping along I-88 for the Illinois Tollway. I-88 is undergoing a mill and resurfacing program, and the design engineers required a high precision base map to prepare their construction documents. By employing a helicopter mapping solution, AeroMetric offered the team a creative and innovative approach to transportation corridor surveying. This is the first time the Illinois Tollway has used helicopter-based high accuracy mapping lidar technology for a corridor survey. This solution will encourage transportation authorities nationwide to make use of leading edge technology when mapping their corridors. AeroMetric used Tuck Mapping Solutions' state-of-the-art eagleeye® corridor mapping systems. This enabled the team to acquire very low altitude, high accuracy lidar data sets, topographic maps, 3D planimetric maps and 3-inch resolution digital orthophoto imagery for the entire corridor. For information, visit www.aerometric.com.

Critigen was awarded a Prime Contract on the U.S. Navy's SeaPort Enhanced (SeaPort-e) contract. The contract is an indefinite-delivery/indefinite-quantity multiple award contract under which the government estimates a maximum of \$5,300,000,000 of services will

be procured per year. Critigen's award has a three-year base period with one five-year award term, and is comprised of seven regional zones in which task orders will be competed based upon the principal place of performance. Critigen is authorized to perform services in all seven zones. The scope of the contract includes 22 functional requirements areas spanning the full spectrum of professional services procured by the U.S. Navy and Marine Corps, as well as other Defense agencies. Critigen and its team partners support all 22 functional areas of the SeaPort-e contract. The following key areas are of particular focus: systems and process engineering; system design and technical data documentation; software engineering, development, programming, and network support; configuration management and quality assurance; information system development, information assurance, and information technology support; test and evaluation; training; and program-level support. For information, visit critigen.com.

East View Cartographic (EVC) has become an official reseller of paper and digital geospatial products produced by the national mapping agency of Tanzania, The Ministry of Lands in Dar-es-Salaam. EVC has acquired and signed digital rights agreements to offer these unique locally produced geospatial data to all of its customer types, which include: academic libraries; regional and international governmental agencies; mil/intell, oil, gas & mining, and avionics corporations. Over the past five years, EVC has embarked on an aggressive mission to acquire the world's largest commercially-available collection of locally produced cartographic and GIS data worldwide with a particular focus on Africa nations. Tanzania now accompanies EVC's similar success in Botswana, Rwanda, Madagascar, Kenya, and South Africa. EVC maintains an office in Nairobi, Kenya, which is staffed primarily to establish and consummate data distribution and value-add agreements.

The University of Arizona's Map Library and GIS Department has requested that East View Cartographic (EVC) procure, structure, translate and host several gigabytes of Mexican-created geospatial vector data. EVC fulfilled the request and additionally built a convenient webapp that allows non-GIS users to also access this dataset. Chris Kollen, the University of Arizona's Data Curation Librarian and sponsor of the effort expressed, "With the geospatial web server, University of Arizona faculty and students are able to easily view and download detailed Mexico geospatial data. By providing access to the data through East View Cartographic's geospatial web services, the University of Arizona Libraries did not need to expend hardware, software or staff resources to create their own service." For information, visit www.cartographic.com.

People

Amar Nayegandhi was named manager of elevation technologies at Dewberry. Based in the firm's Tampa, Florida, office, Nayegandhi will provide management and technical support for lidar-derived projects for local, state, and federal clients. With more than 10 years' experience, he has developed original data processing algorithms for airborne lidar sensors, as well as processed and analyzed waveform, point cloud, and Digital Elevation Model data in submerged, sub-aerial, and vegetative coastal environments. He has presented his research and technological findings at more than 60 international conferences and technical workshops, as well as authored 15 articles and more than 65 reports for the U.S. Geological Survey. Nayegandhi is a member of the team developing the Experimental Advanced Airborne Research Lidar (EAARL) system—a unique topo-bathy lidar system that generates large volumes of green-wavelength, waveform lidar data to measure submerged topography and land elevations seamlessly. Nayegandhi earned his master's degree in computer science from the University of South Florida and bachelor's degree in electrical engineering from the University of Mumbai, India. He is a member of the American Society for Photogrammetry and Remote Sensing, American Geophysical Union, and American Association of Geographers.



Richard Jacobs has been appointed to the position of General Counsel at Pictometry International Corp. In this role, Jacobs will oversee rights management and licensing of Pictometry's vast global image library and will join the Company's Executive Management Team. Jacobs' prior legal experience includes positions with Ashland Inc. and Lexis-Nexis, a division of Reed Elsevier PLC (as well as its predecessor, Mead Data Central, Inc., a subsidiary of The Mead Corporation). While at Lexis-Nexis his roles included Vice President, Licensing and Deputy General Counsel, Vice President, Acquisitions and Deputy General Counsel and the establishment and management of licensing operations to support global expansion of a major online information publishing business during a period of rapid changes in the online publishing industry. In addition to expertise in intellectual property and licensing, he brings significant experience in commercial contracts and international distribution arrangements. Jacobs is a graduate of The Ohio State University where he earned a



bachelor's degree in economics and finance and a Master's of Business Administration degree in finance from the Fisher College of Business, and a Juris Doctor degree from the Moritz College of Law.

Scott Van Dermark has joined Wisser Company, LLC (Wisser) as Senior Vice President, Business Development. In this role, Van Dermark will lead Wisser's business development team's efforts in furthering the company's strategic growth and development within the Intelligence & Security Services, Information Technology Solutions, and Infrastructure Engineering markets. Van Dermark most recently served as the Vice President of Sales and Marketing for Fugro EarthData, Inc. where he directed all sales, marketing, and business development activities within the U.S. geospatial market. He brings over 23 years of geospatial business experience in the field of airborne and satellite remote sensing and is an expert in the application of electro-optical imaging, laser, and radar technologies in support of survey and mapping operations. Van Dermark attended the Community College of the Air Force, Joint Military Intelligence College, and Defense Mapping School and holds multiple certificates in intelligence and counterterrorism analysis.



Products

ERDAS has released ECW for ArcGIS Server, version 11.0.2. This product provides a means for ArcGIS Server to deliver data in the ERDAS-patented Enhanced Compression Wavelet (ECW) format to clients via OGC-compliant Web Coverage Service (WCS) and Web Map Service (WMS). Based on technology originally provided in ERDAS ECW/JP2 SDK version 4.2, ECW for ArcGIS Server enables ArcGIS Server to support ECW imagery, providing the fast decompression. Using minimal memory, ECW can quickly decompress and open massive files, in many cases faster than uncompressed imagery can be opened. Additionally, multi-resolution

level of detail is built into the file, eliminating the need to generate or distribute pyramids or overviews. The ECW technique does not require the creation and storage of intermediate tiles (RRDs), as they are an inherent part of the ECW format. ECW also supports opacity channels, allowing images to overlay other imagery cleanly without showing compression artifacts around the edges. A key enhancement in ECW for ArcGIS Server version 11.0.2 is backward compatibility with ArcGIS Server 9.3 and 9.3.1 in addition to the previously supported ArcGIS Server 10. ECW for ArcGIS Server version 11.0.2 also supports the use of European Petroleum Survey Group (EPSG) codes in ECWP. For information, visit www.erdas.com.

GeoCue Corporation announced the release of GeoCue 2011.1. Advanced enhancements to GeoCue 2011.1 include: native support for 64-bit Windows platforms; significantly enhanced coordinate reference system and datum support, including Horizontal Time Dependent Positioning (HTDP) and ground-grid models; automatic dispatched and distributed processing for local clouds; support for Web Mapping Services (WMS) backdrops in GeoCue Client, including native support for Open Street Map layers; completely new Table of Contents including nested folders and real-time shared layouts; new CuePacs for Intergraph's OrthoPro and Trimble's Rapid Ortho; and, many other new features aimed at improving project quality and reducing production wall-clock time. GeoCue products featured in this release include GeoCue Client, GeoCue Server, GeoCue Federator (Dashboard), and a family of workflow specific CuePacs. GeoCue customers under current maintenance agreements will automatically receive this significant upgrade.

QCoherent Software LLC recently previewed its impending release of the 2011.1 LP360 LIDAR product suite. LP360 includes an ArcGIS extension version as well as standalone versions with no CAD or GIS prerequisites. In addition to numerous new features, the company announced a renaming of the product set:

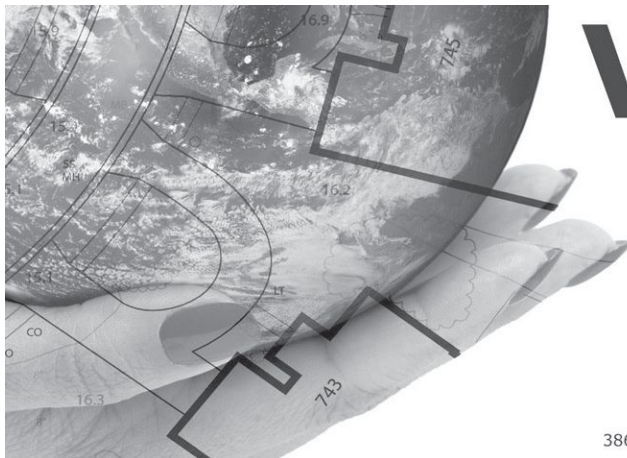
- LP360 Basic (formerly LP360) – Lidar data import, visualization, QC and product generation

- LP360 Standard (formerly Classify) – Adds interactive data classification, geometry-based classification, conflation, breakline and hydrologic enforcement tools to the Basic version
- LP360 Advanced (formerly Extractor) – Add algorithmic classification to the Standard version

Among the many new features are algorithmic tools (LP360 Advanced version) including: Low Points, Isolated Points, Ground Classifier, Statistical Noise, and Point group vectorization. In addition to a number of other new features, LP360 standalone is now available in a 64-bit version. Each license of LP360 32-bit or LP360 64-bit. QCoherent continues to offer its GeoCue integrated solutions for Quality Check/Edit (LP360 EQC) and railway feature extraction (LP360 RFX) through its OEM relationship with GeoCue Corporation. For information, visit www.geocue.com.

Services

Clark Labs of Clark University announced that two new tutorials have been added to the video series on its website. Both videos highlight functionality within the IDRISI software's modeling applications: Land Change Modeler and Earth Trends Modeler. The video entitled "REDD Baseline Modeling with Land Change Modeler in IDRISI," demonstrates its use for REDD—Reducing Emissions from Deforestation and Forest Degradation. Utilizing a case study from Conservation International, the video highlights how Land Change Modeler can be used to prepare the required maps of projected land change. The video entitled "Time Series Analysis with Earth Trends Modeler in IDRISI" provides an introduction to the Earth Trends Modeler application within IDRISI for the analysis of image time series. Earth Trends Modeler is a revolutionary earth observation software tool that allows you to model and analyze earth trends and ecosystem dynamics. The software is specifically developed for global change research and analysis. The videos are available at <http://www.clarklabs.org/resources/videos.cfm>.



Vr Mapping

The NEW Standard

- VrOne
- VrTwo
- VrLiDAR
- VrOrtho
- VrAirTrig
- VrLite
- VrMosaic
- VrBalance
- VrVolumes

386-439-2525 www.cardinalsystems.net

Cardinal Systems

Board of Directors

Officers

President

Gary Florence*
Photo Science, Inc.
gflorence@photoscience.com

President-Elect

Roberta Lenczowski*
scrumpski@sbcglobal.net

Vice President

Stephen D. DeGloria*
Cornell University
sdd4@cornell.edu

Past President

Carolyn J. Merry*
The Ohio State University
merry.1@osu.edu

Treasurer

Donald T. Lauer*
U.S. Geological Survey (Emeritus)
lauer@usgs.gov

Board Members

Alaska Region - 2013

Nicholas William Hazelton
AERO-METRIC Anchorage
nwjh@mac.com
<http://www.asprs.org/All-Regions/Alaska.html>

Central Region - 2014

Barry Budzowski
Western Air Maps
barryb@westernair.com
<http://www.asprs.org/All-Regions/Central.html>

Central New York Region - 2014

John T. Boland
ITT Industries Space Systems Division
john.boland@itt.com
<http://www.asprs.org/All-Regions/Central-New-York.html>

Columbia River Region - 2014

Chris Aldridge*
Continental Mapping Consultants
CAldridge@continentalmapping.com
<http://www.asprs.org/All-Regions/Columbia-River.html>

Eastern Great Lakes Region - 2014

Charles K. Toth
The Ohio State University
toth@cfm.ohio-state.edu
<http://www.asprs.org/All-Regions/Eastern-Great-Lakes.html>

Florida Region - 2013

Thomas J. Young
Pickett & Associates
tjyoung@pickett-inc.com
<http://www.asprs.org/All-Regions/Florida.html>

Geographic Information Systems Division - 2013

David Alvarez
HALCROW
davidalvarez76@gmail.com
<http://www.asprs.org/Divisions/GIS-Division.html>

Intermountain Region - 2013

Lucinda A. Clark
Draper, UT 84020
cclark@utah.gov
<http://www.asprs.org/All-Regions/Intermountain.html>

Lidar Division - 2012

Lewis N. Graham (Interim Director)
GeoCue Corp.
lgraham@niirs10.com
<http://www.asprs.org/Divisions/Lidar-Division.html>

Mid-South Region - 2013

Haluk Cetin
Murray State University
haluk.cetin@murraystate.edu
<http://www.asprs.org/All-Regions/Mid-South.html>

New England Region - 2012

Mark Brennan
BAE Systems
mark.brennan@baesystems.com
<http://www.asprs.org/All-Regions/New-England.html>

North Atlantic Region - 2013

David Stolarz
East Meadow, NY 11554
dstolarz@att.net
<http://www.asprs.org/All-Regions/North-Atlantic.html>

Northern California Region-2012

Lorraine Amenda
Towill, Inc.
Lorraine.Amenda@towill.com
<http://www.asprs.org/All-Regions/Northern-California.html>

Photogrammetric Applications Division - 2014

Douglas Lee Smith
David C. Smith & Assoc, Inc
Doug@davidsmithmapping.com
<http://www.asprs.org/Divisions/Photogrammetric-Applications-Division.html>

Potomac Region - 2014

Barbara A. Eckstein
L-1 MCLENDON
beckstein@surfbest.net
<http://www.asprs.org/All-Regions/Potomac.html>

Primary Data Acquisition Division - 2013

Robert E. Ryan
Stennis Space Center
rryan@I2Rcorp.com
<http://www.asprs.org/Divisions/Primary-Data-Aquisition-Division.html>

Professional Practice Division - 2012

Anne K. Hillyer
Bonneville Power Administration
akhillyer@bpa.gov
<http://www.asprs.org/Divisions/Professional-Practice-Division.html>

Puget Sound Region - 2012

Terry A. Curtis
WA DNR, Resource Map Sect.
terry.curtis@wadnr.gov
<http://www.asprs.org/All-Regions/Puget-Sound.html>

Remote Sensing Applications Division - 2012

Joseph Knight
University of Minnesota
jknight@umn.edu
<http://www.asprs.org/Divisions/Remote-Sensing-Applications-Division.html>

Rocky Mountain Region - 2012

Jeffrey M. Young
Centennial, CO 80115
jeffreymyoung@msn.com
<http://www.asprs.org/All-Regions/Rocky-Mountain.html>

Southwest U.S. Region - 2014

A. Stewart Walker*
BAE Systems
stewart.walker2@baesystems.com
<http://www.asprs.org/All-Regions/Southwest-US.html>

St. Louis Region - 2012

David W. Kreighbaum*
NGA
David.W.Kreighbaum@nga.mil
<http://www.asprs.org/All-Regions/St-Louis.html>

Sustaining Members Council Chair - 2013

Jim Green
Optech Incorporated
jim.green@optech.com
<http://www.asprs.org/About-Us/Sustaining-Members-Council.html>

Western Great Lakes Region - 2013

Douglas Fuller*
Sheboygan, WI 53081
FullerDoug@charter.net
<http://www.asprs.org/All-Regions/Western-Great-Lakes.html>

Division Officers

Geographic Information Systems

Director: David Alvarez
Assistant Director: TBA
<http://www.asprs.org/Divisions/GIS-Division.html>

Lidar

Interim Director: Lewis N. Graham
Assistant Director: TBA
<http://www.asprs.org/Divisions/Lidar-Division.html>

Photogrammetric Applications

Director: Douglas Lee Smith
Assistant Director: TBA
<http://www.asprs.org/Divisions/Photogrammetric-Applications-Division.html>

Primary Data Acquisition

Director: Robert E. Ryan
Assistant Director: Allen E. Cook
ITT Space Systems Division
allen.cook@itt.com
<http://www.asprs.org/Divisions/Primary-Data-Aquisition-Division.html>

Professional Practice

Director: Anne K. Hillyer
Assistant Director: Rebecca Morton
becky.morton@towill.com
<http://www.asprs.org/Divisions/Professional-Practice-Division.html>

Remote Sensing Applications

Director: Joseph F. Knight
Assistant Director: David Szymanski
Dave_Szymanski@alum.rit.edu
<http://www.asprs.org/Divisions/Remote-Sensing-Applications-Division.html>

Sustaining Members Council

Chair: Jim Green
Vice Chair: Brian Murphy
Northrup Grumman
brian.murphy@ngc.com
<http://www.asprs.org/About-Us/Sustaining-Members-Council.html>

*Executive Committee Member

- 3D Laser Mapping LTD**
Bingham, Nottingham, UK
www.3dlasermapping.com
Member Since: 2/2010
- Adageos Research LTD**
St John's, Newfoundland, Canada
Email: d.laprairie@nl.rogers.com
Member Since: 7/2010
- Aerial Cartographics of America, Inc. (ACA)**
Orlando, Florida
www.aca-net.com;
Member Since: 10/1994
- Aerial Data Service, Inc. (ADS)**
Tulsa, Oklahoma
www.aerialdata.com
Member Since: 8/1993
- Aerial Services, Inc.**
Cedar Falls, Iowa
www.AerialServicesInc.com
Member Since: 5/2001
- Aero-Graphics, Inc.**
Salt Lake City, Utah
www.aero-graphics.com
Member Since: 4/2009
- AeroMetric, Inc.**
Sheboygan, Wisconsin
www.aerometric.com
Member Since: 1/1974
- Aeroquest Optimal**
(formerly Optimal Geomatics Inc.)
Huntsville, Alabama
www.optimalgeo.com
Member Since: 2/2006
- AeroTech Mapping Inc.**
Las Vegas, Nevada
www.atmlv.com
Member Since: 8/2004
- AGFA Corporation**
Ridgefield Park, New Jersey
www.agfa.com
Member Since: 1/1990
- Air Photographics, Inc.**
Martinsburg, West Virginia
www.airphotographics.com
Member Since: 1/1973
- Airborne 1 Corporation**
El Segundo, California
www.airborne1.com
Member Since: 7/2000
- American Surveyor Magazine**
Frederick, Maryland
www.TheAmericanSurveyor.com
Member Since: 12/2004
- Applanix, A Trimble Company**
Ontario, Canada
www.applanix.com
Member Since: 7/1997
- Applied Imagery**
Silver Spring, Maryland
www.appliedimagery.com
Member Since: 4/2005
- ASD Inc.**
(formerly Analytical Spectral Devices)
Boulder, Colorado
www.asdi.com
Member Since: 1/1998
- Axis GeoSpatial, LLC**
Easton, Maryland
www.axisgeospatial.com
Member Since: 1/2005
- Ayres Associates, Inc.**
Madison, Wisconsin
www.AyresAssociates.com
Member Since: 1/1953
- BAE Systems**
San Diego, California
www.baesystems.com/gxp
Member Since: 7/1995
- Bohannon Huston, Inc.**
Albuquerque, New Mexico
www.bhinc.com
Member Since: 11/1992
- Booz Allen Hamilton**
Mc Lean, Virginia
www.boozallen.com
Member Since: 10/2004
- Cardinal Systems, LLC**
Flagler Beach, Florida
www.cardinalsystems.net
Member Since: 1/2001
- CRITIGEN**
(formerly CH2M HILL)
Redding, California
www.critigen.com
Member Since: 1/1974
- Clark Labs/Clark University**
Worcester, Massachusetts
www.clarklabs.org
Member Since: 10/1997
- COL-EAST, Inc.**
North Adams, Massachusetts
www.coleast.com
Member Since: 1/1976
- CRC Press - Taylor & Francis Group**
Boca Raton, Florida
www.crcpress.com
Member Since: 9/2006
- DAT/EM Systems International**
Anchorage, Alaska
www.datem.com
Member Since: 1/1974
- Dewberry**
Fairfax, Virginia
www.dewberry.com
Member Since: 1/1985
- DigitalGlobe**
Longmont, Colorado
www.digitalglobe.com
Member Since: 7/1996
- DiMAC sprl**
Gosselies, Belgium
www.dimac.eu
Member Since: 1/2004
- DMC International Imaging Ltd.**
Guildford, Great Britain
www.dmcii.com
Member Since: 3/2008
- Dudley Thompson Mapping Corp. (DTM)**
Surrey, Canada
www.dtm-global.com
Member Since: 9/2006
- Dynamic Aviation Group, Inc.**
Bridgewater, Virginia
www.dynamicaviation.com
Member Since: 4/2003
- Eagle Mapping, Ltd**
British Columbia, Canada
www.eaglemapping.com
Member Since: 1/1999
- Earth Eye, LLC**
Orlando, Florida
www.eartheye.com
Member Since: 7/2009
- Eastern Topographics**
Wolfeboro, New Hampshire
www.e-topo.com
Member Since: 8/1978
- Environmental Research Incorporated**
Linden, Virginia
www.eri.us.com
- ERDAS Inc. & Intergraph**
Norcross, Georgia
www.erdas.com
Member Since: 1/1985
- Esri**
Research Institute, Inc.
Redlands, California
www.esri.com
Member Since: 1/1987
- EUROSENSE**
Wommel, Belgium
www.eurosense.com
Member Since: 1/1982
- Federal Geographic Data Committee**
Reston, Virginia
www.fgdc.gov
Member Since: 1/1998
- Fugro EarthData, Inc.**
(was EarthData, Inc.)
Frederick, Maryland
www.earthdata.com
Member Since: 1/1994
- Fugro Horizons, Inc.**
(was Horizons, Inc.)
Rapid City, South Dakota
www.fugrohorizons.com
Member Since: 1/1974
- GeoBC, Crown Registry & Geographic Base Branch**
Victoria, Canada
www.geobc.gov.bc.ca
Member Since: 12/2008
- GeoCue Corporation**
(was NIIRS10, Inc.)
Madison, Alabama
info@geocue.com
Member Since: 10/2003
- GeoDigital International**
Hamilton, ON V8W 1R9
CANADA
www.geodigital.com
Member Since: 3/2011
- GeoEye**
(was ORBIMAGE Inc.)
Dulles, Virginia
www.geoeye.com
Member Since: 4/1995
- Geographic Resource Solutions**
Arcata, California
www.grsgis.com
Member Since: 12/2006
- Geolas Consulting**
Poing, Germany
www.geolas.com
Member Since: 1/2002
- Global Science & Technology, Inc.**
Greenbelt, Maryland
www.gst.com
Member Since: 10/2010
- GRW Aerial Surveys, Inc.**
Lexington, Kentucky
www.grwinc.com
Member Since: 1/1985
- Harris Corporation**
Melbourne, Florida
www.harris.com
Member Since: 6/2008
- HAS Images, Inc.**
Dayton, Ohio
www.hasimages.com
Member Since: 2/1998
- HyVista Corporation**
Castle Hill, Australia
www.hyvista.com
Member Since: 3/2010
- International Institute for Geo-Information Science and Earth Observation (ITC)**
Enschede, Netherlands
www.itc.nl
Member Since: 1/1992
- ISTS Americas Corporation**
Fremont, California
www.istsamericas.com
Member Since: 5/2010
- ITRES Research Limited**
Calgary, Canada
www.itres.com
Member Since: 1/2003
- ITT Visual Information Solutions**
Boulder, Colorado
www.itvis.com
Member Since: 1/1997
- Keystone Aerial Surveys, Inc.**
Philadelphia, Pennsylvania
www.keystoneaerialsurveys.com
Member Since: 1/1985
- Kim Geomatics Corporation**
Manotick, Ontario, Canada
bryerson@kimgeomatics.com
Member Since: 9/2007
- KLT Associates, Inc.**
Peabody, Massachusetts
www.kltassoc.com
Member Since: 11/1993
- Kucera International**
Willoughby, Ohio
www.kucerainternational.com
Member Since: 1/1992
- LaFave, White & McGivern, L.S., P.C.**
Theresa, New York
www.lwmlspc.com
Member Since: 1/1987

LizardTech

Seattle, Washington
www.lizardtech.com
Member Since: 10/1997

M.J. Harden Associates, Inc.

Mission, Kansas
www.mjharden.com
Member Since: 1/1976

MDA Geospatial Services, Inc.

Richmond, Canada
www.mdacorporation.ca
Member Since: 1/1992

MDA Information Systems, Inc.

(formerly MDA Federal Inc.)
Gaithersburg, Maryland
www.ndaus.com
Member Since: 1/1993 (rejoined in 2011)

Merrick & Company

Aurora, Colorado
www.merrick.com/gis
Member Since: 4/1995

Michael Baker Jr., Inc.

Beaver, Pennsylvania
www.mbakercorp.com
Member Since: 1/1950

NASA Earth Science Division

Washington, DC
www.appliedsciences.nasa.gov
Member Since: 1/2001

NavCom Technology, Inc.

Torrance, California
www.navcomtech.com
Member Since: 3/2004

New Tech Services, Inc.

Sugar Land, Texas
www.nts-info.com
Member Since: 3/2006

NGA-National Geospatial-Intelligence Agency-Bethesda

Bethesda, Maryland
www.nga.mil
Member Since: 11/2008

NOAA National Geodetic Survey

Silver Spring, Maryland
www.ngs.noaa.gov
Member Since: 7/2009

North West Group

Calgary, Canada
www.nwgeo.com
Member Since: 1/1998

Northrop Grumman

Chantilly, Virginia
www.northropgrumman.com
Member Since: 1/1989

NSTec, Remote Sensing Laboratory

Las Vegas, Nevada
www.nstec.com
Member Since: 7/2005

Observera, Inc.

Chantilly, Virginia
www.observera.com
Member Since: 7/1995

Office of Surface Mining

Denver, Colorado
www.tips.osmre.gov
Member Since: 3/2008

Optech Incorporated

Toronto, Canada
www.optech.ca
Member Since: 1/1999

PAR Government

Systems Corporation
Rome, New York
www.pargovernment.com
Member Since: 5/1992

PCI Geomatics

Ontario, Canada
www.pcigeomatics.com
Member Since: 1/1989

Photo Science, Inc.

Lexington, Kentucky
www.photoscience.com
Member Since: 7/1997

Pickett & Associates, Inc.

Bartow, Florida
www.pickett-inc.com
Member Since: 4/2007

Pictometry International Corp.

Rochester, New York
www.pictometry.com
Member Since: 5/2003

Pinnacle Mapping Technologies, Inc.

Indianapolis, Indiana
www.pinnaclemapping.com
Member Since: 7/2002

Pixxures, Inc.

Arvada, Colorado
www.pixxures.com
Member Since: 8/2006

POB Magazine

Troy, Michigan
www.pobonline.com
Member Since: 7/2006

Professional Surveyor Magazine –

Flatdog Media, Inc.
(formerly Reed Business-Geo)
Frederick, Maryland
www.profsurv.com
Member Since: 1/1998

QCoherent Software LLC

Colorado Springs, Colorado
www.qcoherent.com
Member Since: 9/2006

Radman Aerial Surveys

Sacramento, California
www.radaerial.com
Member Since: 1/1971

Riegl USA, Inc.

Orlando, Florida
www.rieglusa.com
Member Since: 11/2004

Robinson Aerial Survey, Inc. (RAS)

Hackettstown, New Jersey
www.robinsonaerial.com
Member Since: 1/1954

Sanborn

Colorado Springs, Colorado
www.sanborn.com
Member Since: 9/1984

Science Applications

International Corporation
Mc Lean, Virginia
www.saic.com
Member Since: 1/1987

The Sidwell Company

St. Charles, Illinois
www.sidwellco.com
Member Since: 1/1973

SimActive, Inc.

Montreal, Quebec, Canada
www.simactive.com
Member Since: 1/2010

Spatial Information Solutions

Starkville, Mississippi
www.spatialis.com
Member Since: 3/2010

Spectral Evolution

North Andover, Massachusetts
www.spectralevolution.com
Member Since: 10/2010

Stewart Geo Technologies

A Division of PropertyInfo Corporation
San Antonio, Texas
www.stewartgeotech.com
Member Since: 1/1978

Supresoft Corporation

San Jose, California
www.supresoft.com
Member Since: 4/2010

Surdex Corporation

Chesterfield, Missouri
www.surdex.com
Member Since: 1/1979

Surveying and Mapping (SAM), Inc.

Austin, Texas
www.saminc.biz
Member Since: 12/2005

TASC

Chantilly, Virginia
www.tasc.com
Member Since: 3/2010

TerraGo Technologies

Atlanta, Georgia
www.terragotech.com
Member Since: 12/2008

TerraSim, Inc.

Pittsburgh, Pennsylvania
www.terrasim.com
Member Since: 9/2003

Terratec AS

Lysaker, Norway
www.terratec.no
Member Since: 9/2004

Topcon Positioning Systems

Livermore, California
www.topconpositioning.com
Member Since: 3/2010

Towill, Inc.

San Francisco, California
www.towill.com
Member Since: 1/1952

Track'Air BV

Ej Oldenzaal, Netherlands
www.trackair.com
Member Since: 6/2001

Trimble Navigation Limited

(formerly INPHO GmbH)
Westminster, Colorado
www.trimble.com/geospatial
Member Since: 4/1994

Trimble Germany GmbH

Stuttgart, Germany
www.trimble.com/geospatial
Member Since: 7/2007

U.S. Geological Survey

Reston, Virginia
www.usgs.gov
Member Since: 4/2002

Urban Robotics, Inc.

Portland, Oregon
www.urbanrobotics.net
Member Since: 3/2008

USDA/National Agricultural Statistics Service

Fairfax, Virginia
www.nass.usda.gov
Member Since: 6/2004

Vexcel Imaging, GmbH

(a Microsoft Company)
Graz, Austria
www.microsoft.com/ultracam
Member Since: 6/2001

Virtual Geomatics

Austin, Texas
www.virtualgeomatics.com
Member Since: 2/2008

VisionMap LTD

Tel Aviv, Israel
www.visionmap.com
Member Since: 1/2010

Watershed Sciences, Inc.

Corvallis, Oregon
www.watershedsciences.com
Member Since: 7/2011

Wehrli & Associates Inc.

Valhalla, New York
www.wehrliassoc.com
Member Since: 5/1994

Wilson & Company, Inc.,

Engineers & Architects
Albuquerque, New Mexico
www.wilsonco.com
Member Since: 3/2007

Wiser Company, LLC

Murfreesboro, Tennessee
www.wiserco.com
Member Since: 7/1997

Woolpert LLP

Dayton, Ohio
www.woolpert.com
Member Since: 1/1985

XEOS Imaging Inc.

Quebec, Canada
www.xeosimaging.com
Member Since: 11/2003

Photogrammetric Engineering and Remote Sensing (*PE&RS*)

Instructions for Authors Submitting a Manuscript for Peer Review

Authors submitting a new manuscript for peer review should follow these instructions. Failure to do so will result in the manuscript being returned to the author.

INTRODUCTION: The American Society for Photogrammetry and Remote Sensing (ASPRS) seeks to publish in *Photogrammetric Engineering & Remote Sensing (PE&RS)* theoretical and applied papers that address topics in photogrammetry, remote sensing, geographic information systems (GIS), the Global Positioning System (GPS) and/or other geospatial information technologies. Contributions that deal with technical advancements in instrumentation, novel or improved modes of analysis, or innovative applications of these technologies in natural and cultural resources assessment, environmental modeling, or the Earth sciences (atmosphere, hydrosphere, lithosphere, biosphere, or geosphere) are especially encouraged. In addition, papers dealing with the practical or applied aspects for these disciplines will be published as “Applications” papers (see additional instructions below).

REVIEW PROCEDURES: Manuscripts are peer reviewed and refereed by a panel of experts selected by the Editor. A double-blind review procedure is used. The identities and affiliations of authors are not provided to reviewers, nor are reviewers’ names disclosed to authors. Our goal is to provide authors with completed reviews within 90 days of receipt of a manuscript by the Editor. Manuscripts accepted for publication will be returned to the author(s) for final editing before being placed in the queue for publication. Manuscripts not accepted will either be (1) rejected or (2) returned to the author(s) for revision and subsequent reconsideration by the review panel. Authors who do not revise and return a “to-be-reconsidered” manuscript within 90 days from receipt of reviews may have their manuscript withdrawn from the review process.

ENGLISH LANGUAGE: Authors whose first language is not English must have their manuscripts reviewed by an English-speaking colleague or editor to refine use of the English language (vocabulary, grammar, syntax). At the discretion of the Editor, manuscripts may be returned for English language issues before they are sent for review.

COVER LETTER: All submissions must also include a separate cover letter. All submissions must also include a separate cover letter. Please modify the sample Cover Letter found at <http://www.asprs.org/pers/CoverLetter> and then convert it to a PDF file.

It is important that we have the full names and titles (Dr. Russell G. Congalton not R. G. Congalton), complete mailing addresses, and email addresses of all the authors and any special instructions about the paper. Papers can not be submitted for review until this information is received by the editor. Also, the paper must be original work and not currently being considered for publication in any other journal. Finally, the authors must pay for any color figures in the manuscript and any page charges for articles longer than 7 journal pages. (Details on color costs can be found at <http://www.asprs.org/pers/ColorOrderForm>.)

“APPLICATIONS” PAPERS: A maximum of one “Applications” paper will be published each month as the last paper in the peer-reviewed section of *PE&RS*. The authors should follow all the instructions in this document. However, the “Applications” paper will be strictly limited to 7 journal pages. These papers will be peer-reviewed, but will emphasize the practical and applied aspects of our discipline. These papers must be identified by the author as an “Applications” paper in the cover letter and will be labeled as an “Applications” paper in the journal.

PREPARING A MANUSCRIPT FOR REVIEW: Authors must submit papers electronically in PDF format. Care must be taken to remove the author(s) name(s) from the electronic document. Please remove all author identification from the Properties of Microsoft Word before creating the PDF. Verify under Properties in Adobe Reader that your identity has been removed.

FORMAT REQUIREMENTS: Manuscripts submitted for peer review must be prepared as outlined below. Manuscripts that do not conform to the requirements described below will be returned for format revisions before they are sent for review.

- 1 TYPING:** All pages must be numbered at the bottom of the page. In addition, manuscripts must be single column and double-spaced. An 11 or 12-point font such as Times New Roman or Arial is preferred. Authors should use 8.5 by 11-inch or A4 International (210- by 297-mm) paper size, with 30-mm (1.25 inch) margins all around. For review purposes every part of the manuscript must be double-spaced, including title page/abstract, text, footnotes, references, appendices and figure captions. Manuscripts that are single-spaced or have no page numbers will be returned to authors.
- 2 PAPER LENGTH:** Authors are encouraged to be concise. Published papers are generally limited to 7-10 journal pages. A 27-page manuscript (including tables and figures), when typed as indicated above, equals about 7 journal pages. Authors of published papers will be charged \$125/page for each page exceeding 7 journal pages. These page charges must be paid before publication; without exception.
- 3 TITLE/ABSTRACT:** Authors should strive for titles no longer than eight to ten words. The first page of the paper should include the title, a one-sentence description of the paper’s content to accompany the title in the *PE&RS* Table of Contents, and the abstract. To facilitate the blind review process, authors’ names, affiliations, and addresses must be provided only in a separate cover letter, not on the title page. Authors should indicate both their current affiliation and, if different, their affiliation at the time the research was performed. Following the title and one-sentence and on the same page must be the abstract. All manuscripts submitted for peer review must include an abstract of 150 words or less. The abstract should include information on goals, methods and results of the research reported. The rest of the paper should begin on the second page.
- 4 FIGURES AND TABLES:** All figures and tables must be cited in the text. Authors should note that figures and tables will usually be reduced in size by the printer to optimize use of space, and should be designed accordingly. For purposes of peer review, figures and tables can be embedded in the manuscript. However, it should be noted that papers, once accepted, will require that all figures be included as separate files (see instructions for accepted papers) If the manuscript contains copyrighted imagery, a copyright statement must be included in the caption (e.g., ©SPOT Image, Copyright [year] CNES).
- 5 COLOR ILLUSTRATIONS:** Authors should use black and white illustrations whenever possible. Authors who include color illustrations will be charged for the cost of color reproduction. These costs must be paid before an article is published. Details on color costs can be found at

<http://www.asprs.org/pers/ColorOrderForm>. Authors should indicate in the cover letter that they have the funds to pay for any color figures in their paper.

- 6 **METRIC SYSTEM:** The metric system (SI Units) will be employed throughout a manuscript except in cases where the English System has special merit stemming from accepted conventional usage (e.g., 9- by 9-inch photograph, 6-inch focal length). Authors should refer to "Usage of the International System of Units," *Photogrammetric Engineering & Remote Sensing*, 1978, 44 (7): 923-938.
- 7 **EQUATIONS:** Authors should express equations as simply as possible. They should include only those equations required by an average reader to understand the technical arguments in the manuscript. Manuscripts that appear to have excessive mathematical notation may be returned to the author for revision. Whenever possible, authors are encouraged to use the Insert and Symbol capabilities of Microsoft Word to build simple equations. If that is not possible, the author must indicate in the cover letter which software was used to create the equations. *Microsoft Equation*, *Microsoft Equation Editor*, or *MathType* format should be used only if absolutely necessary. Equations must be numbered, but unlike tables, figures, color plates, and line drawings should be embedded in the text file.
- 8 **ELECTRONIC JOURNAL:** The ASPRS Journal Policy Committee discourages lengthy appendices, complex mathematical formulations and software programs. These will ordinarily not be published in the hardcopy version of *PE&RS*. However, these materials may be made available on the ASPRS web site (<http://www.asprs.org/>). Authors wishing to have supplemental material posted on the website after their paper is published should submit this material along with their manuscript. All supplemental material must be clearly labeled as supplemental material.
- 9 **REFERENCES:** A complete and accurate reference list is essential. Only works cited in the text should be included. Cite references to published literature in the text in alphabetical order by authors' last names and date, as for example, Jones (1979), Jones and Smith (1979) or (Jones, 1979; Jones and Smith, 1979), depending on sentence construction. If there are more than two authors, they should be cited as Jones et al. (1979) or (Jones *et al.*, 1979). Personal communications and unpublished data or reports should not be included in the reference list but should be shown parenthetically in the text (Jones, unpublished data, 1979). Format for references will be as follows:

BOOKS:

Falkner, E., 1995. *Aerial Mapping: Methods and Applications*, Lewis Publishers, Boca Raton, Florida, 322 p.

ARTICLES (OR CHAPTERS) IN A BOOK:

Webb, H., 1991. Creation of digital terrain models using analytical photogrammetry and their use in civil engineering, *Terrain Modelling in Surveying and Civil Engineering* (G. Petrie and T.J.M. Kenzie, editors), McGraw-Hill, Inc., New York, N.Y., pp. 73-84.

JOURNAL ARTICLES:

Meyer, M.P., 1982. Place of small-format aerial photography in resource surveys, *Journal of Forestry*, 80(1):15-17.

PROCEEDINGS (PRINTED):

Davidson, J.M., D.M. Rizzo, M. Garbelotto, S. Tjosvold, and G.W. Slaughter, 2002. Phytophthora ramorum and sudden oak death in California: II. Transmission and survival. *Proceedings of the Fifth Symposium on Oak Woodlands: Oaks in California's Changing Landscape*, 23-25 October 2001, San Diego, California (USDA Forest Service, General Technical Report PSW-GTR-184, Pacific Southwest Forest and Range Experiment Station, Berkeley, California), pp. 741-749.

PROCEEDINGS (CD-ROM):

Cook, J.D., and L.D. Ferdinand, 2001. Geometric fidelity of Ikonos imagery, *Proceedings of the ASPRS 2001 Annual Convention*, 23-27 April, St. Louis, Missouri (American Society for Photogrammetry and Remote Sensing, Bethesda, Maryland), unpaginated CD-ROM.

THESIS AND DISSERTATIONS:

Yang, W., 1997. *Effects of Spatial Resolution and Landscape Structure on Land Cover Characterization*, Ph.D. dissertation, University of Nebraska-Lincoln, Lincoln, Nebraska, 336 p.

WEBSITE REFERENCES:

Diaz, H.F., 1997. Precipitation trends and water consumption in the southwestern United States, USGS Web Conference, URL: <http://geochange.er.usgs.gov/sw/changes/natural/diaz/>, U.S. Geological Survey, Reston, Virginia (last date accessed: 15 May 2002).

- 10 **ACKNOWLEDGMENTS:** In keeping with the process of blind reviews, authors are asked not to include acknowledgments in manuscripts submitted for peer review. An acknowledgment may reveal a considerable amount of information for reviewers that is not necessary or desirable for their evaluation of the manuscript. After a manuscript is accepted for publication, the lead author will be encouraged to insert appropriate acknowledgments.

INFORMATION ON MANUSCRIPT REVIEW PROCEDURES: Corresponding authors of manuscripts submitted for review will receive an e-mail from the Editor acknowledging receipt of the manuscript. Details on *PE&RS* Manuscript Review Procedures can be found at <http://www.asprs.org/pers/ReviewProcedure>.

MANUSCRIPT SUBMISSION: All peer-reviewed manuscripts should be emailed to:

Dr. Russell G. Congalton, Editor-in-Chief
Photogrammetric Engineering & Remote Sensing
4 Ryan Way
Durham, NH 03824 USA
E-mail: russ.congalton@unh.edu; Tel.: (603) 862-4644

NOTE: Authors should NOT MAIL MANUSCRIPTS TO ASPRS HEADQUARTERS. This will cause the review to be delayed.

***Instructions last updated June 2011*

Quantifying Urban Landscape Water Conservation Potential Using High Resolution Remote Sensing and GIS

Fayek A. Farag, Christopher M.U. Neale, Roger K. Kjelgren, and Joanna Endter-Wada

Abstract

Research goals were to analyze patterns of urban landscape water use, assess landscape water conservation potential, and identify locations with capacity to conserve. Methodological contributions involved acquiring airborne multispectral digital images over two urban cities which were processed, classified, and imported into a GIS environment where landscaped areas were extracted and combined with property and water billing data and local evapotranspiration rates to calculate landscape irrigation applications exceeding estimated water needs. Additional analyses were conducted to compare classified aerial images to ground-measured landscaped areas, landscaped areas to total parcel size, water use on residential and commercial properties, and turf areas under trees when they were leafed out and bare. Results verified the accuracy and value of this approach for municipal water management, showed more commercial properties applied water in excess of estimated needs compared to residential ones, and that small percentages of users accounted for most of the excess irrigation.

Introduction

Competition over scarce water supplies has increased in the rapidly urbanizing Western United States. Building new supply structures to meet increasing urban demand is problematic economically, socially, and politically. Alternative solutions are water reallocation from irrigated agriculture, as urban water uses exercise higher-valued market demand (Pimentel *et al.*, 2004; Postel, 2000), and urban water conservation strategies (Carr and Crammond, 1995; Vickers, 2001). Re-allocating water from agricultural to urban uses comes at the cost of lost farmland, compromised national food security, and dislocations in agriculturally-dependent communities

Fayek A. Farag is with the National Water Research Center Strategic Research Unit, NWRRC, Egypt, and formerly with The Department of Biological and Irrigation Engineering, Utah State University, Logan, UT 84322.

Christopher M.U. Neale is with the Department of Civil and Environmental Engineering, Utah State University, 4105 Old Main Hill, Logan, UT 84322 (christopher.neale@usu.edu).

Roger K. Kjelgren is with the Department of Plants, Soils and Climate, Utah State University, 4820 Old Main Hill, Logan, UT 84322.

Joanna Endter-Wada is with the Department of Environment and Society, Utah State University, 5215 Old Main Hill, Logan, UT 84322.

(National Research Council, 1992; Postel, 2000). Increasingly, water re-allocation from agricultural to municipal use is being scrutinized on the basis of how much water is actually needed by urban areas and how efficiently urban areas use their existing water supplies. Determining urban water needs in relation to urban water use (i.e., identifying potential inefficiencies or waste) can reveal potential conservation savings that could help minimize competing demands on agricultural water as well as on a variety of environmental uses.

In urbanizing parts of the arid U.S. West, irrigation of outdoor landscapes consumes most municipal water, accounting for 50 percent or more of total annual urban-municipal potable water use (Kjelgren *et al.*, 2000). Nationally, it is estimated that approximately 30 percent of total annual municipal water consumption in the U.S. is used on urban landscapes (Solley *et al.*, 1998). Unlike indoor water use, outdoor landscape water use has not been rigorously quantified, but potentially conservable water, or capacity to conserve, can be quantified by comparing actual irrigation usage to estimated water needs (Endter-Wada *et al.*, 2008; Kjelgren *et al.*, 2010). Estimated water needs can be expressed in depth units, and can be determined from local cool-season reference evapotranspiration rate (ET_o). ET_o is a function of local air temperature, wind speed, humidity, and incoming solar radiation that drive evaporation, which is modified by a correction factor unique to a given plant type (Allen *et al.*, 1994). Actual landscape water use can be derived from water purveyor billing data measured in volumetric units. However, in order to compare estimated landscape water needs to actual usage, both ET_o and water use need to be expressed in common units.

Careful measurements of irrigated landscaped areas and determination of plant types are necessary for this conversion. Compared to large-scale agricultural production, measuring irrigated urban areas is difficult because of the wide range in sizes, shapes, and fragmentation of these areas, as well as diversity in plant material used and the types and functions of various landscapes (residential, commercial, institutional, public). Manual measurement is impractical on a large scale, and the great diversity of plant species used in urban landscapes makes area determination from conventional black and white or color aerial images

Photogrammetric Engineering & Remote Sensing
Vol. 77, No. 11, November 2011, pp. 1113–1122.

0099-1112/11/7711-1113/\$3.00/0
© 2011 American Society for Photogrammetry
and Remote Sensing

difficult (Kjelgren *et al.*, 2000). Most satellite multispectral images have too low a spatial resolution for this functional use in urban areas.

The purpose of this paper is to present research findings which demonstrate that high-resolution airborne multispectral imagery can be used to determine irrigated landscaped areas and aid in quantifying urban water conservation potential. Images can be taken over a large area with high spatial resolution, and different vegetation types can be classified based on their spectral properties. A geo-rectified and classified aerial image can then be imported into a geographic information system (GIS) environment and integrated with municipal databases to extract irrigated landscaped areas for individual properties or water users. We argue that this methodology could be employed by water agencies to assess potentially conservable water on both an aggregate (e.g., municipal) and an individual (e.g., customer) basis.

Our research is based on a conceptual approach that uses airborne multispectral imagery to obtain irrigated landscape areas that, when combined with local reference evapotranspiration data, can be used to estimate reasonable, area-specific urban vegetative water demand. The estimated water demand is compared to actual landscape water use by parcel, obtained by mining water supplier billing data. This approach is used to determine potentially conservable landscape irrigation water and to identify end users with high capacity to conserve. This methodological approach is a key component in a trajectory of interdisciplinary research designed to investigate site characteristics and human behaviors affecting urban water use (Endter-Wada *et al.*, 2008; Kilgren *et al.*, 2010).

Methods

Study Areas

Research was conducted in two suburb cities of Salt Lake City, Utah and one northern Utah community. The City of Layton, approximately 35 km north of Salt Lake City (population in 2000 of about 58,000) was the initial project study area. Layton was selected for study as it is rapidly urbanizing, and yet retains older areas that may vary in landscaped area and landscape water use characteristics. We focused on a section of the city, approximately 17 km² that encompassed newer and older residential areas, as well as commercial-industrial and institutional (CII) areas. All customers in this area relied on municipally-supplied culinary water and did not have access to landscape water from secondary irrigation systems. A second suburb of Salt Lake City, the City of West Jordan, was additionally selected in order to validate the image analysis process and assess if the landscaped area and water use trends observed in Layton might be representative of other urban areas in Utah. West Jordan (population in 2000 of about 68,000), located approximately 15 km southwest of Salt Lake City, is mostly residential but with a fast-growing commercial district and covers an area of 80 km². Research conducted in Logan, Utah, approximately 120 km north of Salt Lake City, determined the percentage of turf grass shaded by tree cover. The area of tree canopy in relation to underlying turf area needs to be taken into consideration when estimating the demand for urban irrigation water. Findings from the Logan research were integrated into the calculations of landscape water needs.

Image Acquisition

Multispectral airborne digital images of Layton were taken in August 1998, and repeated for both Layton and West

Jordan in August 2000 using an airborne multispectral digital imaging system (Cai and Neale, 1999; Neale and Crowther, 1984). This system consisted of three Kodak Megaplug 4.2i digital cameras using Nikon 20 mm lenses with interference filters forming spectral bands in the green (0.545 to 0.555 μm), red (0.665 to 0.675 μm) and near infrared (NIR) (0.790 to 0.810 μm) wavelengths mounted in a Piper Seneca II aircraft, dedicated to remote sensing research. The cameras were computer controlled using in-house software. The multispectral images were acquired at 1-meter pixel resolution. In the Logan research (quantifying shaded turf areas under trees), images were acquired at 0.5-meter pixel resolution on 20 May 1999, early enough in the growing season that leaf cover from trees and shrubs was minimal. Images were taken again on 16 September 1999, at the end of the growing season when trees and shrubs were at full leaf cover.

Image Processing

The individual images were corrected for lens vignetting effects and geometric radial distortions, using the same calibration techniques from a previous generation of the airborne digital system developed by Neale and Crowther (1994) and described by Sundararaman *et al.* (1997) for airborne multispectral video images. The removal of the lens vignetting effects in the imagery minimizes image-to-image brightness variations, allowing for the mosaicing of overlapping images along flight lines with no perceivable seams.

The spectral images were then registered into 3-band images and rectified individually to digital 7.5-minute orthophotos quads (1:24 000) with 1-meter pixel resolution, using the Universal Transverse Mercator (UTM) projection and a root mean square error for the transformation of less than 1 meter. The rectified images were mosaiced along the flight lines into image strips of six to ten images each. The strips were joined together into large image mosaics covering the entire study area in each research location (Layton, West Jordan, and Logan). The final images were re-projected to the Utah State Plane coordinate system to match the GIS parcel boundary layers provided by the respective cities.

The 3-band image strips along each flight line were calibrated in terms of reflectance through the ratio of outgoing over incoming radiation. Outgoing radiation was obtained using system calibration curves relating image digital numbers with radiance (W/m²) (Neale and Crowther, 1994). Incoming solar irradiance was measured with an Exotech radiometer with similar spectral bands to the airborne digital cameras, placed at nadir over a leveled barium sulfate standard reflectance panel with known bi-directional reflectance properties (Jackson *et al.*, 1992) located in central locations in each study area. The Exotech radiometer was sampled every minute throughout the image acquisition period using a CS21X data logger synchronized to the GPS time stamp of the airborne system digital images (Chavez *et al.*, 2005; Crosby *et al.*, 1999). Each 3-band image strip was thus calibrated prior to the formation of the final mosaics covering the entire research areas.

Image Classification

Spectral signatures of ground surface classes of interest were extracted and on-site verification through ground measurements and observations were conducted using laminated printed portions of the multispectral mosaics, marked up to indicate the different surface classes visible in the imagery. In agricultural areas adjacent to Layton, signatures from identifiable crop types, evaluated as to stage of growth, were extracted. In the urban areas, the classes trained represented the turf grass, trees, shrubs and other landscape features, physical structures and shadows. Several dozen signatures

were extracted visually and iteratively from each mosaic to cover most agricultural and urban surface classes, using the seed property method of the ERDAS Imagine® (version 8.4; Leica Geosystems; Norcross, Georgia) with the appropriate spectral Euclidian distance.

The high spatial resolution of the airborne digital images complicated the signature extraction and classification. Several spectral signatures were needed in the training set to represent a specific surface's illumination or vegetation density variations. For example, darker reflectance values for shaded portions of trees and large shrubs could lead to misclassifications and thus were extracted as a separate class. Class spectral separability, a statistical measure of distance between two signatures, was studied using the Transformed Divergence Index (TDI) method within ERDAS Imagine® (ERDAS, 1999). For the Euclidean distance evaluation, the spectral distance between the mean vectors of each pair of signatures was computed and evaluated for significance.

The transformed divergence has lower and upper bounds of 0 and 2,000, respectively. If the calculated divergence for a signature pair is equal to the upper bound, then the signatures are considered to be totally separable in the spectral band combination being used (in our case, the three bands of the airborne multispectral system). A calculated divergence of zero means that the signatures are inseparable and should be either merged or one of them discarded. For the classification of the Layton mosaic, signatures below a TDI value of 1,500 were discarded while signatures above 1,500, such as those for trees and shrubs, were added to capture the nuances in variability due to bi-directional effects. TDI values above 1,800 were accepted with little confusion and high relative confidence of separability between the signatures.

Images were iteratively classified using the maximum likelihood scheme. Surfaces with spectral reflectance not encompassed within the selected signatures were successively set as "unclassified" in the classification and the signatures corresponding to the unclassified area re-assessed to the individual pixel level and incorporated to the signature set after every iteration. The final classified image was created by forcing the remaining unclassified pixels into the class with the most similar signature. After filtering using a 3×3 majority filter to remove "salt-and-pepper" pixels, the resulting several dozen classes were re-coded into specific basic classes. The recorded classes were "grass," "trees and shrubs," "concrete," "asphalt," "bare soil," "shadow," "water," and "meadow."

An accuracy assessment was conducted on the urban portion of the classified image product. A stratified random sampling scheme in ERDAS Imagine® was used to generate 217 random points on the classified image, proportional to class surface area present. The urban surface class corresponding to each point was verified on 2006 NAIP (National Agricultural Inventory Program) color, digital orthophotography of the same area. Because of the changes that occurred in some portions of the imagery between the date of multispectral image acquisition (1998 and 2000) and the NAIP image acquisition, 60 points of the 210 had to be verified by visual interpretation of the multispectral image itself. A contingency table was built with this information which allowed for calculation of the errors of omission and commission (Congalton, 1991).

GIS Landscape Area Extraction

Residential and commercial (CII, or "commercial-industrial-institutional") GIS layers were obtained from Layton and West Jordan cities. These layers contained parcel boundaries, streets names, parcel tax identification numbers, and

other information. The Layton residential layer divided parcels into subdivisions or neighborhood areas, designated by name, while the West Jordan layer did not. The Layton commercial GIS overlays were out of date and thus were not usable. The layers were matched to the projection of the high-resolution multispectral mosaic and its classified rendition. In addition, residential and commercial water billing data were also obtained from Layton for 1996 to 2001, and from West Jordan for 2000 and 2001.

The GIS parcels layer was overlaid on the recorded classified images imported to ArcInfo® (version 8; Esri, Inc.; Redlands, California) in GRID format. Water billing database files were linked to the GIS database for both cities using property tax ID number as the common attribute. Within the Layton study area, the number of GIS parcel boundary records we were able to join to residential water billing records varied by year (initially with 1,000 in 1997, but up to 2,800 by 2001) due to updates and changes in the water billing database. We also randomly selected approximately 2,000 residential parcels in West Jordan from the entire city to match Layton residential numbers for 2000 and 2001. Two hundred and thirty-one CII parcels with landscapes were identified within the Layton study area for analysis, and again a similar number of commercial parcels were randomly selected from West Jordan City.

Remotely sensed landscape area accuracy was assessed by regressing against ground-measured landscape areas. In Layton, 53 residential parcels were randomly selected and a walk-behind measuring wheel was used to physically measure dimensions for calculating total lot size and landscaped area. Contiguous shrub areas were physically measured on the ground separately from turf, and irregularly shaped areas beyond simple rectangles or circles were approximated as rectangles. All Layton CII parcels were similarly hand measured but could not be related to GIS-derived areas for lack of an accurate parcel layer, but in West Jordan we were able to link 73 GIS-derived cases, with up-to-date parcel layers, to hand-measured commercial properties. Water billing data collection frequency varied between cities, and between residential and CII areas. All West Jordan and Layton CII parcels had monthly water billing data, while Layton residential billing data were bi-monthly; all water billing data were in volume (gallon) units. All parcels, except for several institutional landscapes, were served by a single water meter and thus indoor water use and outdoor landscape water consumption volumes were combined and could not be directly separated. Since plant dormancy and low temperatures preclude winter irrigation in Utah, we assumed that average monthly winter (December through February) billed water use was exclusively indoors and further assumed that indoor use is constant year round. We estimated landscape water use by subtracting the derived indoor water use from monthly or bi-monthly billed water use during the potential (April through October) irrigation growing season (Endter-Wada *et al.*, 2008). Non-landscape seasonal outdoor water use, for features such as swimming pools, was assumed to be negligible, and CII users with seasonally variable or unusually high non-landscape water use, such as car washes, were excluded.

Parcel landscape area was extracted from the classified and recorded image within the GIS database. The area of each surface cover was obtained by GIS analysis using the tabulated-areas method to obtain the areas of one theme within the zones of another. Total landscaped area was then calculated as the sum of the three turf class areas (good growth, stressed grass, and sparse cover grass) and the tree and shrub class areas, and the output tables were joined with water billing data through the common identifier of tax

ID. Water volume applied to landscapes was extracted from billing data, as described above, and normalized to depth units by dividing by GIS-derived landscaped areas.

Data Analysis

Descriptive statistics were calculated for the percentage area of good, stressed, and sparse grass, as well as for trees and shrubs. Total landscaped area, total parcel size, and percent landscaped area were also analyzed. GIS-derived landscape areas were regressed against landscape areas obtained from on-site ground measurements for verification. GIS-derived landscaped areas were then regressed on total parcel size (ground-measured for Layton CII; GIS parcel boundaries for the others) to evaluate the potential for estimating landscaped areas from total parcel size for the subsets of residential properties in both cities, but for all CII properties within the study areas.

The frequency distribution of percent turf coverage was determined for CII and residential landscapes in Layton and West Jordan. We also calculated frequency distribution for the fraction of total seasonal water use within 500 mm increments of water consumption for CII and residential parcels in Layton (1998 billing data) and West Jordan (2000 billing data) during the period 01 June 1 through 30 September when data were most complete. This period of water consumption was chosen because the two-month residential billing period for Layton limited the availability of reliable irrigation season data to only two billing periods during the growing season of June/July and August/September. Consequently, we constrained the water billing data for Layton CII, and West Jordan residential and CII, to the same four-month time period in order to compare results.

Capacity to conserve water used on landscapes is the difference between water actually applied and water needed which is based on a reasonable estimate of landscape evapotranspiration. Estimated landscape water need is based on local reference evapotranspiration, or ET_0 (Allen *et al.*, 1998), that integrates radiation, air temperature, humidity, and wind into calculated water loss for a hypothetical uniform cool-season turf grass surface for a fixed set of plant characteristics. ET_0 generally ranges from 0 to 6 mm/day in northern Utah, when constraints are not imposed by non-uniform urban conditions (Snyder and Eching, 2005). The product of local ET_0 and an empirical-fractional plant correction factor (Kc; reflecting variable plant characteristics) proportional to plant water needs is the depth of estimated water needs for a regional area defined by the position of the weather station used to calculate local ET_0 . Empirical Kc values are not seasonally well defined for turf, but an intra-seasonal value of 0.8 is commonly used for cool season turf grass (Kneebone *et al.*, 1992). While precise empirical Kc values defined for trees and shrubs require additional research, a value of 0.5 is reasonable (Montague *et al.*, 2004; Costello *et al.*, 1992).

Our initial approach to quantifying capacity to conserve was a frequency distribution end user applied water depth (per parcel, seasonal water use divided by GIS-derived total landscape area) for Layton and West Jordan residential and CII end users for 1998 and 2000, respectively (image acquisition years). Capacity to conserve was identified in those users applying water above a ceiling threshold of estimated needs, defined by seasonal ET_0 (years 1998 and 2000 for Layton and West Jordan, respectively) multiplied by 0.8 Kc that assumes a uniform turf grass surface (Endter-Wada *et al.*, 2008; Kilgren *et al.*, 2010). We constrained seasonal ET_0 to June through September to match the constrained billing data. We did not subtract rainfall, in order to provide a generous estimate from the user point of view, or include an

empirical correction factor for irrigation system non-uniformity because the study did not include on-the-ground irrigation system assessments (Solomon *et al.*, 2007).

Here, we calculated capacity to conserve on an aggregate volume basis. Volume of estimated water need was calculated for each end user parcel using the following equation:

$$V_{\text{water needs}} = \frac{A_{\text{total}} \times ET_0 \times Kc_l}{E_i} \quad (1)$$

where $V_{\text{water needs}}$ is the estimated volume of landscape water needs for given end user, A_{total} is total landscaped area, ET_0 is reference water loss (mm/time period; in this case, the constrained June through September billing periods and data obtained from nearby weather stations in Layton and West Jordan), Kc_l is a composite landscape correction factor that integrates the different Kc values for turf, shaded turf and trees, and shrubs. Finally, E_i is the estimated efficiency of irrigation application where a value of 0.85 was used and chosen to give a more generous estimate of landscape water needs. Kc_l can be further defined such that:

$$Kc_l = \left(\frac{A_{\text{turf}} \times K_{\text{turf}}}{A_{\text{total}}} \right) + \left(\frac{A_{\text{ts}} \times (1 - T_{\text{sh}}) \times K_{\text{ts}}}{A_{\text{total}}} \right) + \left(\frac{A_{\text{ts}} \times T_{\text{sh}} \times K_{\text{turf}}}{A_{\text{total}}} \right) \quad (2)$$

where, A_{turf} , A_{ts} , and A_{total} , are the areas (m^2) of turf grass, trees and shrubs, and total landscape respectively; T_{sh} is the fraction of shaded turf grass under tree canopies; K_{turf} and K_{ts} are the previously defined Kc values for turf and trees/shrubs (0.8 and 0.5, respectively). We assumed a Kc value of 0.8 for turf under trees under the assumption that reduced water loss in shaded turf is compensated by the water loss in overlaying tree canopy. The resulting $V_{\text{water needs}}$ from Equation 1 will vary largely with A_{total} , as Kc_l will vary within the range of 0.5 for an all woody plant landscape to 0.8 for an all-turf grass landscape.

Results and Discussion

Plate 1a shows the location of the Layton study area with the calibrated multispectral mosaic of the research area and the surrounding agricultural fields (Plate 1b). The classified rendition of the image is also shown (Plate 1c) with the property boundary layer used for the extraction of the overlaid landscape vegetation areas. The accuracy assessment of the classified and recoded product is shown in Table 1 including only the urban vegetation classes and bare soil. The overall accuracy was 89 percent, similar to classification accuracy results obtained by Neale *et al.* (2007) for wetland habitats using a similar type of imagery and methodology. Some spectral confusion occurred between the trees and shrubs class and the grass classes, but overall, the results were similar to those obtained by Thomas *et al.* (2003) for an urban setting resulting from the classification of airborne multispectral imagery at the same pixel resolution. The classification accuracy would have been reduced if the impervious surface classes had been included (asphalt, roofs, concrete, etc.) due to the spectral variability of these classes within the urban setting.

Landscaped areas derived from the digital imagery through GIS analysis correlated with those derived from ground truth measurements (Figure 1). For Layton residential parcels over a range of landscaped areas of 200 to 1,200 m^2 , the relationship was reasonable ($r^2 = 0.74$), but still somewhat unexpectedly low. Similarly, correlation of GIS-derived commercial landscaped areas to ground

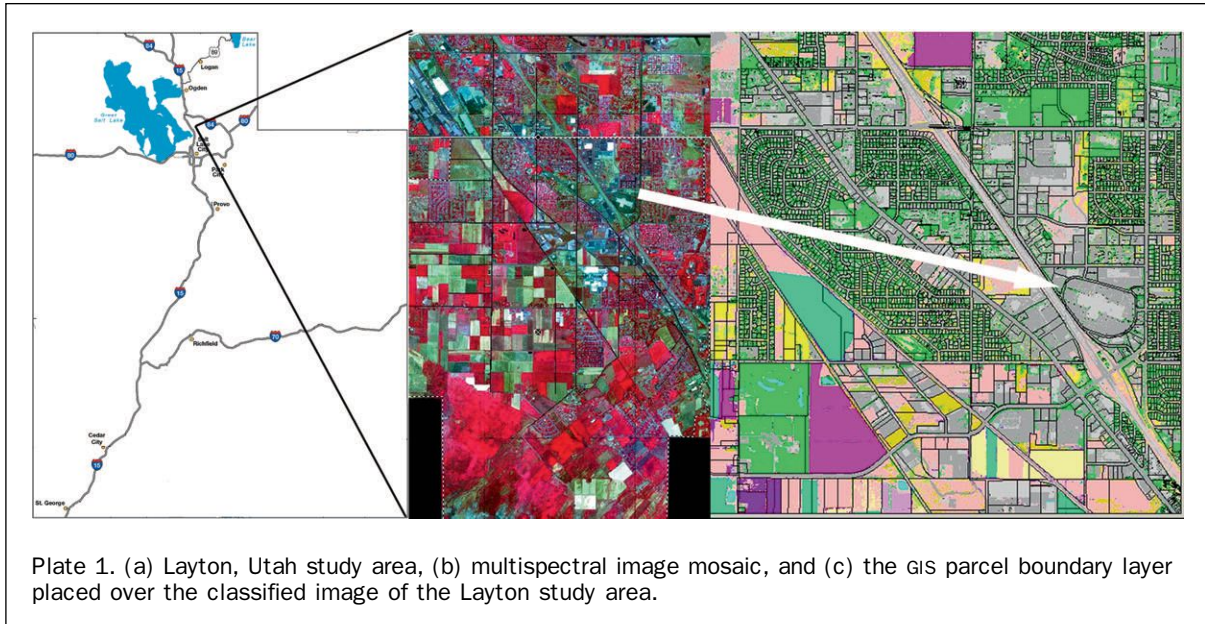


TABLE 1. ACCURACY ASSESSMENT OF THE CLASSIFIED IMAGE PRODUCT INCLUDING ONLY THE URBAN VEGETATION CLASSES

Classified Data	Good Grass	Sparse Grass	Stressed Grass	Trees & Shrubs	Bare Soil	Errors of Commission	
						Row Total	% Correct
Good Grass	58	4	1	2	0	65	89.2
Sparse Grass	4	22	0	2	0	28	78.6
Stressed Grass	0	1	44	4	3	52	84.6
Trees And Shrubs	0	1	0	27	0	28	96.4
Bare Soil	0	1	0	0	36	37	97.3
Column Total	62	29	45	35	39	210	
Errors of Omission							
% Correct	93.5	75.9	97.8	77.1	92.3		187.0
Total Error							89.0

measurements in the City of West Jordan also showed scatter within the range of smaller landscapes, but the large range of landscaped areas up to 30,000 m² yielded a close fit ($r^2 = 0.96$). The scatter at the lower end of the range for the commercial landscapes, as well as the scatter observed for the residential areas, is possibly due to the limits of the 1-meter imagery resolution and uncertainty in the parcel boundary layer. These factors would give greater weight to errors in smaller, fragmented landscapes than would be the case for larger, contiguous landscapes characteristic of large parcels in the Salt Lake City metropolitan region. Possible errors in landscape ground measurements could have also contributed to the scatter, particularly related to the difficulty of measuring irregular shaped landscape areas on the ground. However, given that the residuals in Figure 1a were normally distributed, it appears that errors in remotely sensed and ground measured landscape areas were random. We think these reasonable relationships between ground-measured GIS-derived landscaped areas imparted enough confidence to conduct further analyses using the GIS-derived landscaped areas.

Since parcel size is a key element in municipal construction permitting and property taxation, this information is generally readily available. Landscaped area parameterized as a function of total parcel size can be developed into a model and ultimately a functional tool, when remote

sensing is not possible, to estimate irrigated landscape area. We tested the relationship between GIS-derived landscape area and GIS-derived total parcel area (Figure 2) and found a modest-to-good fit for residential Layton and West Jordan ($r^2 = 0.48$ and 0.91 , respectively), but each relationship exhibited unique properties. As parcel size increased, Layton residential landscape areas formed an upper threshold, under which there was substantial scatter. Since this residential study area contained a large percentage of older homes in subdivisions (dating back to 1940), it included more parcels that had been converted to other non-vegetated uses, such as patios, decks, and building additions. In West Jordan, average parcel size was much larger than in Layton, with upper bounds of nearly 5,000 m² versus 1,400 m². The landscape area to parcel size relationship became weaker above 2,000 m², because the randomly selected residential parcels above this range were higher-income custom-built homes with larger landscaped areas that were customized and irregular rather than standardized, as in a subdivision. Future regression analyses conducted in sections of cities and incorporating census and demographic information could better explain outliers and further refine these data into more robust relationships.

Landscaped area and parcel size for CII parcels in Layton and West Jordan were not statistically related in any meaningful way. Isolated large parcels defined the fit and

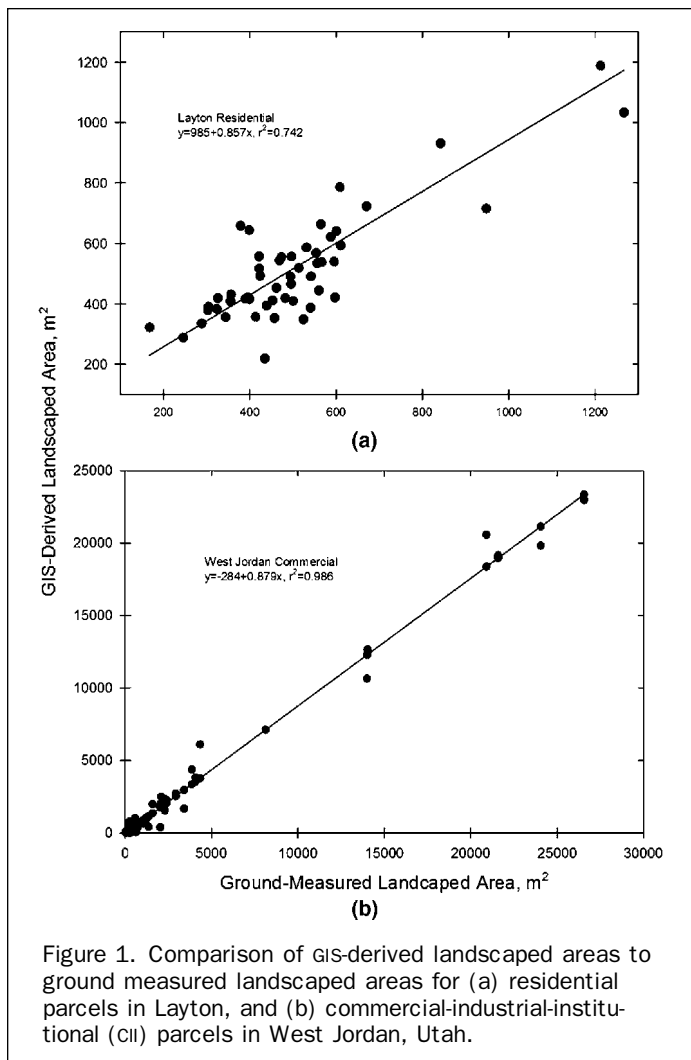


Figure 1. Comparison of GIS-derived landscaped areas to ground measured landscaped areas for (a) residential parcels in Layton, and (b) commercial-industrial-institutional (CII) parcels in West Jordan, Utah.

increased the r^2 values but substantial scatter made the relationships less predicatively useful. The high degree of variability amongst the majority of the CII parcels for both cities suggests that trying to predict landscape area from parcel size would be difficult. Compounding this difficulty would be CII landscape regulations that would vary from municipality to municipality, likely rendering a robust, widely-applicable, predictive model nearly impossible. Thus, the use of high-resolution multispectral imagery to quantify landscaped areas on an individual parcel basis would be an advantage for determining CII irrigated landscaped areas.

The amount of landscaped area in turf varied between the Layton residential and the other three groups (Figure 3). CII landscapes, and West Jordan residential landscapes, all showed somewhat to heavily right hand-skewed frequency distributions in terms of the number of parcels with high turf, and low tree-shrub coverage. West Jordan residential parcels showed a relatively even distribution (12 to 15 percent of the total population for each bin) in the 51 to 90 percent turf coverage range, with a sharp decline in the fraction of water users with turf coverage below 50 percent. West Jordan CII parcels showed a similar percentage of the population having more turf coverage than tree and shrub coverage. Since turf has higher water use and a shallower root zone than trees, quantifying parcels with high turf area is potentially diagnostic and predictive of higher water use.

The skewed distribution of the fraction of parcels with high turf coverage is much sharper for CII parcels in Layton, with about 60 percent of all the parcels falling in the range of 81 to 100 percent turf coverage. This different distribution is due, in part, to a larger number of institutional landscapes within the Layton study area, such as parks and schools that are largely turf grass and used for recreational purposes, and to a larger number of industrial business landscapes where the easiest type of landscape coverage is turf grass that lends itself to uncomplicated irrigation and maintenance. In contrast, the largest fraction of residential parcels in Layton had 41 to 50 percent turf coverage, with a roughly normal distribution on either side. This lower amount of turf grass is due to the many older landscapes in the Layton study area that had mature trees covering more of the landscaped area. An analysis (data not shown) of neighborhood age in Layton showed that about half were older than 20 years at the time of the study. A high proportion of tree cover has water conservation policy implications. Urban trees represent a significant time and financial investment and produce water (as well as energy) savings as they mature and provide shade. Tree water needs during drought should be factored into conservation measures to reduce risk of tree loss, help ensure water user acceptance and compliance, and avoid liability concerns.

Tree cover may include turf growing under the tree canopy, however. The Logan research was conducted on imagery from three residential neighborhoods on the Logan bench and one cemetery selected for analysis because of the diversity and maturity of the trees. After image classification using the same techniques described above, the areas of turf and trees were extracted from the imagery acquired at two different dates in the growing season and shown in Table 2. The average amount of turf under tree canopy weighted according to the size of the section areas analyzed was 34 percent. This overlapping coverage also means that water consumed through evapotranspiration is from a combined turf/tree system and was taken into account in our landscape water need calculations.

Seasonal (01 June through 30 September) water applied to landscapes (year 1998 for Layton; year 2000 for West Jordan) varied the most between residential and CII users in both cities (Figure 4). The largest fraction of residential water users in both Layton (90 percent) and West Jordan (80 percent) used below 1,000 mm/year, showing a sharp left hand distribution. Again, because the residential neighborhood areas in Layton were older, there were fewer automated sprinkler systems and more manual irrigation, which led to lower overall water use (Endter-Wada *et al.*, 2008). In West Jordan, there was a higher percentage of new parcels with automated systems (characteristic of the area), likely leading to higher irrigation application amounts. Average cumulative reference evapotranspiration (Allen *et al.*, 1994) for the Salt Lake City region is approximately 750 mm. Allowing for irrigation non-uniformity that increases water needs (Kjelgren *et al.*, 2000), 1,000 mm of water applied to landscapes can be justified. Thus, the majority of residential water users in Layton and West Jordan appeared to be relatively efficient at irrigating their landscapes. CII parcels exhibited something similar to a bimodal pattern of water use, with only 40 to 45 percent of the total number of parcels using less than 1,000 mm. Both cities had a long tail at the high end of water use for CII parcels where 17 percent of the West Jordan and 7 percent of the Layton CII parcels used in excess of 5,000 mm of water. These potentially excessive water users are most likely businesses with automated systems where water use is not closely monitored; such systems have been shown to contribute to excess irrigation (Endter-Wada *et al.*, 2008; Kilgren *et al.*, 2010).

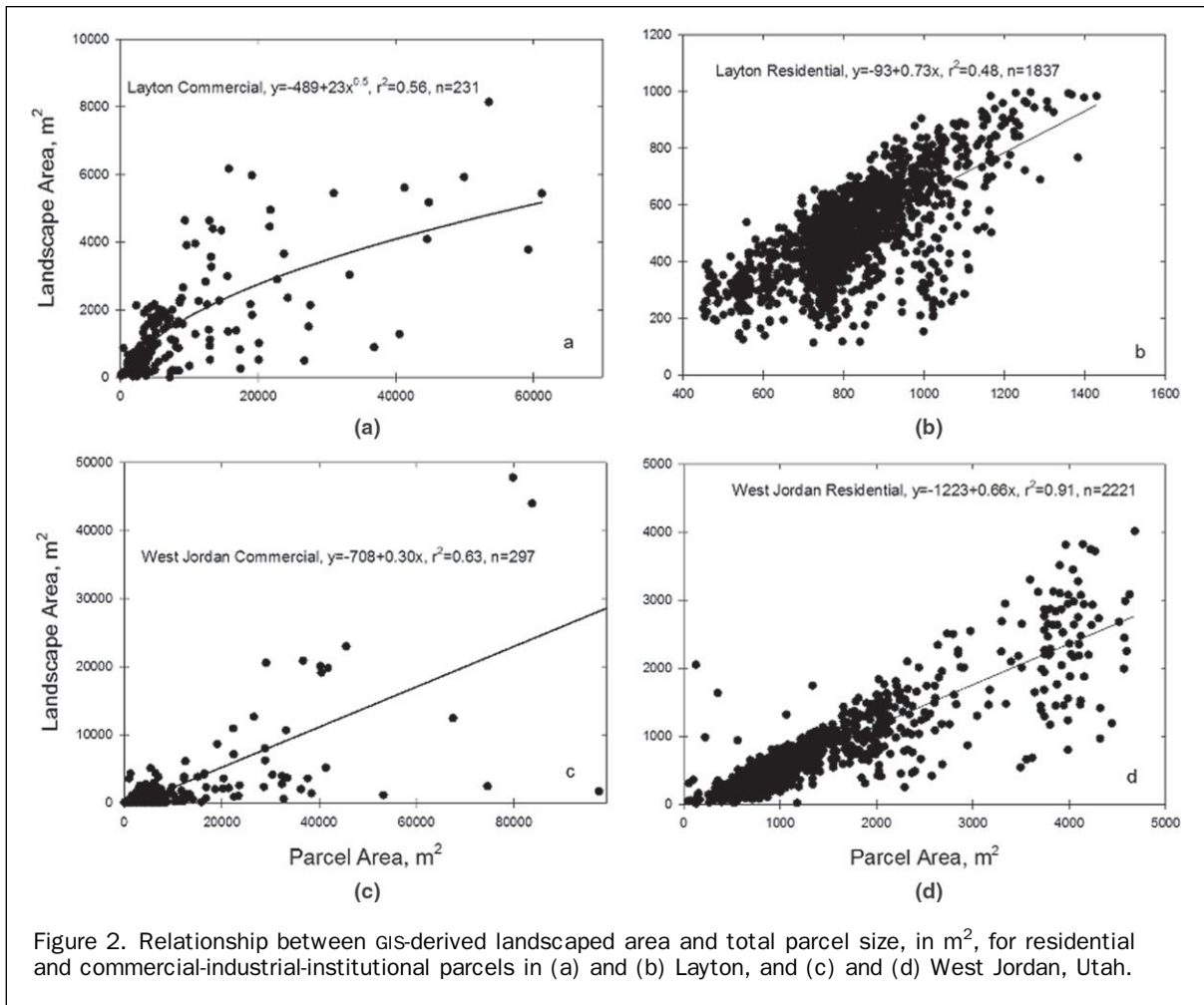


Figure 2. Relationship between GIS-derived landscaped area and total parcel size, in m², for residential and commercial-industrial-institutional parcels in (a) and (b) Layton, and (c) and (d) West Jordan, Utah.

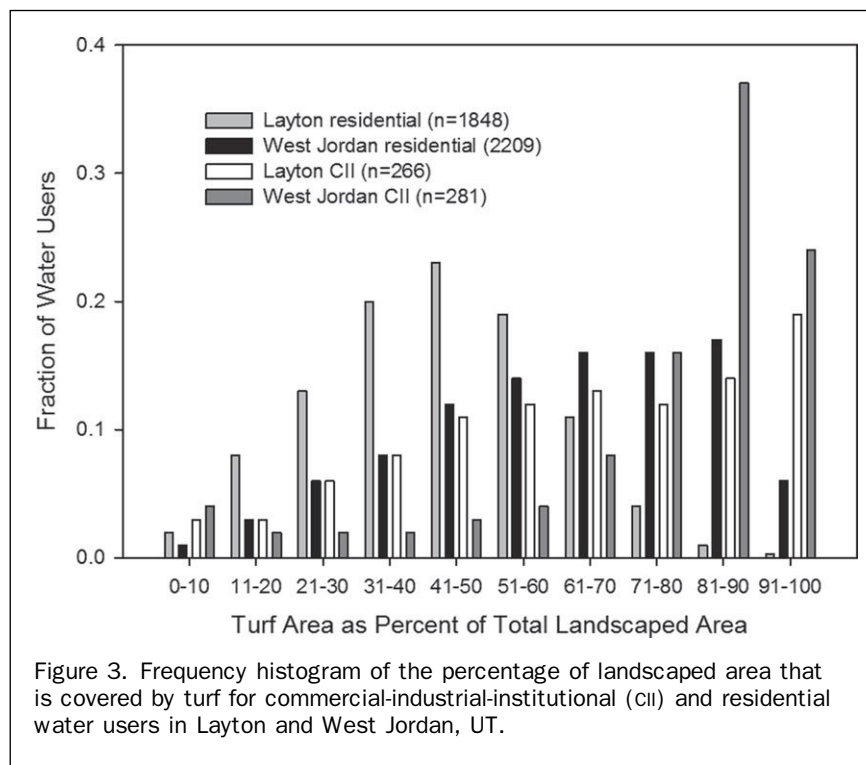


Figure 3. Frequency histogram of the percentage of landscaped area that is covered by turf for commercial-industrial-institutional (CII) and residential water users in Layton and West Jordan, UT.

TABLE 2. TURF AND TREE SURFACE AREAS EXTRACTED FROM MULTISPECTRAL IMAGERY ACQUIRED OVER THE CITY OF LOGAN, UTAH IN EARLY MAY 1999 PRIOR TO FULL TREE LEAF OUT AND IN SEPTEMBER 1999 AFTER FULL LEAF OUT, TO DETERMINE THE PERCENT OF TURF AREA UNDER TREE CANOPY

Image	Turfgrass Area			Tree Area	Size Area	Shaded Grass	
	5-May (m ²)	16-Sept. (m ²)	Difference (m ²)			Actual %	Weighted %
Cemetery	114,365	84,013	30,352	44,394	1	0.68	0.12
Section 1	149,977	132,495	17,482	64,143	1.5	0.27	0.07
Section 2	78,024	61,614	16,410	44,831	1	0.37	0.07
Section 3	162,846	143,097	19,749	98,622	2	0.20	0.07
Average						0.38	0.34

Residential water use in excess of estimated needs in Layton over a five-year period showed substantial variation among years as estimated water needs varied (Table 3). The years 1997 and 2000 were relatively hot and dry, and a higher percentage (68 percent and 66 percent, respectively) of the study population irrigated their landscapes in excess of water needs as estimated from local reference evapotranspiration and landscape areas. Again, the population size varied among years as the water billing data set received from the city varied from year to year in terms of the number of billing records that we were able to link to parcel boundary records. In late 1999, Layton changed to a new water billing system that resulted in more consistent water billing data. In 1998/1999, evapotranspiration was lower and rainfall higher than in 2000 and 2001, thus fewer Layton residential water users irrigated in excess of estimated needs compared to 1997 and 1998 (54 to 59 percent). In 2001, the number of people irrigating their landscapes in excess of estimated needs fell as a result of a state-wide, state-run advertising campaign asking the population of Utah to reduce water consumption due to the third year of below normal winter snow pack. Over all five years, approximately

the same percentage of residential water users, 9 to 13 percent, accounted for 50 percent of the excess irrigation in any given year. This result is consistent with the right hand tail of seasonal water use (Figure 4) where a small number of parcels had very high consumption rates.

Conclusions

High-resolution airborne multispectral imagery obtained over urban areas in northern Utah was classified to extract turf grass, trees, and shrub areas resulting in an accuracy of 89 percent of the final recorded product. This imagery analyzed in a GIS environment can be a very useful tool in urban areas for estimating evapotranspiration from landscaped surfaces, identifying high-end landscape water users, and formulating water management and conservation plans by cities. This process provides data on irrigated landscaped areas of thousands of parcels through remote sensing that would otherwise be logistically impossible to obtain with on-the-ground measurements. Remotely sensed landscaped and total parcel area provided the basis for a practical model to predict residential landscaped area from total parcel area.

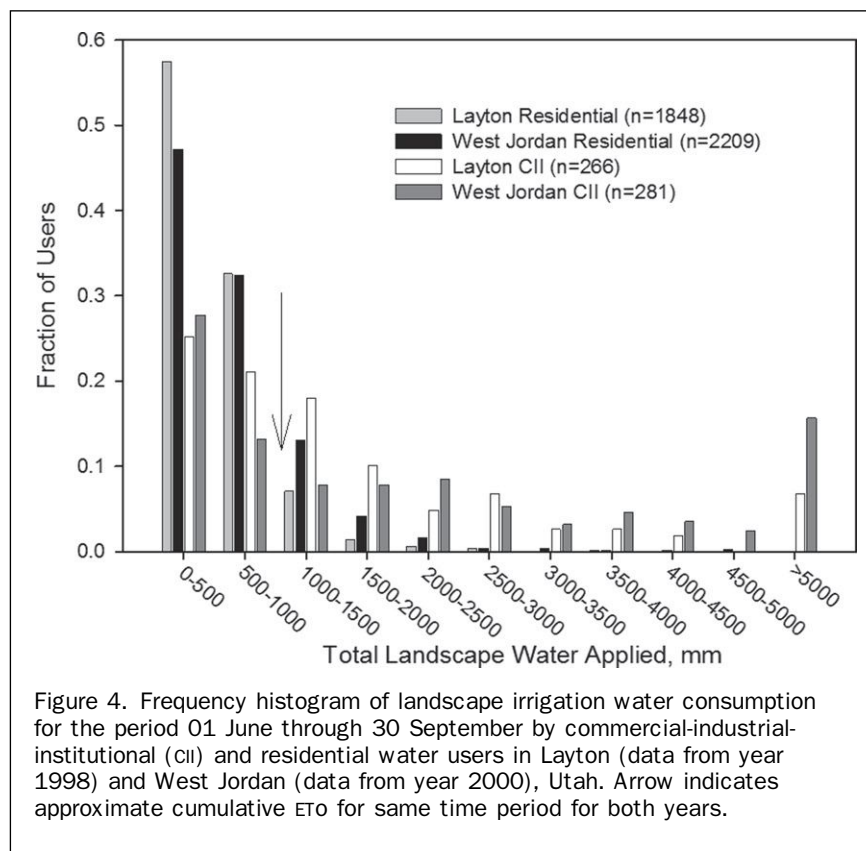


TABLE 3. NUMBER OF PARCELS, LOCAL EVAPOTRANSPIRATION AND RAIN FOR 01 MAY THROUGH 30 SEPTEMBER, PERCENTAGE OF ALL RESIDENTIAL PARCELS CONSUMING WATER FOR LANDSCAPE IRRIGATION ABOVE ESTIMATED NEEDS, PERCENTAGE OF RESIDENTIAL PARCELS ACCOUNTING FOR 50 PERCENT OF THE VOLUME OF LANDSCAPE WATER APPLIED IN EXCESS OF ESTIMATED NEEDS, FOR 1997 TO 2001 FOR LAYTON, UTAH

Year	Total Parcels Examined Number	ET (mm)	Precipitation (mm)	Excess Irrigation (m ³)	% of Parcels Accounting for Excess Irrigation	
					Total	50%
1997	1,034	678	353	100,167	68	12
1998	1,865	720	408	147,538	59	11
1999	2,149	736	312	131,976	54	10
2000	2,862	887	278	310,520	66	13
2001	2,859	903	209	158,703	37	9

Further work is needed to determine if such a model from this data set would be applicable to residential areas in other cities around the western U.S.

Estimating irrigated landscape area and using water billing data allowed us to determine the actual amount of water applied to CII and residential landscapes. This practical analysis of landscape water consumption showed that all the groups studied, residential and CII in Layton and West Jordan, had a small percentage of users accounting for most of the excess irrigation above estimated landscape needs. Thus, if a city wanted to implement water conservation measures, those individual water users could be identified and targeted in an efficient manner without offering or delivering conservation programs to the majority of users already irrigating their landscapes efficiently. However, more CII than residential parcel owners were applying water in excess of estimated needs, and in vastly greater amounts. Thus they would be the most likely targets for conservation interventions in order to most efficiently achieve the greatest water savings from the smallest percentage of users.

Acknowledgments

This research was funded by USDA CSREES National Research Initiative Grant No. 97-35108-5123. It was supported in part by Utah Agricultural Experiment Station Projects UTA00793; Utah State University's Remote Sensing Services Laboratory, Department of Civil and Environmental Engineering; and the Center for Water Efficient Landscaping, Department of Plants, Soils, and Climate. This paper was approved as Journal Paper No. 8064 by the Utah Agricultural Experiment Station, Utah State University, Logan, Utah 84322-4810. The authors thank the Cities of Layton, West Jordan, and Logan for their contributions to this research.

References

Allen, R.G., M. Smith, L.S. Pereira, and A. Perrier, 1994. An update for the definition of reference evapotranspiration, *ICID Bulletin*, 43:35-92.

Allen, R.G., L.S. Pereira, D. Raes, and M. Smith, 1998. *FAO Irrigation and Drainage Paper, No. 56, Crop Evapotranspiration (Guidelines for Computing Crop Water Requirements)*, Food and Agriculture Organization of the United Nations (FAO), Rome, Italy, 300 p.

Cai, B., and C.M.U. Neale, 1999. A method for constructing 3-dimensional models from airborne imagery, *Proceedings of the 17th Biennial Workshop Color Photography and Videography for Resource Assessment*, American Society for Photogrammetry and Remote Sensing, Bethesda, Maryland.

Carr, K.M., and J.D. Crammond (editors), 1995. *Water Law: Trends, Policies, and Practice*, American Bar Association, Chicago, Illinois.

Chávez, J.L., C.M.U. Neale, L.E. Hipps, J.H. Prueger, and W.P. Kustas, 2005. Comparing aircraft-based remotely sensed energy balance

fluxes with eddy covariance tower data using heat flux source area functions, *Journal of Hydrometeorology*, 6(6):923-940.

Congalton, R.G., 1991. A review of assessing the accuracy of classifications of remotely sensed data, *Remote Sensing of Environment*, Vol. 37, pp 35-46.

Costello, L., N. Matheny, and J. Clark, 1992. Estimating crop coefficients for landscape plantings, *University of California Agriculture and Natural Resource Leaflet 21493*.

Endter-Wada, J., J. Kurtzman, S.P. Keenan, R.K. Kjelgren, and C.M.U. Neale, 2008. Situational waste in landscape watering: Residential and business water use in an urban Utah community, *Journal of the American Water Resources Association*, 44(4):902-920.

ERDAS, 1999. *ERDAS Field Guide*, Fifth edition, ERDAS, Inc., Atlanta, Georgia.

Jackson, R.D., T.R. Clarke, and M.S. Moran, 1992. Bidirectional calibration results for 11 Spectralon and 16 Baso4 reference reflectance panels, *Remote Sensing of Environment*, 40(3):231-239.

Kjelgren, R., L. Rupp, and D. Kilgren, 2000. Water conservation in urban landscapes, *HortScience*, (35):1037-1043.

Kilgren, D.C., J. Endter-Wada, R.K. Kjelgren, and P.G. Johnson. 2010. Implementing landscape water conservation in public school institutional settings: A case for situational problem solving, *Journal of the American Water Resources Association (JAWRA)*, 46(6):1205-1220.

Kneebone, W.R., D.M. Kopec, and C.F. Mancino, 1992. Water requirements and irrigation, *Turfgrass, Agronomy Monograph No. 32*, ASA-CSSA-SSSA, Madison Wisconsin.

Montague, T., and R. Kjelgren, 2006. Use of thermal dissipation probes to estimate water loss of containerized landscape trees, *Journal of Environmental Horticulture*, (24):95-104.

Montague, T., R. Kjelgren, R. Allen, and D. Wester, 2004. Water loss estimates for five recently transplanted landscape tree species in a semi-arid climate, *Journal of Environmental Horticulture*, 22:189-196.

National Research Council, 1992. *Water Transfers in the West: Efficiency, Equity, and the Environment*, National Academy Press, Washington, D.C., 320 p.

Neale, C.M.U., and B.G. Crowther, 1994. An airborne multispectral video/radiometer remote sensing system: Development and calibration, *Remote Sensing of Environment*, (48):1-25

Neale, C.M.U., D. Wenger, H. Jayanthi, and F. Farag, 2007. Mapping and monitoring wetlands using airborne multispectral imagery, *Remote Sensing for Environmental Monitoring and Change Detection - Proceedings of Symposium HS3007 at IUGG2007, Perugia*, IAHS Publication 316.

Pimentel, D., B. Berger, D. Filiberto, M. Newton, B. Wolfe, E. Karabinakis, S. Clark, E. Poon, E. Abbett, and S. Nandagopal, 2004. Water resources: Agricultural and environmental issues, *Bioscience*, 54(10):909-918.

Postel, S.L., 2000. Entering an era of water scarcity: The challenges ahead, *Ecological Applications*, 10(4):941-948.

Snyder, R.L., and S.O. Eching, 2005. Microclimate corrections for urban landscape evapotranspiration, *ASCE Conference Proceedings 173*, 544, DOI:10.1061/40792(173)544.

Solley, W.B., R.R. Pierce, and H.A. Perman, 1998. *Estimated Use of Water in the United States in 1995*, U.S.G.S. Circular 1200,

U.S. Dept. of the Interior, U.S. Geological Survey, Reston, Virginia, 27 p.

Solomon, K.H., J.A. Kissinger, G.P. Farrens, and J. Borneman, 2007. Performance and water conservation potential of multi-stream, multi-trajectory rotating sprinklers for landscape irrigation, *Applied Engineering in Agriculture* (23):153–163.

Sundaraman, S., and C.M.U. Neale, 1997. Geometric calibration of the USU videography system, *Proceeding of the 16th Biennial Workshop on Videography and Color Photography in Resource*

Assessment, 29 April - 01 May, Weslaco, Texas, American Society for Photogrammetry and Remote Sensing, Bethesda, Maryland.

Thomas, N., C. Hendrix, and R.G. Congalton, 2003. A comparison of urban mapping methods using high-resolution digital imagery, *Photogrammetric Engineering & Remote Sensing*, 69(9):963–972.

Vickers, A., 2001. *Handbook of Water Use and Conservation: Homes, Landscapes, Industries, Businesses, Farms*, 464p.

(Received 02 January 2009; accepted 30 December 2010; final version 05 April 2011)

Certification Seals & Stamps

- Now that you are certified as a remote sensor, photogrammetrist or GIS/LIS mapping scientist and you have that certificate on the wall, make sure everyone knows!
- An embossing seal or rubber stamp adds a certified finishing touch to your professional product.
- You can't carry around your certificate, but your seal or stamp fits in your pocket or briefcase.
- To place your order, fill out the necessary mailing and certification information. Cost is just \$35 for a stamp and \$45 for a seal; these prices include domestic US shipping. International shipping will be billed at cost. Please allow 3-4 weeks for delivery.

SEND COMPLETED FORM WITH YOUR PAYMENT TO:

ASPRS Certification Seals & Stamps, 5410 Grosvenor Lane, Suite 210, Bethesda, MD 20814-2144

NAME: _____ PHONE: _____

CERTIFICATION #: _____ EXPIRATION DATE: _____

ADDRESS: _____

CITY: _____ STATE: _____ POSTAL CODE: _____ COUNTRY: _____

PLEASE SEND ME: Embossing Seal.....\$45 Rubber Stamp.....\$35

METHOD OF PAYMENT: Check Visa MasterCard American Express Discover

CREDIT CARD ACCOUNT NUMBER _____ EXPIRES _____

SIGNATURE _____ DATE _____

Note: ASPRS certification seals and stamps can only be authorized by ASPRS and manufactured by ASPRS-approved vendors. Unauthorized seal or stamp production is a violation of copyright law and the ASPRS Code of Ethics.

Estimating Aboveground Carbon of Moso Bamboo Forests Using the k Nearest Neighbors Technique and Satellite Imagery

Guomo Zhou, Xiaojun Xu, Huaqiang Du, Hongli Ge, Yongjun Shi, and Yufeng Zhou

Abstract

The extensive distribution of bamboo forests in Southern and Southeast Asia plays an important role in carbon sequestration and climate change. Providing timely and accurate estimates for aboveground carbon (AGC) of Moso bamboo forests is an urgent task. Based on the integration of Landsat Thematic Mapper (TM) and field inventory data, this study explores use of the k Nearest Neighbors (KNN) technique for estimating AGC. A new distance metric named Slope, Intercept, and Correlation Distance (SICD) is introduced and compared with Euclidean Distance (ED) and Mahalanobis Distance (MD). Using leave-one-out (LOO) cross-validation, the estimation performance of KNN technique is then compared with a linear regression model. The research indicates that the SICD is slightly better than ED and MD but no significant differences were found between them in estimating AGC. For extreme AGC conditions, the KNN technique has a greater estimation performance than that of the linear regression model, and is a convenient and effective method for estimating AGC of Moso bamboo forests in a large area.

Introduction

Bamboo forests are extensively distributed in Southern and Southeastern Asia and are continuously increasing. In 2009, the Chinese government reported bamboo forests had reached an area of approximately 6×10^6 ha, in which Moso bamboo accounted for approximately 70 percent of the area. Bamboo serves as an excellent substitute for woods in producing pulp, paper, board, and charcoal and plays an important role in Asia's rural economy (Ruiz-Pérez *et al.*, 1999). Because of bamboo's rapid growth rate and its strong

capacity for storing carbon, carbon sequestration research has increased. For various reasons, it is important to accurately estimate bamboo forest attributes in a timely manner. Forest inventory is the primary source of information for large area estimates. Further, the estimators used to produce the large area estimates are unbiased which cannot be asserted for remote sensing-based estimates. However, forest inventory is time-consuming, labor intensive, and the spatial distribution in a large area is difficult to update. Remote sensing conserves time and labor and is the best approach to estimating forest attributes if maps are also required and/or if small area estimates are required (Mäkelä and Pekkarinen, 2004; McRoberts and Tomppo, 2007).

Previous research has shown the potential of remote sensing imagery for estimating aboveground carbon (AGC) of Moso bamboo with partial least-squares (PLS) regression and Back-Propagation artificial neural network (BP-ANN) (Xu *et al.*, 2011). However, the complexity of PLS and BP-ANN often results in difficulty in choosing optimal parameters (Xu *et al.*, 2011). Both methods are needed to build different models for estimating forest attributes. In contrast, nearest neighbors techniques are easy to apply and have the advantage of simultaneously estimating large numbers of forest attributes. McRoberts (2009) provided and clearly evaluated diagnostic tools for nearest neighbors techniques when used with satellite imagery.

Because it can provide information about forest attributes over large areas, remote sensing imagery is often used as predictor variables with the nearest neighbor techniques. Both predictor and response variables are measured in field sample plot units to construct a reference set. Only predictor variables are measured in pixel units across the entire study area that comprise the target set (Hudak *et al.*, 2008). Nearest neighbor techniques then serve as a bridge between the reference and target sets. The distance metric in nearest neighbor techniques is used to determine nearest neighbors for target sets on the basis of similarity in values of predictor variables. According to the type of distance metric and the number of nearest neighbors, many kinds of nearest neighbors techniques can be used (Moeur and Stage, 1995; Tokola *et al.*, 1996; Nilsson, 1997; Ohmann and Gregory, 2002; Temesgen *et al.*, 2003; McRoberts *et al.*, 2007; Hudak *et al.*, 2008). Of these techniques, the k nearest neighbors

Guomo Zhou, Huaqiang Du, and Hongli Ge are with the School of Environmental Science and Technology, Zhejiang A & F University, Lin'an, Zhejiang, China 311300, Zhejiang Provincial Key Laboratory of Carbon Cycling in Forest Ecosystems and Carbon Sequestration, Zhejiang A & F University, Lin'an, Zhejiang, China 311300, and The Nurturing Station for the State Key Laboratory of Subtropical Silviculture, Zhejiang A & F University, Lin'an, Zhejiang, China 311300 (zhougm@zafu.edu.cn or xuxiaojun83115371@163.com).

Xiaojun Xu, Yongjun Shi, and Yufeng Zhou are with the School of Environmental Science and Technology, Zhejiang A & F University, Lin'an, Zhejiang, China 311300, and Zhejiang Provincial Key Laboratory of Carbon Cycling in Forest Ecosystems and Carbon Sequestration, Zhejiang A & F University, Lin'an, Zhejiang, China 311300.

Photogrammetric Engineering & Remote Sensing
Vol. 77, No. 11, November 2011, pp. 1123–1131.

0099-1112/11/7711-1123/\$3.00/0

© 2011 American Society for Photogrammetry
and Remote Sensing

(KNN) technique combined with remote sensing imagery is one of the more common methods used in estimating forest attributes (Franco-Lopez *et al.*, 2001; Tomppo *et al.*, 2002; McRoberts, 2008; Fuchs *et al.*, 2009; Magnussen *et al.*, 2009). However, results showed KNN prediction error was relatively high (Tokola *et al.*, 1996; Mäkelä and Pekkarinen, 2004; Gjertsen, 2007). In order to continue the credible use of the KNN technique, it is necessary to improve its prediction accuracy.

Previous research has explored some methods for improving KNN technique. For example, a genetic algorithm (GA) was applied to optimize selection of weights for predictor variables (Tomppo and Halme, 2004; Tomppo *et al.*, 2009). A modified KNN technique based on GA to reorder nearest neighbors and to eliminate spurious nearest neighbors (McRoberts, 2008) and a model-assisted KNN technique (Magnussen *et al.*, 2010) were proposed to improve accuracy. A new distance weighted with Fuzzy Weights (FW) or Fuzzy Distance (FD) produced the best results in comparison with ED and MD because it emphasizes the relationship between the response and feature variables (Chirici *et al.*, 2008). A flexible distance metric for selecting the set of potential nearest neighbors is needed because prediction accuracy of the KNN technique mainly depends on the nearest neighbors selected.

According to Im *et al.* (2005), slope, intercept, and correlation images derived from two registered remote sensing images are superior in detecting land use changes because the same geographic area on two dates of imagery tends to be highly correlated if little change has occurred and uncorrelated when change occurs. Ideally, if the sets of values of the feature variables for the target and reference pixels are not significantly different, pairs of feature variable values should be located along $y = x$ in two dimensional space. They should be located far from $y = x$ if the values of the variables are substantially different. Regression lines are computed between the feature variable values of the reference and target pixels. If the differences in values of the feature variables are large, the correlation coefficient of the regression lines between the two sets of feature variable values will fall off to a lower value in which case the slope and intercept of the regression lines will be much larger or smaller than 1 and 0, respectively. Consequently, nearest neighbors can be selected based on estimates of the slope, intercept, and correlation coefficient of the regression lines between the sets of values of the feature variables for the target and reference pixels.

The objectives of this study are (a) to describe and illustrate the new SCID metric for the KNN technique, (b) to compare this new distance metric with the Euclidean distance (ED) and Mahalanobis distance (MD), and (c) to compare the KNN technique with a linear regression model using field plot data and TM imagery for estimating pixel-level AGC (Mg C/ha) of *Moso* bamboo forests.

Study Area

Anji and Lin'an counties, located in the northwestern part of Zhejiang province, China (Figure 1), cover approximately 5,000 km², and were selected for research. Anji County covers 1,886.45 km², and 30.1 percent of the area is occupied by *Moso* bamboo forests. Lin'an County is approximately 3,136.34 km². *Moso* bamboo forests cover approximately 22,000 ha, and are mainly distributed in the eastern part of the county. Both counties have similar geological and climatic conditions. The terrain is undulating with elevation ranging 2 m to 1,629 m above sea level. The average elevation is 403 m. Average annual precipitation is between 1,100 mm and 1,900 mm. The average annual temperature is about 16.0°C.

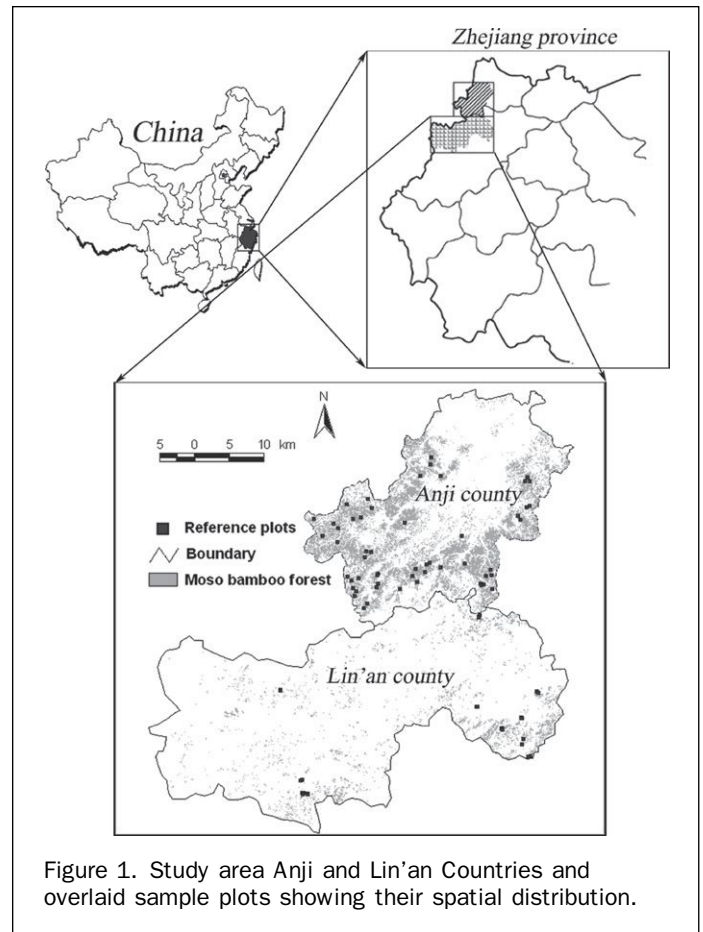


Figure 1. Study area Anji and Lin'an Counties and overlaid sample plots showing their spatial distribution.

Methods

Field Inventory Data and Image Processing

Field inventory was conducted August and September of 2008. Using a stratified random sampling scheme, 92 sample plots of 0.09 ha (30 m × 30 m) were measured. Towns within both counties were used as strata with the percentage of bamboo area of every town as the weight of stratum. Sample plots covered by clouds or with other location errors were excluded. Overall, 54 sample plots in Anji County and 29 sample plots in Lin'an County were surveyed (Figure 1). The survey items included plot longitude and latitude, and tree age, diameter at breast height (DBH, cm), etc. Dry AGC of each individual bamboo tree (kg) was estimated using the Weibull model (Equation 1). This model has an R² value of 0.937 and prediction accuracy of 96.43 percent (Zhou, 2006). The AGC of each sample plot was then estimated as the sum of dry AGC for individual bamboo trees,

$$\hat{AGC} = (747.787DBH^{2.771} \left(\frac{0.148A}{0.028 + A} \right)^{5.555} + 3.772) \times 0.5042 \quad (1)$$

where DBH is diameter at breast height, and A is age. The unit used to denote the age of *Moso* bamboo is called "du." New bamboo or one year bamboo is called 1 du, 2 to 3 years as 2 du, and 4 to 5 years as 3 du, and so on. The expansion factor for the conversion from biomass to carbon for *Moso* bamboo forest is 0.5042 (Zhou, 2006). The AGC of field plots ranges from 9.90 Mg C ha⁻¹ to 38.60 Mg C ha⁻¹.

A Landsat Thematic Mapper (TM) image (WRS = 119/039) acquired on 05 July 2008, was used in this study. The image

was rectified to the Transverse Mercator coordinate system using control points taken from topographic maps, with the root mean square error (RMSE) of 0.51 pixels. The nearest neighbor algorithm was used during the image rectification to resample the TM image into pixel sizes of 30 m × 30 m.

The TM image was radiometrically and atmospherically calibrated using the Dark Object Subtraction (DOS) approach (Chavez, 1996; Song *et al.*, 2001; Schroeder *et al.*, 2006; Vicente-Serrano *et al.*, 2008). The minimum digital number (DN) value and downwelling diffuse irradiance are two very important parameters for the DOS approach. The minimum DN value in each spectral band was selected as the darkest DN with at least a thousand pixels for the entire image (Song *et al.*, 2001; Schroeder *et al.*, 2006). The downwelling diffuse irradiance for a Rayleigh atmosphere was estimated as zero aerosol optical depth at 550 nm using the 6s radiative transfer code (Vermote *et al.*, 1997). After atmospheric calibration, DN values of original image were converted into reflectance values between 0 and 1.

The C correction model was used for topographic correction (Teillet *et al.*, 1982; Chirici *et al.*, 2008) and expressed as:

$$L_T = L \times \left(\frac{\cos(\theta) + c}{\cos(\beta) + c} \right), \quad (2)$$

$$c = \frac{b}{a}, \quad (3)$$

$$\cos(\beta) = \cos(\alpha) \times \cos(\theta) + \sin(\alpha) \times \sin(\theta) \times \cos(\lambda - \omega), \quad (4)$$

where L_T is the normalized reflectance, L is the uncorrected reflectance, θ is the solar zenith angle, β is incidence angle, c is correction factor, a and b are respectively the slope and intercept of a regression line between the cosine of the incident angle and reflectance, α is terrain slope, λ is sun azimuth, and ω is terrain aspect.

Sun elevation and sun azimuth, 65° and 101°, were from the image's header file. Terrain slope and aspect were derived from an ASTER GDEM data with 30 m × 30 m spatial resolution (<http://datamirror.csdn.cn/>).

Linear Regression and kNN Model Development

The mean values of the six TM spectral bands for each field plot were extracted with a window size of 3 pixels × 3 pixels and used to establish AGC estimation models.

Stepwise regression analysis was then used to establish a linear regression model, defining suitable thresholds for adding and removing independent variables. Multi-collinearity issues were addressed by calculating and monitoring the size of the condition index using Statistical Product and Service Solutions software (SPSS13.0). Models with condition index values greater than 30 were not accepted, indicating that there was no serious collinearity inherent in the selected models (Næsset *et al.*, 2005).

The KNN technique, with the combination of Landsat TM imagery and field measurements, has been extensively used for mapping forest attributes (McRoberts, 2008). It can simultaneously estimate all plot attributes using the same underlying remote sensing data. Estimation of forest attributes with KNN can be expressed as:

$$\hat{y}_i = \sum_{j=1}^k w_{i,j} y_j, \quad (5)$$

where \hat{y}_i is the target plot's predicted forest attributes, y_j is the j^{th} nearest reference plot's forest attributes, and k is the number of nearest neighbors. The weight, $w_{i,j}$, is set propor-

tional to the inverse distance between the values of the feature variables for target plot i and the j^{th} nearest reference plots as expressed in Equation 6:

$$w_{i,j} = \begin{cases} \frac{D_{i,j}^{-m}}{\sum_{j=1}^k D_{i,j}^{-m}}, & j \in J \\ 0, & j \notin J \end{cases}, \quad (6)$$

where $D_{i,j}$ denotes the distance in feature space between the values of the feature variables for target plot i and the j^{th} nearest reference plot. J denotes the set of the k reference plots nearest to target set pixel i in feature space when using distance metric, D . In this study, m equals 1. The distance metric is one of the critical parameters used in KNN algorithm, and affects the estimates. Common distance metrics are the ED and MD (McRoberts *et al.*, 2002; McRoberts and Tomppo, 2007; Baffetta *et al.*, 2009). In this study, a new distance metric named Slope, Intercept, and Correlation distance (SICD) was proposed. When the values of feature variables for the target and reference plots are not substantially different, the regression lines between them should be close to $y = x$. If a slope is close to 1, an intercept is near 0, and a correlation coefficient is near 1, the two sets of feature variables are similar.

For each combination of reference and target set elements, the relationship between observations of the feature variables was estimated using a simple linear regression model of the form,

$$y_{i,l} = ax_{j,l} + b + \varepsilon, \quad (7)$$

where $y_{i,l}$ is the observation of the l^{th} feature variable for the i^{th} target set element; $x_{j,l}$ is the observation of the l^{th} feature variable for the j^{th} reference set element; a and b are model coefficients; and ε is residual error. Estimates of a and b respectively are obtained using ordinary least squares techniques.

The SICD, calculated using Equation 8, is used to determine the similarity between the values of the feature variables for target plots and reference plots. Because slope, intercept, and correlation have different scales, the three parameters are normalized by the sum.

$$\text{SICD}_{i,j} = \sqrt{\frac{(a_{i,j} - 1)^2}{\sum_{j=1}^n (a_{i,j} - 1)^2} + \frac{(b_{i,j} - 0)^2}{\sum_{j=1}^n (b_{i,j} - 0)^2} + \frac{(r_{i,j} - 1)^2}{\sum_{j=1}^n (r_{i,j} - 1)^2}}, \quad (8)$$

where $a_{i,j}$, $b_{i,j}$, and $r_{i,j}$ are estimates of the slope, intercept, and correlation coefficient of the regression line (see Equation 7) between the values of the feature variables for the target plot i and reference plot j , and n is the total number of reference plots.

Determining the k value is subjective, and is often selected by a variety of considerations (McRoberts, 2009). Both small and larger numbers of nearest neighbors (k -values) have their own advantages (Tokola *et al.*, 1996; Katila and Tomppo, 2001; Ohmann and Gregory., 2002; McRoberts *et al.*, 2007; McRoberts, 2009). The optimal k -values can be effectively determined using the leave-one-out (LOO) cross-validation technique and statistical measures (Table 1) of prediction quality (Fuchs *et al.*, 2009). Compromise is necessary for determining the optimal k -values in practical application (Katila and Tomppo, 2001; Fuchs *et al.*, 2009). The k -values attaining high correlation coefficient, coefficient of variation (CV), and range values and small relative bias (BIASR), relative root mean square error (RMSER),

TABLE 1. STATISTICAL MEASURES FOR K VALUES SELECTION AND ACCURACY EVALUATION (y_i AND \hat{y}_i ARE OBSERVED DATA i AND PREDICTED DATA i ; n IS NUMBER OF SAMPLE PLOTS)

Measures	Formulas	Measures	Formulas
Range	$\hat{y}_{max} - \hat{y}_{min}$	MRE	$\frac{1}{n} \sum_{i=1}^n \left(\frac{1}{y_i} \hat{y}_i - y_i \right) \times 100\%$
RMSE	$\sqrt{\frac{1}{n} \sum_{i=1}^n (\hat{y}_i - y_i)^2}$	RMSEr	$\frac{RMSE}{y_{mean}} \times 100\%$
BIASr	$\frac{1}{n \times y_{mean}} \sum_{i=1}^n (\hat{y}_i - y_i) \times 100\%$	CV	$\frac{1}{y_{mean}} \sqrt{\frac{1}{n} \sum_{i=1}^n (\hat{y}_i - y_{mean})^2} \times 100\%$

and mean relative error (MRE) values were selected as the optimal number of neighbors to be used.

Model Evaluation and Comparison

The LOO cross-validation and statistical measures (Table 1) were used as an evaluation approach for (a) the choice of k-values, (b) a comparison of distance metrics, and (c) a comparison of the KNN technique and linear regression estimates. In order to reduce the registration errors between sample plots and the imagery, the estimation results were evaluated based on a window size of 3×3 pixels. Significance of difference in absolute residuals between linear regression and KNN technique was tested by the paired sample t test (Altman, 1991), expressed as:

$$t = \frac{d_{mean}}{SE}, \quad (9)$$

$$SE = \sqrt{\frac{\sum_{i=1}^n (d_i - d_{mean})^2}{n \times (n - 1)}} \quad (10)$$

where t is a paired sample t test with $n - 1$ degrees of freedom, d is the difference between two absolute residual samples from linear regression and the KNN technique; d_{mean} is the mean d values, SE is standard error of d values, and n is the number of sample plots.

Results

Linear Regression Models

Pearson's correlation analysis shows that both TM band 2 ($r = 0.24$, $p < 0.05$) and band 4 ($r = 0.26$, $p < 0.05$) are significantly correlated with AGC. The results based on the stepwise regression model (Table 2) show that TM band 4 is a useful variable for estimating *Moso* bamboo forest AGC. According to the F test, the linear regression model for estimating AGC is significant at level $\alpha = 0.01$.

Comparison of Distance Metrics

Correlation coefficients between observations and estimates increase rapidly when the k-values increase from 1 to 10, but

TABLE 2. RESULTS OF STEPWISE LINEAR REGRESSION

Variable	Estimate	Sig.	r	RMSE (Mg C/ha)
Intercept	6.89	0.18	0.29	5.38
Band4	43.13	0.01		

Sig. is level of significance; r is correlation coefficient

decrease slightly after that (Figure 2). RMSEr, MRE, CV, and Range decrease rapidly as the k-values increase from 1 to 10. These statistical measures for the ED and MD curves are quite similar, whereas they are notably different than those of the SICD. When the k-values are from 1 to 20, RMSEr and MRE for SICD are at least 1 percent smaller than those for ED and MD. The correlation coefficient, CV, and Range of the SICD are higher than those of ED and MD (Figure 2). This shows that the SICD is slightly better than ED and MDs in estimating AGC.

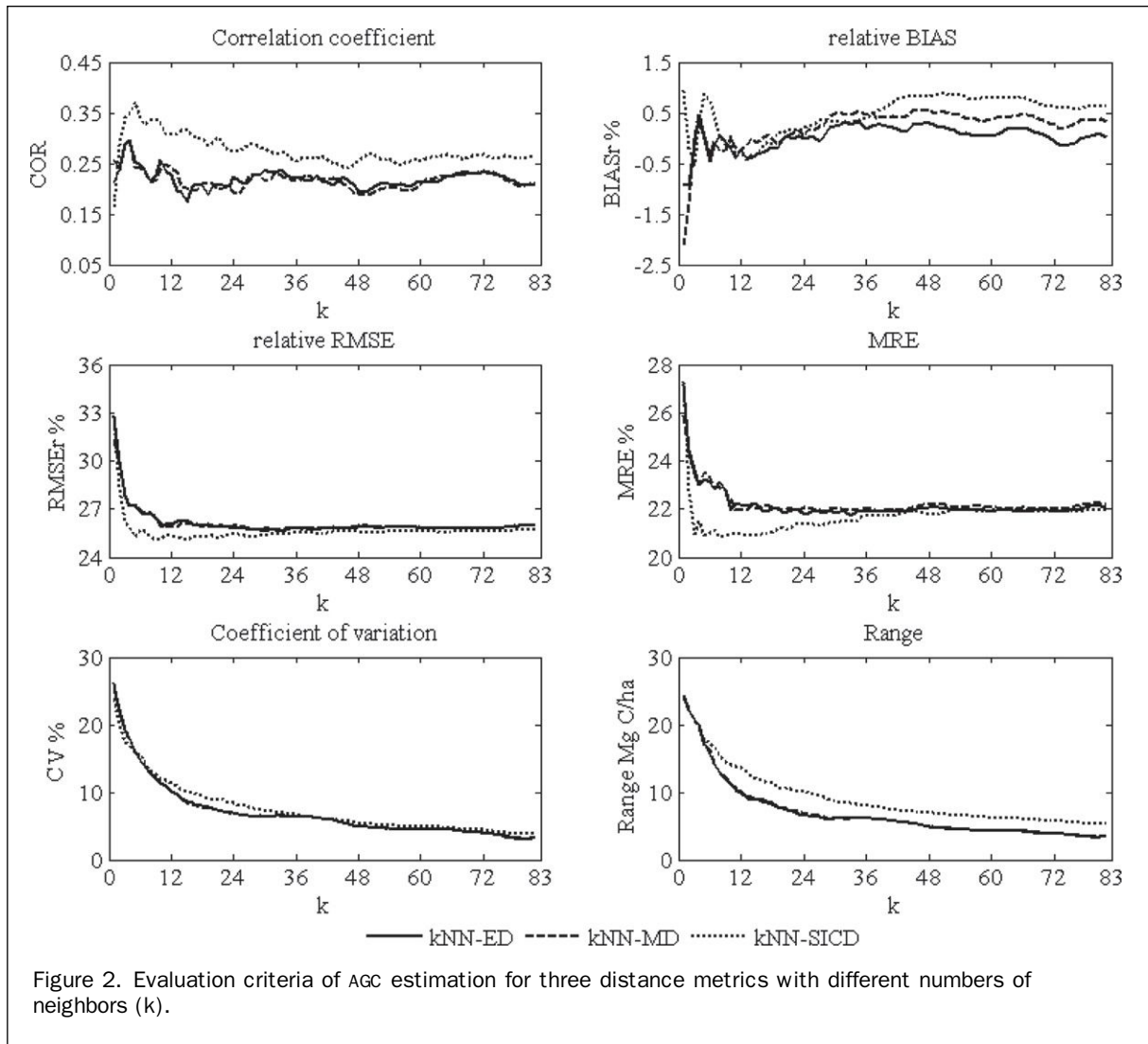
The optimal k-values were selected based on the criteria previously mentioned and were used to estimate AGC of *Moso* bamboo forests. The estimation results of KNN with different distance metrics were evaluated based on the LOO cross-validation (Table 3). The SICD produces the highest correlation coefficient, Range, and CV and the lowest RMSE, RMSEr, and MRE compared with the other two distance metrics. The SICD not only maintains precision but also preserves range and variance better as the CV increases (Figure 2 and Table 3). With the optimal k-values, the SICD is superior to the other two distance metrics. However, results of the paired samples t test show no significant differences in predictive performances of the three distance metrics.

Using the LOO cross-validation technique, the mean and ranges of weight values of the i^{th} nearest neighbors ($I = 1, 2, \dots, k$, $k = 8$) for reference plots are shown in Figure 3a. The weight values for i from 1 to 3 from the SICD are greater than those from the ED and MD. Because a greater weight value reduces the importance of the last nearest neighbors (Katila and Tomppo, 2001), the optimal k-values of the SICD are smaller than those of the ED and MD (Table 3).

The RMSE between the AGC values corresponding to the i^{th} nearest neighbors and AGC observations for reference plots were calculated (Figure 3b). An intrinsic difference between distance metrics was discovered. Nearest neighbors selected by the ED and MD are clearly different than those selected by the SICD. The RMSE between AGC values corresponding to nearest neighbors selected by the SICD and AGC observations for reference plots was less than the RMSE from the ED and MD. The lower RMSE for the SICD shows that nearest neighbors selected by the SICD are more similar to the AGC observations of reference plots, especially for the first three nearest neighbors. Therefore, the SICD can select more suitable nearest neighbors and more effectively display the ordering. With the advantages of greater weight values and better nearest neighbors, the SICD is slightly superior to the ED and MD in estimating AGC values of *Moso* bamboo forests.

Comparison between Linear Regression and kNN-SICD Prediction

A comparative analysis of the predictive performances of KNN-SICD (k-values in Table 3) and linear regression indicates that the KNN-SICD has better estimation performance (Table 4). The CV of the KNN-SICD is much larger than that of linear



regression model. This implies that the KNN-SICD better retains the original variation of the observations in the spatial variation of the estimates.

Field plots were divided into two subgroups according to the AGC values corresponding to field plots. Subgroup 1 consists of field plots with AGC larger than 1 standard deviation from the mean AGC value of all field plots. The AGC values in subgroup 1 are also named as extreme AGC values. The remaining field plots were separated into subgroup 2. Estimation errors are mainly from subgroup 1 (Table 4). The errors for subgroup 1 are much greater than for subgroup 2. Greater RMSEr values are found with linear regression compared with KNN-SICD for subgroup 1, whereas smaller RMSEr values are found with linear regression compared with KNN-SICD for subgroup 2. Results of the paired samples t test show that there is no significant difference between linear regression and KNN-SICD for subgroup 2. However, those observations in subgroup 1 estimated using the KNN-SICD are significantly more accurate ($p < 0.05$) than when using linear regression model.

Scatter-plots of estimates versus observations also show the KNN-SICD prediction accuracy is better than the linear regression model (Figure 4a). For the linear regression model, the resulting scatter diagram reveals the weak

correlation between the observed and estimated AGC. The best-fit line of the linear regression model approaches a horizontal line and its prediction capability is fairly poor. The residual analysis for linear regression and KNN-SICD both show large residuals for small and large AGC values (Figure 4b). Although the linear regression and KNN-SICD methods have similar problems in overestimating small values and underestimating large values, the observations are better estimated by the KNN-SICD than the linear regression models. This result is consistent with result of Fuchs *et al.* (2009).

When predictions are extrapolated beyond the ranges of variable values for the reference data, nearest neighbors techniques are vulnerable to poor performance (McRoberts *et al.*, 2007; McRoberts, 2009). Therefore, the numbers of target set pixels whose variable values beyond the ranges of variable values for reference set were checked. In this study, less than 10 percent of target set pixels were not completely covered by the reference data set. Because the proportion of target set pixels requiring extrapolations was small, the spatial distributions of *Moso* bamboo AGC were produced from the linear regression and KNN-SICD models (Figure 5).

The histograms of AGC estimates for the linear regression and KNN-SICD in Figure 5 show the main difference

TABLE 3. COMPARISON OF DIFFERENT DISTANCE METRICS FOR ESTIMATING AGC BASED ON THE LOO CROSS-VALIDATION

Model	k	RMSE (Mg C/ha)	RMSEr (%)	MRE (%)	BIASr (%)	Range	CV (%)	r
ED	10	5.35	25.90	21.95	-0.22	11.21	11.30	0.26*
MD	10	5.40	26.15	22.36	0.03	11.23	11.39	0.24*
SICD	5	5.22	25.27	20.90	0.87	17.83	15.74	0.37**

Level of significance, * < 0.05, ** < 0.01.

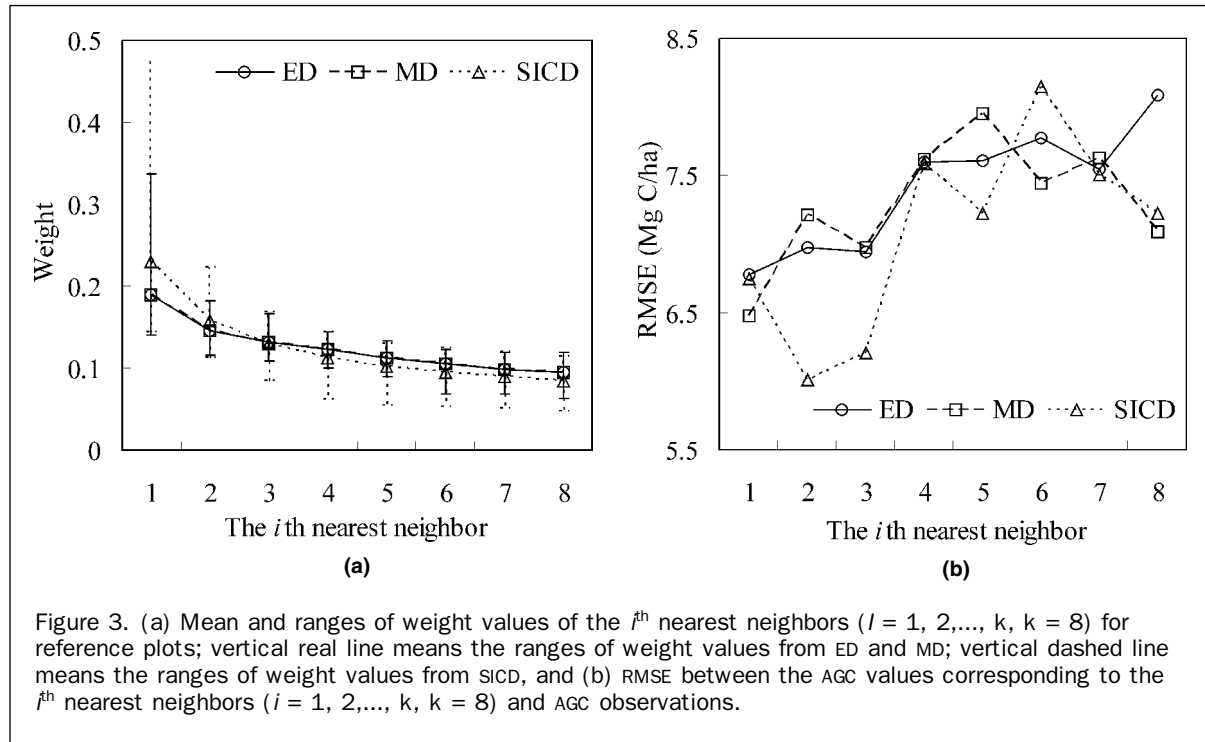


Figure 3. (a) Mean and ranges of weight values of the i^{th} nearest neighbors ($i = 1, 2, \dots, k, k = 8$) for reference plots; vertical real line means the ranges of weight values from ED and MD; vertical dashed line means the ranges of weight values from SICD, and (b) RMSE between the AGC values corresponding to the i^{th} nearest neighbors ($i = 1, 2, \dots, k, k = 8$) and AGC observations.

between the KNN-SICD and linear regression model are the estimates for small and large AGC values. The KNN-SICD estimates extreme values better than linear regression model, which is consistent with the results of Table 4. Mean AGC estimates from the KNN-SICD, for the nine areas of interest, were compared with the mean AGC values of field plots (Figure 5). Mean AGC estimates from the KNN-SICD are close to the mean AGC values of field plots. The difference (field plot observations - KNN-SICD predictions) varies from -8.4 to 2.1 Mg C/ha. The mean difference is -0.9 Mg C/ha (-0.87 percent). The absolute values of relative differences are in most cases less than 10 percent. The relative differences exceed 20 percent only in one area of interest. The large relative difference is due to small AGC values in that area of interest.

Discussion

In this study, when the SICD was applied instead of the ED and MD, the AGC estimates of *Moso* bamboo forest improved. This result is mainly attributed to distance metrics because the predicted AGC are calculated through multiplying the observed AGC associated with nearest neighbors by their weight values. Because the SICD has the advantage of selecting more suitable nearest neighbors, the AGC estimates from the SICD are more similar to observations than those from the ED and MD (see Tables 3 and Figure 3b). Although results of accuracy measures show that the SICD is superior to the ED

and MD, no significant differences were found among the three distance metrics based on the paired samples t test. Since the KNN-SICD needs to calculate slopes, intercepts, and correlation coefficients of regression lines between the values of the feature variables for reference plot and target plot, it takes more time than the KNN-ED and KNN-MD. The applicability of KNN-SICD for other applications should be tested.

The RMSEr of AGC estimates of *Moso* bamboo forests is smaller than in most previous studies of other forests such as *Betula pendula* and *Picea obovata* (Tuominen and Pekkarinen, 2005; Fuchs *et al.*, 2009). The RMSEr of AGC was 25.27 percent as estimated using the KNN-SICD, while for a previous study the RMSEr reached up to 41.21 percent (Fuchs *et al.*, 2009). Most *Moso* bamboo forests are pure forest with high homogeneity. The relatively small errors in this study are possibly due to the homogeneity characteristic of *Moso* bamboo forests. The field inventory data shows the majority of AGC observations of *Moso* bamboo forest are within 1 standard deviation of the mean AGC value of all field plots (Table 4). The spatial variability of AGC values for *Moso* bamboo forest is small. The linear regression and KNN-SICD models both accurately estimate the observations closer to the mean (Table 4). Therefore, the RMSEr of AGC estimates from both methods are small (Table 4). The prediction errors are mainly caused by failure to estimate extreme values in an accurate manner (see Table 4 and residual graphs in Figure 4b). In this study, the large errors for extreme values are partly

TABLE 4. COMPARISON OF AGC ESTIMATES FOR THE KNN-SICD AND LINEAR REGRESSION. THE t IS THE VALUE OF THE PAIRED SAMPLE T TEST AND p IS PROBABILITY VALUE

Plots	n	kNN-SICD		Linear regression		t	p
		RMSEr%	CV%	RMSEr%	CV%		
All plots	83	25.27	15.74	26.03	7.91	-0.42	0.68
Subgroup 1	21	37.12	24.23	40.40	8.38	-2.59	0.02
Subgroup 2	62	18.58	11.87	17.29	7.81	1.90	0.06

due to the limited number of extreme values in reference plots and the relatively weak relationships between TM bands and AGC observations. The prediction accuracy using predictor variables selected by stepwise linear regression was greater than that using the original bands (Fuchs *et al.*, 2009). Another reason for large errors for extreme values may be only use of spectral TM bands. How to accurately estimate those extreme values is a key problem to improving prediction accuracy for AGC of *Moso* bamboo forests. Large quantities of sample data, suitable spectral feature variables, and versatile statistical estimation techniques may solve this problem. The PLS-Bootstrap algorithm is a useful method for selecting suitable variables (Lazraq *et al.*, 2003; Xu *et al.*, 2011).

In comparison with the linear regression model, the KNN-SICD technique improves the AGC estimates of *Moso* bamboo forests. The KNN-SICD performs well and gives estimates with smaller errors than the linear regression model. In estimating extreme AGC values, there are significant differences between the KNN-SICD and linear regression models. The linear regression overestimates the field plots with small observations and underestimates the field plots with large observations, as did another linear regression model based on a different set of variables (Xu *et al.*, 2011). The KNN-SICD considerably improved this situation, and is as efficient as the PLS model (Xu *et al.*, 2011). The BP-ANN model has the advantage of fault tolerance and the ability to estimate extreme values of AGC because it can approximate any arbitrarily complex nonlinear function regardless of the complexity of the relationships between the variables and AGC (Xu *et al.*, 2011). The KNN-SICD is an effective method

that can be used to accurately estimate the mean AGC values of *Moso* bamboo forest at town level.

Conclusions

This study examined the integration of Landsat TM and field measurements for AGC of *Moso* bamboo forests for estimation using the KNN technique and a linear regression model. Using small data sets in this study, the SICD works as well as ED and MD because of its advantage in selecting suitable nearest neighbors. A comparison of the SICD with ED or MD using large data sets would be useful. The prediction accuracy of the KNN-SICD is better than that of the linear regression model. The results show that the KNN technique is a promising tool for estimating AGC of *Moso* bamboo forests for large areas. However, the extreme observations estimation accuracy was still not great enough. In order to acquire accurate as for *Moso* bamboo forests AGC, variable selection and increase in the number of reference plots should be tested in future studies.

Acknowledgments

This work was supported by the funds from National Natural Science Foundation (Grant, 31070564, 30700638, 30771715), 948 item of national forestry bureau (Grants, 2008-4-49), and item of science and technology department of Zhejiang province (Grants, 2008C12068). We also wish to thank three anonymous reviewers for their constructive comments and suggestions.

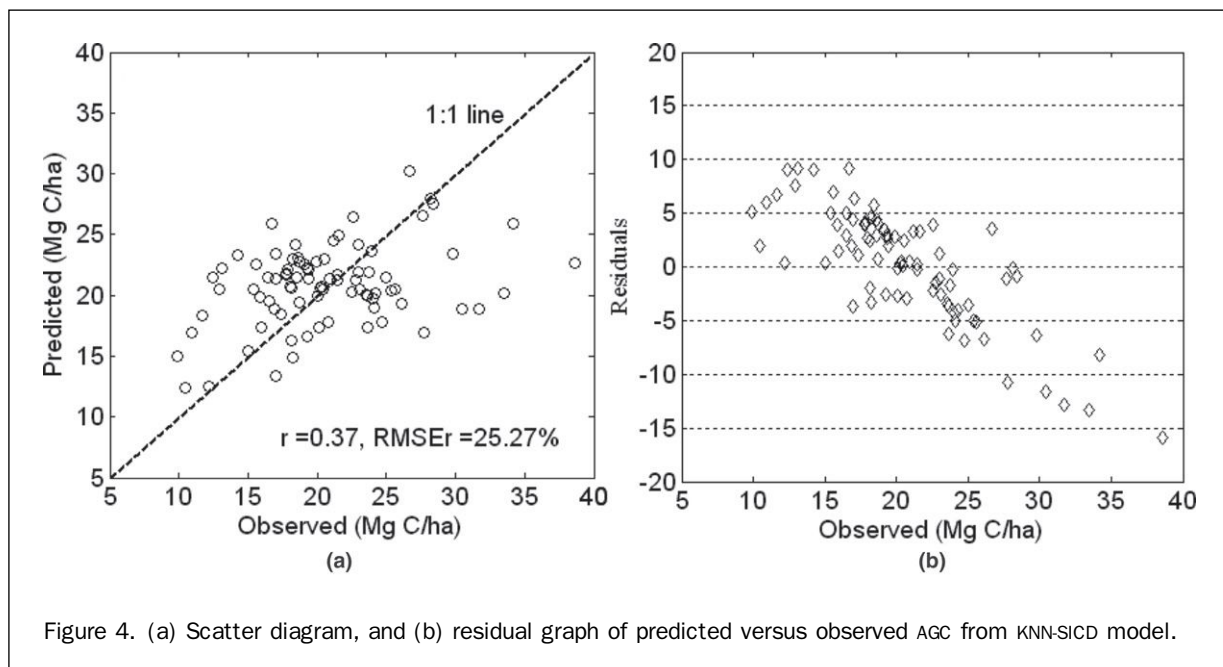
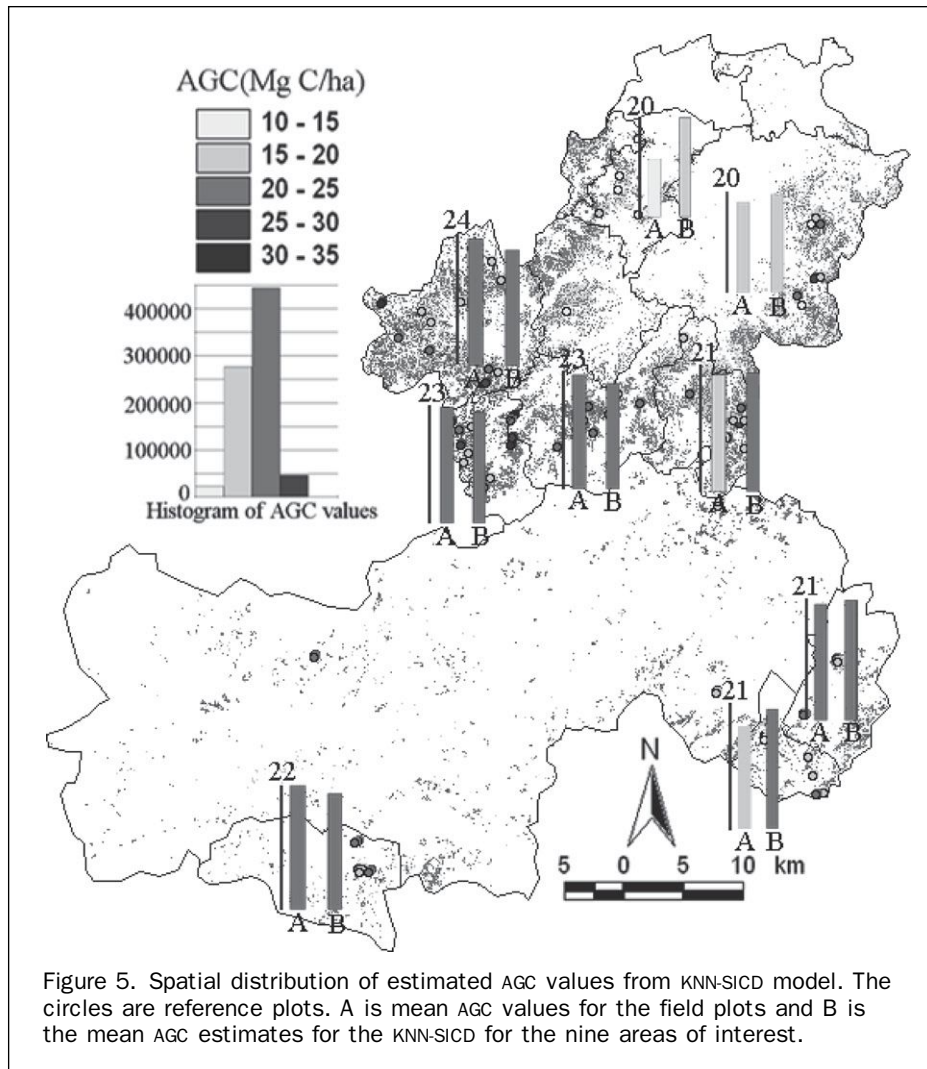


Figure 4. (a) Scatter diagram, and (b) residual graph of predicted versus observed AGC from KNN-SICD model.



References

- Altman, D.G., 1991. *Practical Statistics for Medical Research*, Chapman & Hall, London, 165 p.
- Baffetta, F., L. Fattorini, S. Franceschii, and P. Corona, 2009. Design-based approach to the kNN technique for coupling field and remotely sensed data in forest surveys, *Remote Sensing of Environment*, 113:463–475.
- Chavez, P.S., 1996. Image-based atmospheric corrections-revised and revisited, *Photogrammetric Engineering & Remote Sensing*, 62(10):1025–1036.
- Chirici, G., A. Barbati, P. Corona, M. Marchetti, D. Travaglini, F. Maselli, and R. Bertini, 2008. Non-parametric and parametric methods using satellite images for estimating growing stock volume in alpine and Mediterranean forest ecosystems, *Remote Sensing of Environment*, 112:2686–2700.
- Franco-Lopez, H., A.R. Ek, and M.E. Bauer, 2001. Estimation and mapping of forest stand density, volume, and cover type using the k-nearest neighbors method, *Remote Sensing of Environment*, 77:251–274.
- Fuchs, H., P. Magdon, C. Klein, and F. Heiner, 2009. Estimating aboveground carbon in a catchment of the Siberian forest tundra: Combining satellite imagery and field inventory, *Remote Sensing of Environment*, 113:518–531.
- Gjertsen, A.J., 2007. Accuracy of forest mapping based on Landsat TM data and a kNN-based method, *Remote Sensing of Environment*, 110:420–430.
- Hudak, A.T., N.L. Crookston, J.S. Evans, D.E. Hall, and M.J. Falkowski, 2008. Nearest neighbor imputation of species-level, plot-scale forest structure attributes from LiDAR data, *Remote Sensing of Environment*, 112:2232–2245.
- Im, J., and J.R. Jensen, 2005. A change detection model based on neighborhood correlation image analysis and decision tree classification, *Remote Sensing of Environment*, 99:326–340.
- Katila, M., and E. Tomppo, 2001. Selecting estimation parameters for the Finnish multisource National Forest Inventory, *Remote Sensing of Environment*, 76:16–32.
- Lazraq, A., R. Cléroux, and J. P. Gauchi, 2003. Selecting both latent and explanatory variables in PLS1 regression model, *Chemometrics and Intelligent Laboratory Systems*, 66:117–126.
- Mäkelä, H., and A. Pekkarinen, 2004. Estimation of forest stand volumes by Landsat TM imagery and stand-level field inventory data, *Forest Ecology and Management*, 196:245–255.
- Magnussen, S., R.E. McRoberts, and E. Tomppo, 2009. Model-based mean square error estimators for k-nearest neighbour predictions and applications using remotely sensed data for forest inventories, *Remote Sensing of Environment*, 113:476–488.
- Magnussen, S., E. Tomppo, and R.E. McRoberts, 2010. A model-assisted k-nearest neighbour approach to remove extrapolation bias, *Scandinavian Journal of Forest Research*, 25:174–184.
- McRoberts, R.E., M.D. Nelson, and D.G. Wendt, 2002. Stratified estimation of forest area using satellite imagery, inventory data, and the k-Nearest Neighbors technique, *Remote Sensing of Environment*, 82:457–468.
- McRoberts, R.E., and E. Tomppo, 2007. Remote sensing support for national forest inventories, *Remote Sensing of Environment*, 110:412–419.

- McRoberts, R.E., E.O. Tomppo, A.O. Finley, and J. Heikkinen, 2007. Estimating areal means and variances of forest attributes using the k-Nearest Neighbors technique and satellite imagery, *Remote Sensing of Environment*, 111:466–480.
- McRoberts, R.E., 2008. Using satellite imagery and the k-nearest neighbors technique as bridge between strategic and management forest inventories, *Remote Sensing of Environment*, 112:2212–2221.
- McRoberts, R.E., 2009. Diagnostic tools for nearest neighbors techniques when used with satellite imagery, *Remote Sensing of Environment*, 113:489–499.
- Moeur, M., and A.R. Stage, 1995. Most similar neighbor: an improved sampling inference procedure for natural resource planning, *Forest Science*, 41:337–358.
- Næsset, E., 1997. Estimating timber volume of forest stands using airborne laser scanner data, *Remote Sensing of Environment*, 61:246–253.
- Næsset, E., O.M. Bollands, and T. Gobakken, 2005. Comparing regression methods in estimation of biophysical properties of forest stands from two different inventories using laser scanner data, *Remote Sensing of Environment*, 94:541–553.
- Nilsson, M., 1997. Estimation of forest variables using satellite image data and airborne Lidar, *Silvestria*, Acta Universitatis Agriculturae Sueciae, 17:1–31.
- Ohmann, J.L., and M.J. Gregory, 2002. Predictive mapping of forest composition and structure with direct gradient analysis and nearest-neighbor imputation in coastal Oregon, U.S.A, *Canadian Journal of Forest Research*, 32:725–741.
- Ruiz-Pérez, M., M. Zhong, B. Belcher, C. Xie, M. Fu, and J. Xie, 1999. The role of bamboo plantations in rural development: The case of Anji County, Zhejiang, China, *World Development*, 27:101–114.
- Schroeder, T.A., W.B. Cohen, C. Song, M.J. Canty, and Z. Yang, 2006. Radiometric correction of multi-temporal Landsat data for characterization of early successional forest patterns in western Oregon, *Remote Sensing of Environment*, 103:16–26.
- Song, C., C.E. Woodcock, K.C. Seto, M.P. Lenney, and S.A. Macomber, 2001. Classification and change detection using Landsat TM data: When and how to correct atmospheric effects, *Remote Sensing of Environment*, 75:230–244.
- Teillet, P.M., B. Guindon, and D.G. Goodenough, 1982. On the slope-aspect correction of multispectral scanner data, *Canadian Journal of Remote Sensing*, 8:1537–1540.
- Temesgen, H., V.M. LeMay, K.L. Froese, and P.L. Marshall, 2003. Imputing tree-lists from aerial attributes for complex stands of south-eastern British Columbia, *Forest Ecology and Management*, 177:277–285.
- Tokola, T., J. Pitkänen, S. Partinen, and E. Muinonen, 1996. Point accuracy of non-parametric estimation of forest characteristics with different satellite materials, *International Journal of Remote Sensing*, 17:2333–2351.
- Tomppo, E., M. Nilsson, M. Rosengren, P. Aalto, and P. Kennedy, 2002. Simultaneous use of Landsat-TM and IRS-1C WiFS data in estimating large area tree stem volume and aboveground biomass, *Remote Sensing of Environment*, 82:156–171.
- Tomppo, E., and M. Halme, 2004. Using coarse scale forest variables as ancillary information and weighting of variables in k-NN estimation: a genetic algorithm approach, *Remote Sensing of Environment*, 92:1–20.
- Tomppo, E., C. Gagliano, F. De Natale, M. Katila, and R.E. McRoberts, 2009. Predicting categorical variables using an improved k-Nearest Neighbors estimator, *Remote Sensing of Environment*, 113:500–517.
- Tuominen, S., and A. Pekkarinen, 2005. Performance of different spectral and textural aerial photograph features in multi-source forest inventory, *Remote Sensing of Environment*, 94: 256–268.
- Vermote, E.F., D. Tanre, J.L. Deuze, M. Herman, and J.J. Morcrette, 1997. Second simulation of the satellite signal in the solar spectrum, 6S: An overview, *IEEE Transactions on Geoscience and Remote Sensing*, 35:895–934.
- Vicente-Serrano, S.M., F. Pérez-Cabello, and T. Lasanta, 2008. Assessment of radiometric correction techniques in analyzing vegetation variability and change using time series of Landsat images, *Remote Sensing of Environment*, 112:3916–3934.
- Xu, X., H. Du, G. Zhou, H. Ge, Y. Shi, Y. Zhou, W. Fan, and W. Fan, 2011. Estimation of aboveground carbon stock of Moso bamboo (*Phyllostachys heterocycla* var. *pubescens*) forest with a Landsat Thematic Mapper Image, *International Journal of Remote Sensing*, 32:1431–1448.
- Zhou, G., 2006. *Carbon Storage, Fixation and Distribution in Moso Bamboo (Phyllostachys Pubescens) Stands Ecosystem*, Ph.D. dissertation, Zhejiang University, Zhejiang, China, 55 p. (In Chinese).

(Received 09 July 2010; accepted 27 January 2011; final version 28 March 2011)

Editor *PE&RS*,

Give us your

Regarding the *articles* feedback! in December 2005. Addressing

pertinent chal

As you read *PE&RS* each month if you have comments or questions about the articles and papers that you read we want to hear from you.

in geospatial

Please include your name and contact information with each Letter to the Editor. Your name will be printed with your letter but the contact

today's com.

information will not be published. Please send your letters to

published for end-users

kimt@asprs.org.

educational and professional

Forthcoming Articles

- Tee-Ann Teo*, Bias Compensation in a Rigorous Sensor Model and Rational Function Model for High Resolution Satellite Images.
- Libin Zhou* and *Xiaojun Yang*, An Assessment on Internal Neural Network Parameters Affecting Image Classification Accuracy.
- Rey-Jer You* and *Bo-Cheng Lin*, Building Feature Extraction from Airborne Lidar Data based on Tensor Voting Algorithm.
- Stacey Fairweather*, *Christopher Potter*, *Robert Crabtree*, and *Shuang Li*, A Comparison of Multispectral ASTER and Hyperspectral Endmember Spectral Mixture Analysis for Sagebrush and Herbaceous Cover in Yellowstone.
- Temuulen Sankey* and *Nancy Glenn*, Landsat-5 TM and Lidar Fusion for Sub-pixel Juniper Tree Cover Estimates.
- Wouter Gheyle*, *Jean Bourgeois*, *Rudi Goossens*, and *Karsten Jacobsen*, Scan Problems in Digital CORONA Satellite Images from USGS Archives.
- Stephen C. Medeiros*, *Tarig Ali*, and *Scott C. Hagen*, Development of a Seamless Topographic/Bathymetric Digital Terrain Model for Tampa Bay, Florida.
- Zhixin Qi*, *Anthony G.O. Yeh*, *Xia Li*, and *Zheng Lin*, Integration of Polarimetric Decomposition, Object-oriented Image Analysis, and Decision Tree Algorithms for Land Use and Land Cover Classification using RADARSAT-2 Polarimetric SAR Data.
- Jesús Anaya* and *Emilio Chuvieco*, Accuracy Assessment of Burned Area Products in the Orinoco Basin.
- Xuelian Meng*, *Nate Currit*, *Le Wang*, and *Xiaojun Yang*, Detect Residential Buildings from Lidar and Aerial Photographs through Object-Oriented Land Use Classification.
- Rupert Müller*, *Thomas Krauß*, *Mathias Schneider*, and *Peter Reinartz*, Automated Georeferencing of Optical Satellite Data with Integrated Sensor Model Improvement.
- Yaseen T. Mustafa*, *Valentyn A. Tolpekin*, and *Alfred Stein*, Improving Forest Growth Estimates Using a Bayesian Network Approach.
- Chinsu Lin*, *Khongor Tsogt*, and *Chein-I Chang*, An Empirical Model-based Method for Signal Restoration of SWIR in ASD Field Spectroradiometry.
- Duangduen Roongpiboonsopit* and *Hassan A. Karimi*, Integrated Global Navigation Satellite System (iGNSS) QoS Prediction.
- V.F. Rodríguez-Galiano*, *B. Ghimire*, *E. Pardo-Igúzquiza*, *M. Chica-Olmo*, and *R.G. Congalton*, Incorporating the Downscaled Landsat TM Thermal Band in Land-cover Classification Using Random Forest.
- George Ch. Miliareisis*, Elevation, Latitude/Longitude Decorrelation Stretch of Multitemporal LST Imagery.
- Yuhong He*, *Anum Khan*, and *Amy Mui*, Integrating Remote Sensing and Wavelet Analysis for Studying Fine-scaled Vegetation Spatial Variation among Three Different Ecosystems.
- Wenkai Li*, *Qinghua Guo*, *Marek K. Jakubowski*, and *Maggi Kelly*, A New Method for Segmenting Individual Trees from the Lidar Point Cloud.
- You Kyung Han*, *Young Gi Byun*, *Jae Wan Choi*, *Dong Yeob Han*, and *Yong Il Kim*, Automatic Registration of High-Resolution Images Using Local Properties of Features.
- Abraham Growcott*, *Pascal Sirguey*, and *Stephen M. Dawson*, Development and Assessment of a Digital Stereo Photogrammetric System to Measure Cetaceans at Sea.
- Manuel A. Aguilar*, *Fernando J. Aguilar*, *María del Mar Saldaña*, and *Ismael Fernández*, Geopositioning Accuracy Assessment of GeoEye-1 Panchromatic and Multispectral Imagery.
- Susmita Sen*, *Carl E. Zipper*, *Randolph H. Wynne*, and *Patricia F. Donovan*, Identifying Revegetated Mines as Disturbance/Recovery Trajectories Using Interannual Landsat Chronosequence.

Daily MODIS Data Trends of Hurricane-induced Forest Impact and Early Recovery

Elijah Ramsey III, Joseph Spruce, Amina Rangoonwala, Yukihiro Suzuoki, James Smoot, Jerry Gasser, and Terri Bannister

Abstract

We studied the use of daily satellite data from the Moderate Resolution Imaging Spectroradiometer (MODIS) sensors to assess wetland forest damage and recovery from Hurricane Katrina (29 August 2005 landfall). Processed MODIS daily vegetation index (VI) trends were consistent with previously determined impact and recovery patterns provided by the “snapshot” 25 m Landsat Thematic Mapper optical and RADARSAT-1 synthetic aperture radar satellite data. Phenological trends showed high 2004 and 2005 pre-hurricane temporal correspondence within bottomland hardwood forest communities, except during spring green-up, and temporal dissimilarity between these hardwoods and nearby cypress-tupelo swamp forests (*Taxodium distichum* [baldcypress] and *Nyssa aquatica* [water tupelo]). MODIS VI trend analyses established that one year after impact, cypress-tupelo and lightly impacted hardwood forests had recovered to near pre-hurricane conditions. In contrast, canopy recovery lagged in the moderately and severely damaged hardwood forests, possibly reflecting regeneration of pre-hurricane species and stand-level replacement by invasive trees.

Introduction

In our study of the impacts of Hurricane Katrina (29 August 2005 landfall in Louisiana) to the lower Pearl River flood plain forests of Louisiana, (Ramsey *et al.*, 2009a; Figure 1), we defined spatial patterns of impact and short-term recovery in forested wetlands by using satellite optical and radar image data. Impact and recovery patterns and trends within the wetland forest were determined using change detection analyses of optical vegetation index (VI) products derived from 25 m Landsat Thematic Mapper (TM) imagery (Plate 1) and calibrated 25 m RADARSAT-1 synthetic aperture radar (SAR) intensity images collected before, within a few

Elijah Ramsey III is with the U.S. Geological Survey, National Wetlands Research Center, 700 Cajundome Blvd., Lafayette, LA 70506 (elijah_ramsey@usgs.gov).

Joseph Spruce and James Smoot are with the Computer Sciences Corporation, Stennis Space Center, MS 39529.

Amina Rangoonwala, and Terri Bannister are with Five Rivers Services LLC, Colorado Springs, CO 80918, and formerly with IAP World Services, Inc., Cape Canaveral, FL 32920.

Yukihiro Suzuoki is with Japan Space Imaging Corporation, Tokyo, Japan, and formerly with ASci Corporation, Inc., McLean, VA 22101.

Jerry Gasser is with Lockheed Martin Mission Services, Stennis Space Center, MS 39529.

days after, and about one and two months after the hurricane landfall.

Our success in mapping the storm impact was based on a combination of opportunistic and emergency response collections of satellite images with stand-level (25 m) resolution; an improved approach to forested wetland impact assessment would be based on consistent and higher frequency temporal sampling. The success of emergency response mapping for resource damage assessments is highly reliant on the availability of comparable and timely “before” and “after” recordings of the vegetation condition. In addition to initial emergency response, longer recovery monitoring can expose more subtle abnormalities in phenological trends that indicate latent biophysical changes initiated by a preceding impact event (Middleton, 2009). Trends of relevant coastal ecosystem indicators (e.g., vegetation greenness) based on consistent and appropriate temporal scales are powerful tools for assessing ecosystem change and recovery and functional structure and associations.

The Moderate Resolution Imaging Spectroradiometer (MODIS) offers a source of high temporal resolution data for monitoring vegetation condition at regional scales; however, two noteworthy problems hamper the application of MODIS image data to coastal terrestrial ecosystem monitoring. First, the 250 m (a red and a near-infrared band), 500 m (blue, green, near-infrared, and shortwave infrared bands), and remaining (1,000 m) bands are generally inadequate for most typical forest stand-level mapping applications and tend to be primarily suitable for regional applications which require or otherwise benefit from high temporal fidelity (Ramsey *et al.*, 2009a; Klemas, 2005). For example, AVHRR data at the 1 km scale were useful for assessing forest damage and initial recovery from Hurricane Andrew (Ramsey *et al.*, 1997, 1998, and 2001). More recently, MODIS time-series data have been used to assess Hurricane Katrina impacts on forest biomass (Chambers *et al.*, 2007). In addition, clouds often obscure the landscape, particularly in subtropical to tropical regions (Ramsey *et al.*, 1997, 2009a, and 2009b).

Temporal collection inconsistency in terms of cloud-free data coverage can be a problem with sensors like Landsat, which revisit and collect data at a given spot only once every 16 days. In contrast, the MODIS sensors onboard the Aqua and Terra satellites each collect daily daylight images of a given area. Even though providing two daylight MODIS collections

Photogrammetric Engineering & Remote Sensing
Vol. 77, No. 11, November 2011, pp. 1133–1143.

0099-1112/11/7711-1133/\$3.00/0

© 2011 American Society for Photogrammetry
and Remote Sensing

per 24 hours for a given location, cloud cover can still be problematic. To further increase cloud-free coverage, data from the two MODIS sensors can be fused (Xiong and Barnes, 2006). The dual data source along with time-series data processing software can be used in conjunction with a standard MODIS (MOD35) cloud detection product described by Frey *et al.* (2008) and Ackerman *et al.* (2008) to effectively mask out the clouds and cloud shadows. Further processing enables cloud-related data gaps to be temporally interpolated with appropriate response values obtained from non-cloud-affected temporally adjacent data points from the time series.

Time-series data processing software packages have been developed for temporal processing of MODIS time series, including those for primarily producing vegetation phenology data layers. These software packages are used to generate MOD12 phenology products from MODIS MOD13 enhanced vegetation index (EVI) time-series data (Zhang *et al.*, 2003 and 2006) and phenology products generated from MOD15 leaf area index (LAI; Gao *et al.*, 2008). Similar software has been developed by Reed *et al.* (1994) with respect to AVHRR satellite-based observations of vegetation phenology and by Lunetta *et al.* (2006) regarding MODIS-based land-cover change detection. Other recent relevant examples of satellite time-series data processing include work by Chen *et al.* (2004) and Bradley *et al.* (2007).

Many of these packages were based in part on the TIMESAT package described by Jönsson and Eklundh (2004). The Time Series Product Tool (TSPT) software package developed at the National Aeronautics and Space Administration (NASA) John C. Stennis Space Center also utilizes routines and algorithms from TIMESAT and adds functions for custom processing of multiple standard MODIS and other satellite time-series datasets (e.g., Landsat) into time-series data products for vegetation monitoring (McKellip *et al.*, 2005 and 2008; Spruce *et al.*, 2011). As a precursor to computation of phenology products, time-series processing software programs include algorithms for cloud removal, noise suppression, and data void integration usually through temporal curve-fitting procedures. The intent of temporal data processing is to produce the highest quality time-series dataset possible where the problems of data voids from atmospheric contamination are effectively identified and diminished through interpolation and filtering.

While many software programs exist for MODIS time-series data processing, there can be differences in terms of their effectiveness for a given application. The latter can depend on the application, the sensor characteristics (e.g., spatial, temporal radiometric, and signal to noise resolution), the settings used in running the software (e.g., settings that control allowable data quality, noise detection, and interpolation of data gaps), and other factors (e.g., data storage and computational requirements). The time-series product effectiveness often is gauged through comparison with higher spatial resolution data products, though issues can occur with the suitability of higher resolution products as references. For example, point measurements, or even stand scale compatible measurements, of forest phenology are not necessarily representative of the same phenomenon at the regional MODIS scale (Fisher and Mustard, 2007). One method for increasing the comparability of ground-reference data to satellite-based phenology is to compare plots or ground sampling areas that are of sufficient spatial extent to be comparable to the coarser spatial resolution satellite data (White and Nemani, 2006). In terms of assessing phenology of wetland forest damage from hurricanes, this was accomplished in our study by assessing MODIS vegetation index responses for specific previously defined damage polygons (or equivalently raster bitmaps) created with 25 m optical and radar data analyses (e.g., Plate 1 and Figure 2).

The vegetation index (VI) used for our study was the normalized difference vegetation index described by Tucker (1979). This VI was selected because of its quantitative indication of foliage greenness and quantity and because it is based on the highest spatial resolution MODIS 250 m red and near infrared bands. Even though atmospheric correction was not employed in the computation and application of the MODIS VI products used in our study, these products were computed by using a sequence of rigorous temporal processing (e.g., noise reduction, removal of poor viewing geometry data, multi-MODIS sensor data fusion, and void interpolation) procedures that collectively helped to minimize occurrences of aberrant VI values in the time series caused by inferior (off nadir) illumination and atmospheric contamination. The use of the VI also contributed to the normalization (i.e., mitigation) of effects from atmospheric contamination and inferior viewing geometry (Huete *et al.*, 1999).

The spatial resolution incompatibility of MODIS with Landsat TM and RADARSAT-1 data was minimized by using only the 250 m MODIS bands for computing the VI (e.g., Plate 1 and Figure 2). With the temporal consistency improvement and the spatial restriction to MODIS 250 m VI mapping, we anticipated that the temporal trends in VI would provide additional insight into the damage and recovery of the bottom land hardwood (BLH) forest type. This expectation was based in part on a previous case study in which AVHRR was used with Landsat TM data to assess regionally evident vegetation damage and recovery from Hurricane Andrew's landfall in southeastern Louisiana (Ramsey *et al.*, 1998 and 2001).

For Hurricane Katrina, the first study objective was to determine whether or not the previously documented 25 m stand-level short-term patterns of forest impact and recovery were identifiable on a VI derived from the lower 250 m spatial resolution but higher daily temporal resolution MODIS image data. Within the research process, we examined whether or not the availability of immediately before and after daily and comparable MODIS VI trends enhanced assessment and differentiability of impacts between cypress-tupelo and BLH forests and within evident damage zones of the BLH forest. The second study objective was to demonstrate the advantages of the higher temporal frequency and longer term VI trends in exposing abnormalities in the wetland forest phenological patterns that could indicate latent biophysical changes initiated by Hurricane Katrina impact. To this end, we added 2004 and 2006 yearly trends to the 2005 trend that encompassed the initial impact and short-term recovery periods.

Study Area

The study area included the wetland forests within the State of Louisiana's Pearl River Wildlife Management Area (PRWMA) managed by the Louisiana Department of Wildlife and Fisheries (Figure 1). The PRWMA contains 14,177 ha of flat, low lying terrain largely occupied by wetland forests with poor drainage and subject to annual and episodic flooding. Before Hurricane Katrina, the northern 60 percent of the PRWMA contained a BLH forest of variable age and species that transitioned to a cypress-tupelo forest occupying the more southern PRWMA (Plate 1). According to White's (1983) floristic survey, overstory tree species in the eastern BLH forest were dominated by *Quercus michauxii*, *Magnolia virginiana*, and *Ilex opaca* and the western BLH forests were dominated by *Quercus lyrata*, *Carya spp.*, *Taxodium distichum*, *Nyssa aquatica*, and *Faximas spp.* Cypress-tupelo forests included baldcypress (*Taxodium distichum*) and tupelo gum (*Nyssa aquatica*) communities. Differences in dominant species composition between observed wetland forest cover types represent differences in resiliency to hurricane damage (Ramsey and Ragoonwala, 2010, unpublished data).

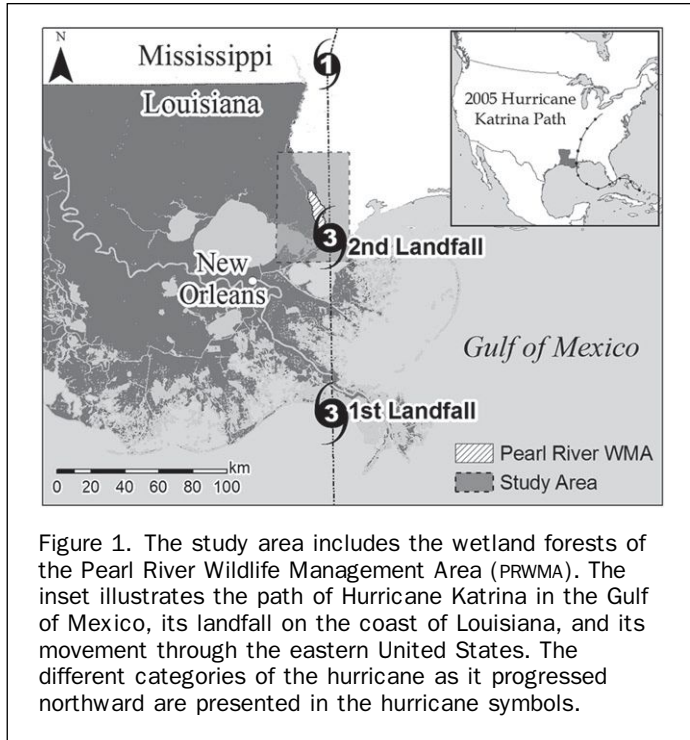


Figure 1. The study area includes the wetland forests of the Pearl River Wildlife Management Area (PRWMA). The inset illustrates the path of Hurricane Katrina in the Gulf of Mexico, its landfall on the coast of Louisiana, and its movement through the eastern United States. The different categories of the hurricane as it progressed northward are presented in the hurricane symbols.

Methods

MODIS VI Time-Series Production

The production of cloud-free daily MODIS VI time-series products involved a multistep process. First, daily Aqua and Terra MODIS sensor reflectance data were acquired as MOD02 reflectance data in the standard MODIS hierarchical data format. Subsequently, TSPT was used to re-project the data and then compute VI values from the input red and near-infrared reflectance data. TSPT then employed the MODIS cloud mask products (MOD35) to remove clouds and further restricted the retained cloud-free data to exclude pixels with sensor zenith angles of more than 47°. Afterward, the retained quality cloud-free data from Aqua and Terra MODIS sensors were fused into a composite image that yielded the best available quality data on a daily basis. The residual data voids were then temporally interpolated and filtered to remove remaining anomalous and erroneous VI values or “spikes” (i.e., residual noise from undetected clouds) using the Savitzky Golay filter (Savitzky and Golay, 1964). The filter was applied with a full width half maximum setting of four time steps (i.e., days), a temporal frame size of 15 time steps, and outlier (spike) removal setting of 0.5. These settings were determined and optimized through trial and error sensitivity analysis. In all of these processing steps, bilinear interpolation resampling was used.

Such processing, where successful, provides a means to compute and assess changes in the digital values of specific VI that are indicative of vegetation vigor, disturbance, and/or recovery status after a major disturbance, like a hurricane. Spike detection settings for identification of residual noise in the intermediate VI products are set conservatively to reduce and alleviate noise artifacts while effectively capturing the vegetation response to the hurricane. In doing so, the output retains and shows the initial VI drop from the hurricane’s impact and subsequent recovery in VI for certain vegetation types in the early months after the hurricane.

Spatial Alignment of the MODIS Images and the 25 m Impact and Recovery Polygons

MODIS images were georeferenced to the Lambert Conformal Conic (LCC) projection (using standard parallels, a central meridian, and false northing and easting as defined by the Louisiana State Plane South) to conform to the Louisiana State georeferencing system. The 25 m image databases were referenced to the same projection (Ramsey *et al.*, 2009a). The georeferenced MODIS data products were then subset to the PRWMA and areas immediately adjacent.

Cypress-tupelo and BLH forest extents were defined by polygons created from the previous classification of a 2004 summer TM image (Ramsey *et al.*, 2009a). Similarly, impact and recovery polygons created from the early (09) and late (25) October 2005 satellite data analyses were used to define the areas with low (slight to moderate defoliation), moderate (widespread defoliation with branch loss), and severe (defoliation, branch loss, and downed trees) impacts to the

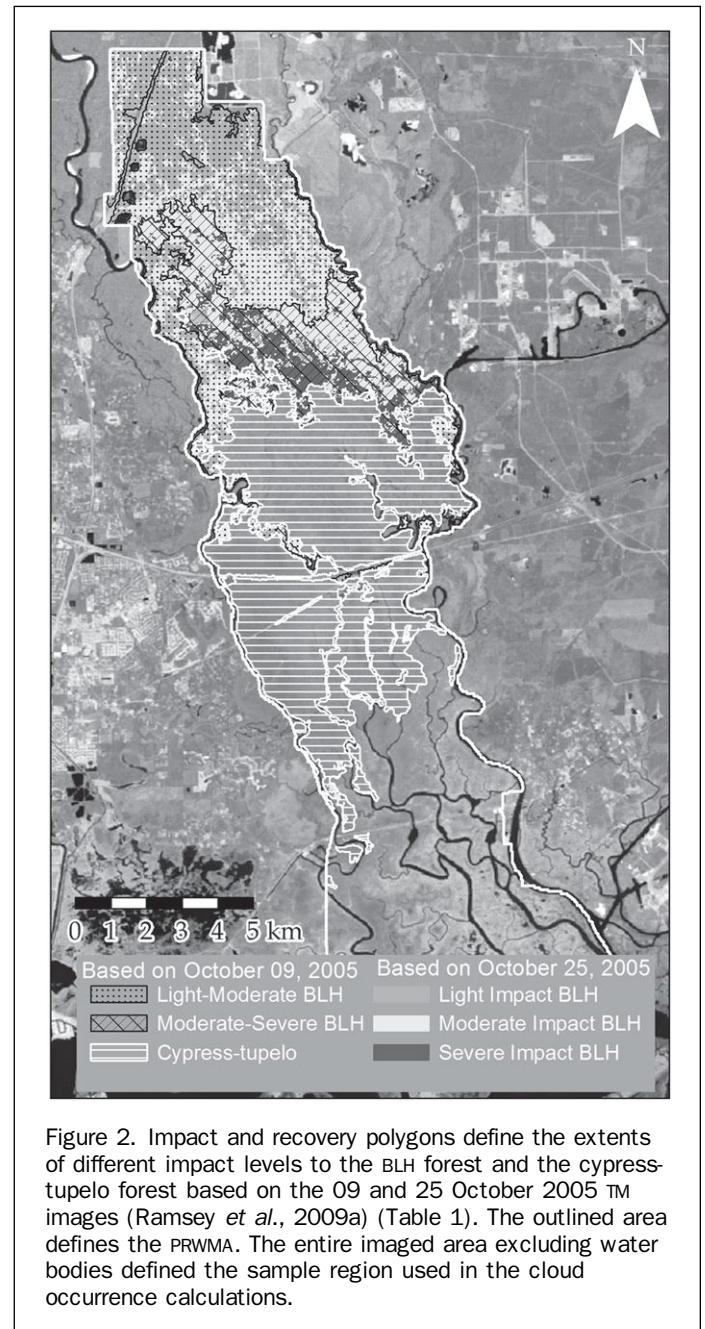


Figure 2. Impact and recovery polygons define the extents of different impact levels to the BLH forest and the cypress-tupelo forest based on the 09 and 25 October 2005 TM images (Ramsey *et al.*, 2009a) (Table 1). The outlined area defines the PRWMA. The entire imaged area excluding water bodies defined the sample region used in the cloud occurrence calculations.

BLH forest (Ramsey *et al.*, 2009a) (Figure 2). Impact severity designations relied on general site assessment, discussions with PRWMA personnel (J. Stafford, Region 7 Biologist Manager, Louisiana Department of Wildlife and Fisheries, personal communication), and previous documentation of cypress-tupelo and BLH forest responses to an intense storm impact (Ramsey *et al.*, 1998). Based on that experience, post-recovery analyses was limited in time in order to alleviate ambiguity in the impact assessments caused by changes brought on by fall senescence and by low-lying shrub and vine growth, particularly where tree fall was widespread (Ramsey *et al.*, 2009a). A combination of site assessment, discussions with PRWMA personnel, mapping experience, and integration of both the initial and short-term recovery assessments were used to define each impact and recovery polygon designation (Ramsey *et al.*, 2009a).

To prepare for comparing these impact and recovery polygons with the MODIS products, vector-smoothing algorithms were applied, and exclusion of polygons encompassing less than 10,000 m² were eliminated to reduce noise (e.g., artifacts in the classification and raster to vector conversion) and increase pertinent information content (PCI Geomatics, 1998).

The Daily Mean VI for each Impact and Recovery Polygon

Cypress-tupelo and BLH forest impact polygons (depicted on Figure 2) based on the 09 and 25 October 2005 25 m satellite data analyses were overlaid on the 2004, 2005, and 2006 suites of MODIS VI images. VI image values were then extracted under each polygon for each day of each year (PCI Geomatics, 1998). Each year spanned from 01 January to 31 December and included 365 days or image layers. (The leap day in 2004 was deleted.)

The ten-fold spatial sampling disparity between the 25 m Landsat and RADARSAT-1 and 250 m MODIS satellite data products had the highest potential for increasing disagreement between the 25 m and 250 m VI comparisons (Plate 1 and Figure 3). The overlay and spatial correspondence calculation was accomplished by reprojecting the bitmaps (raster representation of the polygons) defining the spatial coverages of each impact zone derived from the 25 m analyses to a 250 m representation. A nearest neighbor approach was used to determine which 250 m pixels spatially corresponded with the applied 25 m bitmap. The criteria for inclusion of the 250 m pixel and its associated VI values was whether or not a 25 m bit was located at the

center of the 250 m pixel. Although based on a simplistic approach, visual examination showed the 25 m bitmap and derived 250 m coverages aligned well. The most notable disparities in spatial correspondence were associated with the severe impact polygon (Figure 2; 25 October 2005) exhibiting the highest spatial dispersion of all the impact and recovery polygons.

To quantitatively assess the performance of the simple nearest neighbor approach, we created a procedure within the image processing software (PCI Geomatics, 1998) that associated the spatial location of each bit of each different bitmap with a unique 250 m pixel. For each day and each bitmap (or polygon), the number of spatial co-occurrences per 250 m pixel and its VI values were tracked. That tracked information was used to create a VI frequency distribution that represented the number of bits per bitmap and day that were spatially associated with discrete VI values (at the 0.1 percent level). The bit per VI value frequencies were the weighting values used in the mean and variance calculations (following Andersen *et al.*, 1984; equation 3.12). These statistics based on the VI frequency distributions were compared to the calculated mean and variance statistics based on the nearest neighbor selection of 250 m pixels and their associated VI values. As stated, based on visual inspection of the nearest neighbor results, we expected close correspondences of the means of the two approaches; however, because of the disparity in sample number and the fact that the 25 m bits sampled individually constant valued 250 m pixels, we anticipated higher variances about the 250 m means as compared to the 25 m variance measures.

Daily Cloud Cover Estimates

Initial inspection of the VI trends suggested quasi-sinusoidal cycles that appeared unusual for phenological patterns associated with southern forests. Though trends were largely consistent which might be expected in a forest without hurricane effects, it is possible that cloud occurrences may have impacted the trend results. MODIS data analyses do mitigate most cloud cover impacts, but because they do not completely eliminate them, we visually examined whether the quasi-sinusoidal features could be related to cloud contamination by producing percent cloud occurrence images corresponding to the daily MODIS VI trend products. From each daily cloud occurrence image, the percent of land area within the study area (Figure 1) influenced by clouds

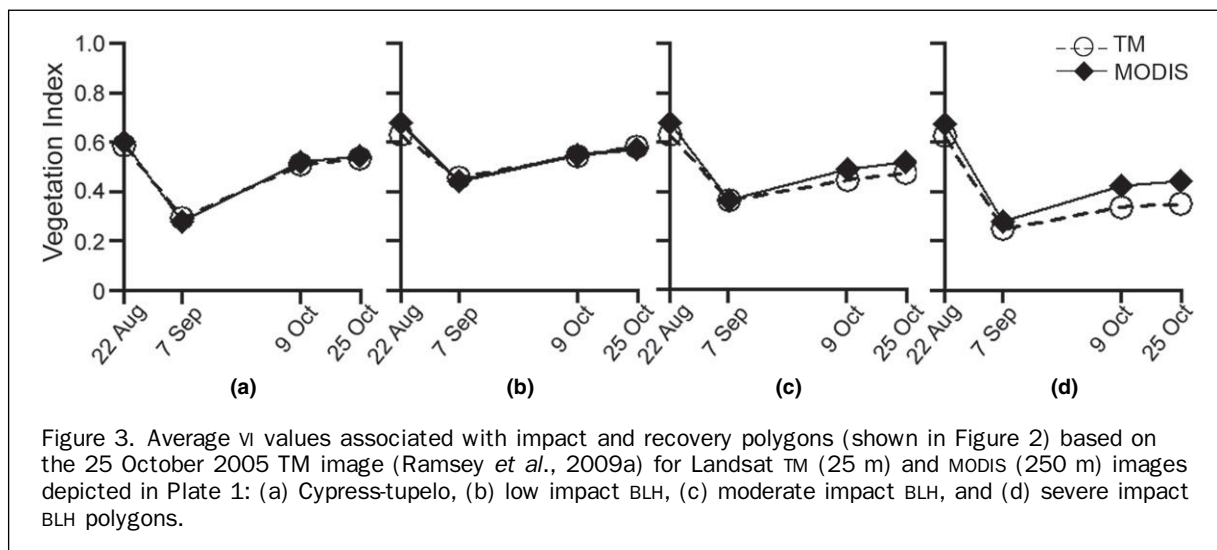


Figure 3. Average VI values associated with impact and recovery polygons (shown in Figure 2) based on the 25 October 2005 TM image (Ramsey *et al.*, 2009a) for Landsat TM (25 m) and MODIS (250 m) images depicted in Plate 1: (a) Cypress-tupelo, (b) low impact BLH, (c) moderate impact BLH, and (d) severe impact BLH polygons.

was calculated. The daily cloud cover was included in the trend graphs for comparison.

Comparison of Yearly VI Trend Differences

To highlight the dissimilarities between pre-hurricane and post-hurricane cypress-tupelo and BLH forests and their associated impact and recovery polygons, MODIS VI differences were calculated between 2004, as the base year, and 2005 and 2006. Pre-hurricane (01 January to 28 August) 2004 versus 2005 VI calculations provided an estimate of nonimpact year to year variability. Post-hurricane (29 August to 25 October and 26 October to 31 December) 2004 versus 2005 VI differences emphasized the immediate impact and near-term recovery. VI differences related to 2004 versus 2006 compared to the 2004 versus 2005 differences provided qualitative assessment of the temporal variability of recovery per forest type and impact level. Errors associated with the VI differences indicated the ability to discern differences given the small 250 m sample size and spatially convoluted impact and recovery polygons. Error estimates of the difference were calculated by propagating the standard deviation (Std) of each VI used in the difference calculation (following Bevington, 1969). The Std indicates how tightly the individual VI values (per pixel) composing each polygon group about the associated polygon VI mean (Streiner, 1996).

In order to further elucidate seasonal patterns in the post-hurricane 2006 recovery, 2004 minus 2005 differences were subtracted from 2004 minus 2006 differences. The direct calculation of the 2004 to 2005 and 2006 difference provided a metric to evaluate the recovery patterns and to quantify their strength per forest type and impact level. These patterns were used to indicate time periods of stability more conducive for assessing recovery.

Results

Assessment of 250-m VI Means and Variance Measures

Daily VI means calculated by using the nearest neighbor selection and the frequency distribution methods differed on average by $<0.1\% \pm 1\%$ (Std) in comparisons that included the 2006 low and severe impact and recovery polygons (extents shown on Figure 2). The closeness of the means justified the use of the simple nearest neighbor approach for extracting the daily polygon VI statistics from the 250 m MODIS data. As expected, the variance magnitudes associated with the frequency distribution were much lower than those calculated from the set of 250 m VI pixels selected with the nearest neighbor approach. Although no compensation for the coarse spatial resolution of MODIS was included in the polygon overlays and VI extractions, we believe the variance calculated at the 250 m level best represented the inherent VI variability considering the relatively small sample size and convoluted spatial coverages of the polygons. Table 1 includes the calculated areas and number of MODIS pixels extracted per polygon (as shown in Figure 2). Each polygon average VI and its associated variance for each year is included in Table 2. The number of observations (250 m pixels) used in the mean and variance calculations is listed in Table 1.

Overlay of TM and MODIS Composite VI Images and VI Aggregate

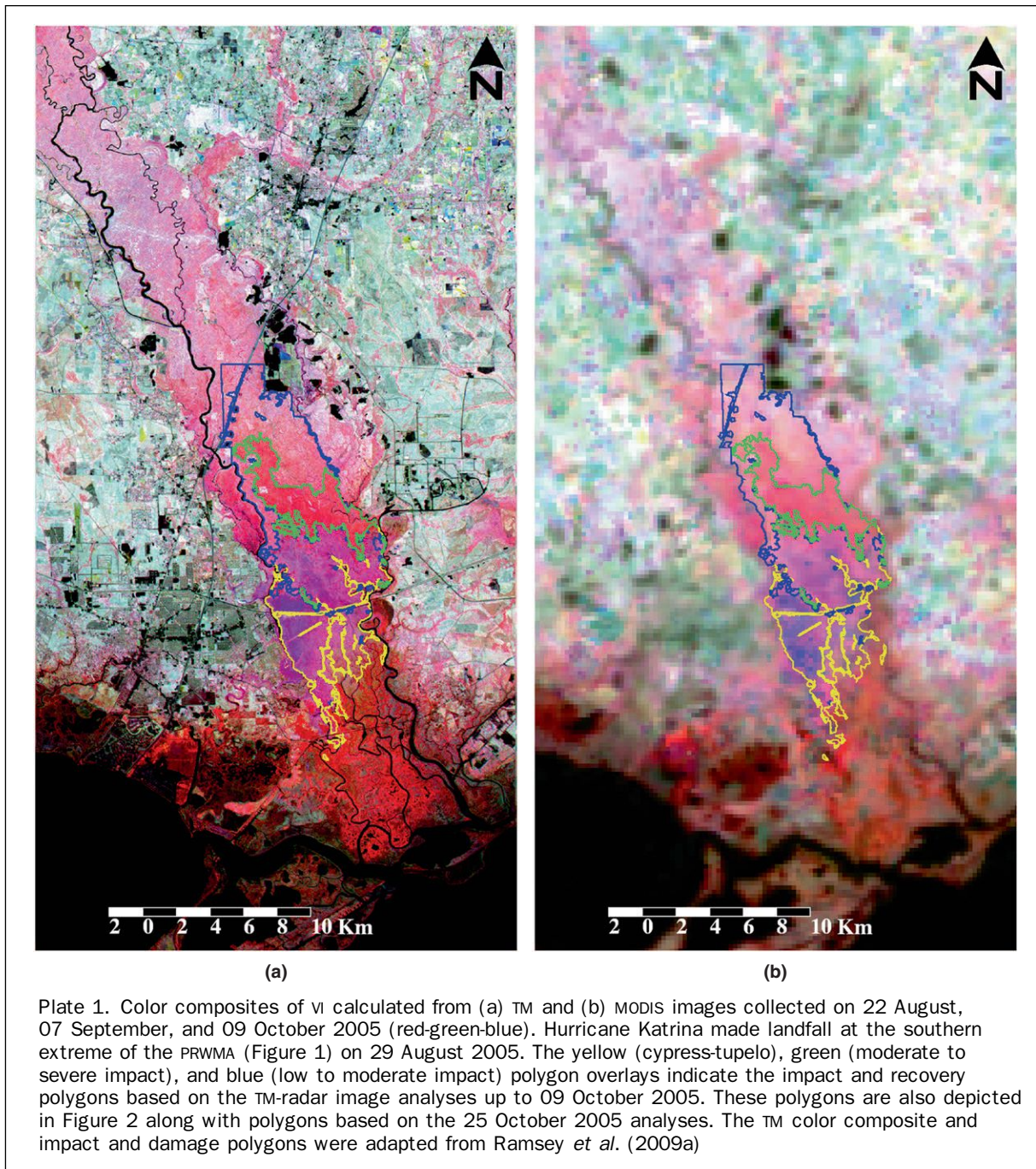
The overlays of 22 August, 07 September, and 09 October 2005 TM and MODIS VI images exhibited remarkable correspondence (Plate 1). Similarly, the TM and MODIS mean VIs associated with the cypress-tupelo forest polygon and the 25 October 2005 low, moderate, and severe BLH impact polygons show nearly replicate trends and magnitudes (Figure 3).

TABLE 1. IMPACT AND RECOVERY POLYGONS IN THE PRWMA

Impact and Recovery Polygons		Observations	
Data	Condition	Total (km ²)	250 m MODIS Pixels
	Cypress-Tupelo	46.5	744
Based on 09 Oct	Low to Moderate Impact BLH	32.5	520
	Moderate to Severe Impact BLH	18.4	294
	Low Impact BLH	17.1	273
Based on 25 Oct	Moderate Impact BLH	26.8	429
	Severe Impact BLH	7.4	118
Total		148.6	2,378

TABLE 2. MODIS VI MEAN AND VARIANCE ESTIMATES PER IMPACT AND RECOVERY POLYGON (MODIS VI AVERAGE VARIANCE ESTIMATES (AVE) ARE COMPUTED USING THE IMPACT AND RECOVERY POLYGONS DERIVED FROM THE 25 OCTOBER 2005 TM COLLECTION AS DEPICTED IN PLATE 1 AND FIGURE 2. THE NUMBER OF OBSERVATIONS USED IN THE STANDARD DEVIATION (STD) CALCULATION ARE LISTED IN THE MODIS PIXELS COLUMN IN TABLE 1.)

Year	Cypress-Tupelo		Low Impact BLH		Moderate Impact BLH		Severe Impact BLH		Averaged by Year	
	Ave	± Std	Ave	± Std	Ave	± Std	Ave	± Std	Ave	± Std
2004	0.488	0.053	0.582	0.044	0.584	0.045	0.570	0.050	0.556	0.048
2005	0.484	0.059	0.558	0.044	0.538	0.048	0.502	0.043	0.521	0.049
2006	0.459	0.056	0.558	0.051	0.516	0.058	0.448	0.049	0.495	0.054
Average	0.477	0.056	0.566	0.046	0.546	0.050	0.507	0.047	0.524	0.050



This high correspondence attests to the quality performance of the TSPT processing.

Cloud Cover and VI Trends

Cloud cover percentages included on the trend graphics illustrate the temporal correspondence between cloud cover and VI trends (Figures 4a, 4b, and 4c). Although the visual correspondence is scarce, there are a few short time periods on the graphs where the rise and fall in cloud cover corresponds to an inverse VI pattern, most notably on Figures 4a and 4c. On the contrary, many abrupt changes in the VI trends are reverse to the above patterns or seem totally independent of the cloud cover trends. This limited evaluation of cloud cover influence on the observed MODIS VI

trends suggests that extensive cloud covers may have impacted the VI estimates at times; however, the relation and magnitude of influence were unclear. The high consistency in TM and MODIS VI results (Plate 1 and Figure 3) and pre-hurricane BLH trends in 2004 and 2005 (and the co-occurrence in Hurricane Katrina landfall and abrupt decrease in VI) substantiated the interpretability of the MODIS VI results with respect to the study objectives.

Early and Late October Impact and Recovery NDVI Trend Comparisons

MODIS VI trends based on the early (09) and late (25) October 2005 impact and recovery zones showed similar patterns differing mainly in VI magnitude (only trend lines associated with 25 October polygons are included; Figures 4a, 4b, and 4c).

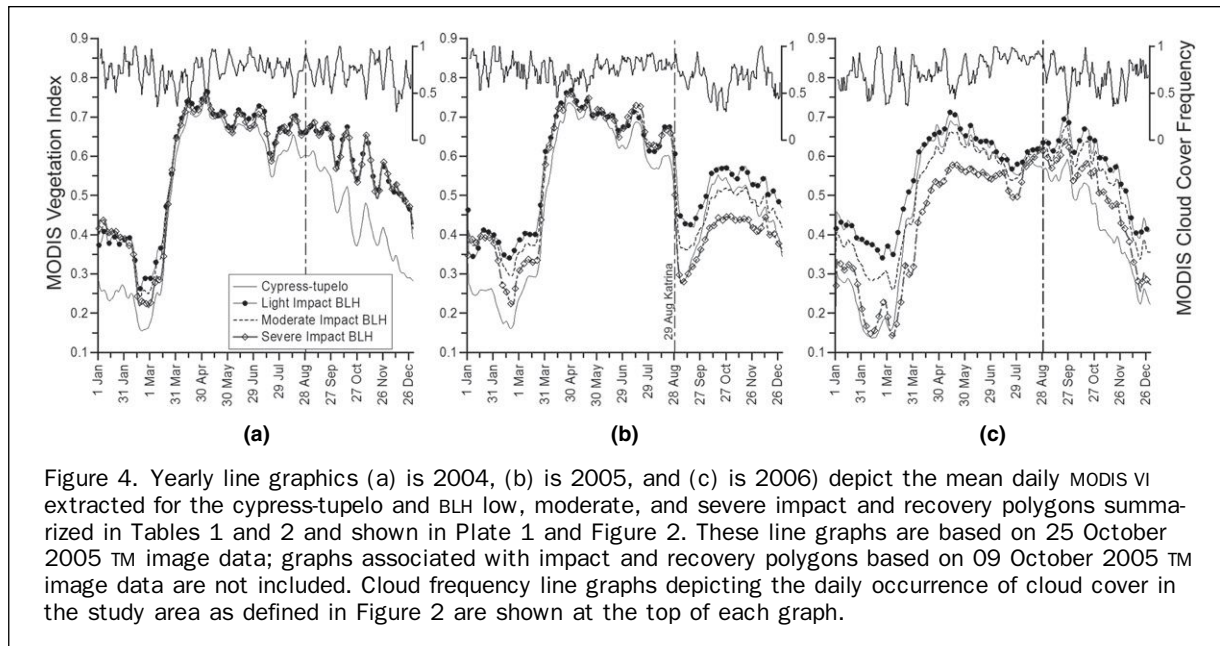


Figure 4. Yearly line graphics (a) is 2004, (b) is 2005, and (c) is 2006 depict the mean daily MODIS VI extracted for the cypress-tupelo and BLH low, moderate, and severe impact and recovery polygons summarized in Tables 1 and 2 and shown in Plate 1 and Figure 2. These line graphs are based on 25 October 2005 TM image data; graphs associated with impact and recovery polygons based on 09 October 2005 TM image data are not included. Cloud frequency line graphs depicting the daily occurrence of cloud cover in the study area as defined in Figure 2 are shown at the top of each graph.

In particular, the trends based on the 25 October VI data showed

- the BLH severe impact trend line lower than the combined moderate to severe impact trend line based on the 09 October VI data;
- the 25 October BLH moderate impact trend line higher than the 09 October VI moderate to severe impact trend line but lower than the 09 October VI combined low to moderate impact trend line;
- the 25 October BLH low impact trend line only slightly higher than the 09 October VI low to moderate impact trend line.

Cypress-tupelo trend lines based on MODIS VI data did not change because its impact and recovery trend was aggregated for the entire cypress-tupelo PRWMA coverage. The near consistent early- and late-October 2005 impact and recovery patterns allowed an effective illustration of the changes in MODIS VI trends relevant to Hurricane Katrina impacts by the trend lines based on the 25 October VI data.

NDVI Trends Based on Late October Impact and Recovery Polygons

The juxtaposition of MODIS VI trends in 2004 representing the 25 October BLH impact and recovery zones supported the spectral similarity of these different impact and recovery patterns documented in the single-date early- and late-October 2005 25 m satellite data analyses (Figure 4a). The only disparity supporting a species dependency to the observed impact and recovery patterns occurred in the spring green-up period between about 01 February and mid-March 2004. The VI trend associated with cypress-tupelo forest in 2004 aligned with the BLH trends from spring to early August then increasingly diverged until reaching maximum differences in the winter. MODIS VI trends in 2005 displayed similar phenological behaviors for these cover types until Hurricane Katrina landfall (Figure 4b). Shortly after the storm, both BLH and cypress-tupelo forests exhibited an atypical sudden and dramatic decrease in VI magnitudes. As revealed in the 25 m analyses, MODIS VI initial impact severities and short-term recoveries trends differed between cypress-tupelo and BLH forests and within the BLH.

As indicated by MODIS VI magnitudes, the cypress-tupelo and the farthest southern BLH forests sustained the highest

damage, while the more northern BLH forest sustained relatively lighter damage (Figure 4b). Based on VI trends, cypress-tupelo forests quickly recovered and surpassed the 2004 VI magnitudes by mid- to late-October 2005 (Figure 4b). Although the change was less dramatic, the lightly damaged BLH forest had similarly recovered to 2004 VI levels by mid-October 2005 (Figure 4b). In contrast, moderate and severe impact BLH forests lagged behind (Figure 4b) and did not approach 2004 VI levels until late-fall 2005 (Figure 4c). MODIS 2006 trends exhibited high disparity between cypress-tupelo and the BLH forests and BLH impact and recovery polygons (Figure 4c).

VI Difference Trends

Yearly VI trends were more fully highlighted in the calculated VI difference trends (Figure 5a, 5b, 5c, and 5d). Pre-hurricane (01 January to 28 August) 2004 versus 2005 VI differences fluctuated ± 5 percent near zero for both cypress-tupelo and BLH forests. As noted in the yearly trends, the largest 2004 versus 2005 difference during the aforementioned pre-hurricane period occurred at spring green-up. A second difference peak occurred in early-July. Post-hurricane (29 August to 31 December) 2004 versus 2005 difference trends exhibited abrupt changes just after impact. In the 2005 post-hurricane period, the level of BLH recovery depended on impact level (Figures 5b, 5c, and 5d; Table 3). While initially defoliated by the hurricane, cypress-tupelo within a matter of weeks exhibited high VI values in this period as these forests grew new canopy foliage. This was already noted in the yearly trends (Figure 4b) and amplified on the 2005 difference trends (Figure 5a; Table 3).

Longer term recovery trend disparities also were represented on the VI difference trends (Figure 5a, 5b, 5c, and 5d). In the pre-hurricane months (01 January to 28 August), the 2006 cypress-tupelo and low impact BLH VI difference trends more closely tracked the 2004 and 2005 pre-hurricane VI trends than did the 2004 versus 2006 moderate and severe BLH impact trends. In the post-hurricane period (29 August to 31 December), near zero 2004 versus 2006 VI differences indicated cypress-tupelo and low impact BLH had recovered to near pre-hurricane levels (Table 3). In the period representing the initial 2005 impact

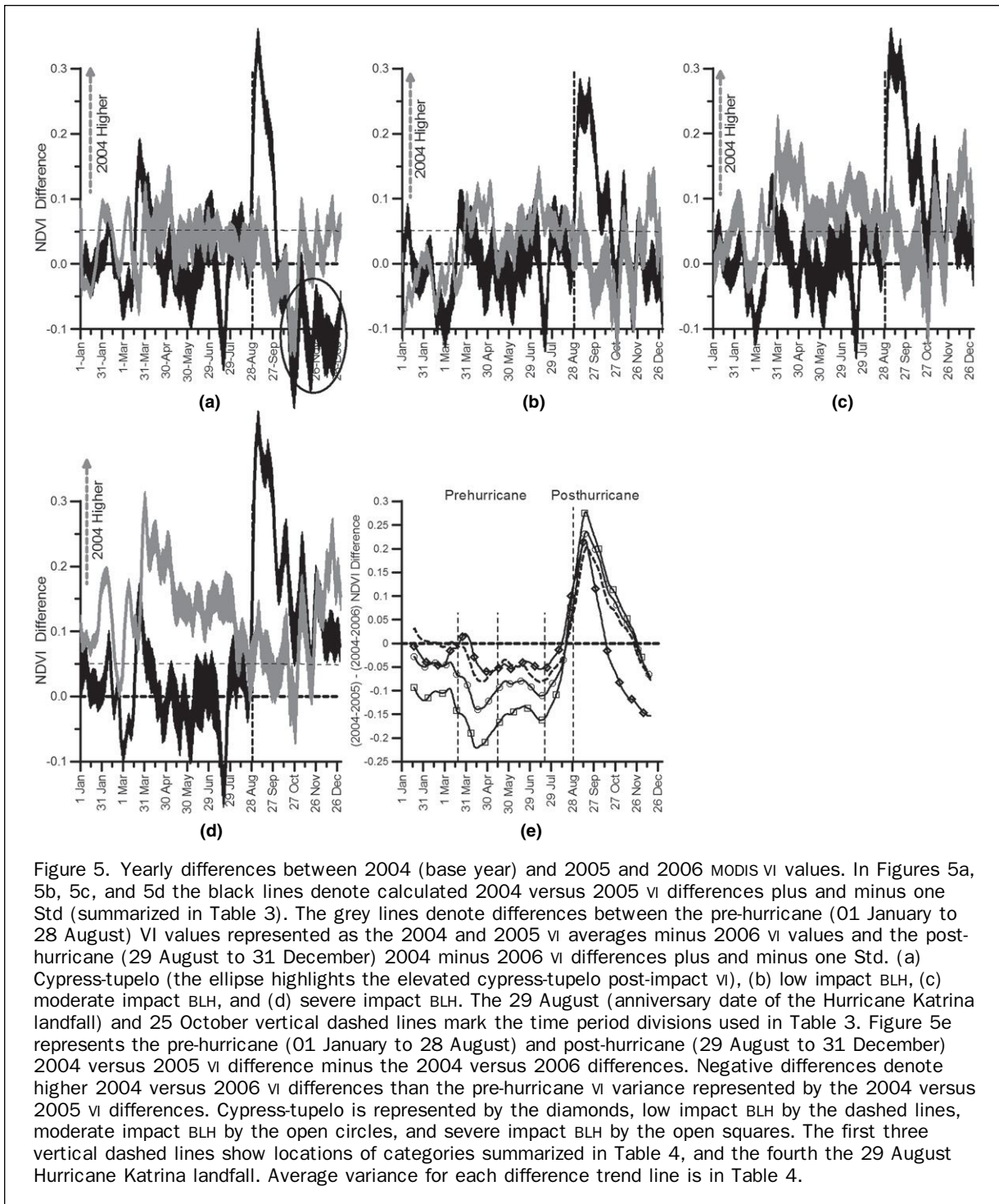


Figure 5. Yearly differences between 2004 (base year) and 2005 and 2006 MODIS VI values. In Figures 5a, 5b, 5c, and 5d the black lines denote calculated 2004 versus 2005 VI differences plus and minus one Std (summarized in Table 3). The grey lines denote differences between the pre-hurricane (01 January to 28 August) VI values represented as the 2004 and 2005 VI averages minus 2006 VI values and the post-hurricane (29 August to 31 December) 2004 minus 2006 VI differences plus and minus one Std. (a) Cypress-tupelo (the ellipse highlights the elevated cypress-tupelo post-impact VI), (b) low impact BLH, (c) moderate impact BLH, and (d) severe impact BLH. The 29 August (anniversary date of the Hurricane Katrina landfall) and 25 October vertical dashed lines mark the time period divisions used in Table 3. Figure 5e represents the pre-hurricane (01 January to 28 August) and post-hurricane (29 August to 31 December) 2004 versus 2005 VI difference minus the 2004 versus 2006 differences. Negative differences denote higher 2004 versus 2006 VI differences than the pre-hurricane VI variance represented by the 2004 versus 2005 VI differences. Cypress-tupelo is represented by the diamonds, low impact BLH by the dashed lines, moderate impact BLH by the open circles, and severe impact BLH by the open squares. The first three vertical dashed lines show locations of categories summarized in Table 4, and the fourth the 29 August Hurricane Katrina landfall. Average variance for each difference trend line is in Table 4.

and short-term recovery (29 August to 25 October), moderate and severe 2004 versus 2006 BLH impact differences also showed dramatic recovery but after that remained at post-hurricane 2004 versus 2005 levels (Table 3).

Pre-hurricane (01 January to 28 August) recovery trends in 2006 were further clarified by comparing 2004 versus 2005 VI and the 2004 versus 2006 VI differences (Figure 5e). In this period, cypress-tupelo and low impact BLH closely aligned with 2004 and 2005 pre-hurricane conditions based on MODIS VI (Figure 5e; Table 4). In contrast, moderate and severe impact BLH trends exhibited successively higher differences

(Figure 5e; Table 4). Within these pre-hurricane overall trends from 01 January through late-July, four time periods exhibiting noticeably different VI difference patterns emerged in the cypress-tupelo and BLH forests. These patterns consisted of (a) the winter flat (01 January to 19 March), (b) the early-spring minimum (20 March to 14 May), (c) the late-spring to early-summer flat (15 May to 19 July), and (d) the summer increase (20 July to 29 August). The first and third periods (the winter flat and the late-spring to early-summer flat) may offer the most stable time periods for monitoring forest recovery in these wetland forests (Figure 5e; Table 4).

TABLE 3. COMPARISONS OF MODIS 2004, 2005, AND 2006 VI DIFFERENCES. (AVERAGES (AVE) WERE CALCULATED FROM 2004 VERSUS 2005 AND 2004 VERSUS 2006 VI DIFFERENCES. THE STANDARD DEVIATIONS (STD) ARE PROPAGATED VARIANCES BASED ON THE STD OF THE INDIVIDUAL YEARLY VI VALUES. NEGATIVES DENOTE LOWER 2004 VERSUS 2005 OR 2006 VI AVERAGED. THE TIME DIVISIONS ARE LOCATED ON FIGURES 5A, 5B, 5C, AND 5D.)

Impact and Recovery Polygon	29 Aug – 25 Oct				26 Oct – 31 Dec			
	2004 vs 2005		2004 vs 2006		2004 vs 2005		2004 vs 2006	
	Ave	± Std	Ave	± Std	Ave	± Std	Ave	± Std
Cypress-Tupelo	0.12	0.04	-0.01	0.04	-0.11	0.04	0.02	0.03
Low Impact BLH	0.15	0.03	0.00	0.03	0.00	0.03	0.02	0.04
Moderate Impact BLH	0.21	0.02	0.03	0.03	0.05	0.05	0.07	0.07
Severe Impact BLH	0.27	0.03	0.06	0.04	0.12	0.04	0.12	0.04

TABLE 4. PRE-HURRICANE AND POST-HURRICANE MODIS VI DIFFERENCE COMPARISONS (AVERAGES (AVE) WERE CALCULATED FROM THE 2004 VERSUS 2005 DIFFERENCE MINUS THE 2004 VERSUS 2006 DIFFERENCES FOR EACH TIME PERIOD. THE TIME PERIODS ARE DEPICTED ON FIGURE 5E. THE STANDARD DEVIATIONS (STD) WERE CALCULATED AS VARIANCE ABOUT THE AVERAGE DIFFERENCES. NEGATIVES DENOTE HIGHER 2004 VERSUS 2006 THAN 2004 VERSUS 2005 DIFFERENCES.)

Impact and Recovery Polygon	01 Jan – 19 Mar		20 Mar – 15 May		16 May – 20 Jul	
	Ave	± Std	Ave	± Std	Ave	± Std
Cypress-Tupelo	-0.02	0.05	-0.02	0.06	-0.05	0.02
Low Impact BLH	0.01	0.04	-0.05	0.05	-0.06	0.03
Moderate Impact BLH	-0.04	0.03	-0.11	0.05	-0.09	0.03
Severe Impact BLH	-0.10	0.05	-0.19	0.06	-0.15	0.03

Discussion

This study showed that, even though extensive cloud cover existed and possibly affected the VI trends at times, its influence on the interpretability of relative trend patterns among impact and recovery zones was substantially eliminated by the TSPT processing of the dual, integrated Aqua and Terra daily MODIS sensor data. MODIS VI trends replicated expected phenologies and hurricane impact responses and aligned remarkably well with VI spatial trends exhibited by Landsat TM impact and recovery images and Landsat TM VI aggregated by impact and recovery polygons. In addition, pre-hurricane MODIS VI BLH trends in 2004 and 2005 further substantiated the consistency of the daily VI record offered by TSPT processing. These and other discussed consistencies confirmed that the relative differences between trends were directly interpretable.

The pre-hurricane daily MODIS VI record considerably improved our understanding of the temporal VI trend associated with hurricane-induced forest damage and subsequent recovery, compared to information available from the snapshot recordings offered by the 25 m Landsat TM and RADARSAT-1 satellite image collections. Replicating the 25 m data analyses, the MODIS VI exhibited different impact and recovery trends in the cypress-tupelo versus BLH forests and within the BLH forest. Even the abnormal and elevated 2005 post-hurricane canopy foliage response associated with the cypress-tupelo forests that were indicated on the 25 m Landsat TM and RADARSAT-1 monitoring was clearly documented and its temporal duration timed in the MODIS VI trend analyses. Not directly distinguishable in the 25 m analyses were the detailed temporal VI response trends representing the cypress-tupelo and different impact and recovery zones within the BLH forest.

Multiple post-hurricane impact trends for these impact and recovery zones were discernable in the MODIS VI record through 2006, more than one year after the Hurricane Katrina Louisiana landfall. By using 2004 and 2005 VI trends

to represent pre-hurricane (01 January to 28 August) vegetation condition, post-hurricane 2004 versus 2006 VI difference analyses showed that by early-2006 cypress-tupelo and light impact BLH canopies had largely recovered to pre-hurricane foliage canopy greenness levels. On the contrary, VI trends of moderate to severe impact BLH forests differed highly from pre-hurricane levels throughout the period from 01 January to 28 August 2006, and although diminished, continued to differ through the end of 2006. A probable reason for the lagging recovery in these more severely impacted BLH forests could be fundamental changes in canopy structure and, in some cases, canopy composition, especially for those areas in the process of stand replacement.

The phenology represented by the severe and moderate impact BLH VI trends seems to correspond to severely damaged stands and subsequent replacement. The most severely impacted BLH forest would include the greatest tree fall, and although diminished, the moderately impacted BLH forest might nevertheless be distinguished by a higher incidence of gap creation and enlargement. Where gaps were created or enlarged, new species and replacement seedlings of similar composition to the pre-hurricane overstory species composition could have quickly established with the newly available light. Creation and enlargement of canopy gaps with the rapid establishment and growth of a sub-canopy or the wholesale replacement of tree stands would alter the site's phenological trends as represented by remotely sensed canopy foliage parameters, such as VI in this case. In fact, widespread replacement of pre-hurricane forest canopies is occurring in severe impact BLH forest zones within the study area (Jimmy Stafford, 2008, Louisiana Department of Wildlife and Fisheries, personal communication). Frequently, this replacement is through regeneration by *Triadica sebifera* (Chinese tallow), an aggressive and highly tolerant invasive tree species (Ramsey *et al.* 2005). The ability to capture these possible forest transitions exemplifies the advantage with MODIS of longer term and higher

frequency monitoring of forest recovery areas and threats to full recovery.

In the pre-hurricane 25 m Landsat TM and RADARSAT-1 analyses, the eastern and western divisions in BLH communities identified in White's (1983) floristic survey were not discernable; however, the pattern of the eastern and western forest communities' dominance coincided with spatial patterns determined in the 25 m impact and recovery analyses (Ramsey *et al.* 2009a; Ramsey and Rangoonwala, 2010, unpublished data). The pre-hurricane MODIS VI trends, however, suggested that spectral separation of the BLH communities may be possible in a fairly narrow time period from late-winter to early-spring encompassing the early-part of leaf regrowth and canopy green-up. Such phenological differences in vegetation greenness can be largely attributable to differences in species composition and other structural attributes (e.g., intra-stand height, density, and arrangement) of the forest overstory within these communities. This apparent distinctiveness in VI response between the BLH communities was achievable because of the availability of the daily MODIS data and the phenological characteristics of these specific communities within the more broadly defined BLH type. The ability to separate spectrally the BLH community types during seasonal canopy foliage changes is supported by mapping based on late-fall and winter color infrared aerial photographic image data (Ramsey and Rangoonwala, 2010, unpublished data). The spatial coincidences in the color infrared and MODIS VI BLH community and impact severity mapping could establish an association between BLH community type and storm impact severity.

Although 25 m Landsat TM and RADARSAT-1 pre-hurricane mapping showed no conclusive spectral disparities between eastern and western BLH forest (Ramsey *et al.*, 2009b), classification of the pre-hurricane 25 m satellite images showed the capacity for spectral differentiation between the BLH and cypress-tupelo forests. The MODIS VI trend analyses confirmed the 25 m satellite data analyses and provided additional information. Pre-hurricane VI trends predicted increasing divergence between cypress-tupelo and BLH trends starting around mid-summer that reached its highest magnitude of difference in winter. Although not determined here, the higher VI differences would most likely suggest higher spectral contrast because the VI magnitudes are primarily driven by green foliage quantities in fully formed canopies and by canopy percent openness and background reflectance in more open canopies. Ramsey *et al.* (2006) noted that many BLH forest species form fuller summer canopies than mixed cypress-tupelo forests and can retain their leaves throughout most of the winter, the leaf turnover transition occurring rapidly within a short time period. The more prolonged retention of leaves and fuller canopies associated with some hardwood species could exacerbate winter VI differences related to canopy closure in cypress-tupelo versus BLH, and thereby, could augment the ability to spectrally differentiate between the more open canopy cypress-tupelo forest and the BLH forest.

Conclusions

The phenological characteristics of impacted wetland forest communities within the lower Pearl River were provided by the integration of 25 m satellite optical and radar satellite stand-level information with the high temporal yet lower spatial resolution 250 m daily MODIS image data. The daily MODIS VI mapping substantiated the overall 2004 and 2005 pre-hurricane consistency in BLH forest canopy foliage and captured the sudden damage to the lower Pearl River's

wetland forest that occurred during Hurricane Katrina's landfall. As in the 25 m Landsat TM and RADARSAT-1 satellite analyses, the MODIS VI showed a dramatic decrease in canopy foliage throughout this wetland forest and corroborated 2005 post-hurricane differential impact patterns. Post-hurricane VI trends documented the rapid and elevated foliage regrowth of the extensively defoliated cypress-tupelo forest and the disparate short-term recoveries associated with the differential BLH impact severities previously documented in 25 m snapshot image collections by Ramsey *et al.* (2009a). The MODIS VI trends, however, changed the monitoring paradigm from one based on chance collections of useable image data from Landsat TM and RADARSAT-1 sources to one based on consistent daily collections of image data from the two MODIS systems.

The MODIS VI trend analyses enabled a more complete description of the pre-hurricane phenologies and post-hurricane damage severities and recovery. Instead of monitoring based on opportunistic snapshots of the wetland forest condition, and even though cloud occurrence was frequently evident and often extensive, specialized processing provided consistent daily MODIS VI estimates of forest greenness conditions. With these daily products, time periods for optimal spectral separation between forest types and communities were observed. This information was not readily available from the alternative 25 m satellite collections of limited temporal availability. For instance, although nearly coincident in pre-hurricane spring to early-winter months, VI analyses identified a separation of BLH community trend in the pre-hurricane spring green-up period, representing observable differences in a specific phenological response per forest community type. In addition, an optimal time period for cypress-tupelo and BLH forest spectral separation was observed. Likewise, hurricane impact and recovery temporal patterns were more fully documented. Lightly damaged BLH and extensively defoliated cypress-tupelo forests exhibited largely pre-hurricane VI trends from 2006 onwards. In contrast, moderately, and especially severely, impacted BLH post-hurricane VI trends revealed lagging recoveries throughout 2006 that may in part be associated with observed stand-level replacement by invasive, non-native trees.

Future works will assess longer term recovery as a function of VI-based wetland forest canopy greenness and compare wetland forest impacts from Hurricane Katrina to those on adjacent upland forests. The spatial and temporal extension of these analyses could help improve the understanding of wetland forest regeneration and forest structure spatial patterns (e.g., composition, density) in order to predict how specific weather events such as devastating storms change these forested ecosystems. In addition, we hope to better define the relationship of observed damage and recovery with respect to timber volume.

Acknowledgments

The authors thank Mike Olinde and James Stafford of the Louisiana Department of Wildlife and Fisheries for access to the Pearl River Wildlife Management Area and Phil Kuper, Slawomir Blonski, and Kara Holekamp of the Computer Sciences Corporation for their contributions. Work at the NASA John C. Stennis Space Center, Mississippi was performed under Task Orders NNS04AB54T and NNS10AA35C and included funding from the USDA Forest Service Eastern Forest Environmental Threat Assessment Center and the Western Wildlands Environmental Threat Assessment Center. Mention of trade names does not constitute endorsement by the US Government.

References

- Ackerman, S., R. Holz, R. Frey, E. Eloranta, B. Maddux, and M. McGill, 2008. Cloud detection with MODIS, Part II: Validation, *Journal of Atmospheric and Oceanic Technology*, 25(7):1073–1086.
- Anderson, E., D. Sweeney, and T. Williams, 1984. *Statistics for Business and Economics*, West Publishing Co., St. Paul, Minnesota, 708 p.
- Bevington, P., 1969. *Data Reduction and Error Analysis for the Physical Sciences*, McGraw-Hill Book Co., New York, 336 p.
- Bradley, A., R. Jacob, J. Hermance, and J. Mustard, 2007. A curve fitting procedure to derive inter-annual phenologies from time series of noisy satellite NDVI data, *Remote Sensing of Environment*, 106:137–145.
- Chambers, J., J. Fisher, H. Zeng, E. Chapman, D. Baker, and G. Hurtt, 2007. Hurricane Katrina's carbon footprint on U.S. Gulf Coast forests, *Science*, 318(5853):1107.
- Chen, J., P. Jönsson, M. Tamura, Z. Gu, B. Matsushita, and L. Eklundh, 2004. A simple method for reconstructing a high-quality NDVI time-series data set based on the Savitzky-Golay filter, *Remote Sensing of Environment*, 91:332–344.
- Fisher, J., and J. Mustard, 2007. Cross-scalar satellite phenology from ground, Landsat, and MODIS data, *Remote Sensing of Environment*, 109:261–273.
- Frey, R., S. Ackerman, Y. Liu, K. Strabala, H. Zhang, J. Key, and X. Wang, 2008. Cloud detection with MODIS, Part I: Improvements in the MODIS cloud mask for collection 5, *Journal of Atmospheric and Oceanic Technology*, 25(7):1057–1072.
- Gao, F., J. Morisette, R. Wolfe, G. Ederer, J. Pedelty, E. Masuoka, R. Myneni, B. Tan, and J. Nightingale, 2008. An algorithm to produce temporally and spatially continuous MODIS-LAI time series, *IEEE Geoscience and Remote Sensing Letters*, 5:60–64.
- Jönsson, P., and L. Eklundh, 2004. TIMESAT – A program for analyzing time-series of satellite sensor data, *Computers and Geosciences*, 30:833–845.
- Huete, A., C. Justice, and W. van Leeuwen, 1999. MODIS vegetation index (MOD 13) Algorithm Theoretical Basis Document, Version 3, Available at: http://modis.gsfc.nasa.gov/data/atbd/atbd_mod13.pdf (last date accessed: 22 July 2011).
- Klemas, V., 2005. Resolution requirements for coastal applications of new geostationary satellites, *Proceedings of OCEANS-05*, Washington, D.C. 20–24 September 2005.
- Lunetta, R., J. Knight, J. Ediriwickrema, J. Lyon, and L. Worthy, 2006. Landcover change detection using multi-temporal MODIS NDVI data, *Remote Sensing of Environment*, 105:142–154.
- McKellip, R., R. Ryan, D. Prados, and S. Blonski, 2005. Crop surveillance demonstration using a near-daily MODIS vegetation index time series, *Proceedings of the 2005 International Workshop on the Analysis of Multi-Temporal Remote Sensing Images, IEEE*, New York, pp. 54–58.
- McKellip, R., D. Prados, R. Ryan, K. Ross, J. Spruce, G. Gasser, and R. Greer, 2008. Remote-sensing time series analysis, a vegetation monitoring tool, *NASA Tech Briefs*, 32(4):63–64.
- Middleton, B., 2009. Regeneration of coastal marsh vegetation impacted by Hurricane Katrina, *Wetlands*, 29:54–65.
- PCI Geomatics. 1998. *Using PCI Software*, Version 6.3 EASZIPACE, PCI Geomatics, Richmond Hill, Ontario, Canada (software documentation).
- Ramsey, E. III, D. Chappell, and D. Baldwin, 1997. AVHRR imagery used to identify Hurricane Andrew damage in a forested wetland of Louisiana, *Photogrammetric Engineering & Remote Sensing*, 63(3):293–297.
- Ramsey, E. III, D. Chappell, D.M. Jacobs, S.K. Sapkota, and D.G. Baldwin, 1998. Resource management of forested wetlands: Hurricane impact and recovery mapped by combining Landsat TM and NOAA AVHRR data, *Photogrammetric Engineering & Remote Sensing*, 64(7):733–738.
- Ramsey, E. III, M. Hodgson, S. Sapkota, and G. Nelson, 2001. Forest impact estimated with NOAA AVHRR and Landsat TM data related to an empirical hurricane wind-field distribution, *Remote Sensing of Environment*, 77(3):279–292.
- Ramsey E. III, A. Rangoonwala, and R. Ehrlich, 2005. Mapping the invasive species, Chinese Tallow with EO1 satellite Hyperion hyperspectral image data and relating tallow percent occurrences to a classified Landsat Thematic Mapper landcover map, *International Journal of Remote Sensing*, 26(8):1637–1657.
- Ramsey, E. III, Z. Lu., A. Rangoonwala, and R. Rykhus, 2006. Multiple baseline radar interferometry applied to coastal landscape classification and change analyses, *GIS Science and Remote Sensing*, 43(4):283–309.
- Ramsey, E. III, A. Rangoonwala, B. Middleton, and Z. Lu, 2009a. Satellite optical and radar image data used to track wetland forest impact and short-term recovery from Hurricane Katrina, *Wetlands*, 29(1):66–79.
- Ramsey, E. III, D. Werle, Z. Lu, A. Rangoonwala, and Y. Suzuoki, 2009b. A case of timely satellite image acquisitions in support of coastal emergency environmental response management, *Journal of Coastal Research*, 25(5):1168–1172.
- Reed, B., J. Brown, D. VanderZee, T. Loveland, J. Merchant, and D. Ohlen, 1994. Measuring phenological variability from satellite imagery, *Journal of Vegetation Science*, 5:703–714.
- Savitzky, A., and M. Golay, 1964. Smoothing and differentiation of data by simplified least squares procedures, *Analytical Chemistry*, 36:1627–1639.
- Spruce, J.P., S. Sader, R.E. Ryan, J. Smoot, P. Kuper, K. Ross, D. Prados, J. Russell, G. Gasser, R. McKellip, and W. Hargrove, 2011. Assessment of MODIS NDVI time series data products for detecting forest defoliation by gypsy moth outbreaks, *Remote Sensing of Environment*, 115:427–437.
- Streiner, D., 1996. Maintaining standards: Differences between the standard deviation and standard error, and when to use each, *Canadian Journal of Psychiatry*, 41:498–502.
- Tucker, J., 1979. Red and photographic infrared linear combinations for monitoring vegetation, *Remote Sensing of Environment*, 8:127–150.
- White, D., 1983. Plant communities of the lower Pearl River basin, Louisiana, *American Midland Naturalist*, 110:381–96.
- White, M., and R. Nemani, 2006. Real-time monitoring and short-term forecasting of land surface phenology, *Remote Sensing of Environment*, 104(1):43–49.
- Xiong, X., and W. Barnes, 2006. An overview of MODIS radiometric calibration and characterization, *Advances in Atmospheric Sciences*, 23(1):69–79.
- Zhang, X., M. Friedl, C. Schaaf, A. Strahler, J. Hodges, F. Gao, B. Reed, and A. Huete, 2003. Monitoring vegetation phenology using MODIS, *Remote Sensing of Environment*, 84:471–475.
- Zhang, X., M. Friedl, and C. Schaaf, 2006. Global vegetation phenology from Moderate Resolution Imaging Spectroradiometer (MODIS): Evaluation of global patterns and comparison with in situ measurements, *Journal of Geophysical Research*, 111, pp. G04017, DOI:10.1029/2006JG00217.

(Received 18 July 2010; accepted 09 April 2011; final version 15 April 2011)

Professional Directory

CALIFORNIA

When you're serious about digital image mosaicking

ORTHOVISTA Direct

Digital Orthophoto Mosaicking Software

- Digital Image Dodging
- Image & Color Matching
- Automatic Seam Placement

www.orthovista.com

WINDOWS LINUX IRIX SOLARIS

COLORADO

Aerial Surveys International, LLC



P.O. Box 130
37500 Astra Way, Unit 3E
Watkins, CO 80137
Phone (303) 261-9990
Fax (303) 261-9996
Mark Schubert
www.aerialsurveysintl.com

DMC
Digital Mapping Company

Precision Aerial Photography LMK 2000 (ABGPS)
Z/I Scanning & B&W/ Color Lab

IDAHO



VALLEY AIR PHOTOS

CATHY GRAVILLE
Owner / Operator

TEL: 208 454-1344 P.O. BOX 1118
FAX: 208 454-1345 CALDWELL, IDAHO 83606-1118
EMAIL: cathy@valleyairphotos.com www.valleyairphotos.com

ILLINOIS



ALT-TERRA SURVEY

LARGE FORMAT VERTICAL PHOTOGRAPHY


DIMAC Digital Aerial Camera
3 Leica RC 30 FMC Cameras
2 IMUs, Airborne GPS/Glonass
4 survey aircraft, 2 Gyro Mounts

Alt-Terra Survey, Inc.
Sheboygan Falls, WI 53085
(920) 467-6720

w.phebus@alt-terra.com
www.alt-terra.com

OHIO

Kenneth R. Stiller Voice: 937-222-3856




HAS Images, Inc.

FULL SERVICE AERIAL PHOTOGRAPHIC LABORATORY
Including Scanning & Digital Photographic Output

136 North St. Clair Street • Suite 300 • Dayton, Ohio 45402
Fax: 937-222-2443 • www.hasimages.com
e-mail: info@hasimages.com

OKLAHOMA

Aerial Data Service, Inc.



Full Service Survey and Mapping
Photography - Survey - LiDAR
Mapping - GIS

For more information call or visit
800.888.9163 www.aerialdata.com

OREGON



Serving the West Since 1975
www.BergmanPhotographic.com
503.239.6010

- Aerial Photography
- ABGPS - Track Air
- Vexcel UltraCam
- Zeiss TOP-15 FMC
- Zeiss TOP-30 FMC
- 4 Survey Aircraft - Piston & Turboprop
- 9X9 Film & Digital Obliques
- Color Prints to 50" wide
- Leica DSW Scanner
- Historical Imagery - Searchable Online

BERGMAN PHOTOGRAPHIC SERVICES, INC.
7816 SE 13TH - PORTLAND, OREGON - 97202

PENNSYLVANIA



KEYSTONE AERIAL SURVEYS

4 Microsoft UltraCam Sensors
ALTM Gemini LiDAR System
17 Survey Aircraft
12 Leica RC Metric Cameras
4 Leica DSW Scanners
Gyro Stabilized Mounts
ABGPS / IMU Processing

KASVIEW.COM
Keystone's Online Image
Catalogue and Search Tool

Offices in Philadelphia, PA and Benson, AZ
www.KASurveys.com
Info@KeystoneAerialSurveys.com
Phone: 215.677.3119 / Fax: 215.464.2889

TEXAS

KRAWIETZ
AERIAL PHOTOGRAPHY LLC

FLYING SERVICES FOR MAPPING

LEICA RC30's STABILIZED MOUNTS AIRBORNE GPS

210 497-4260 Voice P O Box 191
830 438-3023 Fax Bulverde, Texas 78163
email: krawietz@gvtc.com

Serving the southwestern United States since 1966

WEST VIRGINIA



A-P-R Photographics, Inc.

Aerial Photography / Airborne GPS
Airborne IMU Data Collection & Processing
5 Leica Cameras with FMC
5 Stabilized Camera Mounts
Photogrammetric Scanning

Arlie Winters, III, President/CEO
2115 Kelly Island Road
Martinsburg, WV 25405

Toll Free: (800) 624-8993
Fax: (304) 267-0918
www.airphotographics.com

Index to Advertisers

BAE Systems	Cover 4
www.baesystems.com	
(301) 838-6000	
Cardinal Systems, LLC	1107
www.cardinalsystems.net	
(386) 439-2525	
DAT/EM Systems International	1103
http://datem.com	
(907) 522-3681	
ERDAS, Inc.	Cover 2
www.erdas.com	
1-877-GO-ERDAS	
ITT Visual Information Solutions	1070
www.itvis.com	
(303) 786-9900	
Microsoft Corporation	1073
www.microsoft.com/ultracam	
(+43) 316 84 90 66 0	

Advertise with ASPRS

PE&RS
Display Ads
Classified Ads
Professional Directory

Conferences
Programs
Exhibits
Sponsorships
Website Marketing
Medallion Partnership

plus many more opportunities

Contact Don Cooksey at 301-215-6710, ext. 117 or dcooksey@townsend-group.com to obtain more information or request a customized package designed to meet your marketing objectives.

A Volumetric Approach to Population Estimation Using Lidar Remote Sensing

Zhenyu Lu, Jungho Im, and Lindi Quackenbush

Abstract

This research investigated the applicability of lidar data for estimating population at the census block level using a volumetric approach. The study area, near the urban downtown area of Denver, Colorado, was selected since it includes dense distribution of different types of residential buildings. A modified morphological building detection algorithm was proposed to extract buildings from the lidar-derived surfaces. The extraction results showed that the modified morphological building detection algorithm can effectively recover building pixels occluded by nearby trees. The extracted buildings were further refined to residential buildings using parcel data. Two approaches (i.e., area- and volume-based) to population estimation were investigated at the census block level. Four regression models (i.e., simple linear regression, multiple linear regression, regression tree using one variable, and regression tree using multiple variables) were used to identify the relationship between census population and the area or volume information of the residential buildings. The volume-based models overwhelmingly outperformed the area-based models in the study area, and the models using multiple variables yielded more accurate estimation than the single variable models. The volume-based regression tree model using multiple variables yielded the most accurate estimations: $R^2 = 0.89$, $RMSE = 21$ people, and $RRMSE = 26.8$ percent in the calibration site; and $R^2 = 0.80$, $RMSE = 27$ people, and $RRMSE = 30.1$ percent in the validation site. As the results show, the volumetric approach using lidar remote sensing is effective for population estimation in regions with heterogeneous housing characteristics.

Introduction

The application of remote sensing and GIS technologies for population estimation has been intensively investigated during the past two decades (Lo, 1995; Yuan *et al.*, 1997; Harvey, 2002; Wu and Murray, 2005; Lu *et al.*, 2006; Lo, 2008; Liu *et al.*, 2008; Wu *et al.*, 2008; Jensen *et al.*, 2010; Li and Weng, 2010; Lu *et al.*, 2010). In previous studies of population estimation, remote sensing-derived variables were used as population count indicators (such as pixel counts of land use) and population density indicators (such as mean of reflectance data or their transforms) (Wu and Murray, 2007). In most of these studies, these indicators were derived from moderate spatial resolution satellite

imagery (e.g., Landsat Thematic Mapper). Investigation of the relationship between these indicators and census population data has followed (e.g., Lu *et al.*, 2006; Lo, 2008). Approaches using moderate spatial resolution data have two main limitations: a relatively weak relationship between the population indicators (e.g., residential area) and census population, and difficulty in categorizing different types of residential areas (e.g., dominance of multi- versus single-unit residential buildings; and mixtures of tall apartment complexes and one- or two-story residential buildings).

Jensen and Cowen (1999) proposed that spatial resolution between 0.5 m and 5 m would theoretically be appropriate for extracting detailed population information. More recently, several studies reported increased capability for population estimation using high spatial resolution imagery such as QuickBird and Ikonos data (e.g., Liu *et al.*, 2008) or fusing lidar data with high spatial resolution imagery (e.g., Wu *et al.*, 2008; Lu *et al.*, 2010). In addition, many studies have used geographic information system (GIS) tools to collate spatial data from different sources to estimate population. For example, Langford (2006) employed a three-class dasymetric method to estimate population in non-census reporting areas. Interpolation-based approaches have also been investigated for population estimation (Wu and Murray, 2005; Liu *et al.*, 2008).

Remote sensing-derived area information, such as residential area and impervious surface area, has typically been used in population estimation studies. Though the area-based approaches may perform well in homogeneous regions, such as suburban regions where most of the residential buildings are single family houses, they might not work well in heterogeneous areas with various types of residential buildings (single-family houses, apartments, and condominiums). Lu *et al.* (2006) and Wu *et al.* (2008) found that area-based approaches tend to overestimate population in low population density regions, while underestimating population in high density regions. Wu *et al.* (2008) also found that population estimations for multi-family residential areas tend to have higher errors than single-family residential areas. There are two main issues in estimating population in regions with heterogeneous building characteristics: (a) the difficulty in discriminating residential and non-residential buildings, and (b) the difficulty of dividing multi- and single-unit residential buildings (Lo, 1989 and 1995).

Department of Environmental Resources Engineering, State University of New York, College of Environmental Science and Forestry, One Forestry Dr., Syracuse, NY 13210 (imj@esf.edu).

Photogrammetric Engineering & Remote Sensing
Vol. 77, No. 11, November 2011, pp. 1145–1156.

0099-1112/11/7711-1145/\$3.00/0
© 2011 American Society for Photogrammetry
and Remote Sensing

To overcome the limitation of the area-based approaches, a volume-based approach has been introduced (Wu *et al.*, 2008; Lu *et al.*, 2010). The volume-based approach utilizes the volume of residential buildings, rather than the area of the building footprint, to estimate population. The volume-based approach, with its ability to alleviate the prediction bias caused by multi-unit structures, may outperform the area-based method particularly in heterogeneous regions. Lu *et al.* (2010) evaluated both area- and volume-based approaches to population estimation in a suburban area of Denver, Colorado where most of the residential buildings were single-family houses. An object-based decision tree classification algorithm was employed to delineate the residential buildings using QuickBird and lidar data. The volume of residential buildings was then calculated using the previously delineated residential building footprint multiplied by the lidar-derived height. Both the areal and volumetric approaches successfully estimated population at the census block level resulting in $R^2 > 0.8$ and $RMSE < 30$ people. However, the volume-based approach did not significantly outperform the area-based approach mainly because (a) the study site was dominated with single-family houses, and (b) the volume-based approach was more sensitive to residential building classification errors (e.g., confusion with tall trees and other types of buildings such as shopping malls).

Using airborne or satellite imagery or fusing lidar data with such imagery, has been a popular method for delineating building footprints in population estimation studies (Wu *et al.*, 2008; Lu *et al.*, 2010). The fusion process facilitates using the valuable spectral information (e.g., Gong *et al.*, 2011; Ke *et al.*, 2010), which makes the identification of building footprints more accurate. However, this fusion process has several associated challenges: the spatial resolution of the lidar data may be sacrificed to fit other inputs (Tullis and Jensen, 2003); noise, such as shadows, clouds and the building displacements may be introduced due to variation in look angles or other collecting conditions (Meng *et al.*, 2009a); and temporal discrepancy in different data sources can negatively impact population estimation.

Meng *et al.* (2009a) found lidar data adequate for delineating building footprints in urban areas. However, using lidar data solely for estimating population in urban areas has had minimal exploration. In this study, a modified morphological building detection algorithm was proposed to delineate the footprints of all buildings from lidar-derived surfaces around urban downtown areas. Subsequently, the residential building footprints were obtained by intersecting the building footprints delineated from lidar-derived surfaces with land parcel polygons. The volume of the residential buildings was then calculated using lidar-derived height information. The objectives of this research were to (a) investigate the usability of lidar data to delineate residential buildings in urban areas, (b) investigate different lidar-derived products for calculating population indicators (i.e., residential building footprint, residential building volume), and finally (c) evaluate volume and area-based regression models (i.e., simple linear, multiple linear, and regression trees) for population estimation.

Study Area and Data

Study Area

Two sites located near the downtown area of Denver, Colorado were selected for calibration and validation (Figure 1). The calibration site contains three census tracts

which consist of 163 census blocks. Two census blocks in the neighboring tract containing mainly multiple family houses (i.e., apartments and condominiums) were also included to ensure heterogeneity within the calibration site. Of the 165 blocks in the calibration site, 139 contain residential buildings, while 84 of these have multiple family houses. The average number of residents per block in the calibration site is 68.

The validation site includes one census tract with 58 census blocks, 38 of which contain multiple-family houses, and the average number of residents per block is 78. Both sites have heterogeneous characteristics in terms of building components and population intensity, although the validation site is smaller than the calibration site. The buildings in the calibration site consist of 3,041 single-family houses (85.3 percent), 368 multiple-family houses (10.3 percent), and 155 non-residential buildings (4.4 percent), while the buildings in the validation site are 972 single-family houses (79.7 percent), 171 multiple-family houses (14.0 percent), and 77 non-residential buildings (6.3 percent). Table 1 summarizes the basic statistics related to the demographic, economic, and housing characteristics in the calibration and validation sites. One of the census tracts in the calibration site has quite different economic and housing characteristics (i.e., higher income and higher rate of single-family houses) than the other two calibration tracts and the validation tract. This makes the calibration site more heterogeneous, which is good for investigating which modeling techniques are more robust and flexible for population estimation in such a heterogeneous environment. In addition, the different characteristics between the calibration and validation sites will allow us to examine the transferability of the modeling techniques used.

Data

The lidar data were collected on 15 April 2008 by the Sanborn Map Company. The lidar sensor collected small footprint multiple returns (x, y, and z) and intensity data using a 1,064 nm laser with a pulse repetition frequency of 50 kHz. The posting density of the lidar data was about 2.3 pts/m². Three raster surfaces with 0.5 m pixel size were generated from TIN models of the first return, last return, and bare earth data points. Two local height surfaces denoted as the first return height (FRH) surface and the last return height (LRH) surface were created by subtracting the bare earth surface from the first return and last return surfaces, respectively. A first-last difference surface (FLD) was also created by subtracting the last return surface from the first return surface.

The 2000 census block data and land parcel data were downloaded from the GIS Center of Denver City (<http://www.denvergov.org/GIS>). The Denver parcel data describes the rights, interests, usage, and assessed value of property. The parcel polygons approximate the boundaries of land properties. In addition, each parcel data record also has an attribute showing the building construction year, which was used as a reference to exclude residential buildings built after 2000 from the population estimation process.

Methodology

Figure 2 summarizes the research workflow. Three lidar-derived surfaces (i.e., FRH, LRH, and FLD) were initially generated, and then a modified morphological building detection technique (Figure 3) was proposed to delineate building polygons using these surfaces. The extracted building polygons were subsequently intersected with the parcel data to identify the residential building polygons according to the parcel usage. The volume of the residential

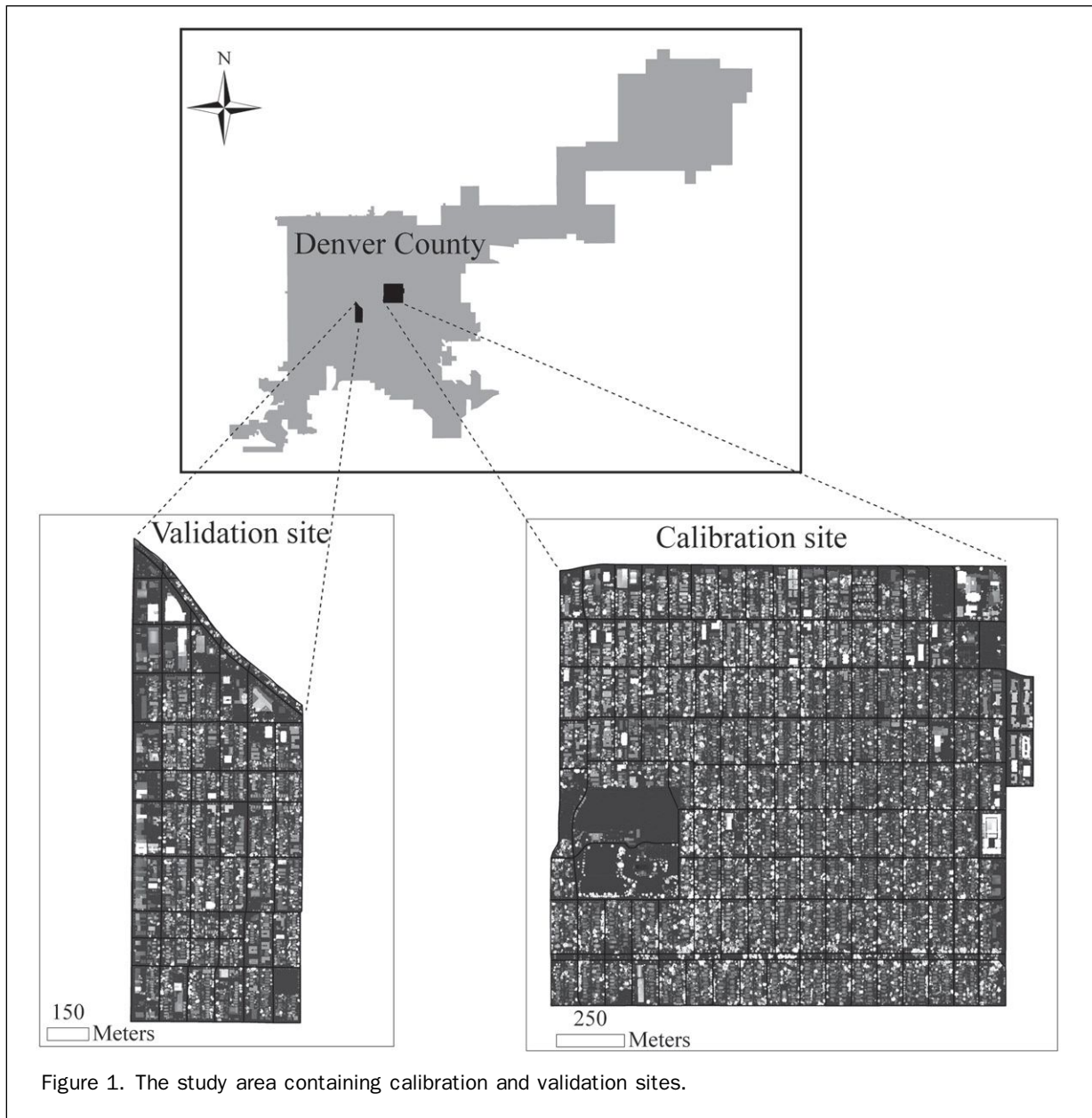


Figure 1. The study area containing calibration and validation sites.

TABLE 1. DEMOGRAPHIC, ECONOMIC, AND HOUSING CHARACTERISTICS OF THE CALIBRATION AND VALIDATION SITES

Statistic	Calibration site	Validation site
Population density	4,119 people/km ²	5,124 people/km ²
Population per block (range)	2 – 462 people	2 – 287 people
Median household income (USD)	\$49,106	\$29,964
Per capita income (USD)	\$36,673	\$23,515
Number of single-family houses	3041/18*	972/17
Number of multiple-family houses	368/2	171/3
Number of non-residential buildings	155/1	77/1

*total/mean at the block level

buildings was calculated by multiplying the delineated footprints of residential buildings with the lidar-derived height. The area and volume information of the residential buildings for each census block were attained using a zonal statistics function in ArcGIS® 9.3. Then, the relationships between the area and volume of the residential buildings and census population were investigated using four

regression models. All the calibrated models were evaluated using data from the validation site.

Modified Morphological Building Detection Algorithm

The morphological building detection algorithm presented by Meng *et al.* (2009a) was developed to utilize lidar-derived surfaces in the extraction process. The use of a

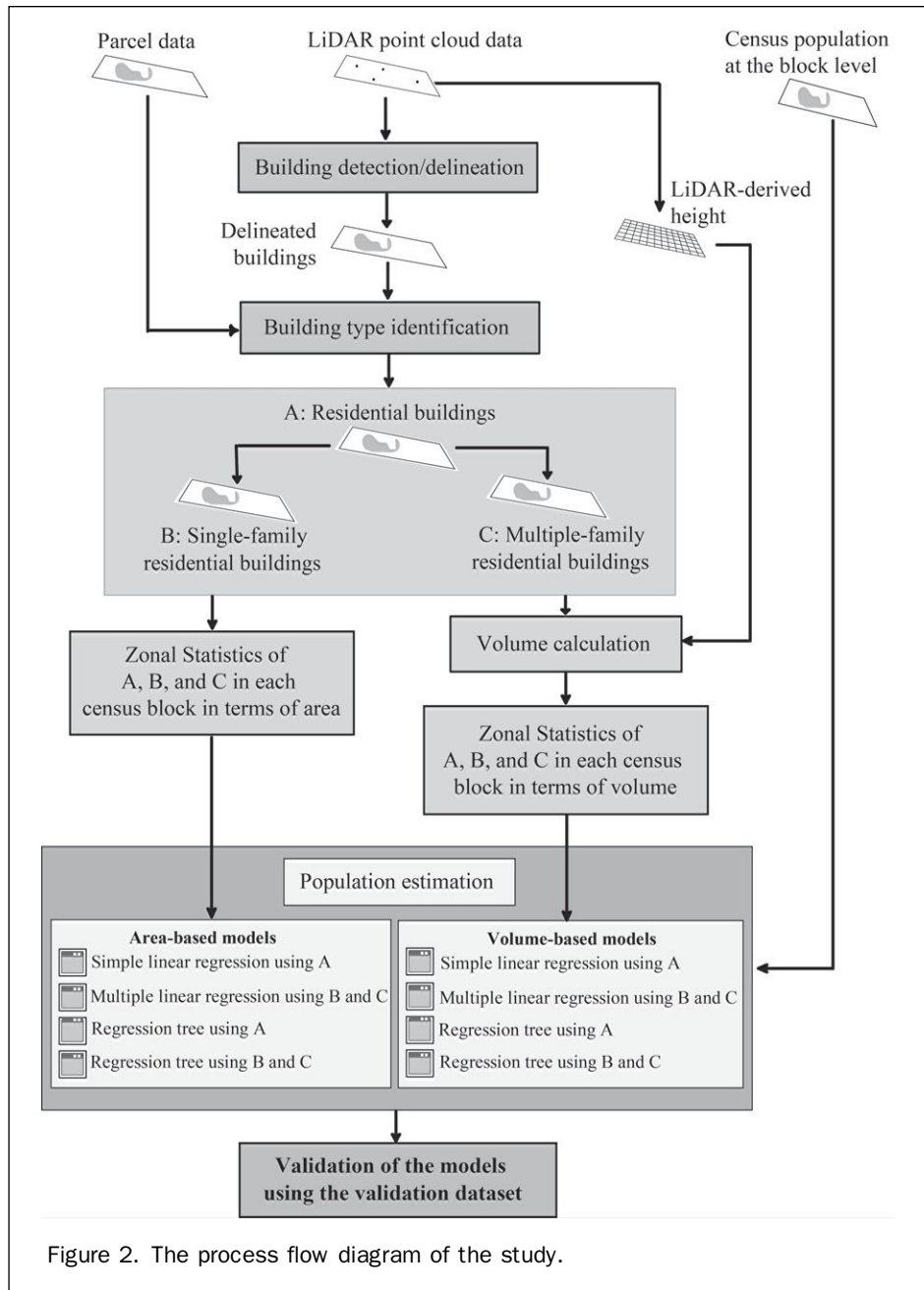


Figure 2. The process flow diagram of the study.

single data source in the algorithm helps mitigate errors and information loss caused by the process of data fusion. There are five main operations in the original morphological building detection method. The first operation is ground filtering, which utilizes a multi-directional ground filtering algorithm (Meng *et al.*, 2009b) to generate the bare earth surface. The second operation uses the FRH and FLD surfaces to separate buildings from other objects. The third operation is morphology filtering to remove misclassified building pixels based on the morphological characteristics of buildings. The fourth operation is building center recovery, which aims to recover the incorrectly filtered pixels that are within the building objects. The last operation is performed to convert the building pixels into vectors and remove non-building polygons using area and compactness thresholds.

The first operation of the morphological building detection algorithm was not necessary in this study because

the bare earth points were identified and delivered by the Sanborn Map Company. Two major improvements have been made to the original method. The first improvement was made to the building center recovery operation. While the original center recovery operation effectively recovered some of the pixels that were misclassified as non-building pixels, the complex urban environment led to substantial enlargement of vegetation fragments within the study site. For this reason, the typical recovery criterion was modified to not only compare the FRH with the average FRH of the neighboring potential buildings, but to also count the number of neighboring building pixels. If the number of neighboring building pixels was less than a user-specified threshold (i.e., four in this study), the non-building label remained even if the pixel satisfied the height criteria.

The second improvement was implementation of a boundary recovery operation to deal with the partial

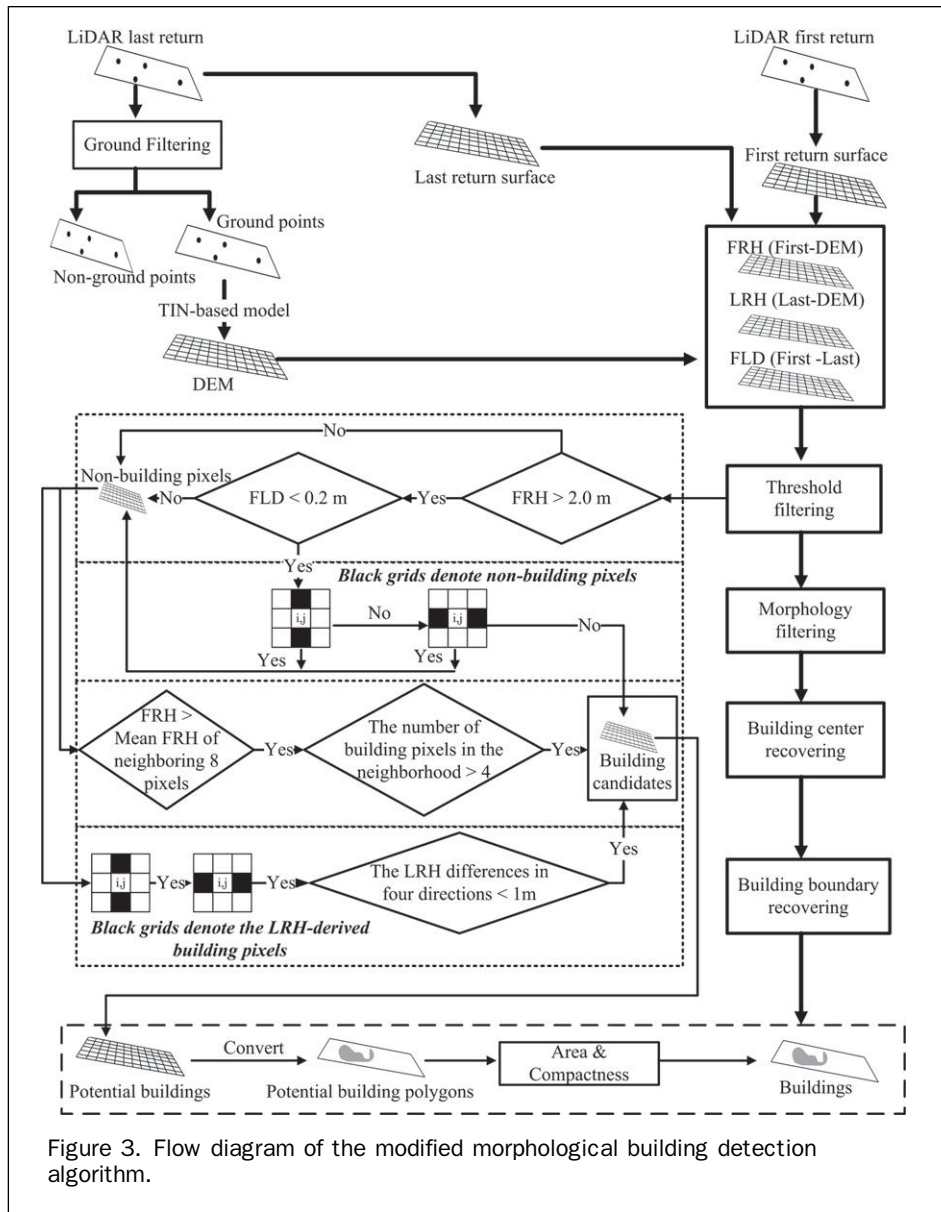


Figure 3. Flow diagram of the modified morphological building detection algorithm.

occlusion of building footprints caused by nearby trees. The boundary recovery operation initially generated another binary image by applying a threshold to the LRH surface. If the height (LRH) of the pixel was larger than the threshold, the pixel would be labeled as a last-return-derived building pixel. Then, a morphology operator was applied to the potential building image obtained after the first four operations of the morphological building detection technique. Pixels incorrectly labeled as non-building pixels were recovered if they satisfied the following two criteria: (a) the pixels below and above or to the left and right were last-return-derived building pixels, and (b) the height difference between the non-building pixel (i, j) and the neighboring last-return-derived building pixels was less than 1 m. The modified morphological building detection algorithm was implemented using the C# programming language and the Geospatial Data Abstraction Library (GDAL).

Volumetric Approach to Population Estimation

The volumetric approach to population estimation uses the volume of residential buildings, which is calculated using the

footprint area and height of the buildings. The footprint of residential buildings was obtained by intersecting the extracted building polygons with the parcel data based on the parcel usage information. Two different lidar-derived height layers (FRH and LRH) were tested for providing the height of residential buildings. To reduce the need for field-collected building height reference data, we performed a relative comparison between the two height layers: the volume of residential buildings was calculated using both height layers for the calibration site, linear regression was investigated between the volume information and census population, and finally, the height layer resulting in better performance was considered the reference "height" layer and used in subsequent population estimation analyses. In addition to the volumetric approach, an areal approach using building footprint size was also employed for comparison.

Four regression models (simple linear regression (SLR), multiple linear regression (MLR), regression tree using a single variable (RTS), and regression tree using multiple variables (RTM)) were used to identify the relationship between both area and volume, and population. Regression

trees are a well accepted machine-learning technique, and have been widely employed in the field of remote sensing (Lawrence and Wright, 2001; Xu *et al.*, 2005; Kocev *et al.*, 2009; Im *et al.*, 2009 and 2011). Regression trees recursively split input reference data to obtain the homogeneous terminal nodes, from which different rulesets are generated. A split occurs if the combined residual error of the model for two subsets is significantly lower than the residual error of the single best model in the process (Huang and Townshend, 2003). This study used Cubist by RuleQuest, Inc., which uses a modified regression tree system to create rule-based predictive multivariate models from the data. It was anticipated that regression tree models (i.e., RTS and RTM) could be valuable for population estimation in heterogeneous regions since the method can generate multiple rulesets that may correspond to census units with different population density and building characteristics. After the four regression models were trained using the calibration site, their performance was evaluated using data from the validation site.

The independent variable for the single variable regression models (i.e., SLR and RTS) was the total area/volume of the residential buildings in each census block. For the multi-variable regression models (i.e., MLR and RTM), the two independent variables were total area/volume of the single family and multiple family houses in each census block. Using the two variables as population indicators, different weights can be assigned to each variable according to its contribution to the population numbers. The performance of the four models (i.e., SLR, MLR, RTS, and RTM) for each input

dataset (i.e., area and volume) was evaluated using coefficient of determination (R^2), root mean square error (RMSE), and relative root mean square error (RRMSE).

Results and Discussion

Residential Building Delineation

Both the original and modified morphological building detection algorithms were applied to the lidar-derived surfaces to delineate building footprints. While the delineated building footprints using both algorithms were generally similar, the modified algorithm dramatically improved the building delineation where there were tall trees next to the residential buildings. In order to conduct a quantitative assessment of the results, a small portion of the study area was selected and buildings were manually digitized based on the visual interpretation of the lidar-derived height (i.e., FRH and LRH) and intensity. The digitized building polygons were further visually examined using Google Earth[®] and were used as a reference for evaluating the two algorithms. Figure 4 shows the reference building polygons and the building footprints delineated using both the original and modified algorithms. The associated accuracy statistics (user's and producer's accuracies, overall accuracy, and Kappa coefficient) are summarized in Figure 4. The statistics showed that the modified algorithm (Kappa of 0.924) outperformed the original one (Kappa of 0.838). When compared to the reference polygons for the building area (5,685 m² based on the reference

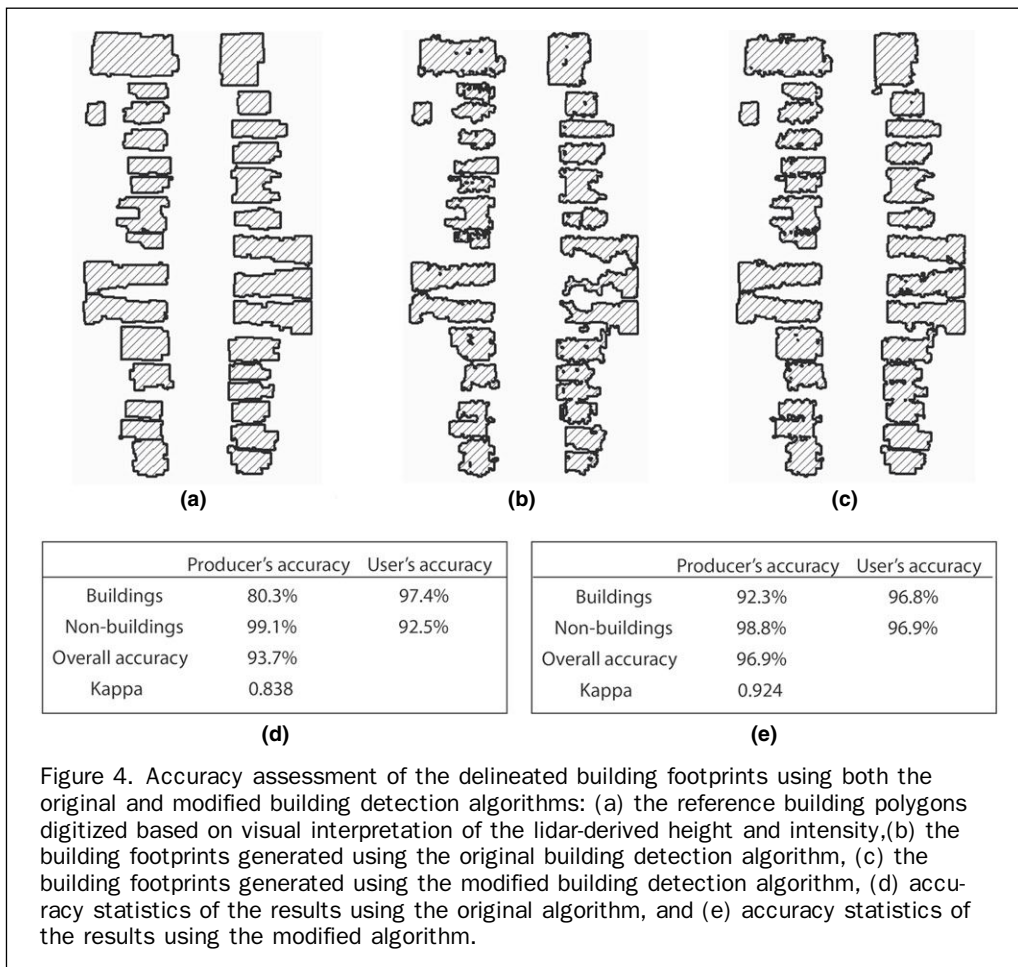


Figure 4. Accuracy assessment of the delineated building footprints using both the original and modified building detection algorithms: (a) the reference building polygons digitized based on visual interpretation of the lidar-derived height and intensity, (b) the building footprints generated using the original building detection algorithm, (c) the building footprints generated using the modified building detection algorithm, (d) accuracy statistics of the results using the original algorithm, and (e) accuracy statistics of the results using the modified algorithm.

polygons), the original algorithm underestimated the building area (4,685 m² or 82 percent of the area of the reference data) while that generated using the modified algorithm was 5,419 m² (95 percent of the area of the reference data). The increase of the building footprint area delineated based on the modified algorithm was mainly attributed to the successful recovery of the building pixels occluded by the nearby tall trees. In addition, the recovery of some pixels that were incorrectly labeled as non-building pixels within the boundary of the building objects also contributed to the increase of the footprint area. However, errors still existed for both the original and modified morphological building detection algorithms since not all incorrectly classified pixels within building objects were recovered and some building boundaries were still irregular. While additional morphology operators such as erosion and dilation might reduce these errors, it is likely that such operations would inappropriately modify the size of the extracted building footprints at the same time. Given the small size of these errors in both the calibration and validation sites, no further processing operations were done for this study.

Having established building footprints, residential buildings were delineated by intersecting the extracted footprints with the parcel data according to the attributes of building type and construction year. All residential buildings were further categorized into two classes (single-family houses (i.e., single-family and row houses) and multiple-family houses (i.e., condominiums and apartments)) according to the usage attribute from the parcel data.

Investigation of Lidar-derived Heights for Calculating Population Indicators

The volume of residential buildings calculated using either FRH or LRH was investigated as a population indicator in this study. Lidar-derived height is typically generated by subtracting a bare earth from a first return surface (i.e., FRH). However, FRH may not provide accurate building height information in certain situations. For example, if a portion of a building rooftop is occluded by nearby tree branches, FRH would overestimate the height, and consequently the building volume. LRH may improve height estimation in this case since the last return comes from the rooftop, not from the occluding tree branches. Table 2 summarizes the performance of the regression models (i.e., SLR and MLR) using building volume based on two different height data (i.e., FRH and LRH) for population estimation in the calibration site. There was not much difference in population estimates using FRH or LRH, although the LRH-derived volume did result in slightly better performance than FRH-derived volume (Table 2). The major reasons for the similarity in results are because (a) occlusion by trees was already improved by the modified morphological algorithm, (b) there are not many building pixels occluded by the tall trees within the site, and (c) the differences between FRH and LRH in the occluded building pixels were generally small. Consequently, the LRH-derived volume information was used in subsequent population estimation.

Population Estimation

We used the parcel data to identify the type of the delineated buildings in terms of usage (i.e., single-family houses, multiple-family houses, and non-residential buildings). As there are many non-residential buildings within the study sites, population estimation based directly on all the delineated buildings could result in very poor performance. A preliminary analysis was conducted in both the calibration and validation sites to see if classification of buildings by their usage could improve population estimation. The analysis evaluated the correlation between the census population and both the area and volume of the residential buildings, extracted based on the parcel data, and all the buildings without using the parcel data. For the calibration site, the R² values between the census population and the area and volume of the residential buildings were 0.23 and 0.73, respectively, compared to 0.10 and 0.14 based on the area and volume of all the extracted buildings. Similar to the calibration site, the R² values between the census population and the area and volume of the residential buildings in the validation site were 0.69 and 0.80, respectively, compared to 0.30 and 0.12 using the area and volume of all buildings. Given that using only the residential buildings dramatically improved population estimation, especially for the volume-based models (i.e., R² value increased from 0.14 to 0.73 and 0.12 to 0.80 in the calibration and validation sites, respectively), the residential building delineation and further classification into single- and multiple-family houses were necessary to increase population estimation accuracy.

Four regression models (i.e., SLR, MLR, RTS, and RTM) based on either the area or volume of the residential buildings were developed in the calibration site (Table 3). The volume-based RTS and RTM models generated two different rulesets for regions with various building characteristics, the remaining six models had only one ruleset. The performances of different models were compared in the following section.

Table 4a shows the calibration results using four regression models (i.e., SLR, MLR, RTS, and RTM) based on either the area or volume of the residential buildings. The volumetric approaches outperformed the areal ones among all the models. In particular, the area-based regression models using a single variable (i.e., SLR and RTS) were poorly calibrated, resulting in R² ≈ 0.23, RMSE ≈ 58 people, and RRMSE ≈ 70.9 percent. The weak performance of the area-based SLR and RTS models indicated that the area of residential building footprints might not be well correlated with the number of people who live within the buildings in certain regions, because important factors, including the number of stories, are not considered. This reason was also supported by a comparison between the area-based and volume-based SLR and RTS models: while there was a tenuous relationship between the area of residential building footprints and the census population, the volume of residential buildings provided much higher correlation (R² > 0.7) with the census population in the calibration site. Among

TABLE 2. REGRESSION MODELS USING TWO DIFFERENT HEIGHT DATA (I.E., FRH AND LRH) FOR POPULATION ESTIMATION IN THE CALIBRATION SITE

Regression model	FRH-derived volume			LRH-derived volume		
	R ²	RMSE (people)	RRMSE (%)	R ²	RMSE (people)	RRMSE (%)
SLR	0.72	34	42.4	0.73	33	42.2
MLR	0.87	23	29.1	0.87	23	29.0

TABLE 3. REGRESSION MODELS DEVELOPED FOR THE CALIBRATION SITE

Regression model	Equation (Ruleset)
Area-based SLR	$P_i = 0.0353 \times A_i - 37.781$
Area-based MLR	$P_i = 0.0583 \times A_{1i} + 0.0026 \times A_{2i} + 31.697$
Area-based RTS	$P_i = 0.0337 \times A_i - 47.800$
Area-based RTM	$P_i = 0.0559 \times A_{1i} + 0.0057 \times A_{2i} + 22.400$
Volume-based SLR	$P_i = 0.0063 \times V_i - 43.985$
Volume-based MLR	$P_i = 0.0065 \times V_{1i} + 0.0013 \times V_{2i} + 24.912$
Volume-based RTS	$P_i = 0.0812 \times V_i - 88.400$ <i>if</i> $V_i > 23505.5$
	$P_i = 0.0030 \times V_i - 0.100$ <i>if</i> $V_i \leq 23505.5$
Volume-based RTM	$P_i = 0.0111 \times V_{1i} - 153.00$ <i>if</i> $V_{1i} > 25122.8$
	$P_i = 0.0069 \times V_{1i} + 0.0016 \times V_{2i} + 17.3$ <i>if</i> $V_{1i} \leq 25122.8$

P_i represents predicted population in the i^{th} census block
 A_i represents the total area of residential buildings in the i^{th} census block
 A_{1i} represents the area of multiple-family housing units in the i^{th} census block
 A_{2i} represents the area of single-family housing units in the i^{th} census block
 V_i represents the total volume of residential buildings in the i^{th} census block
 V_{1i} represents the volume of multiple-family housing units in the i^{th} census block
 V_{2i} represents the volume of single-family housing units in the i^{th} census block

TABLE 4. COMPARISON BETWEEN THE AREA- AND VOLUME-BASED MODELS FOR:
 (A) THE CALIBRATION SITE, AND (B) THE VALIDATION SITE

Regression model	Area-based approach			Volume-based approach		
	R^2	RMSE (people)	RRMSE (%)	R^2	RMSE (people)	RRMSE (%)
SLR	0.23	56	70.9	0.73	33	42.3
MLR	0.75	32	40.3	0.87	23	29.5
RTS	0.23	58	73.5	0.78	31	38.7
RTM	0.75	32	40.9	0.89	21	26.8

(a)

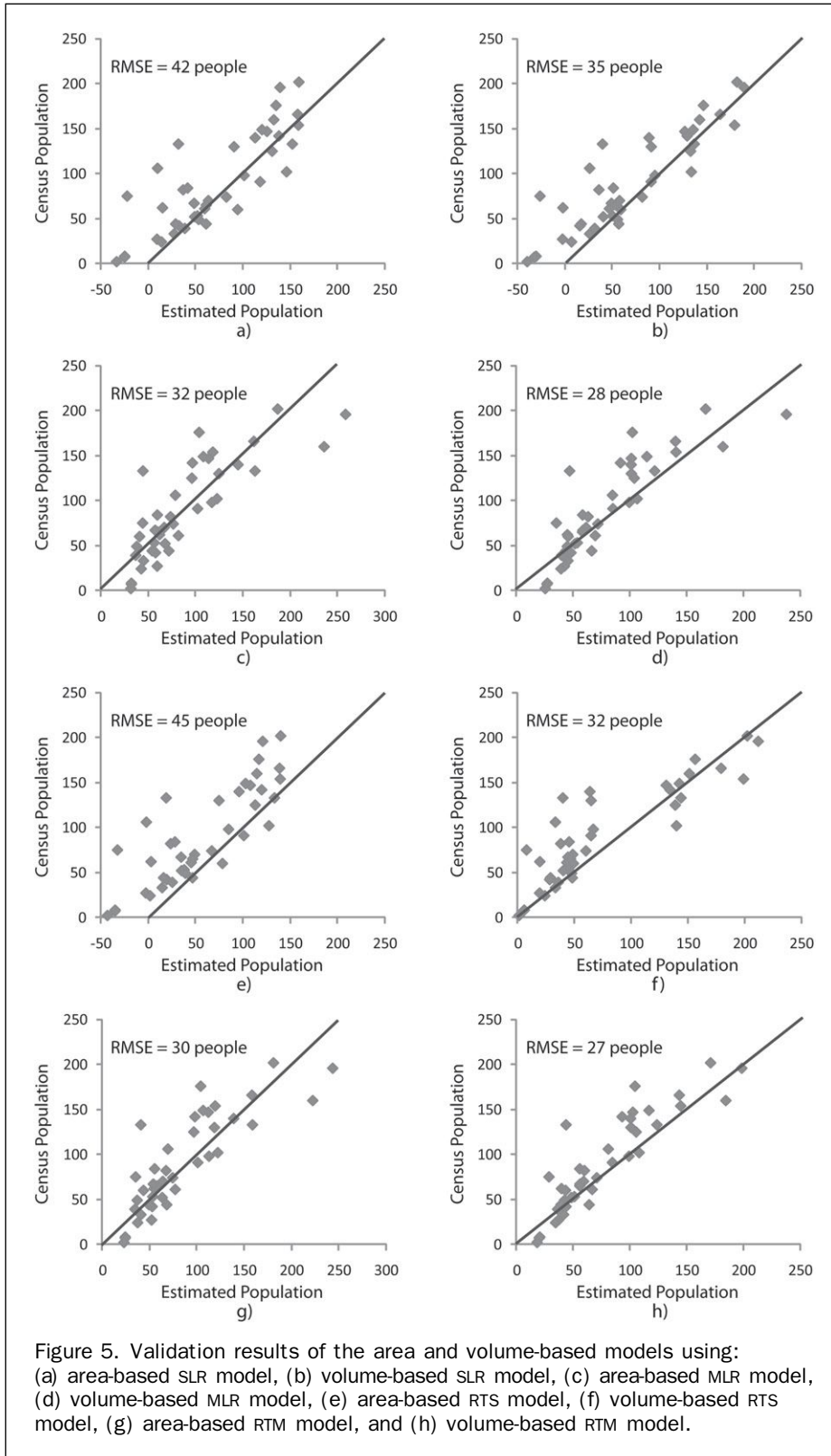
Regression model	Area-based approach			Volume-based approach		
	R^2	RMSE (people)	RRMSE (%)	R^2	RMSE (people)	RRMSE (%)
SLR	0.69	42	43.3	0.80	35	38.8
MLR	0.68	32	32.5	0.76	28	31.1
RTS	0.69	45	50.3	0.78	32	35.9
RTM	0.71	30	33.1	0.80	27	30.1

(b)

all the regression models, the volume-based RTM model yielded the most accurate results, with the highest R^2 value (0.89) and the lowest RMSE (21 people) as well as RRMSE value (26.8 percent). The volume-based MLR model also yielded competitive estimation result with $R^2 = 0.87$, RMSE = 23 people, and RRMSE = 29.5 percent.

The regression models developed for the calibration site were tested on the validation site (Table 4b). The performance of the eight models for the validation site (Figure 5) was similar to that for the calibration site. The volume-based regression models (Figures 5b, 5d, 5f, and 5h) resulted in more accurate population estimation than the area-based models (Figures 5a, 5c, 5e, and 5g). Similar to the calibration results, the volume-based RTM model resulted in the best performance ($R^2 = 0.80$, RMSE = 27, and RRMSE = 30.1 percent) among all the models. The volume-based MLR model yielded competitive estimation results as well ($R^2 = 0.76$, RMSE = 28, and RRMSE = 31.1 percent). It is typical to find

that the validation accuracy is normally lower than the calibration accuracy. However, the performance of the area-based SLR model dramatically increased for the validation site compared to the calibration results (i.e., R^2 increased from 0.23 to 0.69, RMSE decreased from 56 to 42, and RRMSE decreased from 70.9 percent to 43.3 percent), and several other models showed validation accuracy slightly higher than calibration accuracy. The main reason for this is likely the more uneven distribution of multiple-family houses in the calibration site as compared to the validation site (Figure 6). Some blocks in the calibration site have higher proportion of multiple-family houses, while some blocks does not have multiple-family houses (especially in the lower census tract in the calibration site), which resulted in very low correlation when considering the area of the residential buildings. This has less of an impact on the validation accuracy since the validation site has a more even distribution of multiple-family houses. To explore the impact



of the distribution of multiple-family residences on the results, we developed regression models using only one census tract (the upper left one in the calibration site), which has a relatively even distribution of multiple-family houses and a similar rate (~15 percent) of multiple-family houses from the residential buildings. The calibration accuracy

increased using only the census tract. The models were evaluated using the validation dataset and the validation accuracy was slightly lower than the calibration accuracy. This suggests that the different spatial distribution of single- and multiple-family houses between the calibration and validation sites could result in differences in performance.

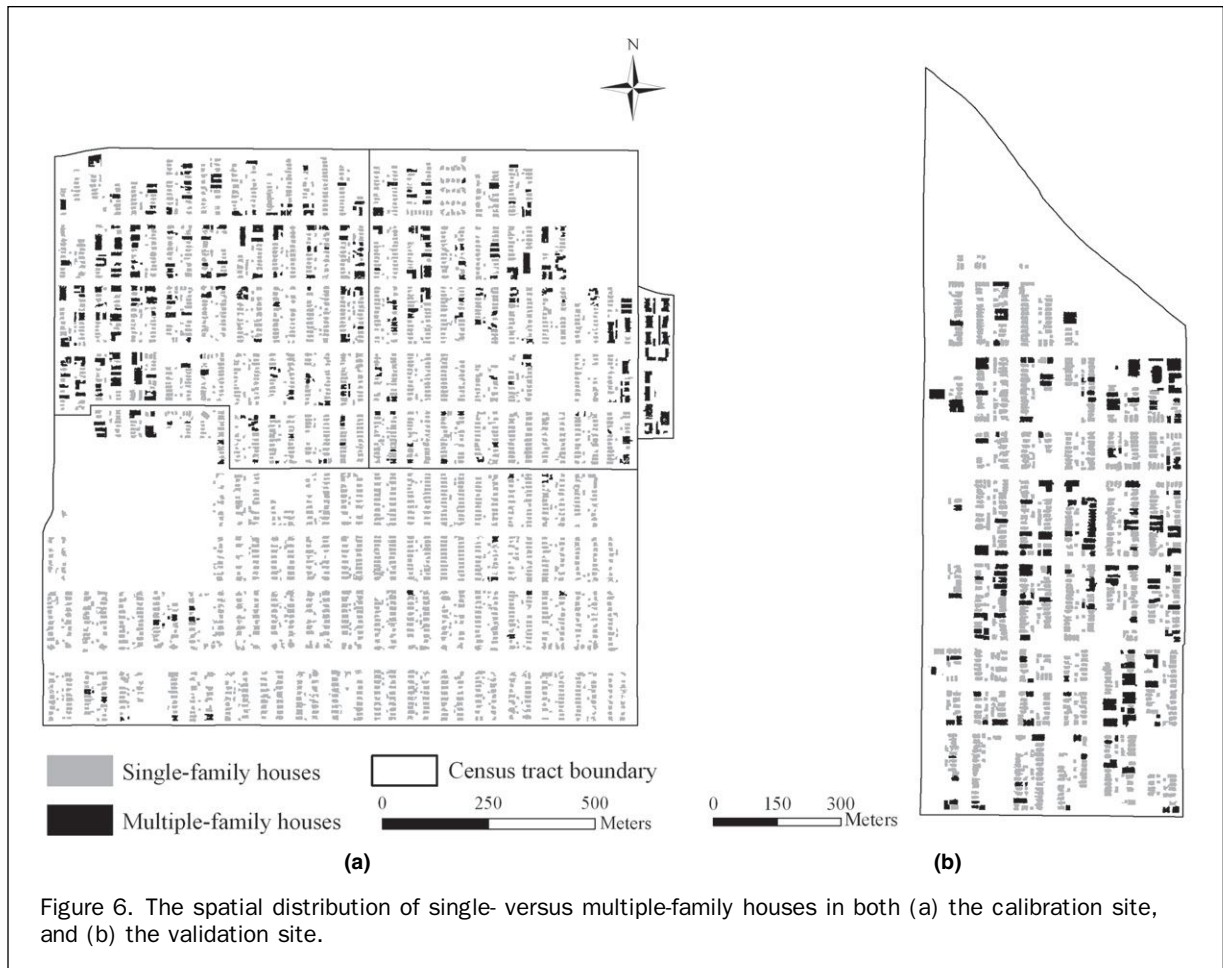


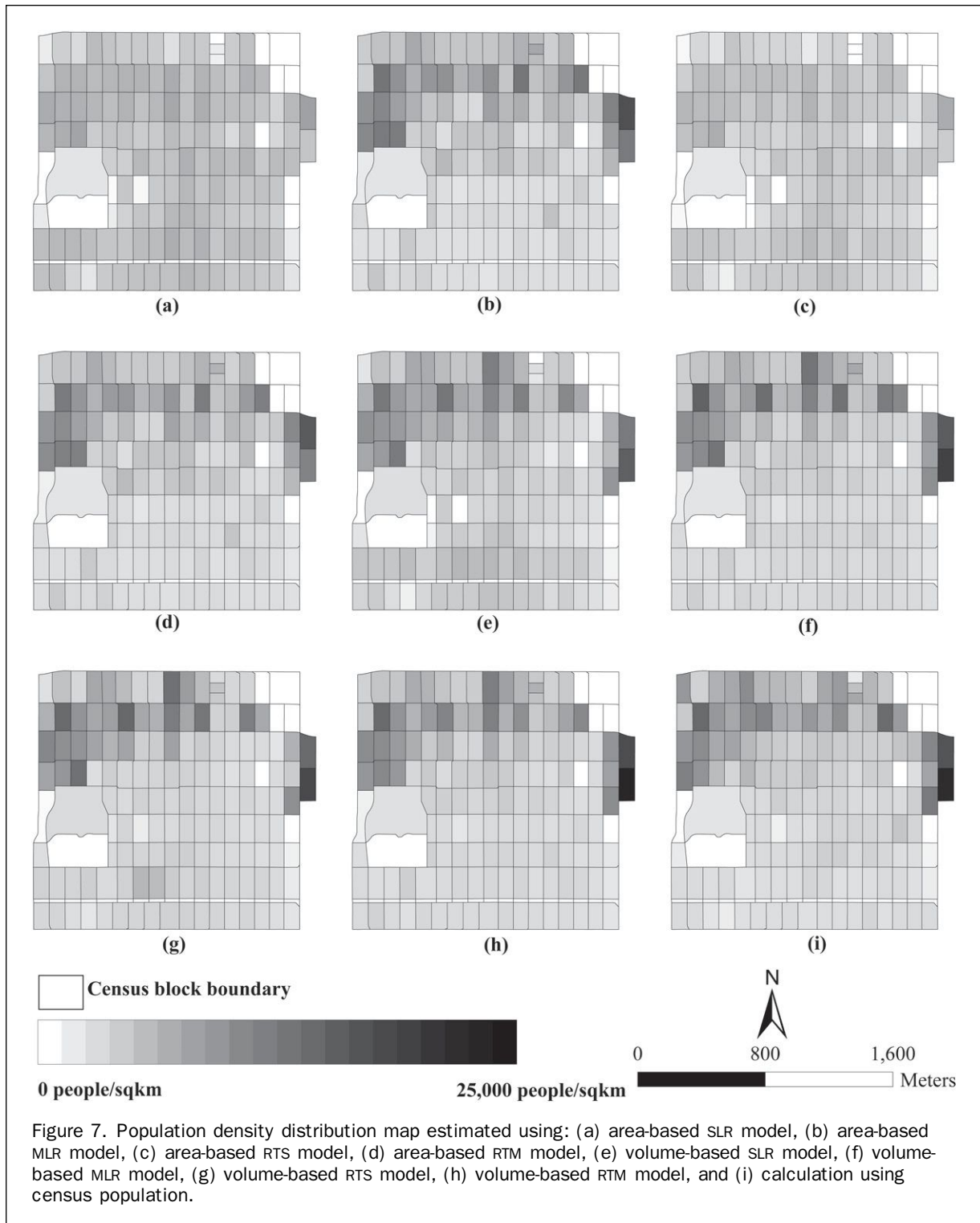
Figure 6. The spatial distribution of single- versus multiple-family houses in both (a) the calibration site, and (b) the validation site.

The performance between the calibration and validation sites of volume-based models did not change as much as the area-based ones according to the RRMSE values. The volume-based single-variable models (SLR and RTS) performed better for the validation site than the calibration site (i.e., RRMSE of the volumetric SLR and RTS models decreased from 42.3 percent to 38.8 percent, and 38.7 percent to 35.9 percent, respectively), while the volume-based multi-variable models (MLR and RTM) resulted in slightly poorer estimations for the validation site than the calibration site (i.e., RRMSE increased from 29.5 percent to 31.1 percent, and 26.8 percent to 30.1 percent). Results show that the performance of population estimation was considerably influenced not only by the models employed but also by the population indicators used. Compared to the dramatic performance fluctuation and relatively poor performance of the areal approach, the performance of the volumetric approach was more accurate and stable.

Regression models using multiple variables, such as high- or low-density urban or commercial use areas, have been commonly used in area-based population estimation (e.g., Lo, 2008; Wu and Murray, 2005; Li and Weng, 2005). In this study, the regression models using two variables (i.e., single- and multiple-family houses) resulted in better performance than the models only using one variable (i.e., residential buildings) for both the area- and volume-based approaches. In particular, the area-based regression models using multiple variables dramatically increased the calibration accuracy compared to the area-based models using a single variable in the calibration site. One possible explanation for this is that the inclusion of two variables allowed different weights to be

assigned for single- and multiple-family houses, which decreased the impact of the lack of information (e.g., the number of stories) in the area-based models. The regression tree models (i.e., RTS and RTM), provided similar or slightly better estimation compared to the linear regression models (i.e., SLR, MLR). In addition, the volume-based RTM model yielded the most accurate estimations in both the calibration and validation sites, which suggested regression tree models could be valuable in remote sensing-based population estimation. The likely reason for more accurate performance of the regression tree models is their ability to generate multiple rulesets, thus better characterizing different housing configurations. For example, the volume-based RTM model generated two rulesets for the calibration site (Table 2). One of the rulesets was for the regions where multiple-family houses were dominant resulting in larger volume of residential buildings, and the other one was for the single-family house-dominant regions with smaller residential building volume.

Figure 7 shows the population density map estimated using the regression models for the calibration site. Both the area- and volume-based models successfully estimated population for most census blocks with population density $< 5,000$ people/km², which contain mainly single family houses. The census blocks with population density between 5,000 and 15,000 people/km² included both single- and multiple-family houses, to different extents, in the study areas. For these census blocks, the volume-based models (i.e., Figures 7e, 7f, 7g, and 7h) performed slightly better than the area-based models (i.e., Figures 7a, 7b, 7c, and 7d). The area-based SLR and RTS models dramatically underestimated population



density in the regions dominated by multiple-family houses, where population density was $>15,000$ people/km². The volume-based MLR and RTM models (Figures 7f and 7h) resulted in accurate estimation regardless of the mixture of single- and multiple-family houses.

Based on a comparison of the area- and volume-based approaches, the volume of residential buildings is a more robust and stable population indicator because the volume-based models were more flexible in considering different housing characteristics. The comparison also suggested the

potential merit of the volumetric approach for remote sensing-based population estimation for urban areas in developing countries, where residential buildings are frequently multiple-family structures such as apartments and condominiums. However, the volume-based approaches are sensitive to the accurate identification of residential buildings. In this study, potential errors due to inclusion of non-residential structures were greatly reduced by the parcel data, which are not always available. Consequently, the accurate extraction of residential buildings from remote

sensing data (e.g., lidar data) without any external information is one of the most significant and challenging problems for remote sensing-based population estimation. While a general land use classification approach may work well for residential building extraction in suburban areas (e.g., Lu *et al.*, 2010), more advanced approaches (e.g., using the association and spatial relationships between residential buildings and other land use classes) are necessary in urban areas with heterogeneous housing characteristics. Building type/usage classification using airborne or satellite remote sensing data only has had minimal exploration.

Conclusions

Compared to population estimation in suburban or rural areas, population estimation in urban areas is particularly challenging due to the heterogeneous characteristics of housing. In this study, five main conclusions can be drawn: (a) the modified morphological building detection algorithm successfully delineated the building footprints, even for buildings partially occluded by nearby tall trees, (b) lidar last return-derived height provided slightly better population estimation results than that using lidar first return-derived height, (c) compared to footprint area, the volume of residential buildings was a more stable population indicator, (d) the regression models using two variables (e.g., single and multiple family houses) outperformed those using only one variable (e.g., residential houses), and (e) the regression tree models (RTS and RTM) increased population estimation accuracy possibly because they were flexible by allowing different rulesets for regions with different housing characteristics.

The main objective of this research was to utilize lidar data for building delineation and compare the performance of volumetric and areal approaches to population estimation in regions with heterogeneous housing characteristics. The results attained using the regression tree model with a volumetric approach provided the best results and is expected to have the greatest extension to other areas. By utilizing the tools generated to accurately delineate building footprints, even where buildings are partially occluded, the utilization of multiple rulesets and inputs provides a population estimation approach that should provide flexibility in a range of urban environments. However, the success of the volumetric approach to population estimation in this study was partially attributed to the parcel data. Using parcel data as an ancillary input to identify residential buildings was an accurate but not ideal solution, since parcel data are not universally available. Accurate building type/usage classification using remote sensing data only would make both the volumetric and areal population estimation approaches more generalized and applicable to different urban environments, which is the main focus of our future research.

References

- Gong, B., J. Im, and G. Mountrakis, 2011. An artificial immune network approach to multi-sensor land use/land cover classification, *Remote Sensing of Environment*, 115: 600–614.
- Harvey, J.T., 2002. Estimating census district populations from satellite imagery: Some approaches and limitations, *International Journal of Remote Sensing*, 23:2071–2095.
- Huang, C., and J.R.G. Townshend, 2003. A stepwise regression tree for nonlinear approximation: Applications to estimating subpixel land cover, *International Journal of Remote Sensing*, 24:75–90.
- Im, J., J.R. Jensen, M. Coleman, and E. Nelson, 2009. Hyperspectral remote sensing analysis of short rotation woody crops grown with controlled nutrient and irrigation treatments, *Geocarto International*, 24(4):293–312.
- Im, J., Z. Lu, J. Rhee, and L.J. Quackenbush, 2011. Impervious surface quantification using a synthesis of artificial immune networks and decision/regression trees from multi-sensor data, *Remote Sensing of Environment*, doi:10.1016/j.rse.2011.06.024.
- Jensen, J.R., and D.J. Cowen, 1999. Remote sensing of urban/suburban infrastructure and socio-economic attributes, *Photogrammetric Engineering & Remote Sensing*, 65(6):611–622.
- Jensen, R.R., J.P. Hardin, and W.M. Jackson, 2010. Spectral modeling of population density: A study of Utah's Wasatch Front, *Photogrammetric Engineering & Remote Sensing*, 76(7):797–806.
- Ke, Y., L.J. Quackenbush, and J. Im, 2010. Synergistic use of QuickBird multispectral imagery and LIDAR data for object-based forest species classification, *Remote Sensing of Environment*, 114(6):1141–1154.
- Kocev, D., S. Dzeroski, M.D. White, G.R. Newell, and P. Griffioen, 2009. Using single- and multi-target regression trees and ensembles to model a compound index of vegetation condition, *Ecological Modelling*, 220:1159–1168.
- Langford, M., 2006. Obtaining population estimates in non-census reporting zones: An evaluation of the 3-class dasymetric method, *Computers, Environment and Urban Systems*, 30:161–180.
- Lawrence, R.L. and A. Wright, 2001. Rule-based classification systems using classification and regression tree (CART) analysis, *Photogrammetric Engineering & Remote Sensing*, 67(11):1137–1142.
- Li, G., and Q.H. Weng, 2005. Using Landsat ETM+ imagery to measure population density in Indianapolis, Indiana, USA, *Photogrammetric Engineering & Remote Sensing*, 71(9):947–958.
- Li, G., and Q.H. Weng, 2010. Fine-scale population estimation: how Landsat ETM+ imagery can improve population distribution mapping?, *Canadian Journal of Remote Sensing*, 36:155–165.
- Liu, X.H., P.C. Kyriakidis, and M.F. Goodchild, 2008. Population-density estimation using regression and area-to-point residual kriging, *International Journal of Geographical Information Science*, 22:431–447.
- Lo, C.P., 1995. Automated population and dwelling unit estimation from high resolution satellite images: A GIS approach, *International Journal of Remote Sensing*, 16:17–34.
- Lo, C.P., 2008. Population estimation using geographically weighted regression, *GIScience and Remote Sensing*, 45:131–148.
- Lu, D.S., Q.H. Weng, and G.Y. Li, 2006. Residential population estimation using a remote sensing derived impervious surface approach, *International Journal of Remote Sensing*, 27:3553–3570.
- Lu, Z., J. Im, L.J. Quackenbush, and K. Halligen, 2010. Population estimation based on multi-sensor data fusion, *International Journal of Remote Sensing*, 31:5587–5604.
- Meng, X., L. Wang, and N. Currit, 2009a. Morphology-based building detection from airborne lidar data, *Photogrammetric Engineering & Remote Sensing*, 75(4):437–442.
- Meng, X., L. Wang, L.C. Jose, and C. Nate, 2009b. A multi-directional ground filtering algorithm for airborne lidar, *ISPRS Journal of Photogrammetry and Remote Sensing*, 64:117–124.
- Tullis, J.A., and J.R. Jensen, 2003. Expert system house detection in high spatial resolution imagery using size, shape, and context, *Geocarto International*, 18(1):5–15.
- Wu, C., and A.T. Murray, 2005. A cokriging method for estimating population density in urban areas, *Computers, Environment and Urban Systems*, 29:558–579.
- Wu, C., and A.T. Murray, 2007. Population estimation using Landsat Enhanced Thematic Mapper imagery, *Geographical Analysis*, 39:26–43.
- Wu, S.S., L. Wang, and X. Qui, 2008. Incorporating GIS building data and census housing statistics for sub-block population estimation, *The Professional Geographer*, 60:121–135.
- Xu, M., P. Watanachaturaporn, P.K. Varshney, and M.K. Arora, 2005. Decision tree regression for soft classification of remote sensing data, *Remote Sensing of Environment*, 97:322–336.
- Yuan, Y., R.M. Smith, and W.F. Limp, 1997. Remodeling census population with spatial information from Landsat TM imagery, *Computer, Environment and Urban Systems*, 21:245–258.

(Received 02 August 2010; accepted 17 April 2011; final version 20 April 2011)

Automatic Georeferencing of Aerial Images Using Stereo High-Resolution Satellite Images

[THIS PAPER WAS THE WINNER OF THE 2010 BAE SYSTEMS AWARD GIVEN AT THE ASPRS 2010 ANNUAL CONFERENCE]

Jaehong Oh, Charles K. Toth, and Dorota A. Grejner-Brzezinska

Abstract

For airborne surveys, the GPS/INS system has become the primary source for aerial image georeferencing. However, alternative automated georeferencing is required to serve as a backup for georeferencing when GPS/INS-based georeferencing is not feasible. High-resolution satellite images (HRSI) have been globally available with better spatial resolution and increasing positional accuracy. Therefore, HRSI has high potential as a ground control source for aerial image georeferencing which usually requires accurate 3D ground control points. Unfortunately, single imagery, which is often used as a reference, contains relief displacement due to objects on the ground introducing positional errors, unless it is not true ortho-rectified which is costly and time consuming. Therefore, in this study, a stereo HRSI-based automated georeferencing approach is proposed. The use of stereo images can avoid the impact of relief displacement and requires no external height information. The proposed method is based on a multi-scale image matching approach utilizing a combination of SIFT (Scale-Invariant Feature Transform) and RANSAC (RANdom SAmple Consensus). In the georeferencing step, the bundle adjustment with outlier removal of Baarda's data snooping was utilized. Experimental results for a strip of aerial images with stereo Ikonos images showed its potential as a backup system for automated georeferencing.

Introduction

Aerial digital imaging systems with direct georeferencing have been widely used for mapping. With the advance in semiconductor technology to produce large CCD arrays, aerial digital cameras have been rapidly spreading all over the world. High-performance airborne digital sensor systems can generally acquire large amounts of data and provide frequent updates of geospatial image information with the capability of fast and automated digital processing. A critical step in aerial image processing is georeferencing, i.e., establishing sensor orientation that is usually performed manually using ground control points. Traditionally, it used to be costly and labor intensive, but now it is highly automated by integrated GPS/INS systems (Global Positioning System/Inertial Navigation System) (Grejner-Brzezinska, 1999; Mostafa and Schwarz, 2000; Mostafa *et al.*, 2001). In the GPS/INS

integration, GPS measurements are used to correct INS measurements through an integration algorithm. However, since GPS is a line-of-sight system and is subject to interference and jamming (Carroll, 2001), any loss of GPS lock results in so-called free inertial navigation of a GPS/INS system, where georeferencing errors increase with time due to inertial sensor drifts. Navigation-grade INS can maintain horizontal position accuracy within 100 m through GPS outages of more than 10 minutes, while the lower cost INS, common in guided weapons, unmanned air vehicles and general aviation (private) aircraft can only maintain this accuracy for 2 to 3 minutes (Runnalls *et al.*, 2005). In addition, there are areas that completely lack the ground-based GPS infrastructure that are often required to maintain mapping accuracy by differential GPS methods.

Image-to-image matching-based indirect georeferencing, also used in terrain-based navigation (Sim *et al.*, 2002; Conte and Doherty, 2008), is rapidly gaining research and practical interest and offers an alternative approach to the georeferencing. By means of image matching, existing reference images can provide newly acquired images with ground control information to perform georeferencing. Therefore, reference data quality is one of the key components for the success of georeferencing. Ideal reference data would be images acquired with the same sensor at a similar geometry, at a similar time and season as that of the new image; obviously, this is rarely the case. Ideally, the sensor used for the reference image should be of high spatial resolution, high temporal resolution, and high positional accuracy.

High-resolution satellite images (HRSI) have good potential as a ground control source for aerial image georeferencing. Since the first 1 m resolution satellite Ikonos-2, was launched in September 1999, many high-resolution satellite images have been available such as QuickBird (DigitalGlobe, launch: 2001, resolution: 60 cm), SPOT-5 (SPOT, 2002, resolution: 2.5 m), OrbView-3 (GeoEye, 2003, resolution: 1 m), KOMPSAT-2 (KARI, 2006, resolution: 1 m), EROS-B (ImageSat, 2006, resolution: 70 cm), WorldView-1 (DigitalGlobe, 2007, resolution: 50 cm), CARTOSAT-2A (ISRO, 2008, resolution: 80 cm), GeoEye-1 (GeoEye, 2008, resolution: 41 cm), WorldView-2 (DigitalGlobe, 2009, resolution: 46 cm). Moreover, more satellites are scheduled in a few years such

Photogrammetric Engineering & Remote Sensing
Vol. 77, No. 11, November 2011, pp. 1157–1168.

0099-1112/11/7711-1157/\$3.00/0
© 2011 American Society for Photogrammetry
and Remote Sensing

Satellite Positioning and Inertial Navigation (SPIN) Laboratory,
The Ohio State University, 470 Hitchcock Hall, 2070
Neil Ave, Columbus, OH 43210 (oh.174@osu.edu).

as EROS-C, and GeoEye-2. HRSI is acquired worldwide with good temporal resolution and is available at good-positional accuracy, up to sub-pixel level accuracy when bundle adjusted using Ground Control Points (GCP) (Fraser and Ravanbakhsh, 2009). These images have a relatively large swath width, usually more than 10 km, and are used to create worldwide image maps, such as Google Earth®. In addition, many images are acquired in multispectral bands, which have advantages in feature extraction.

The image-to-image approach for automatic image co-registration has been studied extensively (Wen *et al.*, 2008; Yi *et al.*, 2008; Wong and Clausi, 2007; Ali and Clausi, 2002; Zhang *et al.*, 2000). Most of these authors focused on two-dimensional co-registration between low-resolution satellite images based on a simple geometric model such as affine geometry and polynomials. Other research utilized a standard ortho-rectified image and an associated low-resolution digital elevation model (DEM) to obtain 3D ground control points to georeference satellite images (Rottensteiner *et al.*, 2009; Gianinetta and Scaioni, 2008). These image-to-image approaches using a satellite image were also investigated in the field of navigation to support unmanned aerial vehicle (UAV) navigation (Sim *et al.*, 2002; Conte and Doherty, 2008).

This study proposes use of stereo HRSI as a ground control source for automatic aerial image georeferencing. Note that a standard ortho-rectified reference image will contaminate ground control point quality due to the still existing relief displacement of the ground features in the image, such as buildings and trees, unless these objects are also rectified; and, a coarse DEM also leads to inaccurate height information. Therefore, the combination of a true ortho-rectified image and a high-resolution DEM should be used for accurate 3D ground control. However, there are practical limitations to the generation and update of a true ortho-rectified image for a large area, including the high production cost of a DEM with accurate break-lines. In addition to the attractive properties of HRSI, stereo HRSI is not subject to the aforementioned effect of relief displacement or the requirement for accurate external height information. Figure 1 compares the proposed method to the conventional method of using a combination of standard ortho-rectified imagery and digital terrain model (DTM) as a reference. Figure 1a shows the main steps of the standard ortho-rectified image and DTM-based registration. Note that there exists relief displacement of the ground features such as buildings and trees in the reference image; the apparent leaning of objects can be observed. Even worse, the DTM does not contain the height information of ground features. When the image points (solid triangles on both aerial image and reference image) are obtained by image matching between the aerial and reference images, erroneous ground point information (hollow triangles) is obtained due to the relief displacement, and due to the missing height information of the ground features in the DTM. In comparison, Figure 1b depicts the case of using stereo HRSI as reference data. By image matching of the aerial image to the left and right HRSI, the image points (solid triangles and squares) are obtained in each stereo image (reference). By utilizing stereo matching along the epipolar line, conjugate image points (hollow triangles and squares) can also be obtained in the stereo image pair. The 3D ground restitution of these conjugate points provide correct 3D ground point coordinates, which are not affected by relief displacement of the ground features in the reference data, and do not require external ground height information.

Besides the reference data, another requirement for successful georeferencing is the robust image matching, because aerial images and HRSI tend to have large image

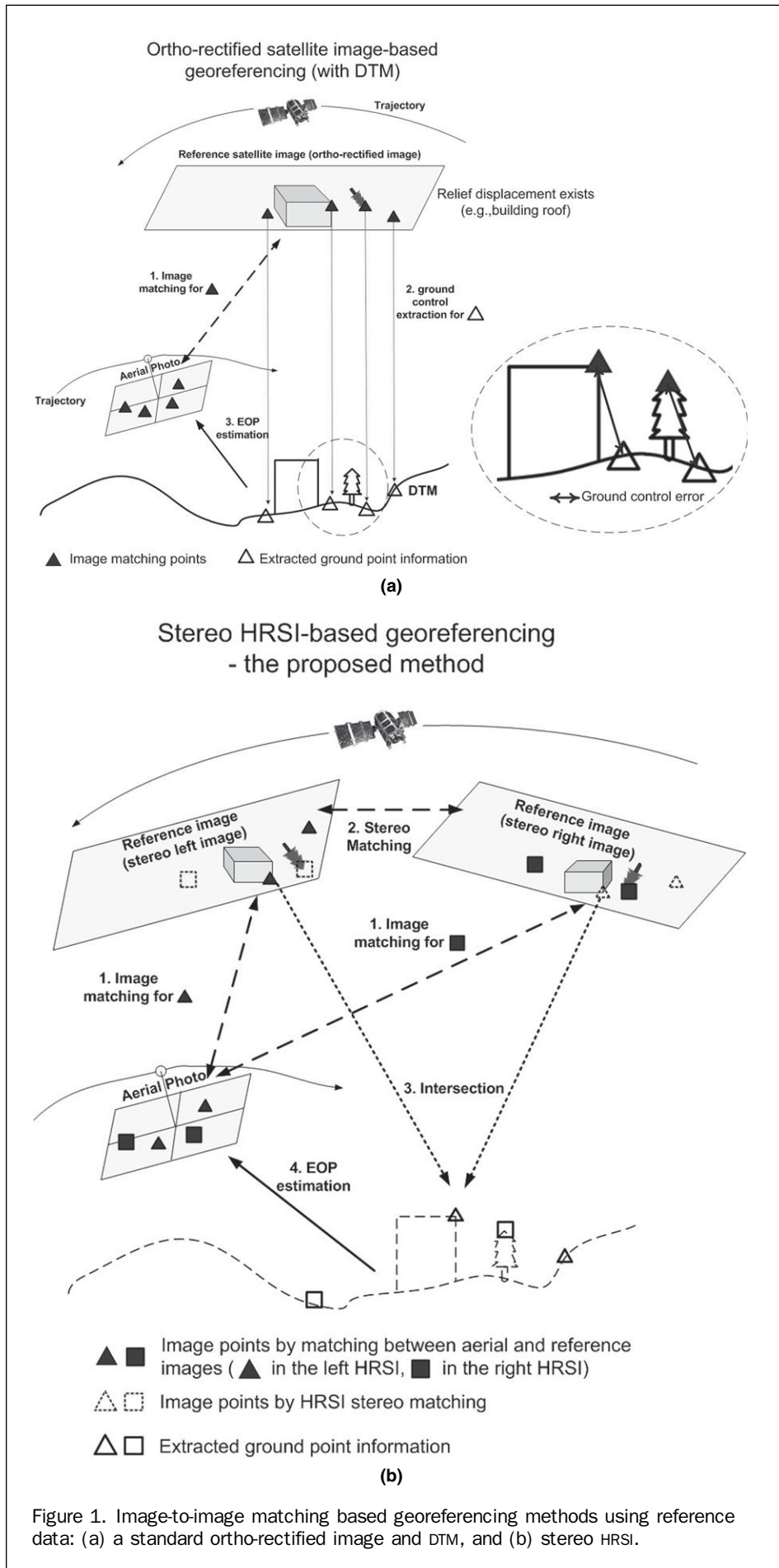
differences due to differences in sensors used, acquisition time and season, camera orientation, and so on. Therefore, the proposed method is based on a multi-scale image matching approach utilizing a combination of the SIFT (Lowe, 1999) and RANSAC (Fischler and Bolles, 1981) methods. Aerial images are matched to stereo HRSI to obtain ground coordinate information of aerial image points. Then, RANSAC implemented with the collinearity constraint is used to eliminate outliers in matching points of each aerial image. In the georeferencing step, exterior orientation parameters (EOP) are estimated from the bundle adjustment with outlier removal based on Baarda's data snooping (Baarda, 1968).

The paper is structured as follows: first, the proposed method will be presented including image matching between aerial images and stereo HRSI and how to remove outliers. Second, experimental results for a strip of aerial images with stereo Ikonos images are presented, followed by a brief summary.

Proposed Method

Robust and accurate image matching is critical since aerial images and the satellite images should have large image differences. To handle these differences, highly invariant feature matching methods are required such as SIFT. SIFT is the popular point feature extraction and matching method, since it was recognized to be very reliable and invariant to changes in image condition. Note that some modifications to SIFT were developed to make it more effective, such as PCA-SIFT (Ke and Sukthankar, 2004), GLOH (Gradient Location-Orientation Histogram) (Mikolajczyk and Schmid, 2005), CSIFT (Abdel-Hakim and Farag, 2006), SR-SIFT (Yi *et al.*, 2008), SURF (Speeded-Up Robust Features) (Bay *et al.*, 2008), and Robust SIFT (Li *et al.*, 2009); although, they are conceptually similar. The major concern in the image matching is the existence of numerous matching outliers, which, for example, can be removed by RANSAC with an appropriate geometric model. Note that RANSAC is a technique to estimate parameters of a model through iteration from a set of observations when they contain outliers. Therefore, this study proposed a multi-scale approach based on SIFT and RANSAC for efficient yet robust image matching between aerial images and HRSI.

Figure 2 depicts the flowchart of the proposed method of automated aerial image georeferencing using stereo HRSI. First, aerial images are matched to each satellite image in a multi-scale approach to extract aerial image points, e.g., n points, and the corresponding left and right satellite image points, e.g., n_L and n_R points, where $n \leq n_L + n_R$. By performing stereo satellite image matching (normalized cross correlation along the epipolar line), conjugate satellite image points can be located in the stereo pair. Of course, poor stereo matching points should be pruned utilizing a threshold at the stage, and it is assumed that m stereo conjugate points remain. Consequently, the number of corresponding aerial image points is also reduced to m . Then, 3D ground coordinates are computed from the m stereo conjugate points by ground restitution using RPC (Rational Polynomial Coefficients) (Grodecki *et al.*, 2004). Since 3D ground coordinates of aerial image points have been obtained, the aerial georeferencing can be carried out indirectly using the collinearity equation. However, there is still a high possibility that numerous image matching outliers exist. Therefore, RANSAC is utilized to remove possible image matching outliers by introducing a geometric constraint of collinearity. Following the successful outlier removal, EOP of the aerial images can be finally estimated using the single photo resection method or the bundle adjustment depending on



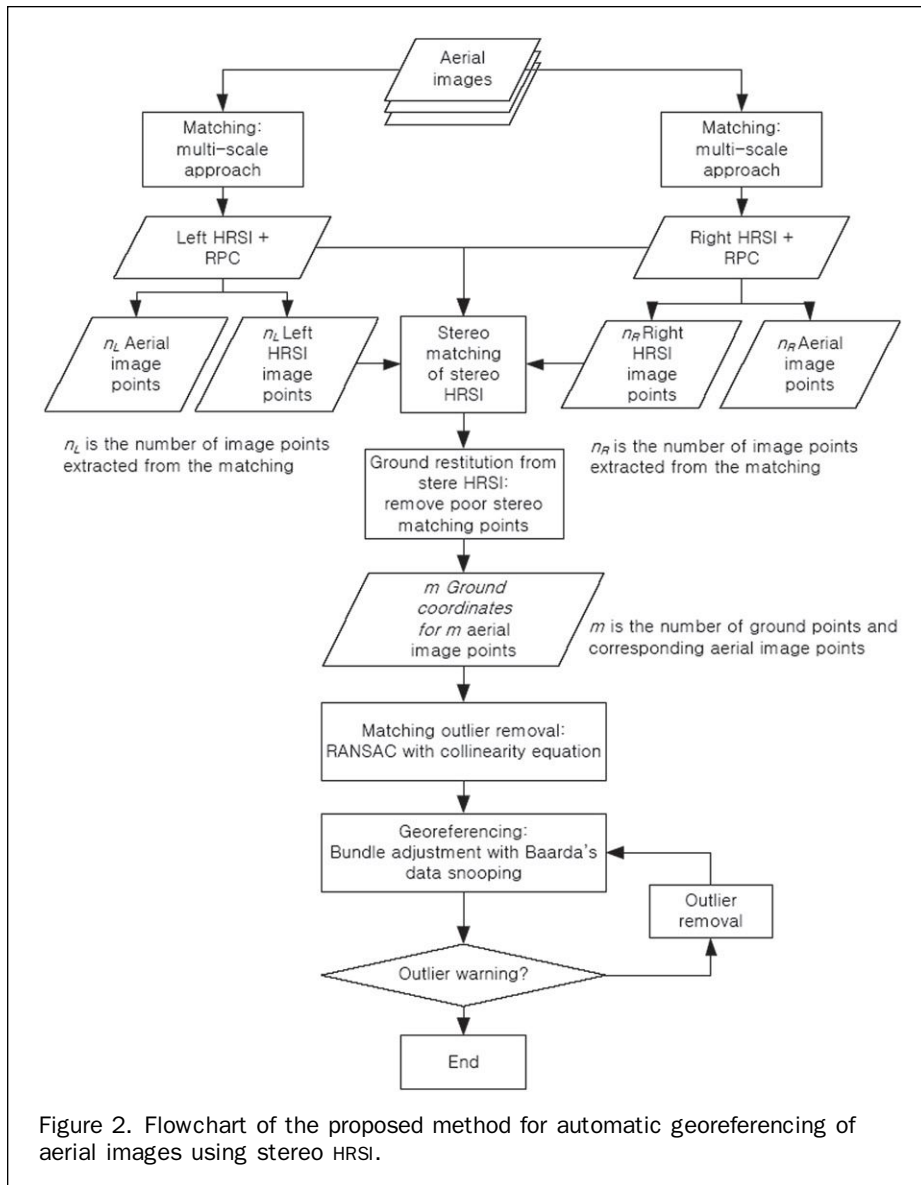


Figure 2. Flowchart of the proposed method for automatic georeferencing of aerial images using stereo HRSI.

the level of overlap between the aerial images. In the bundle adjustment step, a more rigorous outlier removal, based on Baarda's data snooping, is employed as a kind of "safety" because the image overlap can provide a useful geometric constraint to filter out the remaining outliers.

Multi-scale Approach for Matching between Aerial Image and Stereo Satellite Images

A multi-scale approach consisting of coarse and fine image matching between aerial and satellite images is proposed as shown in Figure 3. This multi-scale approach is efficient for practical application since geospatial images acquired for mapping purposes or for terrain-referenced navigation are typically large in size.

By utilizing coarse matching, an aerial image is approximately located and co-registered to satellite images, and the region of interests (ROI) is obtained in satellite images, to which the aerial image will be fine-matched. Note that the coarse matching utilizes down-sampled images. Taking the average is the simplest method of low-pass filter, but in this

study, the Gaussian image pyramid is generated from each aerial and satellite image to attenuate aliasing effects (Fosyth and Ponce, 2000). The top of the image pyramid should have only the low-frequency information. Then, Gaussian down-sampled images of similar spatial resolution are SIFT matched to each other, and outliers in the matching results are removed using RANSAC. Since the down-sampled images are often low-resolution, not significantly affected by relief displacement, the affine model should be satisfactory to model the transformation. Commercial software, such as ERDAS Imagine® AutoSync, requires that at least two conjugate points be measured by users to orient images and constrain automatic image matching. In this case, the coarse matching step would not be required because the manually measured data are available. In addition, when external EOP parameters exist, even though they are not accurate enough, the information will be useful for the initial localization or ROI determination. However, in this study, the coarse matching was activated since no external information is assumed.

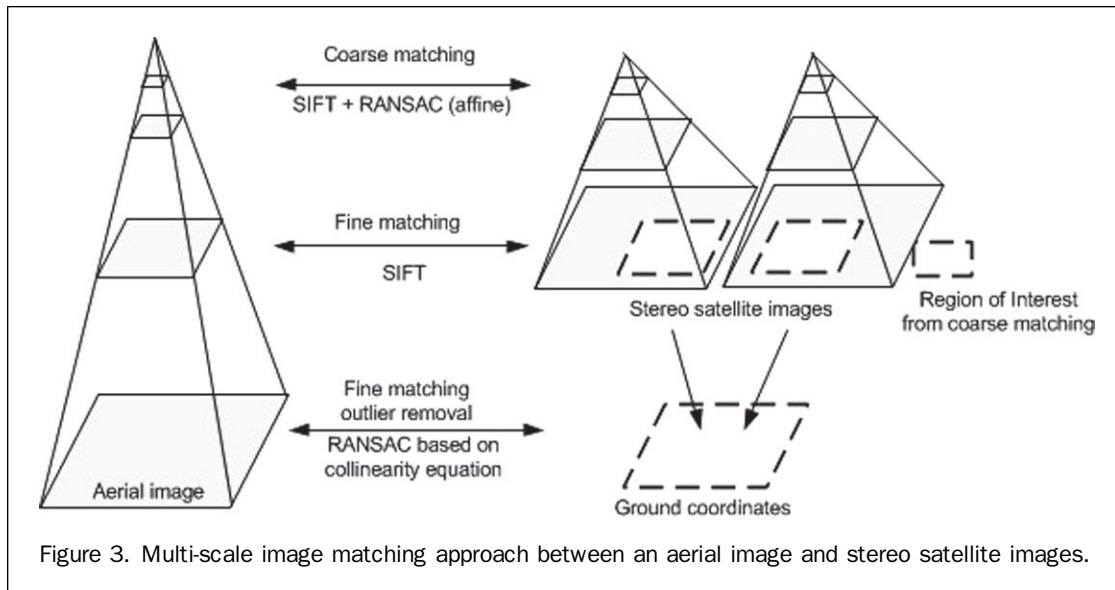


Figure 3. Multi-scale image matching approach between an aerial image and stereo satellite images.

Following the coarse matching, the fine matching is performed between the aerial image and the selected region of satellite images (each stereo image) to obtain control points from the satellite images. Note that aerial images, which usually have higher spatial resolution, need to be down-sampled close to the resolution of satellite images before matching, since resolution difference is one of the factors affecting SIFT matching performance. For example, if the aerial image has 25 cm resolution and satellite images are of 1 m resolution, pyramid level 3 of the aerial image is selected. Use of the down-sampled image has another benefit of significantly reducing computational load in image matching. In contrast to the coarse matching, the outliers in the fine matching results should be suppressed using a rigorous model, such as the collinearity equation, exploiting well-calibrated camera information because relief displacement needs to be handled.

Stereo Matching between Stereo HRSI

Since the geometric and spectral difference between the along-track stereo HRSI are rather small and epipolar geometry is well established, there is no need for SIFT or other sophisticated and computationally expensive feature matching methods. The well-known normalized cross-correlation can be used for the stereo image matching using Equation 1:

$$c = \frac{\sum_{i=1}^{r1} \sum_{j=1}^{c1} [(A_{ij} - \bar{A})(B_{ij} - \bar{B})]}{\sqrt{\left[\sum_{i=1}^{r1} \sum_{j=1}^{c1} (A_{ij} - \bar{A})^2 \right] \left[\sum_{i=1}^{r1} \sum_{j=1}^{c1} (B_{ij} - \bar{B})^2 \right]}} \quad (1)$$

where A is a patch from aerial image, size of $r1 \times c1$, B is a HRSI patch of size equal to that of A , A_{ij}, B_{ij} are the image intensity of A and B at row i and column j , respectively, and \bar{A}, \bar{B} are the average of all intensity values in image A and B , respectively.

Even if the accurate epipolar image resampling significantly reduces the search space to the epipolar line, there is still a computational load for any moving window approach. Therefore, the convolution theorem is utilized for fast matching performance. From Equation 1, it can be seen that B can be computed in the frequency domain by FFT (Fast

Fourier Transform), i.e., convolving B with the window, with all elements equal to one. In other words, if \bar{B} is computed over the entire HRSI in advance, before the correlation computation, the computational load is significantly reduced.

By decomposing the numerator of Equation 1, it is identified that $\sum_{r=1j=1}^{r1 c1} (A_{ij} - \bar{A})$ can be computed once for each aerial image patch, and $\sum_{r=1j=1}^{r1 c1} B_{ij}(A_{ij} - \bar{A})$ can be computed in the frequency domain by convolving B with $(A_{ij} - \bar{A})$. Similarly, the decomposition of the denominator shows that $\sum_{r=1j=1}^{r1 c1} (A_{ij} - \bar{A})^2$ can be computed once for each aerial image patch, and the summation terms $\sum_{r=1j=1}^{r1 c1} B_{ij}$ and $\sum_{r=1j=1}^{r1 c1} B_{ij}^2$ can be computed by convolving B or B^2 with a window that has all elements equal to one. By utilizing this approach, the matching speed can be significantly increased.

Experiment

Test Data

Table 1 presents the specifications of aerial and Ikonos stereo images tested, and Figure 4 and Figure 5 show the test images. Note that the aerial images were acquired in June 2003 and the Ikonos stereos in November 2001. Due to time and seasonal gaps, there are large seasonal and terrain differences between the images. First, the Ikonos RPC were updated using four GCPs by estimating only shift terms in the RPC error adjustment model (Fraser and Hanley, 2005). Image coordinate residuals after adjustment were at the one-pixel level. Then, epipolar image resampling was performed for efficient stereo image handling, and y-parallax in the epipolar resampled images was at a one-pixel level (Note that the epipolar image resampling process is an option.). Ground restitution residuals of the epipolar resampled images were 1 and 0.5 meter for horizontal and vertical, respectively. For the epipolar image resampling method for the same dataset in detail, refer to (Oh *et al.*, 2010). Figure 4

TABLE 1. TEST DATA SPECIFICATION

Data	Site	Date	Focal length	Resolution	Spectral
Ikonos, Level2 Stereo	Daejeon, Korea	Nov 2001	10 m	1 m	Pan
Aerial images	Daejeon, Korea	Jun 2003	55 mm	25 cm	Color

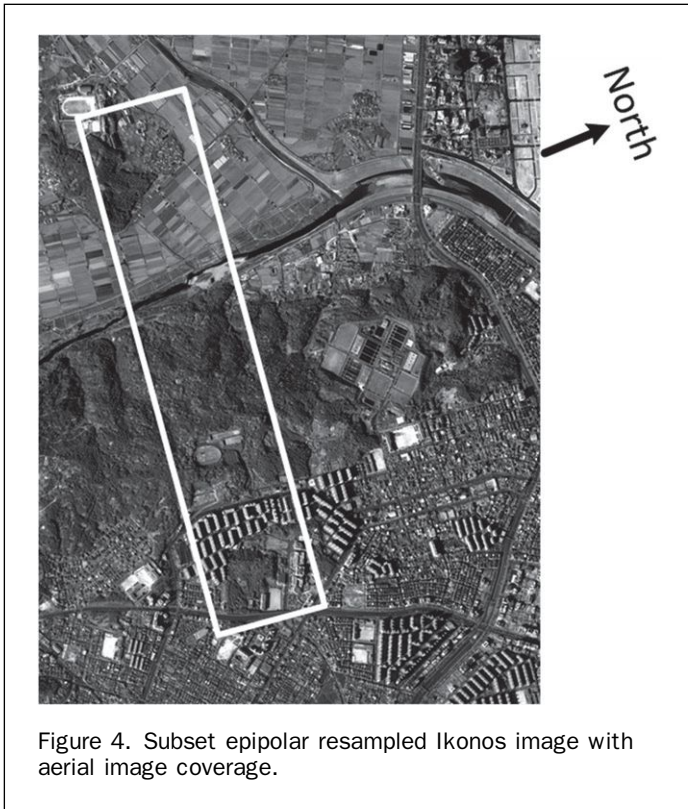


Figure 4. Subset epipolar resampled Ikonos image with aerial image coverage.

presents a subset image of the epipolar resampled images, and Figure 5 shows a strip of aerial images containing various ground textures including open field, forest, and buildings. For the image matching, the red band in the aerial image was selected because the Ikonos relative spectral response (GeoEye, 2008) shows that the red band shows acceptable similarity in terms of spectral responsibility, even though the green band covers a little larger spectral range, i.e., wider in terms of spectral range.

Multi-scale Image Matching

First, the initial localization is carried out by coarse matching, and the results are presented in Figure 6. The first two columns are the aerial image and the left epipolar resampled Ikonos image with the matching points and initial localization results overlaid in them. The last two columns show the aerial image and the right Ikonos epipolar resampled images with the matching points and initial localization results overlaid in them. Note that aerial images and Ikonos images are Gaussian down-scaled to 2 m spatial resolution for matching. Coarse matching is based on SIFT + RANSAC using the affine model. The goal of the coarse matching is only localization, and the threshold for error rejection in RANSAC is loosely set to five pixels with 99 percent probability. Figure 6 shows that regions of interest could be obtained successfully. In the forest area, image matching results seem to be acceptable despite the seasonal difference. Since the images are Gaussian down-scaled, the low frequency terrain features are identified as feature points. Also, another advantage of using stereo images in the matching process

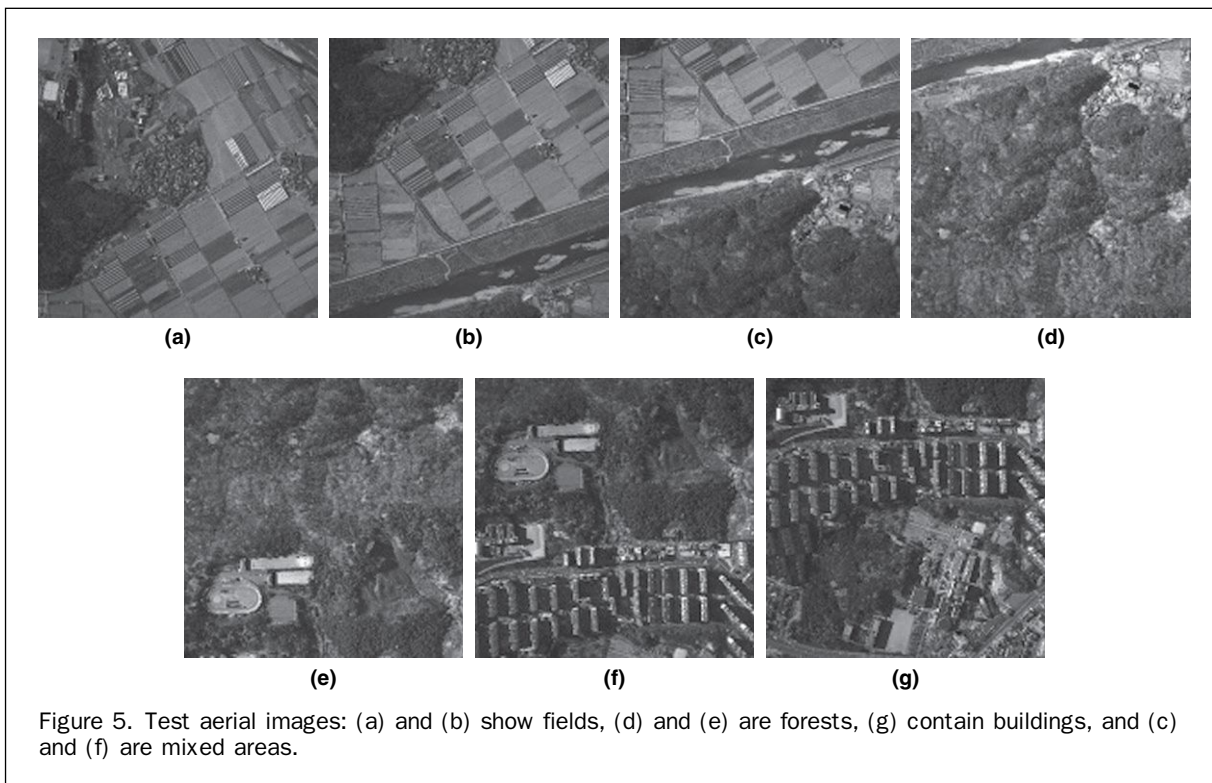


Figure 5. Test aerial images: (a) and (b) show fields, (d) and (e) are forests, (g) contain buildings, and (c) and (f) are mixed areas.

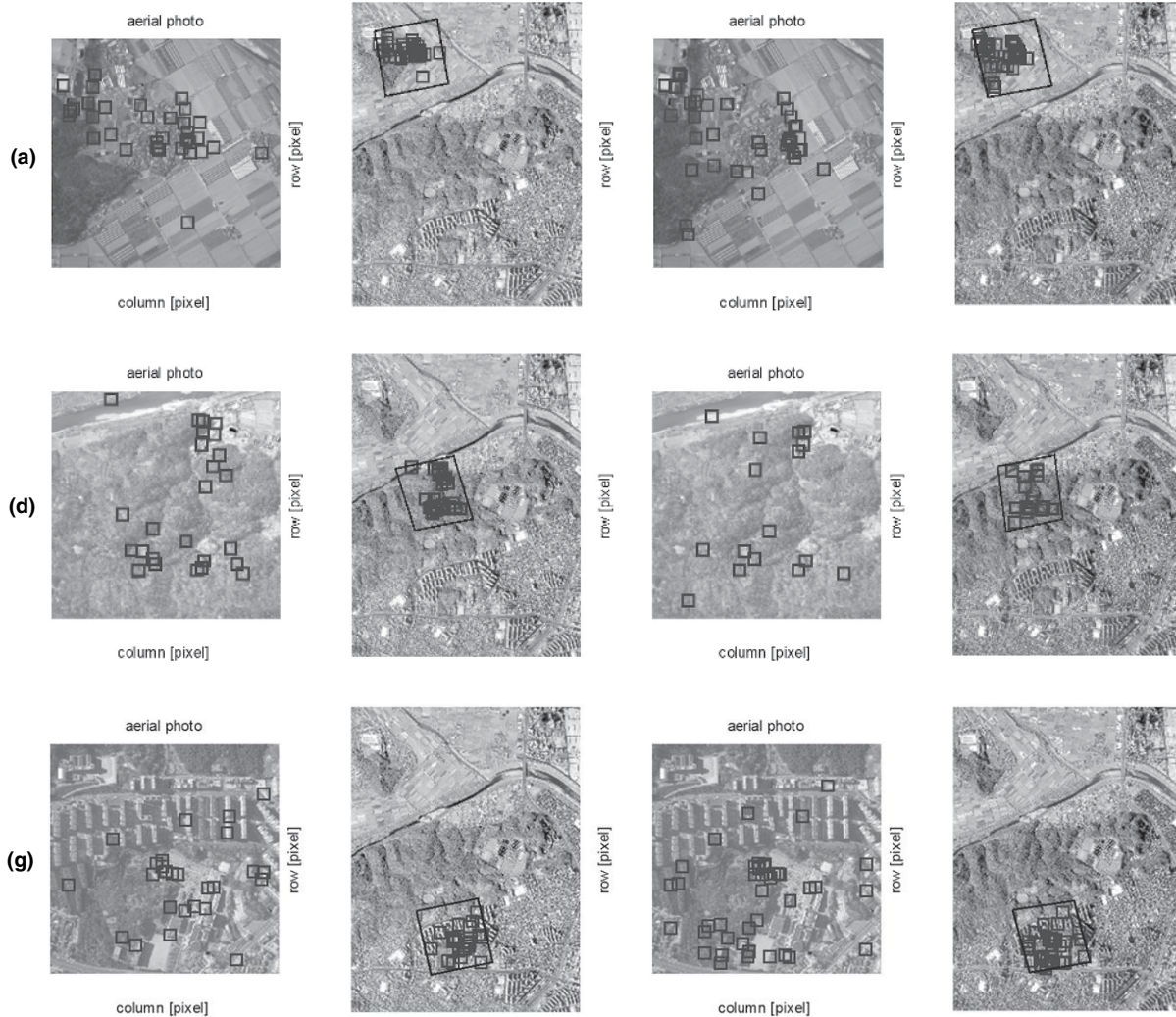


Figure 6. Coarse matching results based on SIFT + RANSAC with affine equation for images (a), (d), and (g).

can be also identified, e.g., more matching points are obtained than in the single image case by combining the points obtained by matching the aerial photos to the left and right Ikonos images, respectively. It is obvious that one of the stereo images should have better similarity in viewing angle than the other.

Based on the region of interest from the coarse matching, subsets of the Ikonos images with a margin were used for fine matching. Since the spatial resolution of Ikonos and aerial images are 1 m and 25 cm, respectively, the aerial images were downscaled to 1 m for efficient matching. Figure 7 shows the fine matching results. The aerial images and the left and right Ikonos images are presented together with the matching points. Note that rectangles are the SIFT matching points from the fine matching. Then, 3D ground coordinates for each SIFT matched point are computed by Ikonos stereo matching (cross-correlation matching with FFT). Then, the ground coordinates and corresponding aerial image points were refined by RANSAC with the collinearity equation. The refined matching point locations are marked by triangles in Figure 7. In RANSAC, the threshold for error rejection is more strictly set to one pixel with 99 percent probability. The images (a) and (g) in Figure 7 show that an

acceptable number of points could be obtained over the image. Note, however, that matching points could hardly be obtained over the forest area due to lack of unique features and large seasonal differences between aerial and satellite imagery. Unlike the coarse matching, which showed moderate image matching for the forest area, the fine matching was not successful over the forest area, as shown in the aerial images (d).

Figure 8 illustrates a sample of fine matching results. It was observed in the test that fine matching could successfully locate identifiable matching points for small and large buildings, road intersections, etc., despite the scale difference.

Georeferencing and Accuracy Assessment

First, single photo resection was tested for EOP estimation from the ground control points obtained by multi-scale image matching. The estimated EOP was compared to the reference EOP known from the bundle adjustment using accurate ground control points, and the differences are presented in Table 2 with the precision is shown in parenthesis. Compared to the forest area (c), (d), and (e), the open field and the urban (building) areas show better estimation performance. Estimation for image (d) is the

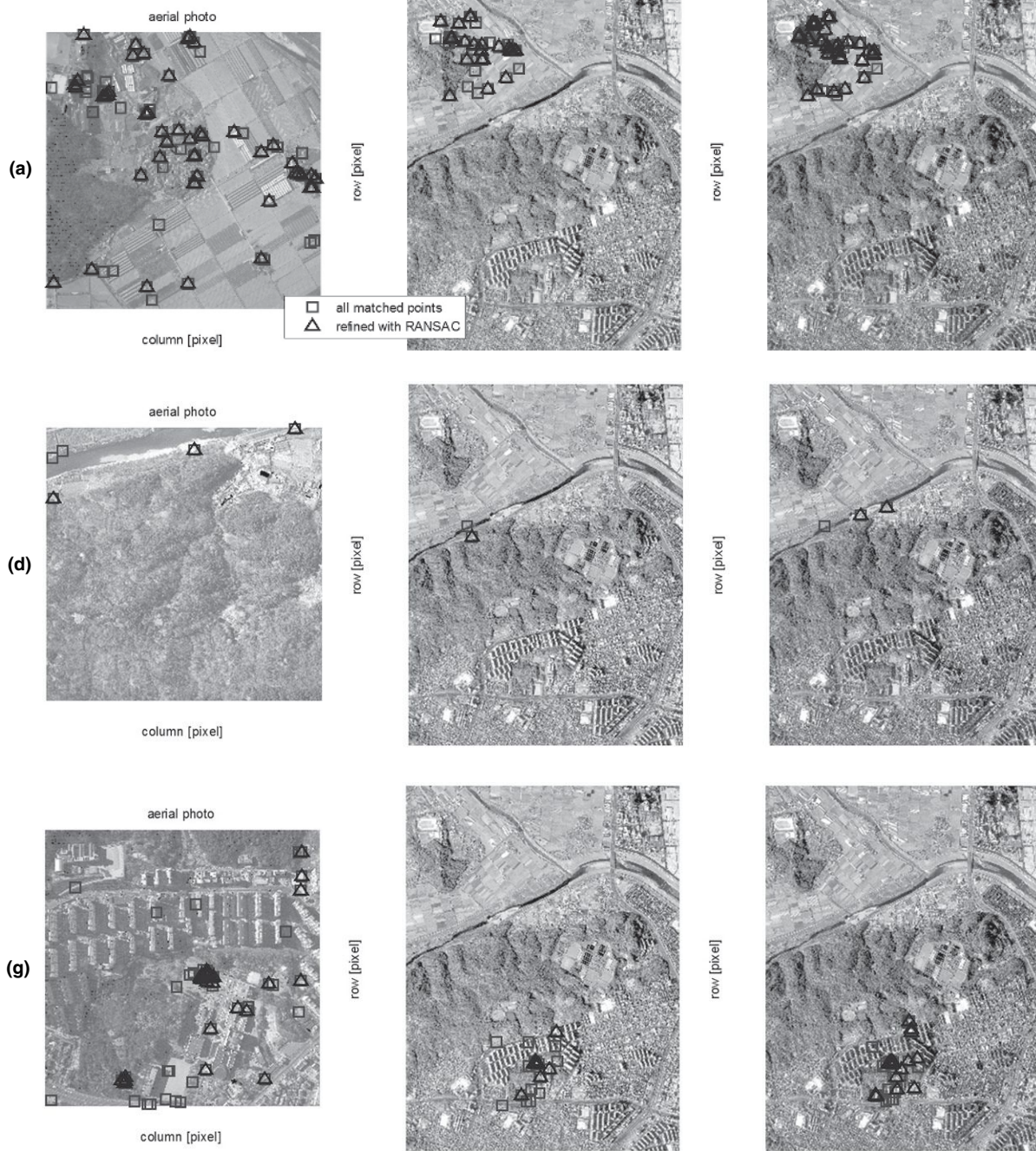


Figure 7. Fine matching results based on SIFT + RANSAC (Collinearity Equations) for images (a), (d), and (g).

worst, because there are not enough invariant features in the forest area due to the large seasonal gap between the aerial and Ikonos images. Most aerial images, except for the forest areas, show an EOP positional accuracy of less than 20 meters; note that the height was relatively well estimated. Note that the East coordinate error is large for (c), and (e), and the pitch angle accuracy is low accordingly as most ground control points are located in the upper part of image (c), and in the lower part of image (e) (figures not presented). Since the East direction is along the row direction of Ikonos, the skewed distribution of points led

to lower estimation. In terms of attitude estimation performance, a sub-degree accuracy could be achieved in most cases, with yaw (heading) angles showing the best accuracy. The precision for forest areas (c) and (e) is roughly twice as worse as the others, as anticipated. Precision for the forest area (d) is infinity, that is, EOP for the area could not be estimated practically.

Image coordinate residuals for the estimated EOP were computed and presented in Table 3. Mean residuals range from three to four pixels. In addition to the residuals, image coordinates computed from the estimated EOP were

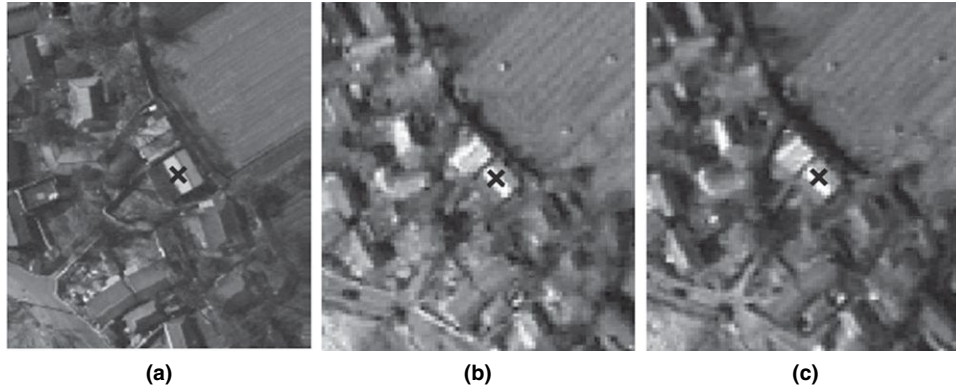


Figure 8. A RANSAC-refined matching point: (a) is an aerial image; (b) and (c) are left and right Ikonos images.

TABLE 2. ERROR AND ONE STANDARD DEVIATION OF THE ESTIMATED EOP USING SINGLE PHOTO RESECTION

	East [m]	North [m]	Height [m]	Roll [deg]	Pitch [deg]	Yaw [deg]
(a) Field	-11.53 (\pm 2.22)	-1.81 (\pm 2.40)	-4.68 (\pm 0.43)	0.067 (\pm 0.112)	-0.533 (\pm 0.104)	0.109 (\pm 0.020)
(b) Field	1.20 (\pm 7.20)	-0.75 (\pm 6.09)	-4.06 (\pm 2.26)	0.019 (\pm 0.282)	0.063 (\pm 0.344)	0.082 (\pm 0.056)
(c) Field + Forest	66.61 (\pm 15.61)	-13.58 (\pm 13.99)	-38.00 (\pm 8.13)	0.526 (\pm 0.652)	3.416 (\pm 0.787)	-0.545 (\pm 0.221)
(d) Forest	534.11 (\pm N/A)	62.75 (\pm N/A)	-603.52 (\pm N/A)	-4.751 (\pm N/A)	40.090 (\pm N/A)	-2.774 (\pm N/A)
(e) Forest	-44.21 (\pm 12.88)	18.48 (\pm 6.54)	-4.46 (\pm 3.65)	-1.025 (\pm 0.339)	-2.221 (\pm 0.685)	0.391 (\pm 0.114)
(f) Forest +	8.26 (\pm 7.13)	4.68 (\pm 5.23)	2.70 (\pm 1.25)	-0.255 (\pm 0.264)	0.452 (\pm 0.344)	0.036 (\pm 0.043)
(g) Building	4.55 (\pm 6.80)	-13.87 (\pm 7.98)	-2.02 (\pm 1.29)	0.679 (\pm 0.396)	0.322 (\pm 0.336)	-0.085 (\pm 0.044)

TABLE 3. IMAGE COORDINATE RESIDUALS AND ERRORS OF THE ESTIMATED EOP USING SINGLE PHOTO RESECTION

	Residual [pixels]				Error [pixels]			
	Column		Row		Column		Row	
	Mean	Max	Mean	Max	Mean	Max	Mean	Max
(a) Field	2.8	12.4	3.3	11.2	4.3	9.1	6.0	17.3
(b) Field	2.5	10.5	4.3	13.5	3.8	9.2	3.1	6.6
(c) Field + Forest	2.9	5.1	1.8	4.4	9.1	24.4	3.3	5.6
(d) Forest	0.0	0.0	0.0	0.0	177.0	392.4	80.7	129.8
(e) Forest	3.5	14.0	4.3	14.0	2.0	6.5	8.1	15.7
(f) Forest + building	4.0	11.0	4.2	12.7	2.3	8.9	5.9	8.7
(g) Building	3.4	8.5	4.1	12.8	2.8	7.5	10.9	18.0

compared to the coordinates from the reference EOP; the image coordinate errors are presented. Most errors are less than 2.5 meters (about ten pixels in aerial images) except for forest areas.

Second, the bundle adjustment was performed by generating tie points between adjacent aerial images, taking advantage of image overlap. Table 4 lists EOP estimation errors. Note that the EOP accuracy of the forest area images ((c), (d), and (e)) significantly improved. However, the EOP for some images are a little deteriorated, most likely due to the fact that the EOP errors of the forest area images are distributed to the adjacent images. The precision also improved overall except for area (a). Note that the precisions are now quite uniform. The precisions for the height

are much better than the precision of the horizontal coordinates, and the yaw precision was superior to the other angles.

Finally, the bundle adjustment with outlier removal was carried out using Baarda's data snooping method. Cumulative F-distribution with $\alpha = 99.99\%$ was used for the hypothesis test. Note that one image point measurement yields two collinearity equations, i.e., one equation for row (line) and one for column (sample) coordinates. Therefore, the image point is flagged as outlier if the null hypothesis is rejected for any one of the two, and the data snooping is iterated until no outlier is detected. In the test, a total of six iterations of data snooping were needed to remove all outliers, as shown in Table 5. The standard deviation of unit

TABLE 4. ERROR AND ONE STANDARD DEVIATION OF THE ESTIMATED EOP USING BUNDLE ADJUSTMENT (WITHOUT OUTLIER REMOVAL)

EOP difference	East [m]	North [m]	Height [m]	Roll [deg]	Pitch [deg]	Yaw [deg]
(a) Field	-2.03 (\pm 4.64)	-6.87 (\pm 5.88)	-6.81 (\pm 1.31)	0.336 (\pm 0.278)	-0.077 (\pm 0.2158)	0.144 (\pm 0.041)
(b) Field	-3.72 (\pm 3.77)	-6.38 (\pm 5.78)	-6.33 (\pm 1.41)	0.352 (\pm 0.274)	-0.123 (\pm 0.174)	0.125 (\pm 0.036)
(c) Field + Forest	-5.96 (\pm 3.31)	-8.79 (\pm 5.41)	-5.62 (\pm 1.66)	0.492 (\pm 0.261)	-0.193 (\pm 0.152)	0.078 (\pm 0.030)
(d) Forest	-5.47 (\pm 2.97)	-6.91 (\pm 5.37)	-4.30 (\pm 1.88)	0.415 (\pm 0.261)	-0.154 (\pm 0.137)	0.006 (\pm 0.031)
(e) Forest	-0.93 (\pm 2.82)	-5.64 (\pm 5.33)	-2.54 (\pm 1.87)	0.340 (\pm 0.263)	-0.328 (\pm 0.139)	-0.063 (\pm 0.034)
(f) Forest + building	-9.25 (\pm 3.68)	-7.10 (\pm 5.59)	-0.64 (\pm 1.64)	0.385 (\pm 0.278)	-0.332 (\pm 0.180)	-0.094 (\pm 0.040)
(g) Building	-8.44 (\pm 5.72)	-7.56 (\pm 5.80)	0.97 (\pm 1.87)	0.375 (\pm 0.288)	-0.294 (\pm 0.278)	-0.120 (\pm 0.051)

TABLE 5. BUNDLE ADJUSTMENT (BAARDA'S DATA SNOOPING)

Bundle adjustment iteration	# of image points	Std of unit weight	Cumulative F-distribution	DOF	# of outlier points detected
1	381	8.58	15.30	761	3
2	378	0.94	15.30	755	6
3	372	0.44	15.30	743	6
4	366	0.37	15.31	731	4
5	362	0.34	15.31	723	1
6	361	0.32	15.31	721	0
					Total 20

weight (the variance component) significantly decreased after the first iteration, and then slowly converged to 0.32. As a result, the total of 20 image points were detected as outliers, which correspond to 12 ground control points

Figure 9 illustrates which ground controls were removed as outliers, marked by 'x'. A total of 12 ground points were removed, which corresponds to 20 outlier image

points as discussed above (Note that most of them are from the aerial images (c), (d), and (e) that are forest areas.). Since a small number of matching points was obtained over the forest area, no redundant ground controls were available to successfully refine control points in the matching and RANSAC process. Table 6 shows the EOP accuracy for bundle adjustment with outlier removal. The EOP accuracy became more uniform and is better than 7 meters. Note that the flight direction is to the East-direction. The negative bias in the East and North coordinates are due to correlation with the negative errors in the pitch angle and the positive errors in the roll angle, respectively. The building area images ((f) and (g)) show fairly accurate Z values. A high ground height variation in the building area seems to lead to a relatively accurate Z value estimation. Among the attitude angles, again the yaw angle shows the best accuracy. Note that precisions of the estimated EOP significantly increased compared to the precisions presented in Table 4. Precisions are not only high, but also uniform for the test areas. Height and yaw angle still show the best precision.

The ground restitution accuracy for tie points was computed and presented in Table 7. Without the outlier removal, the bundle adjustment showed horizontal accuracy up to 3.45 meters and vertical up to 5.77 meters. Considering the existence of outliers, this accuracy is quite good. The effect of the outliers seems to be attenuated by the combined impact of many, good ground control and tie points. In contrast, the bundle adjustment with outlier removal improves horizontal and vertical accuracy to 2.18 and 4.53 meters, respectively. Since 1 m resolution stereo images are used as a reference, these results are relevant.

The error sources affecting the estimation accuracy may be listed as satellite image positional accuracy, epipolar image resampling accuracy, image matching accuracy between aerial and satellite image, stereo matching accuracy, the GCP distribution on the aerial image, and image overlap.

Conclusion

A new automatic aerial image georeferencing using stereo HRSI was proposed. Significant improvements in HRSI specifications, including high spatial and temporal

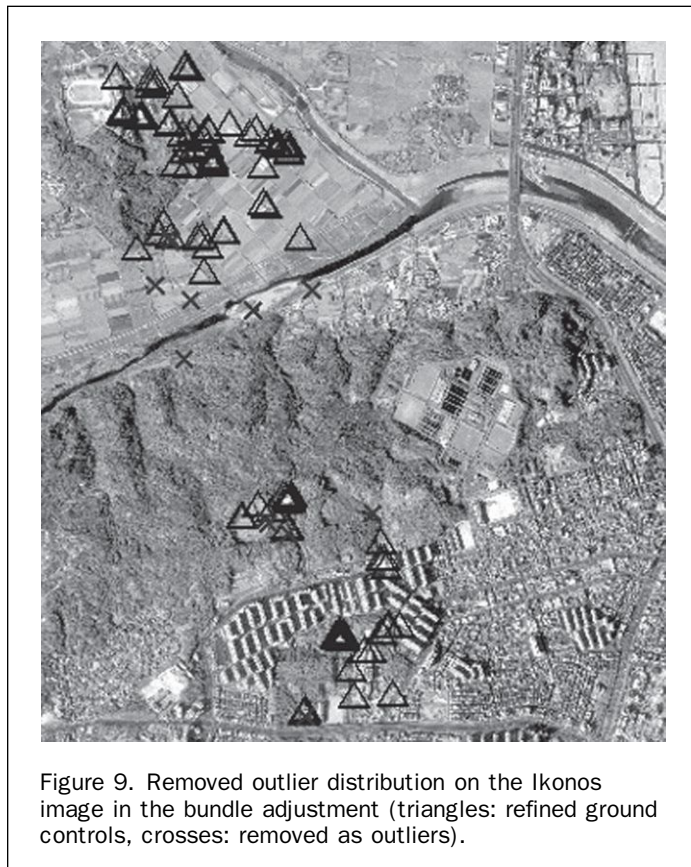


Figure 9. Removed outlier distribution on the Ikonos image in the bundle adjustment (triangles: refined ground controls, crosses: removed as outliers).

TABLE 6. ERROR AND ONE STANDARD DEVIATION OF THE ESTIMATED EOP USING BUNDLE ADJUSTMENT (WITH OUTLIER REMOVAL)

EOP difference	East [m]	North [m]	Height [m]	Roll [deg]	Pitch [deg]	Yaw [deg]
(a) Field	-6.10 (\pm 0.94)	-4.70 (\pm 1.20)	-5.05 (\pm 0.27)	0.196 (\pm 0.057)	-0.280 (\pm 0.044)	0.047 (\pm 0.008)
(b) Field	-5.22 (\pm 0.79)	-3.65 (\pm 1.20)	-3.45 (\pm 0.30)	0.159 (\pm 0.057)	-0.224 (\pm 0.036)	0.040 (\pm 0.007)
(c) Field + Forest	-5.16 (\pm 0.68)	-4.68 (\pm 1.13)	-2.39 (\pm 0.36)	0.217 (\pm 0.055)	-0.212 (\pm 0.031)	0.034 (\pm 0.006)
(d) Forest	-3.39 (\pm 0.59)	-4.51 (\pm 1.13)	-1.54 (\pm 0.41)	0.217 (\pm 0.055)	-0.124 (\pm 0.027)	0.022 (\pm 0.006)
(e) Forest	-5.72 (\pm 0.57)	-3.21 (\pm 1.11)	-0.79 (\pm 0.40)	0.156 (\pm 0.055)	-0.210 (\pm 0.028)	-0.006 (\pm 0.007)
(f) Forest + building	-4.42 (\pm 0.76)	-4.23 (\pm 1.16)	0.11 (\pm 0.35)	0.202 (\pm 0.058)	-0.131 (\pm 0.037)	-0.012 (\pm 0.008)
(g) Building	-3.76 (\pm 1.15)	-4.28 (\pm 1.19)	0.53 (\pm 0.39)	0.197 (\pm 0.059)	-0.083 (\pm 0.056)	-0.029 (\pm 0.010)

TABLE 7. GROUND RESTITUTION ACCURACY

Ground restitution accuracy		X [m]	Y [m]	Z [m]
Bundle adjustment (without outlier removal)	Mean	2.15	0.98	2.77
	Max	3.45	2.69	5.77
Bundle adjustment (with outlier removal)	Mean	1.15	0.30	1.56
	Max	2.18	0.76	4.53

resolutions, good positional accuracy and large swath width, motivated the idea of using satellite imagery as a reference for image-to-image-based indirect georeferencing. For aerial image georeferencing that requires accurate 3D ground coordinates, the use of stereo satellite images was proposed as a reference to provide 3D ground coordinates. The use of stereo images can avoid the impact of relief displacement in the reference data and the requirement of accurate external height information.

For the approach, a robust and efficient image matching scheme with outlier removals was proposed. A SIFT-based multi-scale image matching scheme, including coarse and fine matching, was used for efficient matching between aerial and satellite images. The coarse matching performs the initial localization of aerial images on the satellite image based on a combination of SIFT and the affine model-based RANSAC to model the geometric difference between Gaussian down-scaled images. The coarse matching is followed by fine image matching to obtain accurate matching points. Then, ground coordinates are computed from satellite stereo pairs by cross-correlation matching, implemented by FFT, followed by the collinearity equation-based RANSAC to further refine matching points.

An experiment was carried out for a strip of aerial images and Ikonos stereo images. Test results showed that acceptable matching results could be obtained over open and built-up areas; however, the matching was poor over forest areas, especially when there is a large seasonal difference between the aerial image and the reference. EOPs of aerial images are estimated from ground control information acquired from the matching points. Both single photo resection and bundle adjustments were tested. Using the bundle adjustment approach with blunder removal, relatively accurate EOPs could be obtained and the ground restitution accuracy could be improved up to the level that can be expected from the positional accuracy of stereo satellite images. Even though georeferencing performance is highly subjected to many error sources, including reference data positional accuracy and matching quality, the high potential of stereo HRSI as reference data has been confirmed. The approach could be used not only for aerial image georeferencing in mapping at small scale, but also provides a good basis for robust navigation under GPS signal loss, since it is capable of providing position of the platform, facilitating image-based terrain-referenced navigation.

References

- Abdel-Hakim, A.E., and A.A. Farag, 2006. CSIFT: A SIFT Descriptor with color invariant characteristics, *Proceedings of the 2006 IEEE Computer Society Conference on Computer Vision and Pattern Recognition*, Vol.2, pp. 1978–1983.
- Ali, M., and D. Clausi, 2002. Automatic registration of SAR and visible band remote sensing images, *Proceedings of IEEE International Geoscience and Remote Sensing*, Vol.3, pp. 1331–1333.
- Baarda, W., 1968. *A Testing Procedure for Use in Geodetic Networks*, Netherlands Geodetic Commission, Publications on Geodesy, New Series, Delft, 2(5).
- Bay, H., A. Ess, T. Tuytelaars, L.V. Gool, 2008. SURF: Speeded Up Robust Features, *Computer Vision and Image Understanding (CVIU)*, 110(3):346–359.
- Carroll, J., 2001. *Vulnerability Assessment of the Transportation Infrastructure Relying on the Global Positioning System*, Technical report, Volpe National Transportation Systems Center, August, Report for US Department of Transportation.
- Conte, G., and P. Doherty, 2008. An integrated UAV navigation system based on aerial image matching, *Proceedings of the 2008 IEEE Aerospace Conference*, 01-08 March, Big Sky, Montana, pp. 1–10.
- Fischler, M.A. and R.C. Bolles, 1981. Random sample consensus: A paradigm for model fitting with applications to image analysis and automated cartography, *Communications of the ACM*, 24:381–395.
- Fosyth, D., and J. Ponce, 2000. *Computer Vision: A Modern Approach*, Prentice Hall, 154 p.
- Fraser, C.S., and H.B. Hanley, 2005. Bias-compensated RPCs for sensor orientation of high-resolution satellite imagery, *Photogrammetric Engineering & Remote Sensing*, 71(8):909–915.
- Fraser, C.S., and M. Ravanbakhsh, 2009. Georeferencing accuracy of GeoEye-1 imagery, *Photogrammetric Engineering & Remote Sensing*, 75(6):634–638.
- GeoEye, Inc. 2008. Ikonos Relative Spectral Response. URL: <http://www.geoeye.com/CorpSite/resource/white-papers.aspx> (last date accessed: 03 August 2011).
- Gianinetto, M., and M. Scaioni, 2008. Automated geometric correction of high resolution pushbroom satellite data, *Photogrammetric Engineering & Remote Sensing*, 74(1):107–116.
- Grejner-Brzezinska, D.A., 1999. Direct exterior orientation of airborne imagery with GPS/INS system: Performance analysis, *Navigation*, 46(4):261–270.
- Grodecki, J., G. Dial, and J. Lutes, 2004. Mathematical model for 3D feature extraction from multiple satellite images described by RPCs, *Proceedings of the ASPRS 2004 Annual Conference*, 23–28 May, Denver, Colorado (American Society for Photogrammetry and Remote Sensing, Bethesda, Maryland), unpaginated CD-ROM.
- Ke, Y., and R. Sukthankar, 2004. PCA-SIFT: A more distinctive representation for local image descriptors, *Proceedings International Conferences on Computer Vision*, Washington, D.C., pp. 506–513.
- Li, Q., G. Wang, J. Liu, and S. Chen, 2009. Robust scale-invariant feature matching for remote sensing image registration, *IEEE Geoscience and Remote Sensing Letters*, 6(2):287–291.
- Lowe, D.G., 1999. Object recognition from local scale-invariant features, *Proceedings of the International Conference on Computer Vision*, 20-25 September, Corfu, Greece, pp. 1150–1157.

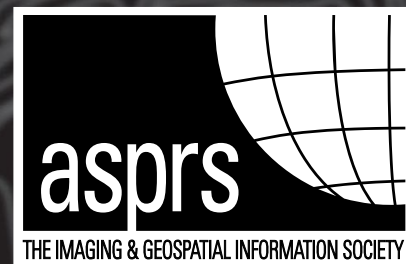
- Mikolajczyk, K., and C. Schmid, 2005. A performance evaluation of local descriptors, *IEEE Transactions on Pattern Analysis and Machine Intelligence*, 27(10):1615–1630.
- Mostafa, M.M.R., and K. Schwarz, 2000. A multi-sensor system for airborne image capture and georeferencing, *Photogrammetric Engineering & Remote Sensing*, 66(12):1417–1423.
- Mostafa, M.M.R., J. Hutton, and E. Lithopoulos, 2001. Airborne direct georeferencing of frame imagery: An error budget, *Proceedings of the 3rd International Symposium on Mobile Mapping Technology*, Cairo, Egypt, 03–05 January.
- Oh, J.H., W.H. Lee, C.K. Toth, D.A. Grejner-Brzezinska, and C.N. Lee, 2010. A piecewise approach to epipolar resampling of pushbroom satellite images based on RPC, *Photogrammetric Engineering & Remote Sensing*, 76(12):1353–1363.
- Rottensteiner, F., T. Weser, A. Lewis, and C. Fraser, 2009. A strip adjustment approach for precise georeferencing of ALOS optical imagery, *IEEE Transactions on Geoscience and Remote Sensing*, 47(12):4083–4091.
- Runnalls, A.R., P.D. Groves, and R.J. Handley, 2005. Terrain-referenced navigation using the IGMAP data fusion algorithm, *Proceedings of the 61st Annual Meeting of the Institute of Navigation*, June 2005, pp. 976–86.
- Sim, D.G., R.H. Park, R.C. Kim, S.U. Lee, and I.C. Kim, 2002. Integrated position estimation using aerial image sequences, *IEEE Transactions on Pattern Analysis and Machine Intelligence*, 24(1):1–18.
- Wen, G.J., J. Lv, and W. Yu, 2008. A high-performance feature-matching method for image registration by combining spatial and similarity information, *IEEE Transactions on Geoscience and Remote Sensing*, 46(4):1266–1277.
- Wong, A., and D.A. Clausi, 2007. ARRSI: Automatic Registration of Remote-Sensing Images, *IEEE Transactions on Geoscience and Remote Sensing*, 45(5):1483–1493.
- Yi, Z., C. Zhiguo, and X. Yang, 2008. Multi-spectral remote image registration based on SIFT, *Electronic Letters*, 44(2):107–108.
- Zhang, Z., J. Zhang, M. Liao, and L. Zhang, 2000. Automatic registration of multi-source imagery based on global image matching. *Photogrammetric Engineering & Remote Sensing*, 66(5):625–629.

ASPRS MEMBERSHIP

Your path to success in the geospatial community

ASPRS Members Are Individuals Like You...

Become a member of the American Society for Photogrammetry and Remote Sensing (ASPRS), the premier international society of over **6,500 geospatial professionals from private industry, government, and academia**. Together we advance imaging and geospatial information into the 21st century.



To join, go to www.asprs.org

Detection of Swimming Pools by Geographic Object-based Image Analysis to Support West Nile Virus Control Efforts

Minho Kim, James B. Holt, Rebecca J. Eisen, Kerry Padgett, William K. Reisen, and Janet B. Croft

Abstract

The recent economic crisis in United States has led to an increase in home foreclosures and subsequent abandonments. A by-product of this trend has been an associated rise in the number of neglected swimming pools, which provide new habitats for the larval stages of the *Culex* mosquito vectors of West Nile Virus (WNV) in urban and suburban environments. WNV has been major concern related to neglected swimming pools in California. Our research focused on using very high spatial resolution (VHR) satellite imagery and processing techniques, including image pansharpening, normalized difference water index, and geographic object-based image analysis (GEOBIA), to develop a geographic information system (GIS) database of swimming pool locations. This research demonstrated that GEOBIA with VHR imagery could produce a GIS database of swimming pools with the high accuracy of 94 percent. The analytic approach of this research is expected to economically facilitate the location of swimming pools for ground inspection and mosquito control.

Introduction

West Nile Virus (WNV) (family *Flaviviridae*, genus *Flavivirus*) emerged in New York City in late August 1999 and quickly spread westward across the United States (US), reaching California in 2003 (Reisen *et al.*, 2004). WNV is now considered to be established in all continental states except

Maine and Alaska. According to the US Center for Disease Control and Prevention (CDC, 2010), a cumulative total of 29,681 WNV cases were reported from 1999 to 2009 across US with the highest numbers in Colorado, Nebraska, and California. WNV is maintained and amplified within an enzootic cycle among passeriform birds and *Culex* mosquitoes, with tangential transmission to humans and equines, which may suffer severe disease but are functionally “dead end” hosts for the virus (Komar, 2003; Kramer *et al.*, 2007). In urban/suburban habitats, members of the *Culex pipiens* complex are the primary WNV vectors (Turell *et al.*, 2005) and exploit manmade containers that hold standing water for larval development.

Neglected (or abandoned) swimming pools are suitable larval habitats for several WNV mosquito vectors (Epstein, 2001; Caillouët *et al.*, 2008; Kern County, 2008; Reisen *et al.*, 2008; Reisen *et al.*, 2009a). Although the putative link between mosquitoes emerging from neglected pools and WNV transmission has not been directly assessed, increases in the numbers of home foreclosures and abandonments has paralleled increases in human cases in several areas of California such as Kern County (Reisen *et al.*, 2008; Reisen *et al.*, 2009b). Colonization of pools was associated with the decline in pool chemicals, followed by algal blooms and an accumulation of organic material (Epstein, 2001; Reisen *et al.*, 2008). The current financial crisis and associated home foreclosures was considered to be a driving factor triggering a marked increase in the number of neglected private swimming pools (Reisen *et al.*, 2008), which provided an extensive array of urban mosquito habitats.

The location and treatment of neglected pools has become a difficult and expensive problem for local mosquito and vector control programs in California responsible for extensive residential areas; the Greater Los Angeles County Vector Control District, for example, contains >1.1 million parcels and >9.8 million residents. Examination of aerial photographs has been used to locate and attempt to identify neglected pools because there may be little current information about the geographic location of each private swimming pool (John Newton, Orange County Vector Control

Minho Kim, James B. Holt, and Janet B. Croft are with the Emerging Investigations and Analytic Methods Branch, Division of Adult and Community Health, Centers for Disease Control and Prevention, 4770 Buford Highway., NE, MS K-67, Atlanta, GA 30341 (htj0@cdc.gov or mhkim73@gmail.com).

Rebecca J. Eisen is with the Bacterial Diseases Branch, Division of Vector-Borne Diseases, Centers for Disease Control and Prevention, 3150 Rampart Road, Fort Collins, CO 80522.

Kerry Padgett is with the Vector-borne Disease Section, California Department of Public Health, 850 Marina Bay Parkway, Richmond, CA 94804.

William K. Reisen is with the Center for Vectorborne Diseases, School of Veterinary Medicine, University of California, Old Davis Road, Davis, CA 95616.

Photogrammetric Engineering & Remote Sensing
Vol. 77, No. 11, November 2011, pp. 1169–1179.

0099-1112/11/7711-1169/\$3.00/0
© 2011 American Society for Photogrammetry
and Remote Sensing

District, personal communication). However, the manual interpretation of aerial photography is a time-consuming and labor-intensive procedure compared to an automated image analysis. Furthermore, aerial surveys are too expensive to be conducted repeatedly over short time periods.

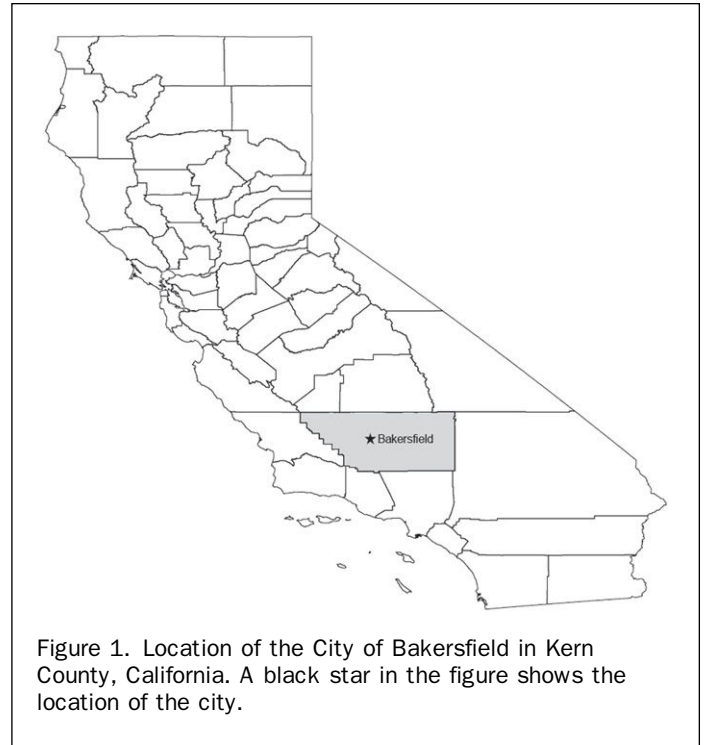
In recent years, very high spatial resolution (VHR) satellite imagery has become available with pixel sizes (i.e., spatial resolution) similar to those of aerial photographs. In addition, VHR satellites generally have the capability to revisit the same locations every two to three days, which allows the rapid detection of changes in Earth surface features. For this reason, automated swimming pool detection using remote sensing techniques and VHR satellite imagery may expedite neglected pool surveillance by extracting the locations of private swimming pools and constructing a geographic information system (GIS) database. Nevertheless, there have been few attempts to use automatic image analyses with VHR satellite imagery for that purpose. In the current study, we explore the potential for using automated remote sensing techniques with VHR satellite imagery to develop a spatial database of swimming pool locations, which may aid in the surveillance and treatment of neglected pools by vector control programs.

Study Area and Data

The US recently has experienced a financial crisis that has caused a considerable increase in mortgage delinquencies and foreclosures. According to the US Federal Reserve Bank of New York (FRB, 2010), Kern County in California had a mortgage delinquency rate of 11.7 percent for over 90 days in 2010, which was nearly double the national rate of 5.7 percent. The unemployment rate of the Bakersfield-Delano Metropolitan Statistical Area was 15.7 percent in June 2010, also higher than a national rate of 9.5 percent (BLS, 2010). This recent economic downturn may have made it difficult for pool-permit holders to pay maintenance costs for their backyard swimming pools, which in turn may increase the possibility of neglected swimming pools to be utilized by WNV vector mosquitoes. In Kern County, *Cx. tarsalis*, a highly efficient WNV vector that is typically associated with wetland and agricultural habitats (Reisen and Reeves, 1990), was found frequently in neglected urban swimming pools (Reisen *et al.*, 2008).

Taking into account the magnitude of the abandoned swimming pool problem, we selected the City of Bakersfield in Kern County, California, for this research (Figure 1). The population of the city was estimated at 328,692 in 2008, and it is one of fast growing cities in California (CDF, 2010). The Kern River flows through Bakersfield City but remains dry during spring and summer seasons (Reisen *et al.*, 2008). Average temperature was approximately 18.6°C in the city, but the average monthly temperature during May to September ranged from 29.2°C to 36.9°C with little precipitation (less than 0.5 cm). Limited summer precluded cloud cover. In addition, Bakersfield has had consistent WNV enzootic and epidemic activity since 2004 (Reisen *et al.*, 2009a).

GeoEye-1 satellite imagery, acquired on 12 September 2009, was delivered with panchromatic and multispectral images from the US National Geospatial-Intelligence Agency. Table 1 describes the spatial resolutions and spectral wavelength regions of the two images, and Plate 1a shows multispectral GeoEye-1 image for the Bakersfield study area. We extracted a residential area in 1.6 km × 1.5 km from the satellite imagery, indicated by a white-hollow box in Plate 1a, and it was utilized to develop swimming pool detection procedures. The study area included residential swimming



pools as well as other land-use and land-cover types such as buildings, roads, grass, trees, bare soil, and lakes (see Plate 1b).

Methods

Image Pansharpening and Visual Interpretation of Swimming Pools

The GeoEye-1 satellite provides panchromatic and multispectral images (see Table 1). The spatial resolution of the panchromatic image is higher than the multispectral image, but it does not contain color information. On the other hand, GeoEye-1 multispectral imagery includes colors, albeit with coarser spatial resolution than the GeoEye-1 panchromatic imagery. Therefore, we employed pansharpening (also called image fusion) from the GeoEye-1 panchromatic and multispectral images to create high spatial resolution imagery containing color information. We used a high pass filter (HPF) technique, implemented in ERDAS Imagine® (version 9.3), because it has the capability of producing high-quality pansharpened imagery, compared with the original multispectral VHR imagery (Gangkofner *et al.*, 2008; Kim *et al.*, 2011a). HPF pansharpening method is a spatial-domain

TABLE 1. SPATIAL AND SPECTRAL RESOLUTIONS OF GEOEYE-1 IMAGERY

		Spatial resolution	Spectral resolution
Panchromatic image		0.40 m	450–800 nm
	Blue	1.65 m	450–510 nm
Multispectral image	Green	1.65 m	510–580 nm
	Red	1.65 m	655–690 nm
	NIR	1.65 m	780–920 nm



(a)



(b)

Plate 1. (a) GeoEye-1 full scene delivered from the United States National Geospatial-Intelligence Agency, and (b) its subset image used in this study. The GeoEye-1 imagery is rendered as a true color composite using blue, green, and red bands for RGB. Visually-identified private outdoor pools of the study area are shown in (b).

image fusion approach that involves high pass filtering of high-resolution imagery, its addition to each multispectral band, and linear histogram match of mean and standard deviation between pansharpened and original multispectral images (Gangkofner *et al.*, 2008).

We then visually identified private swimming pools in our study area using Google Earth® aerial photographs, supplemented with the pansharpened GeoEye-1 imagery to assist in pool identification. In the interpretation, we excluded pools completely covered by tree canopy and

shadow. We obtained a total of 822 visually-interpreted pools (see Plate 1b) that were utilized as the reference to validate the classification accuracy of private swimming pools.

Geographic Object-based Image Analysis (GEOBIA) Private Pool Classification

Conventional pixel-based image classification approaches have been widely utilized with medium- and coarse-resolution satellite images to perform the classification (or

extraction) of landscape features. However, pixel-based approaches decreased the accuracies of image classification when they were used with VHR imagery (Woodcock and Strahler, 1987; Hay *et al.*, 1996; Kim, 2008; Myint *et al.*, 2011). In the late-1990s, an alternative remote sensing approach, known as geographic object-based image analysis (GEOBIA), has emerged to overcome the limitations of conventional pixel-based approaches with VHR imagery. It has gained much attention among remote sensing scientists in recent years (Blaschke, 2010). GEOBIA is also called object-based image analysis (OBIA), and readers are advised to refer to Blaschke (2010) for in-depth literature review about it.

In this study, we adopted GEOBIA to extract private swimming pools from the pansharpened GeoEye-1 imagery. Two major steps are involved in GEOBIA: image segmentation and classification (Wang *et al.*, 2004; Kim *et al.*, 2008; Kim *et al.*, 2009). A segmentation produced the vector boundaries of individual image objects (or segments), which provided a distinguished functionality compared with conventional pixel-based approaches. This means that we can obtain spatial attributes such as size and shape, spectral values for each image object, and contextual information between image segments to be utilized in thematic classification.

The spectral (or color) information from multispectral imagery plays an important role in separating a targeted feature from background or non-targeted features. However, our initial analysis discovered that the spectral reflectance of swimming pools was close to that of the other landscape features such as building rooftops and roads (Figure 2). For this reason, there is the possibility of a high degree of classification confusion when using only the multispectral image. Taking this into account, we used the normalized

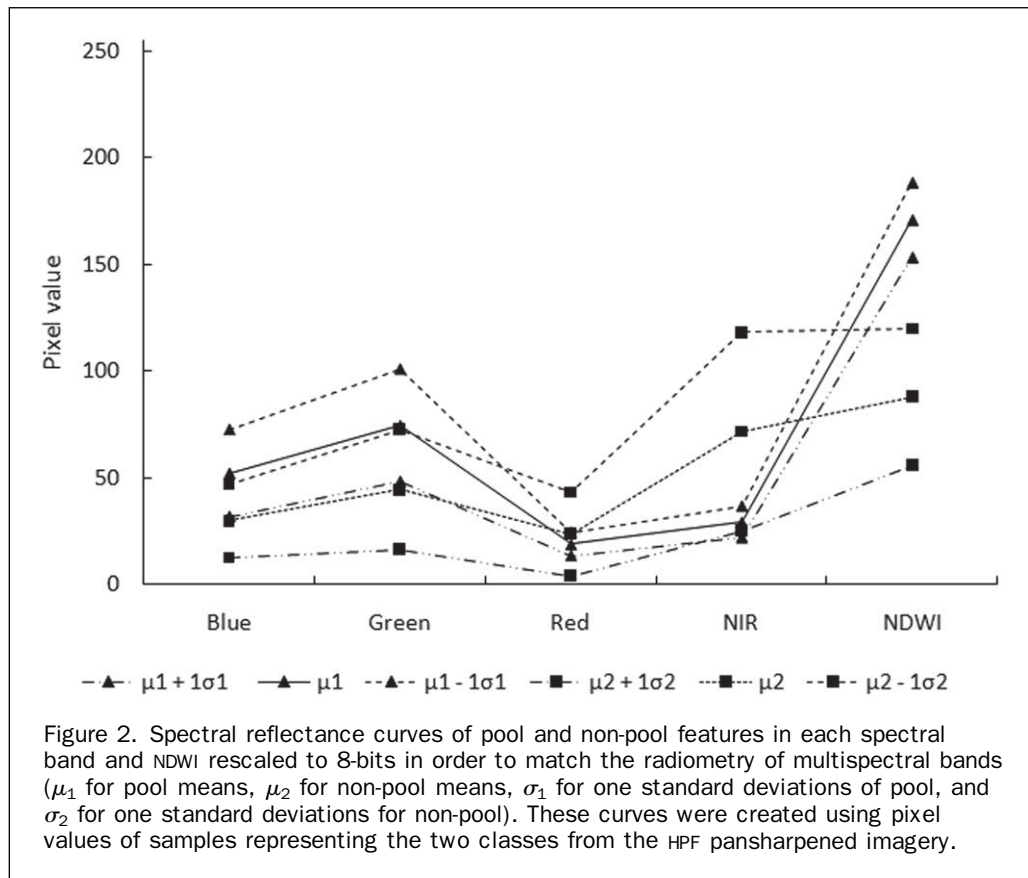
difference water index (NDWI) (McFeeters, 1996) to extract water bodies from remote sensing imagery. NDWI is calculated using green and near infrared (NIR) bands and has values ranging from -1 to $+1$:

$$NDWI = \frac{Green - NIR}{Green + NIR}$$

As shown in Figure 2, the separation of swimming pools from other landscape features using NDWI was improved in comparison with the original multispectral image, and the image was used as our major data source to conduct GEOBIA-based swimming pool classification. We utilized the spectral value of the NDWI image and the spatial attributes associated with image objects: rectangular fit (RF) and size. RF is a spatial metric to describe how well an image object fits in a rectangular shape with a range of 0 (no fit) to 1 (complete fit) (Definiens, 2009). We utilized the number of pixels within an image object to estimate the physical area of each segment by applying Trimble (formerly Definiens) eCognition® Developer (version 8) for segmenting the NDWI imagery and deriving relevant spectral and spatial attributes of each image object. We derived a total of 800 random samples for non-pools, and they were used with visually identified pools for accuracy assessments. We employed overall and individual accuracies for this purpose, including overall accuracy, producer's and user's accuracies, overall Kappa coefficient, and individual Kappa coefficient.

Results

A pansharpened image was obtained using the HPF fusion technique, with correlation coefficients of 0.93 for all four



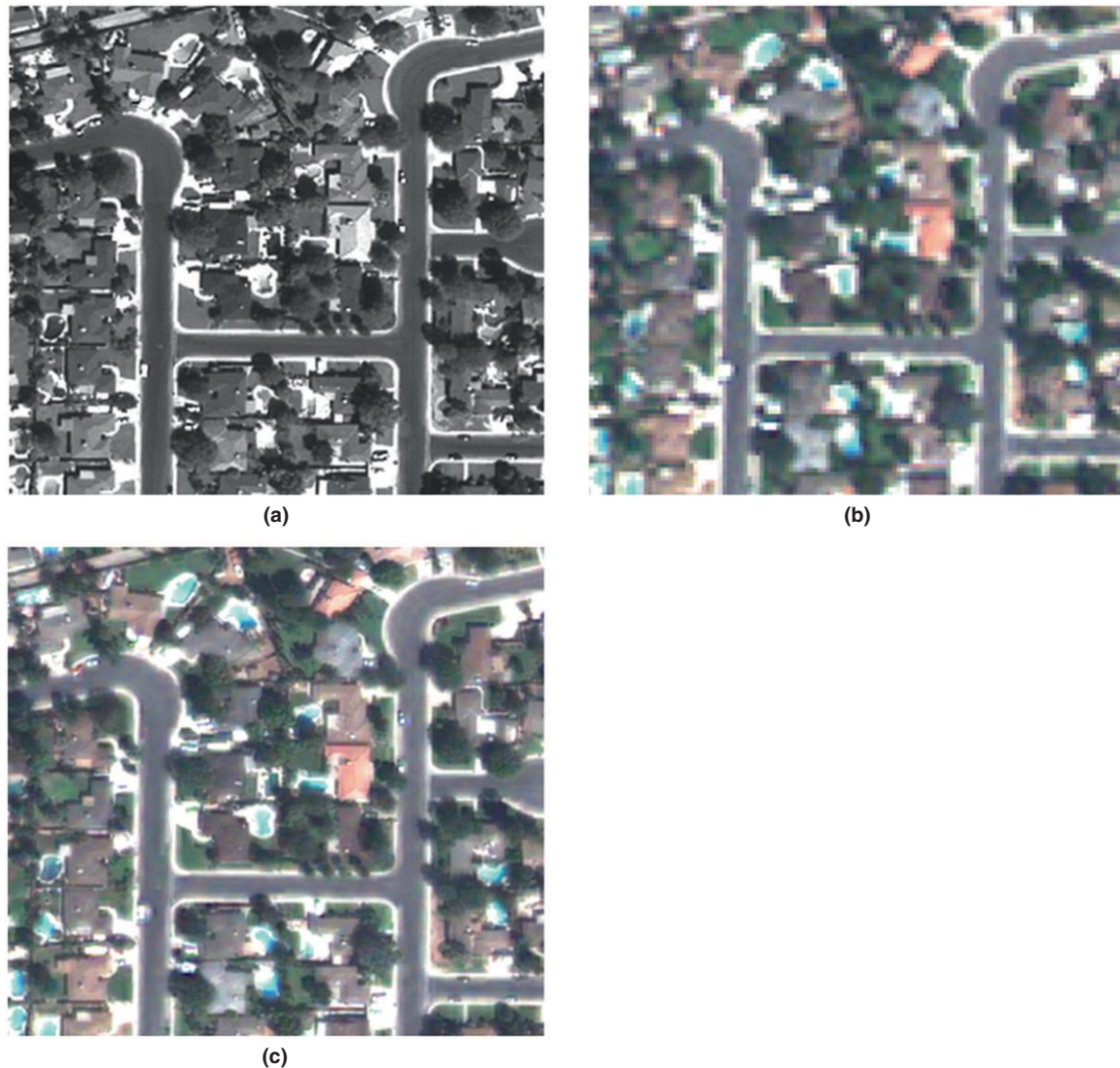


Plate 2. GeoEye-1 (a) panchromatic image, (b) multispectral image, and (c) HPF pansharpened image. All the images are shown at 1:1000 scale.

spectral bands. The correlation coefficient is a band-by-band evaluation metric of pansharpening color quality, compared to the original multispectral image. The value of 1 indicates an ideal case that the pixel values of a fused image are the same as those of an original multispectral image. Higher correlation coefficients reflect better pansharpening quality in terms of color information. Plate 2 shows a panchromatic, multispectral, and HPF pansharpened subset of images derived from the original GeoEye-1 imagery. As shown in the plate, the fused image retains the spatial resolution of the GeoEye-1 panchromatic image, resulting in obvious boundaries of spatial features and the color information from the GeoEye-1 multispectral image.

Figure 3a shows an NDWI image that was computed from the pansharpened imagery. When visually assessing the NDWI image with the pansharpened multispectral image, swimming pools have a relatively higher positive value compared to the other landscape features. We observed that negative NDWI values were assigned to most non-pool features, as shown in Table 2. We utilized the same sample

of each non-pool feature, used for Figure 3, to derive the mean pixel values of each land cover in the table. Therefore, we performed a density slicing in such a way that negative values were assigned to 0 and non-negative values retained their original values. Figure 3b depicts the result of the density slicing and provides greater insight about the location of individual swimming pools. All the interpreted swimming pools were located in the density-sliced image, but shadows were not totally excluded. Therefore, we focused on excluding shadows in subsequent GEOBIA procedures.

We used the *Multiresolution Segmentation* algorithm, implemented in eCognition® Developer, in our GEOBIA pool classification. The algorithm places seed pixels across an entire image and combines adjacent pixels around the seed pixels to create image objects in the segmentation procedures. Very small differences in neighboring pixel values do not produce appropriate boundaries of segments using floating-point values inherent in NDWI imagery. Therefore, we rescaled the density-sliced NDWI imagery to 8-bit radio-

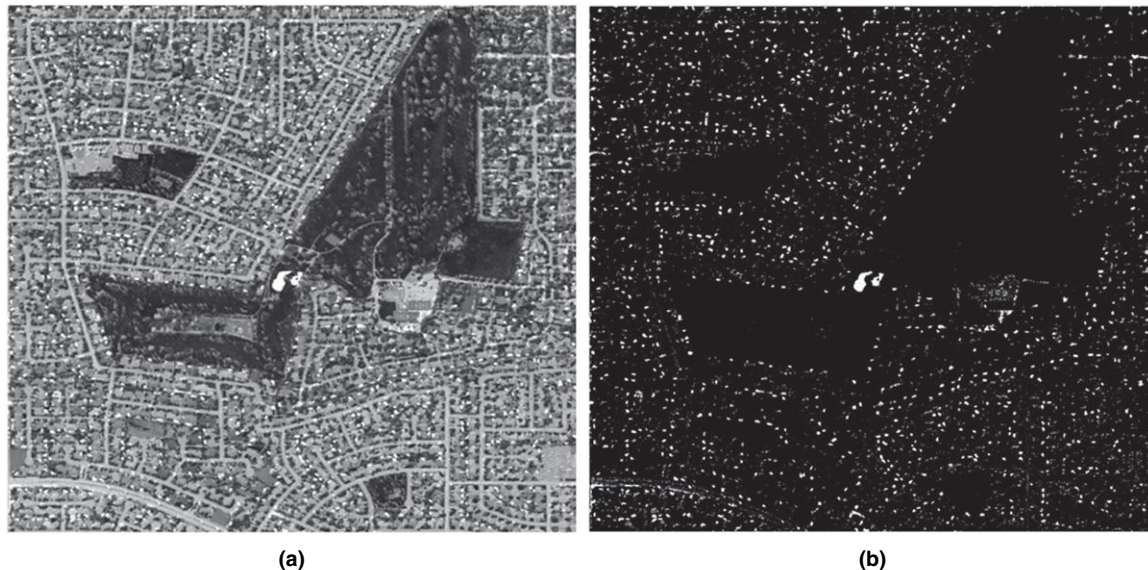


Figure 3. NDWI imagery derived from green and near infrared bands of (a) pansharpended GeoEye-1 image, and (b) its density-sliced image. In the figures, higher NDWI values are represented in light color and lower values in dark color.

metric resolution for GEOBIA pool classification. When using GEOBIA approach, the size of image objects has been known to affect segmentation quality and classification results (Tian and Chen, 2007; Kim *et al.*, 2009; Kim *et al.*, 2010; Kim *et al.*, 2011b; Myint *et al.*, 2011; Kim *et al.*, in press). We conducted image segmentations with various scale parameters that have an effect on deciding the size of segments in the Multiresolution Segmentation of eCognition® Developer. The scale parameter of 5 was found to produce the best segmentation result from the input NDWI imagery that contained private swimming pools with various sizes. We employed the default settings of the other segmentation parameters for shape/color ratio and compactness/smoothness ratio, i.e., 0.9 for color ratio and 0.5 for compactness ratio.

Our initial segmentation generated image objects with a total of 18,666 that included swimming pools and shadows (Figure 4a). The total number of swimming pool, discovered by this method, was much greater than determined by manual interpretation. For this reason, the mean values, RFs, and the number of pixels of individual segments were derived to exclude shadows from the initial segmentation. When examining the histogram of the density-sliced NDWI image (Figure 4b) and the pansharpended image, we found that shadows have lower pixel values than the average value of the NDWI image (refer to Table 2). Taking it into account, image objects that have spectral values smaller than the

global mean value of 36 were classified as non-swimming pools. Figure 4c shows 987 segments combining swimming pools and shadows. This total number of segments was considerably reduced, compared with the initial segmentation of 18,666 segments.

Table 3 shows the classification results of pools and non-pools with the mean value. We obtained an overall accuracy of 85.3 percent with an overall Kappa of 0.70. The use of the global mean correctly identified 775 pools with an accuracy of 94.3 percent as compared to 822 reference pools. Nevertheless, there were 212 image segments that were incorrectly classified as private pools, which resulted in lower user's accuracy of 80.1 percent than the producer's accuracy for pools, as shown in the table.

We then employed spatial metrics to exclude the remaining shadows. In an urban environment, shadows cast from buildings would be rectangular in shape, which is not the case for most private swimming pools. The value of 1 for RF was used to filter rectangular-shaped shadows. Table 4 describes the classification result of employing the RF value to differentiate non-pool segments from pool image objects. Compared with Table 3, the addition of the RF value had a minimal effect on the performance of pool and non pool

TABLE 3. ERROR MATRIX OF A CLASSIFICATION RESULT ONLY WITH NDWI VALUE

Classification	Reference		User's accuracy
	Pool	Non pool	
Pool	775	192	80.1%
Non-pool	47	608	92.8%
Producer's accuracy	94.3%	76.0%	

Overall accuracy: 85.3 percent, Overall Kappa coefficient: 0.70

Pool Kappa coefficient: 0.60

Non-pool Kappa coefficient: 0.86

TABLE 2. MEAN PIXEL VALUES OF NDWI IMAGERY FOR EACH LAND-COVER CLASS

Land-cover class	Mean value
Bare earth	-0.256
Road	-0.035
Building rooftop	-0.158
Vegetation	-0.535
Shadow	0.089
Pool	0.419

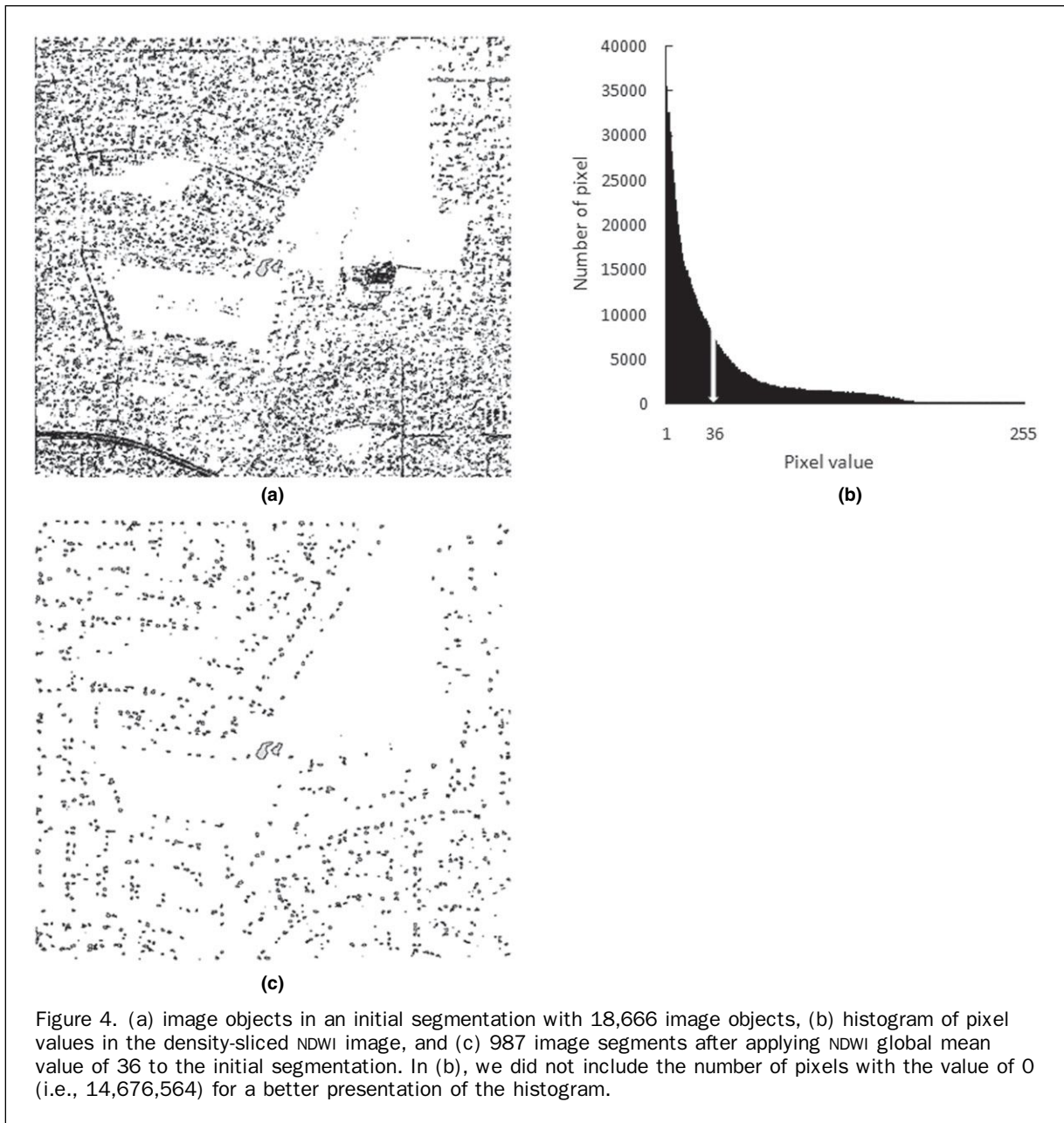


Figure 4. (a) image objects in an initial segmentation with 18,666 image objects, (b) histogram of pixel values in the density-sliced NDWI image, and (c) 987 image segments after applying NDWI global mean value of 36 to the initial segmentation. In (b), we did not include the number of pixels with the value of 0 (i.e., 14,676,564) for a better presentation of the histogram.

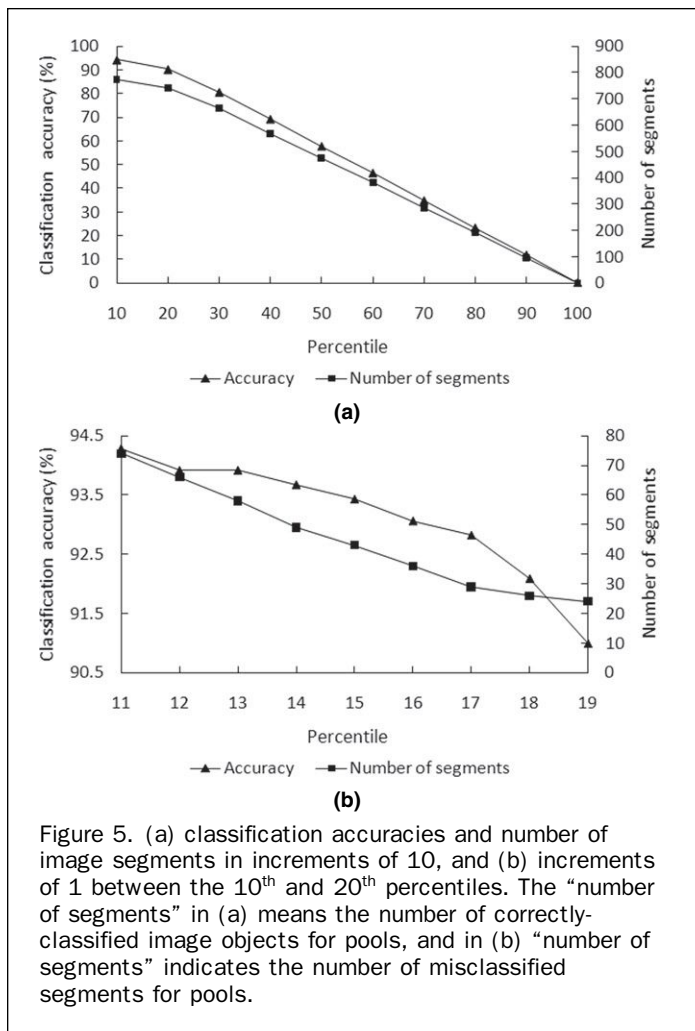
classification. We found that a total of 34 segments were correctly assigned to non-pool class with the use of the RF value of 1, but we still had 178 image objects that were not incorrectly classified as pool in the classification result.

In the final stage, size-controlled shadow masking was applied to image segments that were produced with RF. Because there were few reports about the physical dimensions of private outdoor swimming pools, we computed percentile values of image objects' size that were utilized as cut-off values to remove image segments below the percentile values. Figure 5 shows the classification accuracies of pools generated by dividing the total number of correctly-classified pools by that of referenced pools. As shown in Figure 5a, both accuracy and the number of correctly-classified segments for pool decreased with an increase in percentile ranking. The 10th percentile generated the most

TABLE 4. ERROR MATRIX OF CLASSIFICATION RESULTS WITH RECTANGULAR FIT AS WELL AS NDWI VALUE

Classification	Reference		User's accuracy
	Pool	Non pool	
Pool	775	190	80.3%
Non-pool	47	610	92.9%
Producer's accuracy	94.3%	76.3%	

Overall accuracy: 85.4 percent, Overall Kappa coefficient: 0.71
 Pool Kappa coefficient: 0.60
 Non-pool Kappa coefficient: 0.86



accurate result with 94.3 percent, followed by the 20th percentile with an accuracy of 90.1 percent. We performed the same analysis between the 10th and 20th percentiles in steps of 1. Figure 5b shows their accuracies and the numbers of misclassified image segments for pool, and Table 5 describes percentile values employed in the procedure.

TABLE 5. IMAGE OBJECT'S SIZE FOR EACH PERCENTILE USED IN SIZE-CONTROLLED SHADOW MASKING PROCEDURE

Percentile	Number of pixels	Percentile	Number of pixels
10	48	20	153
11	55	30	222
12	64	40	277
13	71	50	320
14	79	60	360
15	92	70	404
16	105	80	457
17	115	90	548
18	131	100	9329
19	143		

TABLE 6. ERROR MATRIX OF FINAL POOL AND NON-POOL CLASSIFICATION RESULT USING SIZE AS WELL AS NDWI AND RECTANGULAR FIT

Classification	Reference		User's accuracy
	Pool	Non pool	
Pool	772	77	90.4%
Non-pool	50	723	93.5%
Producer's accuracy	93.9%	90.9%	

Overall accuracy: 92.2%, Overall Kappa coefficient: 0.84

Pool Kappa coefficient: 0.82

Non pool Kappa coefficient: 0.86

According to the figure, accuracies decreased as the percentile ranking increased. However, the decrease of classification accuracy was insignificant until the 15th percentile.

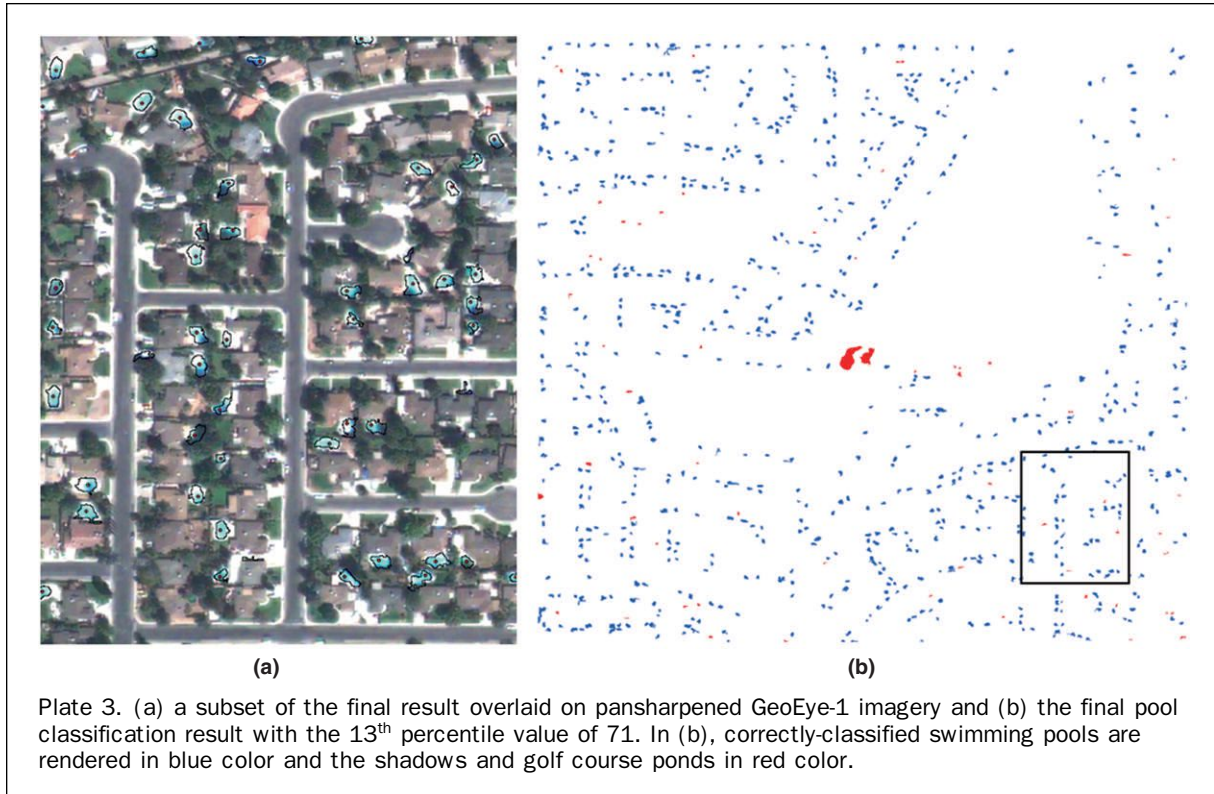
In particular, the 13th percentile value of 71 produced a maximum classification accuracy of 93.9 percent, and it produced the number of misclassified image segments for pool less than the values of 11th and 12th percentiles. Table 6 summarizes the classification accuracies of size-controlled GEOBIA with the 13th percentile value. The size-controlled GEOBIA yielded an overall accuracy of 92.2 percent and a Kappa coefficient of 0.84 that increased by approximately 6.9 percent and 0.14 for overall accuracy and Kappa, respectively, compared with previous classification results. In addition, the size-controlled GEOBIA enhanced the accuracies of individual classes by the increased ability of differentiating non pools from pools (see Tables 3 and 4). We obtained producer's and user's accuracies over 90 percent for both pool and non-pool classes with Kappa coefficients of 0.82 and 0.86 for pool and non-pool, respectively.

Plate 3 shows the final classification result of swimming pools with the 13th percentile value of 71. The area of Plate 3a corresponds to the lower-right portion of Plate 3b marked with a black-hollow rectangle. The boundary of each classified swimming pool is delineated in black color, and manually-interpreted pools are located in Plate 3a. As shown in the plate, each extracted swimming pool can be located in a GIS spatial database, which will expedite ground truthing and the identification of neglected pools. Meanwhile, shadows could not be totally excluded in the final classification result, and non-pool water features such as lakes in a golf course were confused with swimming pools. The lakes are located in the center of Plate 3b.

Discussion

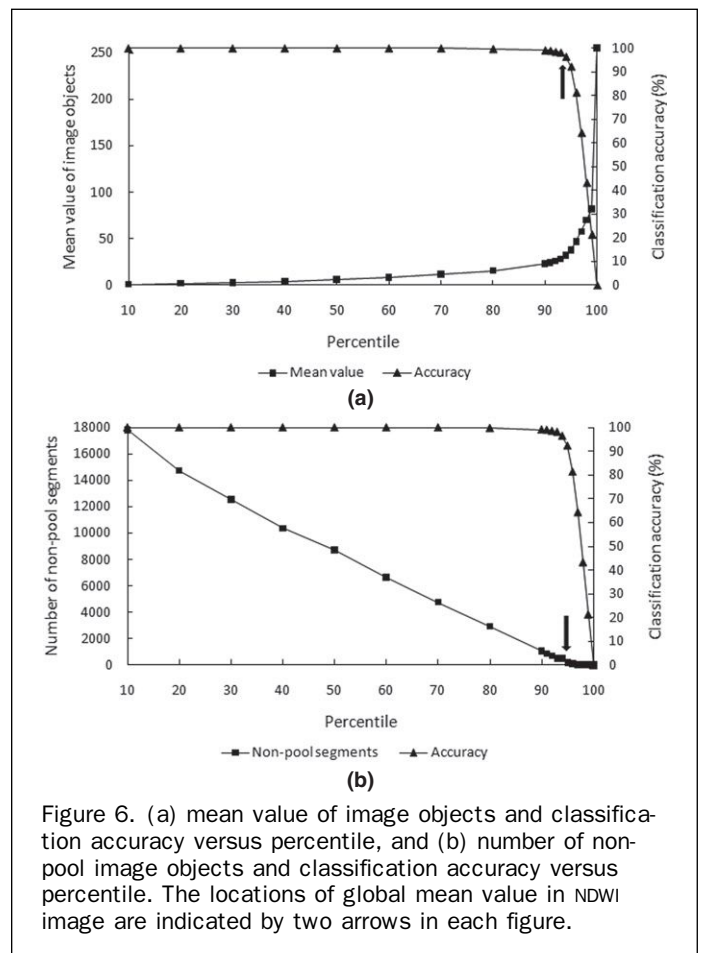
Our research demonstrated that remote sensing techniques and VHR satellite imagery could be utilized to detect private swimming pools and to construct a GIS database with a high accuracy. In particular, NDWI was found to be a valuable remote sensing index that accurately separated swimming pools from most other landscape features. NDWI has proven to be successful in extracting open water and monitoring vegetation moisture with medium resolution imagery (McFeeters, 1996; Dennison *et al.*, 2005). On the contrary, few studies have combined the NDWI with VHR satellite imagery. In our study, all manually-interpreted pools were successfully located in NDWI imagery, but shadows remained within the NDWI image that should be removed.

The global spectral mean of the NDWI image was a useful cut-off (or threshold) value that reduced the number of image segments and resulted in high classification



accuracy by separating swimming pools from shadows. Figure 6 shows the graphs of the mean object values, classification accuracy, and the number of non-pool segments as a function of these percentiles. The classification accuracy of the figure was derived with the same way for Figure 5. The global mean 36 of 8-bit NDWI image was between the 94th percentile of 32 and 95th percentile of 38 in terms of image objects' mean value, as indicated by an arrow in Figure 6a. The classification accuracy of the 94th percentile was 96.5 percent and that of the 95th percentile 92.3 percent. As marked by an arrow in Figure 6b, a mean object value between the two percentiles was a critical point associated with the number of non-pool segments. In the 94th percentile, 514 image objects were found to be incorrectly classified as swimming pools. On the contrary, there were 175 segments that were incorrectly extracted in the 95th percentile. Taking it into account that a global mean value would be different scene by scene, the incorporation of a global mean with the percentile of mean value of image objects is expected to provide a valuable clue in deciding a threshold NDWI value for differentiating pools and non pools.

The GEOBIA approach has valuable functional aspects compared with the conventional pixel-based approach in landscape feature extraction. In the traditional pixel-based approach, it was hard to derive spatial attributes such as size and shape, because individual pixels were the basic processing units. However, GEOBIA enabled us to generate spatial attributes because the image objects have their own vector boundaries to differentiate them from adjacent segments. In our study, spatial attributes such as RF and size played important roles in separating shadows from swimming pools. Particularly, when using the 13th percentile value of 71 as minimum size, the classification accuracy of 93.9 percent was acquired with a minimum number of shadow segments. In remote sensing imagery, outdoor swimming pools may be partly covered by vegetative



canopies and shadows, which makes it difficult to determine their average size even though we have that information. For this reason, the percentile value will be more appropriate to differentiate swimming pools from shadows when considering size as a classification criterion.

The final GEOBIA classification result revealed that shadows inherent from buildings and vehicles on roads were confused with swimming pools. Auxiliary information can be incorporated in segmentation and classification procedures, which improves the performance of GEOBIA (Dragut and Blaschke, 2006; Kim *et al.*, 2009; Kim *et al.*, 2010; Kim *et al.*, 2011b). Regarding shadow issue, the incorporation of an additional data set, *i.e.*, light detection and ranging (lidar) data, has been made to differentiate shadows from non-shadows with high-resolution digital aerial imagery (Zhou *et al.*, 2009). Taking it into consideration, the additional data set such as building footprints and road networks may reduce classification confusion between pools and shadows. Moreover, additional data on size range for private swimming pools would facilitate the separation of pools from non-pool water bodies (e.g., lakes and reservoirs) that are larger than pools. Besides size information, contextual relationship between land-cover features, e.g., topological relation such as adjacency and containment would be helpful to differentiate pools from non-pool water bodies. The contextual and spatial information of image objects has been utilized to conduct thematic classification of a dense urban area (Shackelford and Davis, 2003).

In recent years, an attempt has been made to study neglected pools and find their correlation with WNV mosquito production status using remote sensing imagery (Weinhold, 2009). Our proposed spatial database derived from GEOBIA and VHR satellite imagery is expected to facilitate the identification and location of neglected pools. Nevertheless, manual interpretation will be required to create a complete coverage of swimming pools. The accuracy of 94 percent in pool detection is suitable from the perspective of remote sensing, but 6 percent of the swimming pools may be missed (or 46 of the 775 correctly identified pools). Therefore, the combination of GEOBIA and manual interpretation is recommended to develop a system for the detection of all swimming pools before surveying for neglected pools.

Besides remote sensing pool surveys, it also is important to continue community education efforts to encourage residents to report neglected pools in their neighborhoods to local vector control programs. The combination of remote sensing and neighborhood patrols will aid efforts to control urban *Culex* mosquitoes, including those who carry WNV or other mosquito-borne pathogens. In addition, we utilized NDWI imagery in image segmentation and pool classification procedures based on our initial analysis associated with the spectral reflectance of pools and the other land cover features (see Figure 2). However, the incorporation of multispectral bands with NDWI may have any effects on GEOBIA pool classification since segmentation quality and its associated classification result could be affected by the types of input data set (Blaschke, 2003; Kim *et al.*, 2010; Kim *et al.*, 2011b; Kim *et al.*, in press). Taking it into consideration, the use of NDWI and VHR multispectral image would help improve the performance of GEOBIA pool classification as well as the separation of neglected pools from normal pools in a further image analysis step.

Health scientists have utilized remote sensing imagery to extract environmental variables that are related to vector-borne diseases, and VHR imagery would be appropriate for urban feature classification (Beck *et al.*, 2000). Nonetheless, the spatial resolution of original VHR multispectral imagery may be insufficient to resolve small features in epidemiological research. For instance, it was pointed out that VHR

multispectral images were not appropriate to detect and extract small malaria mosquito habitats because their spatial resolution was generally larger than the malaria mosquito habitats (Mutuku *et al.*, 2009).

In the current study, image pansharpening enabled us to create higher-resolution color imagery that is appropriate for extracting smaller spatial features, but still may miss objects such as hot tubs or Jacuzzis. Existing VHR satellites, such as Ikonos, QuickBird and GeoEye, provide multispectral images with blue, green, red, and NIR wavelength regions. However, recent advances in sensor technology have expanded the number of spectral wavelength regions. For example, the WorldView-2 satellite, launched in October 2009, provides the additional spectral bands of coastal, yellow, red edge, and NIR-2 as well as the conventional four spectral bands at spatial resolution of 1.84 m (DigitalGlobe, 2010). The panchromatic image of 0.46 m spatial resolution is also available from the same satellite. Increased spatial and spectral resolutions of current remote sensing imagery are anticipated to aid in acquiring information about environmental risk factors for human diseases.

Conclusions

Our research demonstrated that GEOBIA and VHR satellite imagery could be used for the accurate construction of GIS spatial databases for detecting private swimming pools. The spectral and spatial attributes of individual image objects played important roles in reducing classification confusion between swimming pools and non-pool features, particularly shadows. The current GIS pool database is expected to assist mosquito control programs to detect mosquito larval sources within urban communities, especially for West Nile Virus epidemic in the United States. We plan to expand this research to develop an unsupervised classification scheme to separate neglected swimming pools from clean swimming pools using GEOBIA and VHR satellite imagery.

Acknowledgments

The authors thank John Newton of Orange County Vector Control District (VCD), Russell Parman of Santa Clara County VCD, and Richard Takahashi, Kern County MVCD, California, for providing valuable information on their aerial pool surveillance programs. We acknowledge that the findings and conclusions in this report are those of the authors and do not necessarily represent the official position of United States Centers for Disease Control and Prevention.

References

- Beck, L.R., B.M. Lobitz, and B.L. Wood, 2000. Remote sensing and human health: New sensors and new opportunities, *Emerging Infectious Diseases*, 6:217–226.
- Blaschke, T., 2003. Object-based contextual image classification built on image segmentation, *Proceedings of the 2003 IEEE Workshop on Advances in Techniques for Analysis of Remotely Sensed Data*, 27–28 October, Washington, D.C., pp. 113–119.
- Blaschke, T., 2010. Object based image analysis for remote sensing, *ISPRS Journal of Photogrammetry and Remote Sensing*, 65:2–16.
- BLS (Bureau of Labor Statistics), 2010. *Labor Force Statistics from the Current Population Survey*. Department of Labor, United States, URL: <http://www.bls.gov/cps/> (last date accessed: 04 August 2011).
- Caillouët, K.A., J.C. Carlson, D. Wesson, and F. Jordan, 2008. Colonization of abandoned swimming pools by larval mosquitoes and their predators following Hurricane Katrina, *Journal of Vector Ecology*, 33:166–172.
- CDC (Centers for Disease Control and Prevention), 2010. *Statistics, Surveillance, and Control Archive, United States*, URL:

- http://www.cdc.gov/ncidod/dvbid/westnile/surv&control_archive.htm (last date accessed: 04 August 2011).
- CDF (California Department of Finance), 2010. *City/County Population Estimates with Annual Percent Change*, URL: <http://www.dof.ca.gov/research/demographic/reports/estimates/e-1/view.php> (last date accessed: 04 August 2011).
- Definiens, 2009. *eCognition Developer 8: Reference Book*, Definiens AG, München, Germany.
- Dennison, P.E., D.A. Roberts, S.H. Peterson, and J. Rechel, 2005. Use of normalized difference water index for monitoring live fuel moisture, *International Journal of Remote Sensing*, 26:1035–1042.
- DigitalGlobe, 2010. *Spectral Response for DigitalGlobe WorldView 1 and WorldView 2 Earth Imaging Instruments*. URL: http://www.digitalglobe.com/downloads/spacecraft/DigitalGlobe_Spectral_Response.pdf (last date accessed: 04 August 2011).
- Dragut, L., and T. Blaschke, 2006. Automated classification of landform elements using object-based image analysis, *Geomorphology*, 81:330–344.
- Epstein, P.R., 2001. West Nile virus and the climate, *Journal of Urban Health*, 78:367–371.
- FRB (Federal Reserve Bank), 2010. *U.S. Credit Conditions*, New York, URL: <http://www.newyorkfed.org/creditconditions/> (last date accessed: 04 August 2011).
- Gangkofner, U.G., P.S. Pradhan, and D.W. Holcomb, 2008. Optimizing the high-pass filter addition technique for image fusion, *Photogrammetric Engineering & Remote Sensing*, 74(11):1107–1118.
- Hay, G.J., K.O. Niemann, and G.F. McLean, 1996. An object-specific image-texture analysis of H-resolution forest imagery, *Remote Sensing of Environment*, 55:108–122.
- Kern County, 2008. *West Nile Virus Strategic Response Plan*, California, URL: <http://www.kernpublichealth.com/departments/cdc/westnile/pdfs/WNVStrategicResponsePlan.pdf> (last date accessed: 04 August 2011).
- Kim, M., M. Madden, and T. Warner, 2008. Estimation of optimal object size for the segmentation of forest stands with multispectral Ikonos imagery, T. *Object-based Image Analysis – Spatial Concepts for Knowledge-driven Remote Sensing Applications* (T. Blaschke, S. Lang, and G.J. Hay, editors.), Springer-Verlag, Berlin, pp. 291–307.
- Kim, M., 2008. Performance comparison of object- and pixel-based land cover classifications using a color infrared aerial photograph, *The Geographical Journal of Korea*, 42:1–10 (in English).
- Kim, M., M. Madden, and T. Warner, 2009. Forest type mapping using object-specific texture measures from multispectral Ikonos imagery: Segmentation quality and image classification issues, *Photogrammetric Engineering & Remote Sensing*, 76(2):137–149.
- Kim, M., M. Madden, and B. Xu, 2010. GEOBIA vegetation mapping in Great Smoky Mountains National Park with spectral and non-spectral information, *Photogrammetric Engineering & Remote Sensing*, 76(2):137–149.
- Kim, M., J.B. Holt, and M. Madden, 2011a. Comparison of global- and local-scale pansharpening for the rapid assessment of humanitarian emergencies, *Photogrammetric Engineering & Remote Sensing*, 77(1):51–63.
- Kim, M., T. Warner, M. Madden, and D. Atkinson, 2011b. Multi-scale GEOBIA with very high spatial resolution digital imagery: Scale, texture and image objects, *International Journal of Remote Sensing*, 32(1): 2825–2850.
- Kim, M., J.B. Holt, C.Y. Ku, and M. Madden, (in press), GEOBIA building extraction of Mae La refugee camp, Thailand: Step-wise multi-scale approach, *Landscape Analysis using Geospatial Tools: Community to the Globe* (M. Madden and E. Allen, editors), Springer-Verlag, New York.
- Komar, N., 2003. West Nile virus: Epidemiology and ecology in North America, *Advances in Virus Research*, 61:185–234.
- Kramer, L.D., J. Li., and P.Y. Shi, 2007. West Nile virus, *Lancet Neural*, 6:171–181.
- McFeeters, S.K., 1996. The use of the normalized difference water index (NDWI) in the delineation of open water features, *International Journal of Remote Sensing*, 17:1425–1432.
- Mutuku, E.M., M.N. Bayoh, A.W. Hightower, J.M. Vulue, J.E. Gimnig, J.M. Mueke, F.A. Amimo, and E.D. Walker, 2009. A supervised land cover classification of a western Kenya lowland endemic for human malaria: Associations of land cover with larval Anopheles habitats, *International Journal of Health Geographics*, 8, DOI:10.1186/1476-072X-8-19.
- Myint S.W., P. Gober, A. Brazel, S. Grossman-Clarke, and Q. Weng, 2011. Per-pixel vs. object-based classification of urban land cover extraction using high spatial resolution imagery, *Remote Sensing of Environment*, 115:1145–1161.
- Reisen, W.K., and W.C. Reeves, 1990. Bionomics and ecology of *Culex tarsalis* and other potential mosquito vector species, *Epidemiology and Control of Mosquito-Borne Arboviruses in California, 1943–1987* (W.C. Reeves, S.M. Asman, J.L. Hardy, M.M. Milby, and W.K. Reisen, editors), California Mosquito and Vector Control Association, Inc., Sacramento, California, pp. 128–144.
- Reisen, W.K., H. Lothrop, R. Chiles, M. Madon, C. Cossen, L. Woods, S. Husted, V. Kramer, and J. Edman, J., 2004. West Nile virus in California, *Emerging Infectious Diseases*, 10: 1369–1377.
- Reisen, W.K., R.M. Takahashi, B.D. Carroll, and R. Quiring, 2008. Delinquent mortgages, neglected swimming pools, and West Nile virus, California, *Emerging Infectious Diseases*, 14:1747–1749.
- Reisen, W.K., B.D. Carroll, R. Takahashi, Y. Fang, S. Garcia, V.M. Martinez, and R. Quiring, 2009a. Repeated West Nile virus epidemic transmission in Kern County, California, 2004–2007, *Journal of Medical Entomology*, 46:139–157.
- Reisen, W.K., R.M. Takahashi, B.D. Carroll, and R. Quiring, 2009b. Letter – Delinquent mortgages, neglected swimming pools, and West Nile virus, California, *Emerging Infectious Diseases*, 15:508–509.
- Shackelford, A.K., and C.H. Davis, 2003. A combined fuzzy pixel-based and object-based approach for classification of high-resolution multispectral data over urban areas, *IEEE Transactions on Geoscience and Remote Sensing*, 41:2354–2363.
- Tian, J., and D.M. Chen, 2007. Optimization in multi-scale segmentation of high-resolution satellite images for artificial feature recognition, *International Journal of Remote Sensing*, 28:4625–4644.
- Turell, M.J., D.J. Dohm, M.R. Sardelis, M.L. O’Ginn, T.G. Andreadis, and J.A. Blow, 2005. An update on the potential of North American mosquitoes (*Diptera: Culicidae*) to transmit West Nile virus, *Journal of Medical Entomology*, 42:57–62.
- Wang, L., W.P. Sousa, and P. Gong, 2004. Integration of object-based and pixel-based classification for mapping mangroves with Ikonos imagery, *International Journal of Remote Sensing*, 25:5655–5668.
- Weinhold, B., 2009. Infectious disease: WNV thrives in financial crisis, *Environmental Health Perspectives*, 117:A18.
- Woodcock, C.E., and A.H. Strahler, 1987. The factor of scale in remote sensing, *Remote Sensing of Environment*, 25:349–379.
- Zhou, W., G. Huang, A. Troy, and M.L. Cadenasso, 2009. Object-based land cover classification of shaded areas in high spatial resolution imagery of urban areas: a comparison study, *Remote Sensing of Environment*, 113:1769–1777.

(Received 20 January 2011; accepted 27 March 2011; final version 26 April 2011)

Everyone will benefit if YOU



Make a commitment to *Your* Profession and Join ASPRS Today.

Which membership is right for me?

ASPRS membership is for one year (12 months) and all **Active** and **Associate** members receive 12 issues of *PE&RS*. All **Student** members receive *PE&RS* in digital form only. Membership renewal is based on the anniversary date of the month you joined. Membership certificates are available for an additional charge (see below). Please allow 4–6 weeks for delivery of your membership materials.

Active

- Involved or interested in the practice of photogrammetry, remote sensing, and/or geographic information systems and related sciences.
- Full member benefits including; the right to vote and hold office, discounts on ASPRS conference registration fees, group insurance policy, eligibility for awards, discounts off ASPRS publications.

\$135.00 Domestic, 2nd Class \$184.00 Canada, Air¹ \$195.00 Foreign, ISAL

Associate

- Have been a student member for at least one year but are no longer eligible for student membership status.
- Eligible for this membership for a period of no more than three years immediately following their time as a student member.
- Associate Members shall be entitled to the same rights and privileges of the Society as an Active Member.

\$90.00 Domestic, 2nd Class \$137.00 Canada, Air¹ \$150.00 Foreign, ISAL

Student

- A Student Member shall be working towards a degree at a university or college. Certification of student status (examples may include copies of student identification or current registration, faculty or sponsor signature, etc.) is required for each year of student membership. **Attach a copy of your student ID or certifying faculty name and institution** _____
- A person is not eligible for student membership if he/she has previously held an Active or Associate Member status.
- Student members do not vote or hold office until they advance to Associate Membership.

\$45.00 Domestic \$48.00 Canada \$55.00 Foreign

Membership Certificate

Hand-engrossed, frangible certificate of membership is available for additional charge. \$20.00

Member Sponsorship (not mandatory)

Sponsor's Member ID: _____

Sponsor's Name: _____

Member Information

Technical Division Preferences: Number the following 6 ASPRS divisions in order of preference where your primary interests lie so you can be kept up to date on their activities (Order of Preference 1–6).

___ GIS Geographic Information Systems ___ PA Photogrammetric Applications
___ PDA Primary Data Acquisition ___ PP Professional Practice
___ Lidar Division (new) ___ RSA Remote Sensing Applications

New Member Renewal (ID number _____)

Mr. Ms. Dr. other: _____

Name (please print): _____

Check appropriate box for mailing address home business

Address: _____

Country: _____

Company's name/workplace: _____

Business Phone*: _____ Home Phone*: _____

fax*: _____ e-mail*: _____

*DO NOT PUBLISH: Business Phone Home Phone Fax E-mail

Method of Payment: Payment must be submitted with application.

Payment must be made in US Dollars drawn on a US Bank or appropriate credit card. Make checks payable to ASPRS.

- Check (Print name on check.)
 Visa MasterCard American Express Discover

Credit Card Account Number _____ Expires (MO/YR) _____

Signature _____ Date _____

Total Amount Enclosed: \$ _____

Membership dues includes an annual subscription to *PE&RS* valued at \$68.00. Non-member subscription price is \$410.00 (libraries, universities, private companies etc.) Members may NOT deduct the subscription price from dues. ASPRS is an educational organization exempt from taxation under the 501(c) (3) code of the Internal Revenue Service. Dues payments are not deductible as a charitable contribution for federal tax purposes, but may be deductible as a business expense. Please check with your tax preparer.

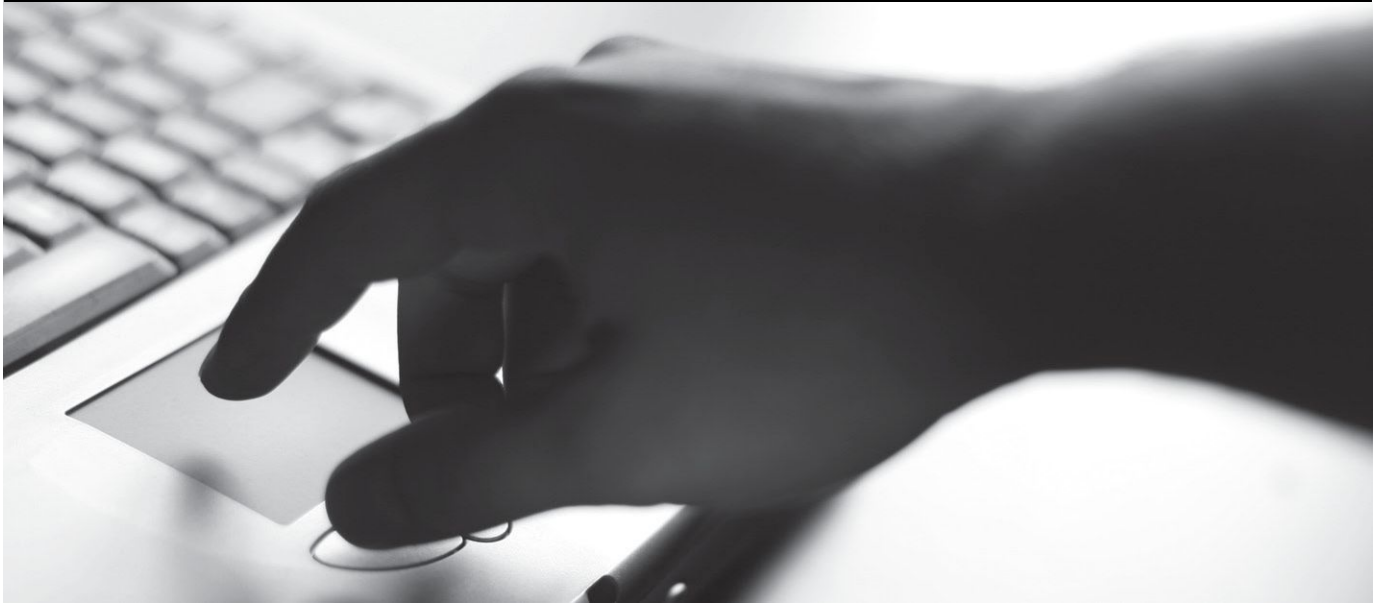
Dues for Active and Associate domestic members includes Second Class Postage for *PE&RS*. Dues for Mexico and all other foreign countries include Airmail Publication Service postage for *PE&RS* (7–20 day delivery time worldwide). In addition, all dues include a postage surcharge. Student members residing outside of the U.S., including Mexico and Canada, receive a Full digital version of *PE&RS* only.

¹DUES INCLUDES POSTAGE AND GST. (ASPRS is required by the Canada Customs and Revenue Agency to collect 5% of the total amount of dues and postage for Canada's Goods and Services Tax — GST #135123065.)

5410 Grosvenor Lane, Suite 210, Bethesda, Maryland 20814-2144 · tel 301.493.0290 · fax 301.493.0208 · email asprs@asprs.org · www.asprs.org

ASPRS WEBINAR SERIES

Have you wanted to attend an ASPRS conference workshop but didn't have the time to spend away from the office? Are your travel funds limited? No problem. Here's why.



ASPRS Workshops are at your fingertips with the ASPRS Webinar Workshop Series. Now you can take popular ASPRS Workshops from your home or office through the ASPRS Webinar Workshop Series. Just sign up and log in on the Webinar date. You will be able to interact with others attending the Webinar and ask questions, just as if you were attending the Workshop at one of our conferences. The only thing you'll miss is the coffee break!

You benefit from having these excellent ASPRS workshops delivered to you. So don't wait; sign up today.

For deadlines & fees, see the URL below.

Webinar Calendar

December 2, 2011

Basic Principles of Spatial Data Analysis

January 17, 2012

Object-based Image Analysis

January 26-27, 2012

Preparation for ASPRS Certification

<http://asprs.org/Webinar-Series/>

**GXP XPLORER™ SOFTWARE.
TAKE COMMAND OF YOUR DATA UNIVERSE.**



Discover a revolutionary way to organize and access data — from a handheld device, desktop or enterprise-wide server cluster. Build a common data environment and promote collaboration between peers, within a workgroup or across an enterprise. With a single query, connect to multiple data stores to discover and display images, maps, terrain, videos, features and documents. Just one of the ways BAE Systems delivers real performance.